Université du Québec
à Rimouski

Variabilité climatique et reconstitution des conditions océanographiques dans le golfe de San Jorge (Patagonie, Argentine) au Pléistocène supérieur et à l'Holocène

Thèse présentée

dans le cadre du programme de doctorat en Océanographie

en vue de l'obtention du grade de Philosophiae Doctor (Ph.D.)

PAR

© Simon Waly Faye

Novembre 2020

Composition du jury :

Gwénaëlle Chaillou, présidente du jury et évaluatrice interne, UQAR

André Rochon, directeur de recherche, ISMER-UQAR

Guillaume St-Onge, codirecteur de recherche, ISMER-UQAR

Anne de Vernal, examinatrice externe, UQAM

Dépôt initial le 16 Juillet 2020 Dépôt final le 25 Novembre 2020

À mes parents et à l’ensemble de mes professeurs pour les valeurs et connaissances transmises.

REMERCIEMENTS

Ce présent document n'a pu être rédigé que grâce au concours de nombreuses personnes auxquelles je tiens à exprimer ma profonde gratitude et mes sincères remerciements.

Je tiens à remercier mon directeur de thèse André Rochon de m'avoir donné l'opportunité d'enrichir mes connaissances dans le cadre de ce projet de recherche. Je le remercie de m'avoir initié dans l'univers des kystes de dinoflagellés et pour sa prompte présence toutes les fois où j'avais des doutes pour la reconnaissance de certains palynomorphes. Merci pour sa patience et sa disponibilité à chaque fois que de besoin pour discuter de diverses questions. Ses critiques constructives et ses suggestions ont constitué un appui inestimable à l'aboutissement de ce travail. Qu'il soit rassuré de ma profonde gratitude. Je remercie également mon co-directeur Guillaume St-Onge pour ses conseils et son soutien moral. Ses suggestions de nouvelles pistes de réflexion ont amélioré considérablement ces travaux de recherche. Qu'il soit rassuré également de ma profonde reconnaissance.

Un grand merci à Isabel Vilanova d'avoir accepté de superviser mon stage en Argentine qui m'a permis de me familiariser avec l'identification des grandes familles de pollen spécifique de la Patagonie. Merci pour sa joie de vivre et son aide inestimable.

Mes remerciements à Anne de Vernal et Gwénëlle Chaillou pour le temps et l'énergie accordés à l'évaluation de ce document. Je remercie également Elisabeth Levac et Jean Carlos Montero-Serrano d'avoir agi respectivement à titre de membre externe et interne de mon comité de thèse.

Je tiens à remercier également Quentin Beauvais pour sa disponibilité et sa proactivité à chaque fois que nécessaire pour retrouver les carottes et les données recueillies lors de la mission MARGES. Je remercie également Pierre-Arnaud Desiage (PAD) pour les intéressantes discussions et d'avoir mis à ma disposition l'ensemble des données dont j'ai eu

besoin pour mes travaux de recherche. Le pire que je puisse te souhaiter est une brillante carrière dans la recherche PAD.

Ce travail a pu être fait grâce à l'appui financier du FRQNT (*Fonds de recherche du Québec – Nature et technologies*) et du CRSNG (*Conseil de recherche en sciences naturelles et en génie du Canada*) auxquels nous adressons nos chaleureux remerciements. Un grand merci également à UQAR-ISMER et au GEOTOP pour les soutiens financiers complémentaires et à l'ensemble des structures qui ont financé mes congrès, mes expéditions en mer et mon stage en Argentine en l'occurrence le RQM et Québec Océan.

Au moment d'achever cette fabuleuse aventure, mes pensées vont tout naturellement à ma famille (Pa léo, Ma thérèse, Agnès, Rose, Eli, Vero, Michel, Marie) à laquelle je tiens à manifester ma profonde gratitude pour le soutien sans failles tout au long de ma scolarité. Ce présent travail vous est dédié. Diokodial a paax!

À mes amis et collègues sans distinction, j'aimerai tout simplement dire merci pour ces sourires, ces rires, cette joie de vivre, ces moments de partage et de réconfort dans le doute. À chacun de ces mercis, je pense naturellement à Yan Lévesque, Omnain Kutos, Atif Waqas, Pierre Arnaud Desiage, Quentin Duboc et Arthur Bieber. Une mention spéciale à Yan Lévesque qui a su me révéler la beauté du Québec et les joies de l'hiver. Je garde en souvenir nos journées de raquettes, les campings en forêt et le plaisir de faire du canoé.

À Pape et Thierry (colocs de choc), j'aimerai dire un grand merci pour les moments de joies partagées et le soutien collectif. Je remercie également l'ensemble de mes amis qui ont égayé mes journées à Rimouski. Un grand merci à Claire, elle a été présente au bon moment de ma vie et m'a accompagné dans l'aboutissement de ce projet. Merci pour ton soutien!

Au-delà de répondre à une problématique, la thèse a été pour moi une expérience de vie enrichissante en tout point de vue parsemée de moments de temps forts et temps faibles tels les mesures d'une musique. L'objectif a toujours été d'essayer de ramener la mesure vers un temps fort dans les moments de doutes et de questionnements. Je rends un vibrant hommage à toutes ces personnes citées ci-haut qui m'ont permis de garder la note haute.

RÉSUMÉ

La circulation atmosphérique dans l'hémisphère Sud est principalement contrôlée par les forts vents de la ceinture des vents d'ouest. Ces vents ont une influence considérable sur la circulation océanique dans l'Atlantique Sud et le Pacifique Sud. La Patagonie est la seule masse continentale qui intercepte l'essentiel des vents d'ouest et représente donc une région clé pour l'étude des variations passées de ces vents. Cependant, l'étude sur la dynamique de ces vents fait l'objet de discussion dans la littérature scientifique. En outre, la majeure partie de ces études en lien avec les conditions océaniques dans le Pacifique Sud est localisée dans la partie ouest de la Patagonie. Par contre, la variation passée de ces vents en relation avec les conditions océaniques dans l'Atlantique Sud reste faiblement documentée. Sous cet angle, 52 échantillons de surface et 3 carottes sédimentaires prélevés dans le golfe de San Jorge (GSJ), situé dans l'Atlantique Sud-Ouest, ont été étudiés dans cette thèse. L'objectif était de mieux saisir les interactions entre le climat actuel et passé, la végétation et les conditions océaniques dans l'Atlantique Sud.

Dans le chapitre 1, la distribution spatiale des assemblages modernes de kystes de dinoflagellés à partir des échantillons de surface a permis d'établir une base de données de référence pour les interprétations paléocéanographiques en identifiant les assemblages qui reflètent les conditions modernes de surface dans le golfe. À partir des résultats, deux assemblages ont été identifiés. Le premier assemblage est situé dans le GSJ alors que le second assemblage est localisé au large du GSJ. Les assemblages de kystes de dinoflagellés sont dominés par les taxons autotrophes avec une forte présence de taxons hétérotrophes au nord et au large du GSJ. La distribution des kystes de dinoflagellés semble être contrôlée par l'upwelling au large, la présence de proies (e.g. les diatomées) et la productivité primaire.

Dans le Chapitre 2, les patrons de dispersion moderne du pollen et des spores ont été caractérisés en relation avec les provinces phytogéographiques adjacentes au golfe à partir des échantillons de surface. Les résultats ont permis également d'établir une base de données moderne pour décrire l'histoire de la végétation et de décrire les flux d'apports éoliens afin d'identifier des indicateurs pour étudier les variations passées des vents d'ouest. Les résultats attestent que la distribution pollinique reflète la végétation adjacente au GSJ et ainsi démontrent la validité des études polliniques dans la zone d'étude. Dans les sédiments, nous avons retrouvé le pollen de *Nothofagus* et de *Podocarpus* transportés sur une longue distance (~350 km) par les vents d'ouest vers le GSJ. L'abondance de ces taxons dans les sédiments du golfe a été identifiée comme un excellent traceur pour décrire la dynamique passée des vents d'ouest.

Dans le chapitre 3, les assemblages fossiles de pollen & spores et de kystes de dinoflagellés préservés dans 3 séquences sédimentaires dans le GSJ ont permis de

documenter l'histoire de la végétation, de retracer la migration latitudinale de la ceinture des vents d'ouest dominants en relation avec les conditions océaniques dans le golfe durant le Pléistocène supérieur et l'Holocène. Les résultats des chapitres précédents ont été utilisés comme bases de données modernes dans l'interprétation des archives sédimentaires. Les assemblages sporo-polliniques fossiles et de kystes de dinoflagellés combinés aux données sédimentologiques, géochronologiques (AMS-^{14}C) suggèrent des conditions arides et un environnement subaérien probablement lagunaire avant 14 000 cal BP dans le GSJ. Cette période est suivie d'une immersion du golfe et d'une transition vers des conditions semi-arides sur le continent marquées par le développement de la steppe patagonienne. L'indice P:D (indicateur des apports continentaux) et les flux de pollen de *Nothofagus* dans le GSJ ont été identifiés comme des indicateurs de l'intensité des vents d'ouest. Les résultats suggèrent une position nord des vents d'ouest au cours du Pléistocène supérieur, puis une migration sud durant l'Holocène inférieur suivi d'une migration progressive vers le nord durant le reste de l'Holocène. Cette migration progressive est marquée par une intensification des vents d'ouest au centre de la Patagonie à la fin l'Holocène inférieur jusqu'à l'Holocène moyen entrainant une augmentation de la productivité dans le GSJ en raison de la fertilisation du golfe par les flux terrigènes.

Mots clés : Ceinture des vents d'ouest, distribution pollinique, kystes de dinoflagelés, Patagonie, plateau continental argentin.

ABSTRACT

Atmospheric circulation in the Southern Hemisphere is mainly controlled by the strong winds of the Southern Westerly Wind Belt (SWWB). These winds have a significant influence on ocean circulation in the South Atlantic and South Pacific Oceans. The Patagonian region is the only continental mass intercepting the core of the SWWB and constitutes a key region for documenting the latitudinal shifts of these winds. The dynamics of these winds have been well recorded, particularly in relation to oceanic conditions of the South Pacific Ocean (Western Patagonia). Conversely, past variations of these winds in relation to oceanic conditions of the South Atlantic Ocean (Eastern Patagonia) remain poorly documented. In this investigation, 52 surface samples and 3 sediment cores taken from the San Jorge Gulf (SJG), located in the Southwest Atlantic, were studied to better understand the interactions between current and past climate, vegetation and oceanic conditions in the South Atlantic Ocean.

In Chapter 1, the spatial distribution of modern dinoflagellate cyst assemblages from surface samples was analyzed so that the environmental preferences of each taxon be inferred and used to reconstruct paleoenvironmental conditions. The results helped identifying two main assemblages. The first one is located in the inner part of the SJG while the second is located at offshore sites. The dinoflagellate cyst assemblages are dominated by autotrophic taxa, but with strong presence of heterotrophic taxa in the northern part of the SJG and offshore sites. The distribution of dinoflagellate cysts appears to be controlled by offshore upwelling, the presence of prey (e.g. diatoms) and primary productivity.

In Chapter 2, pollen and spore dispersal patterns from surface samples of SJG bottom sediments were characterized in relation to the phytogeographic provinces adjacent to the gulf. The results helped to establish a modern database to describe the vegetation history and to identify the best proxies to study past variations of the SWWB. The results demonstrate that the pollen distribution reflects the vegetation adjacent to the SJG and thus confirms the validity of the pollen records in the study area. In the sediments, we found pollen from *Nothofagus* and *Podocarpus* transported by the SWWB over long distances (~ 350 km) to the SJG. The abundance of these taxa in the SJG sediments have been proposed here as indicators of the past dynamics of the SWWB.

In chapter 3, the fossil assemblages of pollen & spores and dinoflagellate cysts preserved in three sedimentary sequences in the SJG were used to document the vegetation history, and to trace the latitudinal migration of the SWWB in relation to oceanic conditions in the SJG during the Late Pleistocene and Holocene. The results of previous chapters were used as a modern database for the interpretation of the palynological records (pollen, spores and dinocysts). The interpretation of the fossil assemblages combined with sedimentological

and geochronological data (AMS-^{14}C) suggest a subaerial environment in the SJG and possibly a coastal lagoon environment under arid conditions before 14,000 cal BP. This period was followed by an immersion of the SJG and a transition to semi-arid conditions in the adjacent continent marked by the development of the Patagonian steppe. The P:D index (proxy of continental inputs) and *Nothofagus* pollen were identified as indicators of the intensity of the SWWB in the SJG. The results suggest a northern position of the SWWB during the Late Pleistocene, followed by a southward shift during the Early Holocene and a gradual northward migration onwards. This gradual migration is marked by an intensification of the SWWB in the center of Patagonia from the end of the Early Holocene to the Middle Holocene that produced high terrigenous inputs, leading to increased ocean fertilization and primary productivity in the SJG.

Keywords: Southern Westerly Winds; pollen patterns; dinoflagellate cyst assemblages; Patagonia; Argentinian Continental shelf.

TABLE DES MATIÈRES

LISTE DES TABLEAUX

LISTE DES FIGURES

LISTE DES ABRÉVIATIONS, DES SIGLES ET DES ACRONYMES

AAO	*Antarctic Oscillation,* oscillation antarctique
ACC	*Antarctic Circumpolaire Current,* courant circumpolaire antarctique
AMS	*Accelator Mass Spectrometry,* spectrométrie de masse par accélérateur
BP	*Before present,* avant le présent
Cal	*Calibrated dates,* âges calibrés
CONICET	Conseil national argentin de recherche en sciences et techniques
ENSO	*El Niño Southern Oscillation,* El Niño-oscillation australe
GEOTOP	Centre de recherche en Géochimie isotopique et en Géochronologie
GSJ	Golfe de San Jorge
HSCW	*High Salinity Coastal Water,* masse d'eau côtière de salinité élevée
ISMER	Institut des sciences de la mer de Rimouski
LGM	*Last Glacial Maximum,* dernier maximum glaciaire
LSCE	Laboratoire des sciences du climat et de l'environnement
LSCW	*Low Salinity Coastal Water,* plume d'eau côtière de faible salinité
MARGES	*MARine GEology, sedimentology, stratigraphy, basin architecture and paleoceanography of the San Jorge Gulf*
MC	*Malvinas Current,* courant des Malouines
MINCyT	Ministère argentin des sciences, de la technologie et de l'innovation

PC	*Patagonian Current,* courant patagonien
PROMESse	PROgramme Multidisciplinaire de recherche en océanographie pour l'étude de l'Écosystème et de la géologie marine du golfe San Jorge et de la région côtière des provinces de Chubut et Santa Cruz
SAM	*Southern Annular Mode,* mode annulaire australe
SJG	*San Jorge Gulf,* golfe de San Jorge
SWWB	*Southern Westerly wind Belt,* ceinture des vents d'ouest
UQAR	Université du Québec à Rimouski

LISTE DES SYMBOLES

μ	Mu
σ	Sigma

INTRODUCTION GÉNÉRALE

Au cours des dernières décennies, la communauté scientifique s'est attachée à mesurer et à comprendre les facteurs contrôlant les changements climatiques. Cependant, les études sur le climat ne peuvent se limiter aux périodes couvertes par les archives météorologiques, aussi longues et complètes soient-elles. C'est pourquoi la connaissance des changements climatiques requiert que le climat soit placé dans une perspective historique de manière à connaître les variations naturelles à des échelles séculaires ou millénaires. Ainsi, des outils de mesures indirectes ont été développés qui permettent d'estimer le climat passé à partir d'analogues modernes (traceurs micropaléontologiques, dendrochronologiques, biomarqueurs, traceurs géochimiques, etc.). Ainsi donc, plusieurs études réalisées ont montré qu'au Pléistocène supérieur, notamment pendant le dernier maximum glaciaire (LGM~18 000 cal BP), les calottes glaciaires occupaient une grande partie de la surface de la Terre (Ray et Adams, 2001). Cette période fut suivie par un réchauffement au cours de la dernière transition glaciaire/interglaciaire jusqu'à l'Holocène (~11 800 cal BP à l'actuel) en raison des changements d'insolation. Au cours de cette transition, on observe des changements climatiques rapides mis en évidence par la composition isotopique des carottes de glace (*Epica Dôme C* : EDC, *North Greenland Ice Core Project* : NGRIP) et qui diffèrent d'un hémisphère à l'autre (Figure 1). Ces variations climatiques asynchrones entre l'Antarctique et le Groenland montrent la complexité du système climatique. Pour expliquer ce phénomène, des arguments ont été développés, notamment le concept "*bipolar see-saw* ", qui prend en compte les réorganisations internes, dans les circulations atmosphérique et océanique ainsi que la fonte des calottes glaciaires. Ces dites réorganisations sont associées à l'insolation en lien avec les variations des paramètres orbitaux de la Terre (Broecker, 1998 ; Stoker et Johnsen, 2003). En conséquence, la circulation atmosphérique dans l'hémisphère Sud, contrôlée principalement par les vents d'ouest, a une influence considérable sur la circulation océanique dans l'Atlantique Sud et le climat global (Mayr et al., 2006). Des études ont montré

que la variation latitudinale des vents d'ouest module le dégazage de CO_2 dans l'Atlantique Sud (Toggweiler et al., 2006 ; Anderson et al., 2009 ; Denton et al., 2010), et est reliée aux variations de températures de surface du Pacifique Sud (Lamy et al., 2002 ; Caniupàn et al., 2014) et de l'Atlantique Sud (Bianchi et Gersonde, 2004).

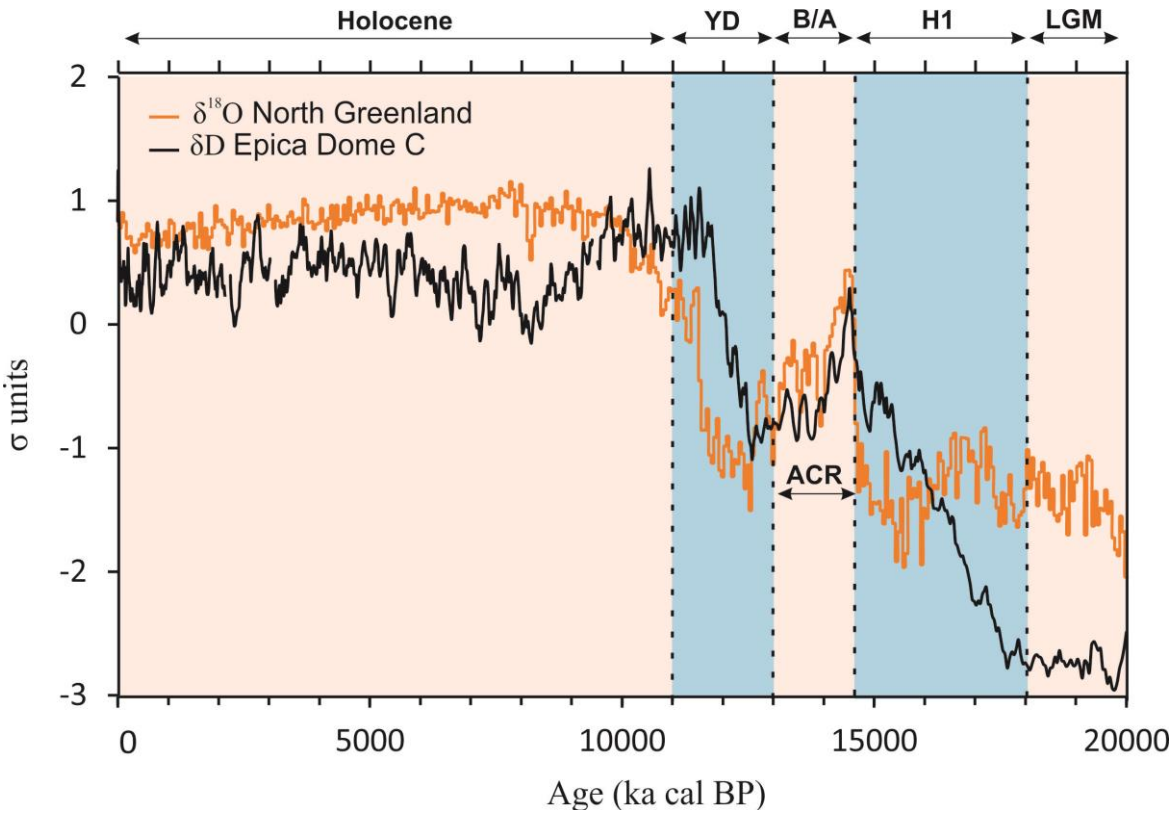

Figure 1. Variation du rapport isotopique de l'oxygène ($\delta^{18}O$) enregistrée au Groenland et la teneur en deutérium (δD) enregistrée en Antarctique (EDC) durant le dernier maximum glaciaire et l'Holocène. LGM : *Last Glacial Maximum* (Dernier Maximum Glaciaire), H1 : Heinrich 1, B/A : Bølling-Allerød, ACR : *Antarctique Cold Reversal*, YD : *Younger Dryas* (Dryas récent, NGRIP, 2004; Parrenin et al., 2013)

À cet effet, la Patagonie, seule bande de terre dans l'hémisphère Sud entièrement traversée par la ceinture des vents d'ouest, ou *westerlies*, demeure une région clé pour documenter la variation latitudinale de ces vents. Cependant, plusieurs études menées sur ces

variations et ne prenant en compte qu'un seul site ne permettent pas de reconstituer avec exactitude la position latitudinale de la ceinture des vents d'ouest depuis le LGM (Bertrand et al., 2014). Par conséquent, les résultats de ces études sont souvent contradictoires et ont fait l'objet de discussions dans la littérature scientifique (Heusser, 1989 ; Markgraf, 1989). Par exemple, Moreno et al. (2010) suggèrent un affaiblissement des vents d'ouest vers le sud de la Patagonie à l'Holocène inférieur (entre 10 et 8 ka cal BP) sur la base de compilations de données polliniques le long de la Patagonie, alors que Lamy et al. (2010) proposent pour la même période une intensification de ces vents. En se fondant sur cette littérature, il n'est donc pas facile de déterminer la position des vents d'ouest depuis le LGM. Notre site d'étude, le golfe de San Jorge est localisé entre 45 et 47°S et se trouve au centre de la ceinture de vent d'ouest (30 et 60°S, Bertrand et al., 2014). Ainsi, ce site offre-t-il une opportunité unique de décrire la variation des vents d'ouest et leur influence sur les conditions océaniques dans l'Atlantique Sud depuis le LGM en utilisant des enregistrements marins et en les comparants avec les archives continentales. La première partie de cette introduction de thèse décrit de façon synthétique le contexte géographique, la circulation atmosphérique et océanographique ainsi que le contexte climatique du site d'étude. La seconde partie réunie les objectifs de ce projet de recherche et l'état des connaissances actuelles liées à la problématique. La troisième partie décrit le matériel et la méthodologie employés. Enfin dans la dernière partie, l'organisation générale de la thèse et les réalisations obtenues au cours de cette thèse seront présentées.

CONTEXTE GÉOGRAPHIQUE

La Patagonie, incluant la *Tierra del Fuego*, est un vaste territoire de 900 000 km^2 localisé entre 39° et 55°S en Amérique du sud (Figure 2 ; Bullard et al., 2016). Du point de vue de la géomorphologie, cette région est marquée à l'échelle régionale par la cordillère des Andes (~1500 m au-dessus de niveau marin dans la province Chilienne) à l'ouest avec des plaines basses avec un faible relief vers l'est (Garreaud, 2009). Le site d'étude, le golfe de San Jorge (GSJ), est localisé au centre de la Patagonie argentine dans l'Atlantique Sud-Ouest.

Il s'étend entre les latitudes 45°S et 47°S pour une superficie supérieure à 39 000 km^2 (Glembocki et al., 2015).

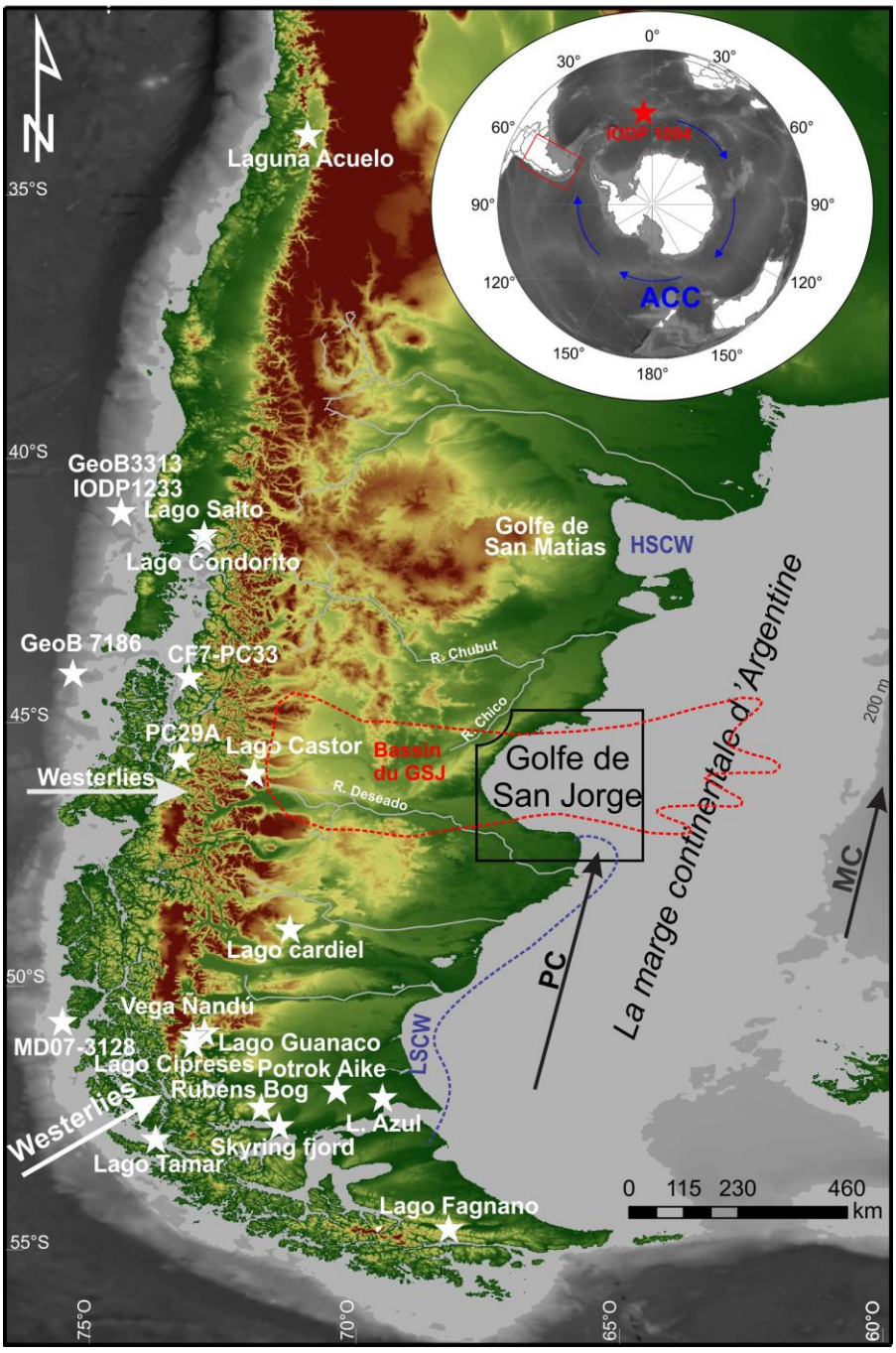

Figure 2. Localisation de la zone d'étude et des sites cités dans l'introduction et délimitation du bassin du GSJ. PC : le courant patagonien, MC : le courant des Malouines, ACC : le courant circumpolaire antarctique, LSCW : *Low Salinity Coastal Water*, HSCW : *High Salinity Coastal Water*.

CONTEXTE GÉOLOGIQUE ET VARIATION DU NIVEAU MARIN

Le GSJ est un bassin intracratonique avec une forme allongée de direction Est-Ouest (Figure 2 ; Fitzgerald et al., 1990). La genèse du bassin du GSJ est expliquée par une tectonique d'extension liée à la fragmentation du supercontinent du Gondwana au cours du Jurassique (Fitzgerald et al., 1990). Ce mouvement extensif a généré des structures tectoniques formées de series de grabens associées à un volcanisme représenté par le complexe Marifill qui affleure au nord du GSJ (Fitzgerald et al., 1990 ; Foix et al., 2013). Après cette période, le bassin a été rempli par des formations sédimentaires oblitérant les structures tectoniques héritées du mouvement extensif (Fitzgerald et al., 1990). Ces formations sédimentaires témoignent de divers environnements sédimentaires liés aux oscillations eustatiques, à la tectonique extensive, aux changements climatiques et aux épisodes glaciaires de la région (Sylwan, 2001). La période couvrant le Jurassique supérieur et le Crétacé est représentée par des roches sédimentaires lacustres (Groupe de Las Heras) et les sédiments continentaux du Groupe Chubut asssociés à une accélération de la subsidence thermique durant le Crétacé (Fitzgerald et al., 1990; Foix et al., 2013). Du Paléocène au Pliocène, la sédimentation dans le bassin du SJG est contrôlée par la tectonique extensive et par des séries de transgression et de regression dues à des variations eustatiques avec une faible subsidence thermique (Figure 3 ; Fitzgerald et al., 1990 ; Sylwan, 2001). Durant cette période, les formations sédimentaires suggèrent un environnement estuarien (e.g. Formation de Salamanca), fluviatile (e.g. Rio Chico) avec des évènements pyroclastiques (e.g. Formation de Sarmiento). La formation de Chenque suggérant un environement néritique et littoral couvre les formations de Rio Chico et Sarmiento et indique une transgression dans le bassin du GSJ. La formation de Santa Cruz caractérisée par des sédiments continentaux et

pyroclastiques s'est déposée sur la formation de Chenque (Nullo et Combina, 2002; Paredes, 2002; Foix et al., 2013). Les dépôts du Quaternaire représentent la période post-tectonique dont les mécanismes de sédimentation sont contrôlés par les variations du niveau marin et les épisodes glaciaires du Pléistocène (Sylwan, 2001). Le Pléistocène est représenté par la formation Rodados Patagonicos qui couvre une grande partie de la Patagonie et affleurant autour du GSJ (Figure 3C). Cette Formation est formée de rochers issus de produits volcaniques des Andes qui sont transportés sur de longues distances et suggérant des processus fluvoglaciaires (Sylwan, 2001). Durant le dernier maximum glaciaire (~20 ka cal BP), une grande partie du plateau continental argentin était émergé et le niveau marin était à -105 m sous le niveau actuel suivi d'une remontée progressive du niveau marin durant le reste du Pléistocène supérieur jusqu'à l'Holocène (Violante et al., 2004). Les évidences de ces fluctuations du niveau marin sont préservées sous forme de quatre terrasses de largeurs et profondeurs variables au niveau du plateau continental argentin (Parker et al., 1997). Dans l'emplacement actuel du GSJ, les données stratigraphiques mettent en évidence la présence d'un réseau fluvial durant cette période de bas niveau marin (Desiage, 2020). Ce système de drainage a incisé des chenaux et des vallées qui auraient été comblés par une succession de dépôts fluviaux, lagunaires et estuariens (Desiage, 2020). L'immersion de GSJ est estimée à ~14500 cal BP lors de la dernière transgression marine (Figure 3B ; Violante et Parker, 2004, Ponce et al., 2011). La lithostratigraphie des séquences post-transgressions a été décrite par Desiage (2020) et marque l'installation de conditions marines dans le GSJ. D'après Schellman et Radtke (2010), le niveau marin était à environ 2 à 3 m au desssus du niveau actuel durant l'Holocène moyen (7,4 à 6,6 ka cal BP) avant de régresser jusqu'à son niveau actuel. Cette régression semble être contrôlée en grande partie par la glacio-isostasie qui se traduit par une remontée du continent estimée à environ 0,3 et 0,4 mm/an depuis de début de l'Holocène moyen sur les côtes atlantiques de la Patagonie (Schellman et Radtke, 2010).

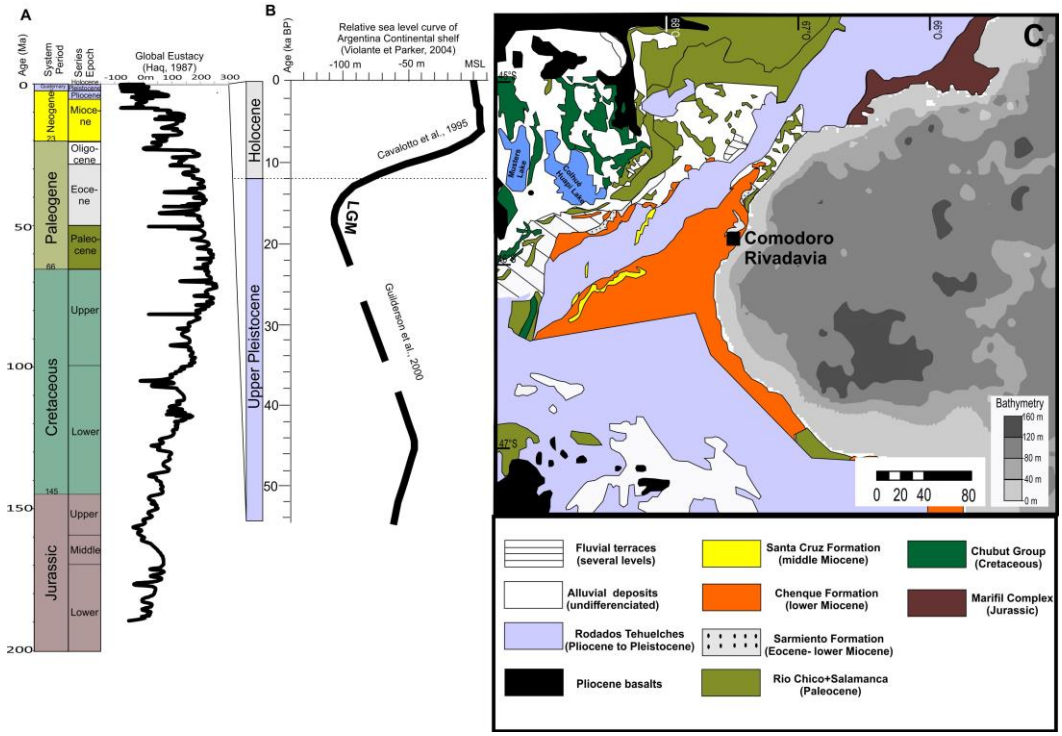

Figure 3. Variation globale du niveau de la mer (A, Haq, 1987) et dans le plateau continental argentin (B, Violante et Parker, 2004). Carte géologique simplifiée du GSJ (C, adaptée de Foix et al., 2013 et de Paredes et al., 2015)

CIRCULATION ATMOSPHÉRIQUE

La circulation atmosphérique, dans la région de la Patagonie, est fortement sous l'influence de la ceinture des vents d'ouest ou *westerlies* (Aravena et Luckman, 2009). En effet, cette zone se trouve entre la ceinture semi-permanente de haute pression subtropicale (anticyclone de l'île de Pâques dans le Pacifique Sud et anticyclone de Sainte-Hélène dans l'Atlantique Sud) et la ceinture de basse pression subpolaire. D'après Compagnucci (2011), les faibles variations de ces centres de haute pression contrôlent l'intensité et la direction des vents. Durant l'hiver austral, les vents d'ouest deviennent plus faibles en raison de la migration de la ceinture de haute pression subtropicale vers le nord. Par contre pendant l'été

austral, la ceinture de haute pression subtropicale migre vers le sud et induit une intensification des vents d'ouest (Figure 4 ; Lamy et al., 2010).

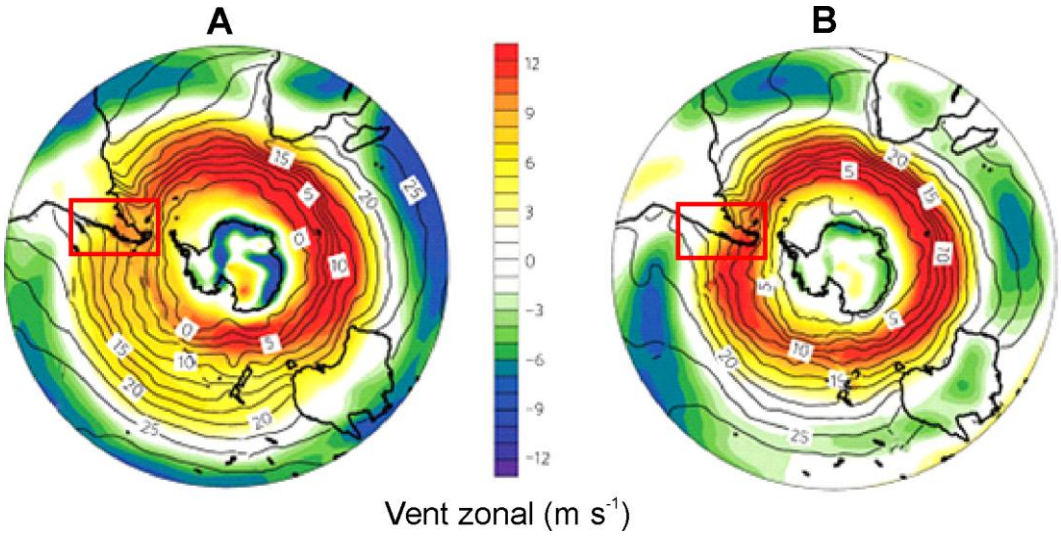

Figure 4. Vent zonal à 850 hPa pendant l'hiver austral (A) et l'été austral (B). Les isolignes indiquent les isothermes de la température de surface de l'océan tirée de Lamy et al. (2010).

CIRCULATION OCÉANIQUE

La circulation océanique générale dans l'Atlantique sud-ouest consiste en un écoulement du courant des Malouines (Malvinas Current : MC) depuis le passage de Drake (55°S) jusqu'à 38°S (Palma et al., 2004 ; Matano et al., 2010 ; Piola et al., 2010). En effet, le MC constitue l'une des branches du courant circumpolaire antarctique (Matano et al., 2010). Il occupe le rebord du talus continental et transporte des eaux subantarctiques froides, salées (S>34) et riches en nutriments (azote inorganique et phosphate ; Piola et al., 2010). Ainsi, les masses d'eau au niveau du plateau continental provenant des eaux subantarctiques par le courant du Cap Horn, ont une salinité beaucoup plus faible (S<34) en raison de l'influence des décharges d'eaux douces du détroit de Magellan (Bianchi, 2005 ; Romero et al., 2006).

La circulation océanique sur le plateau continental argentin est caractérisée par un écoulement vers le nord du courant patagonien (Patagonian Current en anglais : PC ; Matano et al., 2010). Au niveau des côtes argentines, on note la présence d'une plume d'eau côtière de faible salinité (Low Salinity Costal Water en anglais : LSCW ; S<33, 4), associée aux décharges d'eau douce du détroit de Magellan, qui s'étend jusque dans le GSJ (Bianchi et al., 2005). On note également la présence d'une masse d'eau côtière de salinité élevée (High Salinity Coastal Water en anglais : HSCW ; S~34) à proximité de *San Matias* et du *Nuevo Golf* (42°S), due à une évaporation intense (Bianchi, 2005 ; Krock et al. 2015). Les interactions de ces différentes masses d'eau sur le plateau continental argentin sont particulièrement importantes pour la compréhension des caractéristiques des masses d'eau au sein du GSJ.

D'après Krock et al. (2015), les masses d'eau dans le GSJ sont constituées par les eaux du plateau continental argentin qui sont fortement influencées au nord par le HSCW et au sud par le LSCW. La circulation générale dans le GSJ varie saisonnièrement durant l'été et l'hiver australs (Figure 5; Matano and Palma, 2018). La circulation durant l'été austral constitue la configuration la plus courante et est caractérisée par un gyre délimité à l'ouest par les courants côtiers et à l'est par le PC avec une intrusion maximale du PC dans le golfe (Matano et Palma, 2018). Durant l'hiver austral, le gyre s'affaiblit considérablement et les forts vents génèrent deux anticyclones (Matano and Palma, 2018). La circulation actuelle suggère que les vents, les flux de chaleur, la dépression topographique au centre du GSJ et le développement saisonnier de fronts de marées contrôlent l'hydrodynamisme (Krock et al., 2015; Matano and Palma, 2018).

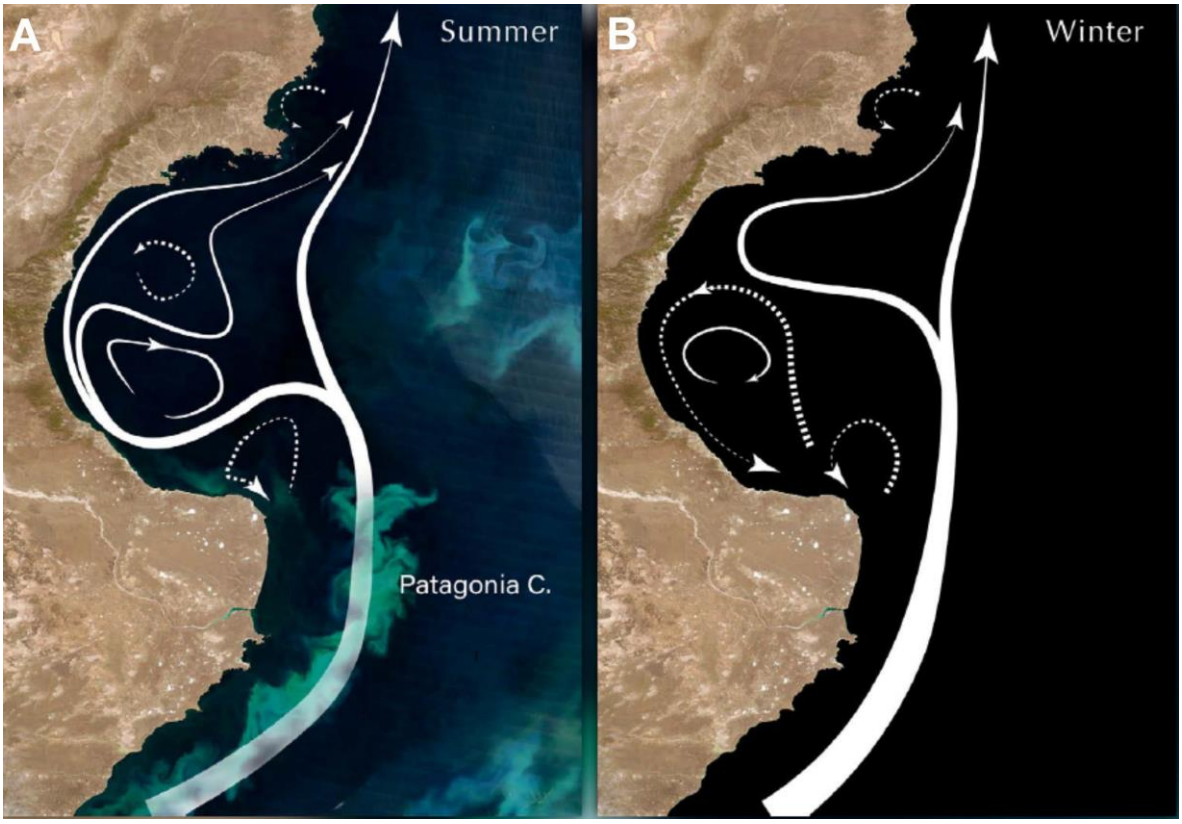

Figure 5. Représentation schématique de la circulation océanique dans le golfe de San Jorge en été et en hiver tirée de Matano et al., 2018.

Dans la partie intérieure du golfe, les eaux sont très stratifiées (Krock et al., 2015). Le réchauffement pendant le printemps et durant l'été induit des fronts thermiques qui délimitent les eaux stratifiées (Rivas et al., 2006). Ce phénomène est associé à de forts courants de marées qui peuvent inhiber le développement saisonnier de la thermocline et générer des fronts tidaux observés dans le GSJ et au niveau de l'isobathe 200 m (Rivas et al., 2006; Carbajal et al., 2018). D'après Sabatini et Martos (2002), ces fronts tidaux sont caractérisés par des zones de forte production primaire. Tonini et al. (2006) mettent en évidence à partir de simulations numériques la présence d'un système de downwelling et d'upwelling localisé respectivement au nord et au sud-sud-ouest du GSJ. On y note également la présence d'un

upwelling, localisé le long de l'isobathe 200 m, dont les mécanismes sont peu compris. Des auteurs suggèrent que les forçages externes comme le vent et la marée ne semblent pas être la cause de ce phénomène (Matano et al., 2010). Par ailleurs, Matano et al (2010) ont émis l'hypothèse selon laquelle la diffusion latérale du MC sur le plateau continental pourrait être à l'origine de cet upwelling.

CONTEXTE CLIMATIQUE

Le climat régional en Patagonie est contrôlé par les vents d'ouest, la différence altitudinale des Andes et la latitude (Borromei et Musotto, 2016). En effet, la cordillère des Andes coupe la trajectoire des vents d'ouest qui amènent de l'air humide provenant du Pacifique. Cela engendre des ombres pluviométriques dans la partie occidentale des Andes alors que la partie orientale demeure sèche en raison de l'effet de foehn (Aravena et Luckman, 2009 ; Coronato et al., 2008). On observe ainsi, au sud de 40°S, un fort gradient de précipitations annuelles qui varient entre 7000 et 4000 mm à l'ouest à 200 mm vers l'est (Garreaud, 2007). Ce gradient constitue l'un des contrastes pluviométriques les plus importants au monde associé à des températures annuelles qui varient entre 8 et 10°C sur le plateau patagonien puis entre 5 et 6°C à l'ouest (Aravena et Luckman, 2009 ; Coronato et al., 2008 ; Mancini, 2009). C'est pourquoi la Patagonie orientale est caractérisée par un climat semi-aride alors que la Patagonie occidentale a un climat très humide soumis aux influences océaniques du Pacifique (Borromei et Musotto, 2016). D'après Agosta et al. (2015), les alizés, associés au centre de haute pression subtropicale situé dans l'Atlantique, apportent aussi de l'humidité jusqu'au centre de la Patagonie.

Par ailleurs, il a été démontré que les variations des températures de surface dans le Pacifique, qui sont associées au mode de variations de l'ENSO (*El Niño Southern Oscillation*), constituent l'un des phénomènes les plus importants régissant des variations interannuelles des précipitations en Patagonie (e.g. Scheinder et Gies, 2004 ; Aravena et Luckman, 2009 ; Moy et al., 2009). Durant la phase positive de l'ENSO (El Niño), la cellule

de haute pression du Pacifique diminue et entraîne une réduction de l'intensité des vents d'ouest au sud de 40°S (Scheinder et Gies, 2004). À cet effet, on note une baisse des précipitations en Patagonie occidentale (Chili) alors que dans la partie orientale (Argentine) les précipitations sont au-dessus de la normale annuelle (Pittock, 1980 ; Scheinder et Gies, 2004). Par contre, la phase négative de l'ENSO (la Niña) est corrélée avec des anomalies de précipitations positives au Chili (Aceituno, 1988). En plus, l'indice de SOI (Southern Oscillation Index) est corrélé négativement aux précipitations au nord de 50°S (Pittock, 1980). De ce point de vue, Thompson et Salomon (2002) estiment que la pointe de la Patagonie est plutôt influencée par le SAM (Southern Annular Mode) également appelé AAO (Antarctic Oscillation). Ce paramètre indique la différence de pression entre le Pôle Sud et la latitude 20°S et caractérise les fluctuations des vents d'ouest au niveau du vortex circumpolaire autour de l'Antarctique (Thompson et Wallace, 2000 ; Thompson et Salomon, 2002 ; Aravena et Luckman, 2009).

OBJECTIF DE LA THÈSE

Ce projet de recherche a pour objectif de comprendre et décrire les changements climatiques au cours du Pléistocène supérieur et de l'Holocène dans le GSJ afin de mieux saisir les interactions entre le climat actuel et passé, la végétation et les conditions océaniques dans l'Atlantique Sud. Pour répondre à cet objectif principal, trois objectifs spécifiques ont été identifiés et correspondent chacun à un article scientifique :

Objectif 1. Distribution des kystes de dinoflagellés dans les sédiments de surface du GSJ.

La distribution des kystes de dinoflagellés dans les environnements marins est contrôlée par les paramètres océanographiques tels que la température, la salinité, le couvert de glace, mais aussi la disponibilité des nutriments (e.g. Rochon et al., 1999 ; de Vernal et

al., 2001). Sous ce rapport, les kystes de dinoflagellés sont couramment utilisés comme des traceurs pour les reconstitutions paléocéanographiques (e.g. Ledu et al., 2010 ; Durantou et al., 2012 ; de vernal et al., 2013). Cependant, la majorité des études sont localisées dans l'hémisphère Nord (e.g. Rochon et al., 1999 ; de vernal et al., 2001). Dans l'Atlantique Sud-Ouest, les études sur la distribution de surface des kystes de dinoflagellés sont rares (e.g. Wall et al., 1977 ; Akselman, 1987 ; Orozco et Carreto, 1989 ; Akselman, 1999 ; Borel et al., 2012 ; Krock et al., 2015). Seule l'étude de Krock et al. (2015) est localisé dans le GSJ. Cette dernière étude est basée sur l'analyse de 5 échantillons de surface répartis dans le golfe. Les résultats montrent que les assemblages de kystes de dinoflagellés sont dominés essentiellement par des espèces autotrophes dont *Spiniferites ramosus, Operculodinium centrocarpum* et *Alexandrium tamarense*, avec une forte présence d'organismes hétérotrophes au sud du GSJ représentés par *Protoperidinium minutum, Polykrikos kofoidii* et *P. schwartzii*. Ces travaux n'ont cependant pas pu établir de relation entre la distribution des kystes de dinoflagellés et les dinoflagellés vivant dans la colonne d'eau. Par ailleurs, les fortes concentrations au centre du golfe ont été corrélées à la granulométrie fine des sédiments de surface. En effet, les kystes de dinoflagellés ont la même taille que les silts. De ce fait, ils ont un comportement hydrodynamique similaire et ont tendance à être concentrés avec les sédiments fins par les courants marins (e.g. Dale, 1976). D'autres études ont été faites plus au sud de la Patagonie (Tierra del Fuego) par Candel et al. (2012) pour documenter la distribution des kystes de dinoflagellés dans le chenal de Beagle en relation avec les conditions océanographiques de surface. Les résultats de cette étude suggèrent que les assemblages de kystes de dinoflagellés sont dominés par *Brigantedinium* spp., *Echinidinium* spp. et *Selenopemphix quanta* associés aux kystes de *Pentapharsodinium dalei*, *Islandinium minutum* et *Votadinium spinosum* (Candel et al., 2012). Les assemblages de kystes de dinoflagellés ont été aussi étudiés sur la base de quinze échantillons sur un transect allant des îles Falkland à la mer de Weddel par Harland et al. (1998). Les résultats montrent deux tendances, la première au sud de 60°S qui est caractérisée par de faibles concentrations associées à une faible diversité (e.g. *Impagidinium pallidum, Islandinium minutum* et le kyste de *Pentapharsodinium dalei*, des « ronds bruns » (e.g. le genre *Brigantedinium*) et

Selenopemphix antarctica). Le second assemblage est caractérisé par une forte diversité avec la présence de *Dalella chathamense*, *Impagidinium sphaericum*, *Nematosphaeropsis labyrinthus* asssociées à une forte concentration de *Selenopemphix antarctica*. D'après Harland et al. (1998), cette subdivision coïncide avec la limite nord de la couverture de glace et celle du front polaire (55 et 60°S) qui sépare les eaux subantarctiques froides et riches en nutriments et les eaux atlantiques moins riches en nutriments. Esper et Zonneveld (2002) ont fait une étude similaire à celle de Harland et al. (1998) sur la base de trente-deux échantillons de surface dans l'Atlantique Est entre le front subtropical (40°S) et polaire pour mieux documenter les relations entre la distribution des kystes de dinoflagellés et les fronts océaniques dans l'Atlantique Sud. Les résultats montrent une abondance des espèces du genre *Impagidinium* autour du front subtropical et la présence de *Nematosphaeropsis labyrinthus* et *Operculodinium centrocarpum* entre les zones de transitions subtropicale et subantarctique, puis une dominance des espèces du genre *Protoperidinium* spp. autour du front subantarctique avec une de forte concentration de *Selenopemphix antarctica* plus au sud (Esper et Zonneveld, 2002). Cependant, la position géographique de ces fronts océaniques (polaires et subtropicaux) a pu changer dans le passé avec les fluctuations du climat global induisant ainsi une migration des zones d'assemblages.

Un phénomène d'upwelling est localisé le long de l'isobathe 200 m sur le plateau continental de la Patagonie. Cet upwelling renforce la production primaire par un apport en nutriments venant du fond marin. Les assemblages de kystes de dinoflagellés ont été étudiés dans les zones d'upwelling et on retrouve souvent des espèces du genre *Bringantedinium*, kyste de *Protoperidinium americanum*, *Echinidinium* spp., *Quinquecuspis concreta* associés à des zones de fortes productivité (Pospelova et al., 2008). D'après Smayda et al. (2010), ces zones d'upwelling favorisent aussi l'expansion et la prolifération de dinoflagellés toxiques (e.g. *Alexandrium catenella*, *Dinophysis* spp., *Gymnodinium catenatum*, *Lingulodinium polyedra*, *Protoceratium reticulatum*).

Sur la base de ces éléments, nous pouvons retenir que la distribution des kystes de dinoflagellés est faiblement documentée dans l'Atlantique Sud-Ouest. Cet objectif vient combler ce manquement et demeure la première étude qui va analyser **la distribution spatiale des assemblages modernes de kystes de dinoflagellés** en identifiant les assemblages qui reflètent les conditions de surface dans le golfe et l'upwelling au niveau du plateau continental. En outre, cette étude va nous permettre de disposer d'une base de données de référence pour les reconstitutions paléocéanographiques. Dans ce chapitre, nous essayerons de répondre à la question suivante :

- Quel est le lien entre les assemblages modernes de kystes de dinoflagellés et les paramètres écologiques et physiques du GSJ?

Objectif 2. Patrons de dispersions du pollen et de spores dans les sédiments de surface du GSJ.

Les assemblages polliniques fossiles constituent d'excellents traceurs pour évaluer les changements environnementaux passés et étudier le climat (e.g. Mancini et al., 2008). Par conséquent, il est important de très bien connaître la dispersion du pollen dans les sédiments de surface afin de mieux interpréter les archives paléoclimatiques (e.g. Heusser, 1983; Melia, 1984; Dupont and Wyputta, 2003; Hooghiemstra et al., 2006). De ce fait, plusieurs études menées dans des secteurs continentaux en Patagonie ont montré avec succès une relation cohérente entre la végétation et la distribution du pollen (Paez et al., 2001; Burry et al., 2005; Mancini, 2012). Par ailleurs, nous ne disposons d'aucune étude de ce genre dans le GSJ et encore moins dans l'Atlantique Sud-Ouest. Ainsi, le deuxième objectif cette thèse vise à établir **les patrons de dispersion moderne du pollen et de spores** en relation avec les provinces phytogéographiques adjacentes au golfe à partir des échantillons de surface. Les résultats serviront à établir une base de données moderne pour décrire l'histoire de la végétation et caractériser les flux d'apport éoliens afin d'identifier les meilleurs indicateurs pour étudier les variations passées des vents d'ouest. Dans cette partie l'objectif est de répondre à la question suivante :

- Quels sont les relations entre les patrons de dispersion moderne du pollen et de spores dans le GSJ et la végétation adjacente au golfe ?

Objectif 3. Variations latitudinales des vents d'ouest en relation avec les conditions océaniques dans le GSJ au cours du Pléistocène supérieur et de l'Holocène.

Le climat en Patagonie est fortement influencé par la ceinture des vents d'ouest qui contrôle la distribution latitudinale des précipitations, la répartition de la végétation et l'étendue des glaciers (Garreaud, 2013). Actuellement, la position et l'intensité de ces vents varient saisonnièrement subséquemment aux changements de la température de surface de l'océan Pacifique Sud et Atlantique Sud qui contrôlent la position de la ceinture de haute pression subtropicale (Lamy et al., 2010). Les reconstitutions des vents d'ouest depuis le dernier maximum glaciaire suggèrent que la position de la ceinture des vents d'ouest ait fluctué au cours du Pléistocène supérieur et de l'Holocène en relation avec les variations du climat global et les conditions océaniques dans le Pacifique Sud et l'Atlantique Sud. Des auteurs suggèrent que la ceinture des vents d'ouest se déplace vers l'équateur durant les périodes glaciaires puis migre vers le Pôle Sud durant les périodes interglaciaires (Toggweiler et al., 2006). Des études ont également montré que la ceinture des vents d'ouest jouait un rôle déterminant sur le climat global durant la dernière déglaciation par un dégazage de CO_2 induit par un upwelling intense dans l'Atlantique Sud (Toggweiler et al., 2006 ; Anderson et al., 2009 ; Toggweiler, 2009 ; Denton et al., 2010). En effet, les vents d'ouest contrôlent la force du courant ACC (Antarctic Circumpolar Current) qui module la libération du CO_2 de l'océan profond vers l'atmosphère, particulièrement durant les phases interglaciaires, et accentue le réchauffement (Anderson et 2009 ; Denton et al., 2010). Les variations latitudinales de ces vents sont relativement bien connues durant les phases glaciaires/interglaciaires (Toggweiler et al., 2006). Par contre, les études sur la position de la ceinture de vents d'ouest depuis la dernière déglaciation sont rares, parfois contradictoires, et ont fait l'objet de discussion dans la littérature (Heusser, 1989 ; Markgraf, 1989 ; Lamy, 2010 ; Moreno, 2010 ; Fletcher et Moreno, 2011).

Plusieurs études basées sur des traceurs paléoclimatiques, incluant les assemblages de pollen, des analyses géochimiques, magnétiques et sédimentologiques, ont été réalisées pour décrire les variations de la ceinture des vents d'ouest durant l'Holocène (e.g. Figure 1 ; Tableau 1 ; Lago Aculeo (34°S, Jenny et al., 2003), Lago Condorito / El Salto (41°S , Moreno et al., 2010 ; Moreno and Videla, 2016), Lago Castor (46°S , Van Daele et al., 2016); Quitralco fjord (49°S, Bertrand et al., 2014), Lago Cardiel (49°S, Gilli et al., 2001 ; Ariztegui et al., 2010 ; Quade et Kaplan, 2017), Lago Guanaco / Vega Ñandú/ Lago Cipreses (51°S, Villa-Martinez et Moreno, 2007 ; Moy et al., 2008 ; Moreno et al., 2010 ; Moreno et al., 2014), Lago Tamar (52°S, Lamy et al., 2010), Rio Rubens Bog/Laguna Azul (52°S, Mayr et al., 2007, Zolitschka et al., 2019), Potrok Aike (52°S, Mayr et al., 2007 ; Haberzettl et al., 2007 ; Mayr et al., 2013 ; Zolitschka et al., 2013 ; Lisé-Pronovost et al., 2015), Marcelo Arevalo Cave (53°S, Schimpf et al., 2011), Gran Campo Nevado (53°S, Lamy et al., 2010), Skyring fjord (53°S, Lamy, 2010) et Lago Fagnano (54°S, Waldmann et al., 2011 ; Moy et al., 2011). La majeure partie des conclusions issues de ces études sont déduites des variations des précipitations ou d'humidité au niveau des sites situés au sud-ouest de la Patagonie où les précipitations sont positivement corrélées avec l'intensité des vents d'ouest. Sur la base d'une compilation de ces investigations, plusieurs travaux mettent en évidence une antiphase en lien avec la position et l'intensité des vents d'ouest entre les sites situés au nord et ceux localisés au sud de la Patagonie (e.g. Moreno et al., 2010 ; Lamy et al., 2010 ; Kilian et Lamy, 2012 ; Fletcher et Moreno, 2011 ; Van Daele et al., 2016).

Ces travaux suggèrent que la ceinture des vents d'ouest était localisée au nord de la Patagonie durant la transition Pléistocène-Holocène (14 – 11,5 ka cal BP) en accord avec l'augmentation de l'humidité à Lago Condorito (41°S, Moreno et al., 2010) et une diminution de l'humidité dans les sites situés au sud-ouest de la Patagonie (51° et 53°S, Moreno et al., 2010 ; Lamy et al., 2010). Ensuite, elle aurait migré vers le sud durant l'Holocène inférieur en accord avec les fortes intensités des vents d'ouest enregistrées à Laguna Potrok Aike (52°S, Lisé-Pronovost et al., 2015). Cette position sud favorise une augmentation de l'humidité à Lago Tamar, Gran Campo Nevado, Skyring Fjord (52° - 53°S, Lamy et al., 2010). Par contre Moreno et al. (2010), se basant uniquement sur les enregistrements

polliniques à Lago Condorito (41°S) et Lago Guanaco (52°S), suggèrent un affaiblissement des vents d'ouest à l'Holocène inférieur en Patagonie. Ensuite, à l'Holocène moyen, Van Daele et al. (2016) suggèrent une expansion de la ceinture des vents d'ouest vers le nord déduit de données sédimentologiques à Lago Castor (46°S) en accord avec l'augmentation de l'humidité à Lago Condorito et Lago Salto (41°S, Moreno et al., 2010 ; Moreno and Videla, 2016) alors que dans les sites situés au sud-ouest de la Patagonie on note une diminution de l'humidité (Lamy e al., 2010). Durant l'Holocène supérieur, une faible intensité des vents d'ouest est enregistrée au sud de la Patagonie (51° et 53°S, Lamy et al., 2010) avec une légère diminution de l'intensité des vents d'ouest à Lago Castor (46°S, Van Daele et al., 2016) et Lago Condorito (41°S, Moreno et al., 2010). Cela suggère une expansion vers le nord de la ceinture des vents d'ouest en accord avec l'élévation du niveau du lac à Lago Aculeo où sa recharge est en lien avec les westerlies (34°S, Jenny et al., 2003).

En outre, quelques investigations offrent l'avantage de décrire les variations de la ceinture des vents d'ouest en relation avec les reconstitutions des températures de surface dans le Pacifique Sud et l'Atlantique Sud (e.g. Lamy et al., 2010 ; Kilian et Lamy, 2012 ; Bertrand et al., 2014). En effet, les reconstitutions des températures de surface couvrent près de 10° de latitude dans le Pacifique Sud (e.g. GeoB3313 - 41°S, Lamy et al., 2002 ; ODP 1233 - 41°S, Kaiser et al., 2005 ; GeoB7186 – 44°S, Mohtadi et al., 2007 ; CF7-PC33 - 44°S, Sepúlveda et al., 2009; MD07-3128 - 51°S, Caniupán et al., 2014) et permettent de suivre les variations de température en lien avec la position des vents d'ouest (Bertrand et al., 2014). Cependant, dans l'Atlantique Sud nous ne disposons que d'une seule étude en lien avec les reconstitutions des températures de surface (e.g. Bianchi et Gersonde, 2004). Ainsi, notre site d'étude (GSJ) offre l'opportunité de mieux documenter les variations de ces conditions de surface en lien avec la position des vents d'ouest dans l'Atlantique Sud depuis la dernière déglaciation en utilisant des enregistrements marins puis en les comparants avec les conditions de surface dans le Pacifique Sud. De plus, l'Atlantique Sud est particulièrement intéressant, car il constitue la zone de HNLC (High Nitrate Low Chlorophyll) la plus étendue dans le monde (NASA). Dans cette région, la production primaire est limitée par le Fe

(Gledhill et Buck, 2012) et la Patagonie représente la seule source de Fe par les apports éoliens (feldspath, calcite, fer, phosphore, pollen, diatomées, bactéries etc. ; Bullard et al., 2016). De ce fait, le GSJ est idéalement localisé pour retracer les flux d'apports éoliens dans cette région en lien avec la position de la ceinture des vents d'ouest et la paléoproductivité dans l'Atlantique Sud.

Ce troisième objectif consiste à retracer **la migration latitudinale de la ceinture des vents d'ouest dominants et des zones de végétation** en relation avec **les conditions océaniques de surface** dans le GSJ depuis le dernier maximum glaciaire à partir respectivement des assemblages de pollen et spores et les assemblages de kystes de dinoflagellés préservés dans trois séquences sédimentaires prélevées dans le GSJ. Dans cette troisième partie, l'objectif est de répondre aux questions suivantes :

- Le GSJ enregistre-t-il la migration de la ceinture des vents d'ouest depuis le LGM et quelles sont les positions de cette dernière au cours de cette période?
- Quelles sont les conditions océaniques de surface dans l'Atlantique Sud liées à ces migrations?
- Quelles sont les variations de la végétation adjacente au GSJ au cours du Pléistocène supérieur et de l'Holocène

Tableau 1. Localisation des sites cités dans le texte

		Sites	Latitude (°S)	Longitude (°O)	Periode couverte (cal ka BP)	Traceurs	Références
Archives	Paléo-vents	Lago Aculeo	33°50'	70°54'	0-10	Simulations	Jenny et al., 2003
		Lago Condorito	41°45'	73°07'	0-14	Polliniques	Moreno et al., 2010
		Lago El Salto	41°38'	73°50'	0-16	Polliniques	Moreno and Videla, 2016
		Lago Unco	45°34'	71°43'	10-17,5	Polliniques	Vilanova et al., 2019
		Lago Castor	45°60'	71°80'	0-17	Sédimentologiques	Van Daele et al., 2016
		Quitralco fjord (PC29A)	45°71'	73°42	0-2	Géochimiques	Bertrand et al., 2014
		Lago cardiel	48°90	71°24	0-25	Polliniques	Gilli et al., 2005; Ariztegui et al., 2010; Quade et Kaplan, 2017
		Lago Guanaco	50°52'	72°52'	0-13	Polliniques	Moy et al., 2008; Moreno et al., 2010
		Lago Cipreses	51°28'	72°85	0-14	Polliniques	Moreno et al., 2014; Moreno et al., 2018
		Vega Ñandú	51°00'	72°45'	0-12,6	Pollliniques	Villa-Martinez et Moreno, 2007
		Rubens Bog	52°08'	71°52'	0-11,5	Polliniques	Mayr et al., 2007
		Potrok Aike	51°96'	70°39'	0-51,2	Polliniques/ sédimentologiques	Mayr et al., 2007; Haberzetltl et al., 2007; Mayr et al., 2013; Zolitschka et al., 2013; Lisé-Pronovost et al., 2015
		Laguna Azul	52°04'	69°35'	0-11,6	Palynologiques/ Géochimiques	Zolitschka et al., 2019
		Marcelo Arevalo Cave	52°41'	73°23'	0-4,5	Géochimie	Schimpf et al., 2011
		Gran Campo Nevado	52°48'	72°56'	0-13	Polliniques	Lamy et al., 2010
		Skyring fjord	52°31'	72°08'	0-13	Polliniques	Lamy, 2010
		Lago Fagnano	54°35'	68°00'	0-12	Géochimiques	Waldmann et al., 2011; Moy et al., 2011
	Paléo-températures	GeoB 3313-1	41°00'	74°27'	0-8	Alkénones	Lamy et al., 2002
		ODP 1233	41°00'	74°27'	0-70	Alkénones	Kaiser et al., 2005
		GeoB7186	44°08'	75°09'	0-2,2	$\delta^{18}O$	Mohtadi et al., 2007
		Jacaf fjord (CF7-PC33)	44°20'	72°58'	0-1,8	Alkénones	Sepúlveda et al., 2009
		MD07-3128	52°39	75°33	0-60	$\delta^{18}O$	Caniupán et al., 2014
		ODP 1094	53°10'	5°7' E	0-25	Diatomées	Bianchi et Gersonde, 2004

MATÉRIELS ET MÉTHODES

Ce projet fait partie d'un vaste programme multidisciplinaire appelé PROMESse (PROgramme Multidisciplinaire de recherche en océanographie pour l'étude de l'Écosystème et de la géologie marine du golfe San Jorge et de la région côtière des provinces de Chubut et Santa Cruz). Ce programme s'appuie sur un partenariat tripartite entre l'ISMER (Institut des sciences de la mer de Rimouski), le CONICET (Conseil national argentin de recherche en sciences et techniques) et le MINCyT (Ministère argentin des sciences, de la technologie et de l'innovation). Dans le cadre de cette collaboration, la campagne océanographique MARGES (*MARine GEology, sedimentology, stratigraphy, basin architecture and paleoceanography of the San Jorge Gulf*) a été effectuée dans le GSJ et sur le plateau continental à bord du N/R Coriolis II, du 17 février au 4 mars 2014. L'objectif de MARGES était d'acquérir des connaissances sur l'architecture du bassin du GSJ et de l'ensemble de ses processus sédimentologiques, mais aussi de reconstituer l'évolution des changements climatiques du Pléistocène supérieur et de l'Holocène par une approche multiproxy. Ladite campagne a permis de récolter 52 échantillons de surface, 8 carottes à boîte, 9 carottes à gravité, 5 carottes à piston et environ 2000 km de lignes géophysiques (Figures 6 et 7). Dans le cadre de mon projet de thèse, mon étude se base sur l'ensemble des sédiments de surface et sur 3 séquences sédimentaires qui ont été sélectionnées de manière à disposer d'un transect de la côte vers le large. Les échantillons de surface ont été prélevés à l'aide d'une benne *Van Veen* dans le GSJ et le long du plateau continental. Ces prélèvements serviront à établir la distribution actuelle des assemblages de kystes de dinoflagellés ainsi que les patrons de dispersion du pollen en fonction de la végétation actuelle et des conditions océaniques et climatiques. Trois carottes à piston (06PC, 08PC, 11PC), positionnées au nord du GSJ de la côte vers le large, ont été choisies sur la base de la continuité de l'enregistrement sédimentaire et des datations radiochronologiques disponibles. Ces enregistrements sédimentaires vont permettre de décrire la variation latitudinale des vents d'ouest à partir des assemblages de pollen et spores puis de retracer l'évolution des conditions de surface au

cours du Pléistocène supérieur et de l'Holocène en se basant sur les assemblages de kystes de dinoflagellés.

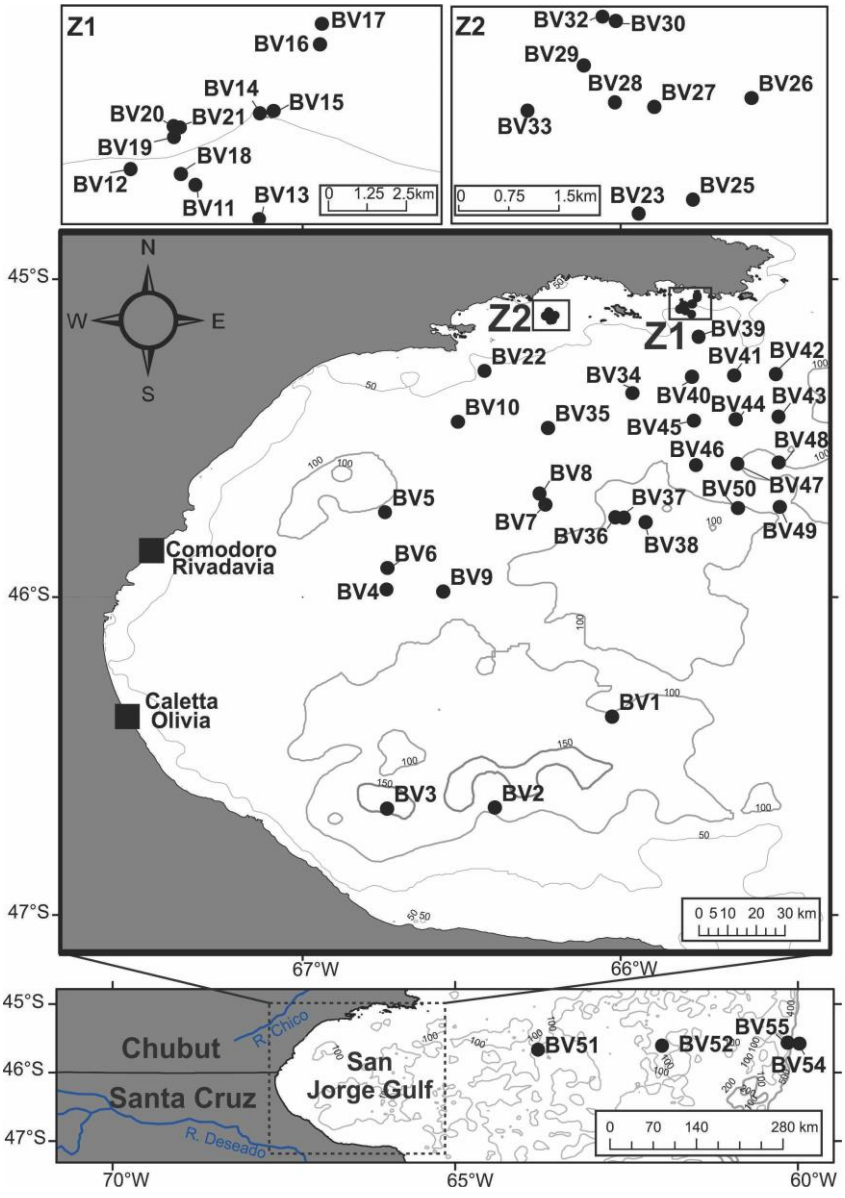

Figure 6. Localisation des échantillons de surface.

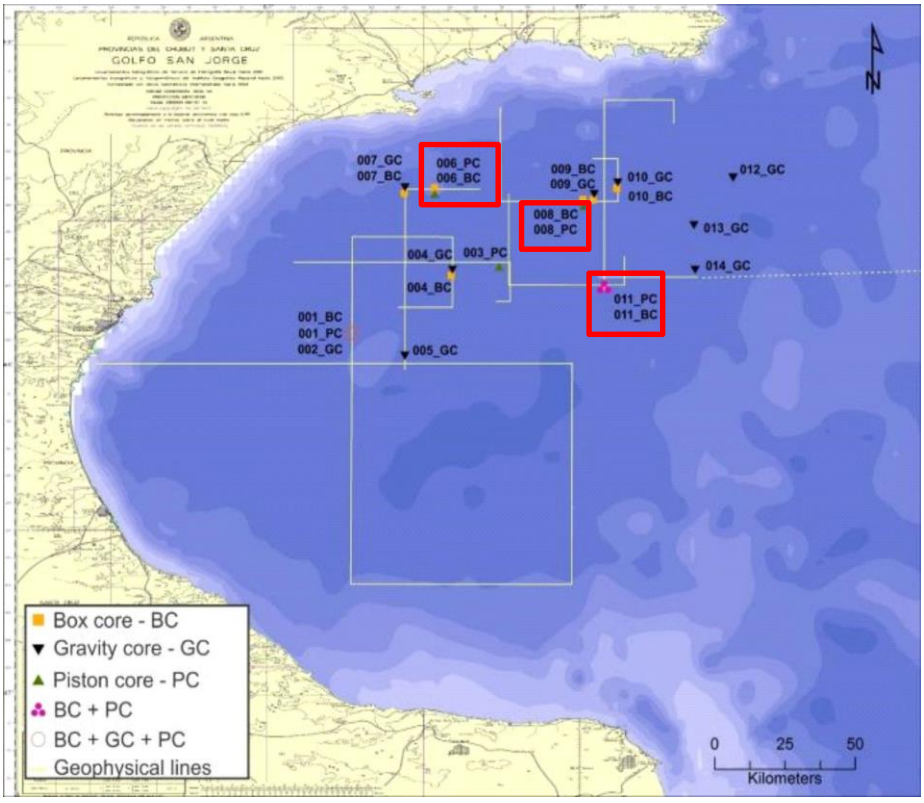

Figure 7. Localisation des carottes sédimentaires (rapport de mission MARGES).

MODÈLE D'ÂGE

Le modèle d'âge des trois carottes (06PC 08PC, 11PC) a été établi sur la base de treize âges ^{14}C obtenus à partir de coquilles de bivalves prélevées dans les carottes. Ces prélèvements ont été envoyés pour des datations AMS-^{14}C au laboratoire W.M. Keck (Université de Californie à Irvine). De plus, deux datations (AMS-^{14}C) ont été effectuées sur la carotte 08PC à partir de microfragments de bois et d'algue au laboratoire des sciences du climat et de l'environnement (LSCE, CNRS-CEA-UVSQ, Desiage, 2020). Les âges obtenus ont été calibrés en utilisant le logiciel CALIB7.1 (Stuiver and Reimer, 1993) en utilisant la courbe Marine13 de Reimer et al. (2013) avec une correction de l'effet réservoir marin (ΔR = 0, Desiage, 2020). Le modèle d'âge a été construit par Desiage (2020) en utilisant une

approche bayésienne avec le logiciel Bacon (v2.2 package) sous R (Blaauw and Christen, 2011).

PALYNOLOGIE MARINE : PROXY PALÉOENVIRONNEMENTAL

La palynologie vient des mots grecs *palunein* qui signifie saupoudrer et *logos* qui veut dire discours (Pons, 1958). De nos jours, la palynologie marine est définie comme étant l'étude des organismes fossiles à paroi organique appelés palynomorphes (de Vernal, 2009). On peut distinguer les palynomorphes d'origine continentale (pollen & spores, algues d'eau douce) et d'origine marine (kystes de dinoflagellés, les thécamœbiens, les tintinnides, les réseaux organiques de foraminifères et les œufs de copépodes, etc.). Les applications de la palynologie sont multiples. Elle est principalement utilisée dans plusieurs études pour reconstituer avec précision les conditions environnementales passées (pour plus d'informations voir de Vernal, 2009 & Marret et Zonneveld, 2003). Dans le cadre de cette thèse de doctorat, les grains de pollen et de spores ainsi que les kystes de dinoflagellés seront utilisés pour les reconstitutions paléoenvironnementales des environnements terrestres et marins respectivement.

POLLEN & SPORES

Toutes les espèces végétales forment au cours de leur vie un élément de petite taille (25-200 µm), appelé spore ou grain de pollen, entouré par une membrane organique composée d'un biopolymère résistant : la sporopollénine. Le grain de pollen représente le gamétophyte mâle chez les plantes à fleurs alors que la spore représente un organe de résistance chez les algues et les champignons puis l'élément sexuel mâle ou femelle chez les mousses et les cryptogames (Pons, 1958). Ces derniers se trouvent dans l'anthère ou le sporange et se forment à partir d'une cellule spéciale qui se divise pour donner un ensemble de 4 spores ou grains de pollen appelé tétrade (Borg et Twell, 2011). Au printemps, durant la pollinisation, les tétrades sont libérées par milliers et disséminées par le vent, les insectes

ou par l'eau. Certaines se déposent dans l'océan puis sont transportées par les courants marins avant d'être incorporées dans les sédiments marins. L'intérêt d'étudier les grains de pollen et les spores résulte du fait qu'en les observant au microscope on peut reconnaître l'identité de la plante (Pons, 1958). C'est pourquoi les applications de l'analyse pollinique sont multiples. Son utilisation permet, entre autres, de faire une reconstitution quantitative des végétations passées en analysant le contenu pollinique d'un enregistrement sédimentaire (e.g. Tonello et al., 2009). Ils sont utilisés en palynologie marine comme traceurs des apports terrestres (de Vernal, 2009) ou comme proxies de la provenance des apports éoliens et de l'intensité des vents (e.g. Rochon et de Vernal, 1994 ; Moreno et al., 2010).

Dans le cadre d'une approche paléovironnementale, il est important de dire que certains processus comme le vent et les courants marins pourraient faire l'objet d'un biais dans la reconstitution des végétations passées. À titre d'exemple, les grains de pollen de plantes anémophiles sont plus favorables au transport par le vent et pourraient être retrouvés préférentiellement dans les sédiments marins par rapport au pollen de plantes entomophiles (e.g. Heusser et Balsam, 1977).

LES KYSTES DE DINOFLAGELLÉS

Les dinoflagellés sont des organismes unicellulaires biflagellés. Ces micro-organismes sont dulcicoles et marins et renferment une grande diversité dans leurs formes et leurs habitats (Evitt, 1985 ; Taylor et al., 1987). On les retrouve sous toutes les latitudes, mais plus particulièrement dans les eaux côtières (Marret et Zonneveld, 2003). Certaines espèces produisent des proliférations d'algues nuisibles ou des marées rouges spécialement dans les zones côtières (Glibert et al., 2005). La plupart des dinoflagellés sont autotrophes (50%), d'autres ont un régime alimentaire hétérotrophe, mixotrophe, parasitaire ou symbiotique (Taylor et al., 1987). Les organismes autotrophes forment une partie de la production primaire alors que les organismes hétérotrophes se nourrissent essentiellement de diatomées, de nanoflagellés, de bactéries ou d'autres dinoflagellés (Jacobson et Anderson, 1986 ; Hansen, 1992 ; Jeong et al., 2010). La plupart des dinoflagellés sont pourvus d'une thèque

cellulosique qui se dégrade après la mort de l'organisme. Par ailleurs, environ 10 à 20% des espèces, produisent au cours de leur cycle de vie une cellule diploïde dotée d'une membrane organique résistante appelée kyste qui permet la survie de l'organisme pendant la période de dormance (Head, 1996). La membrane organique est composée de dinosporine et semble être à base de glucide (Versteegh et al., 2012). D'autres espèces, ont une membrane calcaire (Calciodinellaceae*, Scrippsiella*) rarement silicatée (Evitt, 1985). Durant la phase de dormance, le kyste ainsi formé est préservé dans les sédiments jusqu'à ce que les conditions du milieu redeviennent favorables à la floraison, c'est la phase d'exkystement. Durant cette étape, la cellule diploïde s'extirpe du kyste, et peut développer ou non (e.g. Gymnodiniales) une thèque dont les caractéristiques sont spécifiques à chaque espèce.

Les dinokystes sont utilisés dans de nombreuses études comme proxies paléocéanographiques pour la reconstitution de certains paramètres environnementaux (salinité, température des eaux de surface, durée du couvert de glace, productivité) (e.g. Ledu et al., 2010 ; Durantou et al., 2012 ; de vernal et al., 2013). Dans le cadre d'une approche paléoenvironnementale, il est donc nécessaire de dire que certains processus, notamment la dissolution, l'oxydation ou le transport par les courants marins pourraient induire des biais dans la reconstitution des conditions environnementales (Zonneveld et al., 2007).

ÉCHANTILLONNAGE ET TRAITEMENTS PALYNOLOGIQUES

Pour réaliser les analyses palynologiques, les carottes sédimentaires (03PC, 08PC, 11PC) sont échantillonnées à 6 ou 8 cm d'interval représentant ∼100 à ∼300 ans de résolution selon les modèles d'âges établis (Desiage, 2020). Les échantillons de surface et des carottes sédimentaires sont traités à l'aide d'un protocole décrit par Rochon et al. (1999). Un volume entre 3 et 5 cm^3 est prélevé par déplacement d'un volume égal d'eau distillée dans un cylindre gradué. On mesure le poids du sédiment à l'aide d'une balance à précision Mettler PE 160. On prélève une petite quantité de sédiment pour séchage et mesure du poids sec. Puis, deux tablettes de *Lycopodium clavatum* (concentration 12 100 ± 1892, Batch

414831 ; Université de Lund) sont ajoutées pour déterminer la concentration des palynomorphes. Le sédiment est ensuite tamisé à 100 et 10 µm à l'aide de membranes Nitex afin d'éliminer les sables grossiers, les silts fins et les argiles. La fraction entre 100 et 10 µm est traitée alternativement à l'acide chlorhydrique (HCL, 10%) et à l'acide fluorhydrique (HF, 49%) pour éliminer les carbonates et la fraction siliceuse respectivement. Les traitements au HCl et au HF chauds, d'une dizaine de minutes chacun, sont répétés en alternance 3 fois, à l'exception d'un des traitements au HF qui est fait de nuit (~8 heures). Un quatrième et dernier traitement au HCl chaud est réalisé à la toute fin pour dissoudre les minéraux et gels fuorosilicatés produits durant les traitements aux acides. Le résidu final est tamisé à 10 µm pour éliminer les particules fines, puis transféré dans un tube à fond conique. Pour le montage des lames, les tubes de 15 ml sont centrifugés à ~2500 rpm pendant 10 minutes. Le surnageant est vidé et le résidu est homogénéisé quelques secondes sur un vortimixer. Une goutte est ensuite prélevée et montée entre lame et lamelle dans de la gélatine glycérinée pour l'observation au microscope. Le résidu est finalement conservé dans un tube à fond conique (15 ml) auquel on ajoute une goutte de phénol pour la préservation.

IDENTIFICATIONS ET COMPTAGES

Les comptages sont réalisés à l'aide d'un microscope à lumière transmise (Nikon Eclipse 80i) à × 400 de grossissement pour les comptages et l'identification et ×1000 pour l'identification de spécimens problématiques. L'identification des grains de pollen & spores est réalisé à partir d'ouvrages de référence, tels que *Pollen flora of Argentina* de Markgraf et Antoni (1978) et *Pollen and spores of Chile* de Heusseur (1971). Enfin, pour l'identification des kystes de dinoflagellés des ouvrages de référence tels que Rochon et al. (1999) et Zonneveld et Pospelova (2015) ont été utilisés.

ORGANISATION DE LA THÈSE

Cette thèse englobe trois objectifs spécifiques structurés en chapitres pour répondre à chacun des buts visés dans ce projet de recherche. Chaque chapitre correspond à un article publié ou en voie de soumission dans une revue avec un comité de lecture.

Le premier chapitre (Article 1) présente la première étude sur la distribution spatiale des assemblages modernes de kystes de dinoflagellés en relation avec les conditions modernes de surface dans le GSJ (température, salinité, productivité). Les conclusions obtenues en réponse à ce premier objectif ont été publiées dans le cadre d'une édition spéciale sur le GSJ dans la revue *Oceanography* en décembre 2018.

Faye, S., A. Rochon, and G. St-Onge. 2018. Distribution of modern dinoflagellate cyst assemblages in surface sediments of San Jorge Gulf (Patagonia, Argentina). *Oceanography* 31(4):122–131, https://doi.org/10.5670/oceanog.2018.416.

Le deuxième chapitre (Article 2) présente la première étude sur les patrons de dispersion moderne du pollen & spores lesquels ont été mis en lien avec les provinces phytogéographiques adjacentes au GSJ. L'objectif de cette investigation est de disposer une base de données moderne pour mieux interpréter les archives marines. Les conclusions de ce chapitre ont été publiées dans la revue *Palaeogeography, Palaeoclimatology, Palaeoecology* en juin 2020.

Faye, S., A. Rochon, G. St-Onge and I, Vilanova. 2020. Pollen dispersal patterns in marine surface sediments from San Jorge Gulf, SE Patagonia (Argentina). *Palaeogeography, Palaeoclimatology, Palaeoecology*, https://doi.org/10.1016/j.palaeo.2020.109869.

Le troisième chapitre (Article 3) décrit l'histoire de la végétation sur le continent adjacent au GSJ et retrace la migration latitudinale de la ceinture des vents d'ouest en relation avec les conditions océaniques dans le GSJ durant le Pléistocène supérieur et l'Holocène. Pour ce faire, les assemblages sporo-polliniques fossiles et de kystes de dinoflagellés combinés aux

données sédimentologiques et géochronologiques (AMS-^{14}C) de trois séquences sédimentaires prélevées dans le GSJ ont été utilisés.

Faye, S., A. Rochon, G. St-Onge, I. vilanova and P-A, Desiage. L'article sera soumis prochainement dans *Quaternary Science Reviews*. Southern Westerly Winds and palaeo-oceanography relationship in San Jorge Gulf (SW-Atlantic Ocean, Argentina) during Late Pleistocene and Holocene.

À titre de conclusion générale, j'ai discuté de l'ensemble des principaux résultats de chaque article en dégageant quelques perspectives en lien avec la problématique générale. À noter que les références bibliographiques de chaque chapitre constituant un article sont présentées à la toute fin de ce dernier et sont conformes aux styles prévus par la revue. Les références bibliographiques de l'introduction et de la conclusion générales sont présentées à la fin de ce document.

Autres réalisations

Au cours de mes recherches doctorales, j'ai eu l'opportunité de participer à deux congrès internationaux (Dino 11 et AGU) et six congrès nationaux (Geotop, Québec Océan, Acfas) pour présenter les résultats de mes travaux de recherche. J'ai également participé à deux missions océanographiques dans l'Arctique pour récupérer des carottes sédimentaires et des échantillons de plancton à bord du brise-glace canadien NGCC Amundsen en 2017 et 2019.

Communications orales

Faye, S., Rochon, A., St-Onge, G. **2019**. Latitudinal variations of westerly winds in the Southern Hemisphere and relationship to oceangraphic changes in San Jorge Gulf during the Late Pleistocene and Holocene. Congrès *American Geophysical Union*, San Francisco, États-Unis, 9 au 14 décembre.

Faye, S., Rochon, A., St-Onge, G. **2018**. Distribution des assemblages de kystes modernes de dinoflagellés dans les sédiments de surface du golfe de San Jorge (Patagonie, Argentine)

en relation avec les conditions océaniques. Congrès étudiants du GEOTOP, Malbaie, Québec, Canada, 21 au 23 mars.

Faye, S., Rochon, A., St-Onge, G. **2017**. Distribution of modern dinoflagellate cyst assemblages in surface sediments of the Gulf of San Jorge (Patagonia, Argentina). Argentina workshop, Rimouski, Québec, Canada, 7 au 10 mars.

Faye, S., Rochon, A., St-Onge, G. **2017**. Variabilité climatique et reconstitution des conditions océanographiques dans le golfe de San Jorge (Patagonie, Argentine) au Pléistocène supérieur et Holocène. Congrès de l'ACFAS, Université McGill, Québec, Canada, 8 au 12 mai.

Faye, S., Rochon, A., St-Onge, G. **2017**. Distribution spatiale des kystes de dinoflagellés dans les sédiments de surface du golfe de San Jorge (Patagonie, Argentine). Réunion scientifique annuelle de Québec-Océan, Rivière du loup, Québec, Canada, 13 au 15 novembre.

Communications par affiche

Faye, S., Rochon, A., St-Onge, G. **2019**. Pollen dispersal patterns in marine surface sediments from San Jorge Gulf, SE Patagonia (Argentina). Congrès étudiants du GÉOTOP, Orford, Québec, Canada, 22 au 24 mars.

Faye, S., Rochon, A., St-Onge, G. **2017**. Climate variability and reconstruction of sea surface conditions in the Gulf of San Jorge (Patagonia, Argentina) during the Late Pleistocene and Holocene. Congrès étudiants du GEOTOP, Forêt Montmorency, Québec, Canada, 24 au 26 mars.

Faye, S., Rochon, A., St-Onge, G. **2017**. Spatial distribution of dynocysts in surface sediments from the Gulf of San Jorge (Patagonia, Argentina). Congrès DINO11 - 11th International Conference on Modern and Fossil Dinoflagellates, Bordeaux, France, 17 au 21 juillet.

ARTICLE 1

DISTRIBUTION OF MODERN DINOFLAGELLATE CYST ASSEMBLAGES IN SURFACE SEDIMENTS OF SAN JORGE GULF

1.2 RÉSUMÉ EN FRANÇAIS DU PREMIER ARTICLE

La présence de systèmes d'upwelling et de fronts océaniques fait du sud-ouest de l'Océan Atlantique une région à forte productivité primaire. Des conditions similaires sont présentes dans le GSJ où la production primaire est dominée par les dinoflagellés et les diatomées. La répartition de ces micro-organismes, y compris les kystes produits par certains dinoflagellés au cours de leur cycle de vie, est contrôlée dans les environnements marins par des paramètres océanographiques tels que la salinité, la température, la durée de la couverture de la glace de mer et la disponibilité de nutriments. L'objectif de cette étude est de documenter la distribution moderne des assemblages de kystes dinoflagellés dans les sédiments de surface du GSJ afin d'identifier les préférences environnementales de chaque taxon pour mieux interpréter les archives sédimentaires. Les assemblages de kystes dinoflagellés issus de l'analyse de 52 échantillons de surface ont été décrits et comparés aux conditions océanographiques de surface et et à la granulométrie des sédiments. Les résultats indiquent que les concentrations de kystes de dinoflagellés varient entre 64 kystes g^{-1} et 45 848 kystes g^{-1}, avec une dominance des espèces telles que *Spiniferites ramosus* et *Operculodinium centrocarpum* accompagnées de *Spiniferites mirabilis, Dubridinium* sp., *Polykrikos kofoidii*

et les ronds bruns (*Brigantedinium simplex, Brigantedinium auranteum* et *Brigantedinium* spp.). À partir de la distribution des kystes de dinoflagellés, nous avons défini deux domaines spatiaux situés respectivement dans la partie interne et au large du golfe. Nous avons trouvé une augmentation des concentrations de kystes de dinoflagellés le long d'un gradient nord-sud dans le golfe et de faibles concentrations au niveau des sites situés au large. De plus, des analyses multivariées révèlent que la productivité primaire, l'upwelling en offshore et la granulométrie fine des sédiments (<63 μm; silt et argiles) semblent contrôler la majeure partie de la distribution des kystes de dinoflagellés.

Cet article, intitulé *Distribution of modern dinoflagellate cyst assemblages in surface sediments of San Jorge Gulf (Patagonia, Argentina),* a été rédigé par moi-même sous la supervision de mon directeur André Rochon (UQAR-ISMER) et de mon co-directeur Guillaume St-Onge (UQAR-ISMER). Il a été accepté pour publication dans sa version finale le 14 novembre 2018 par l'éditrice de la revue *Oceanography* pour le numéro spécial sur le GSJ. Les résulats de ces travaux ont été présentés sous forme d'affiches au congrès annuel du Géotop qui a eu lieu dans la forêt de Montmorency en mars 2017 et au congrès international Dino 11 qui s'est déroulé à Bordeaux en juillet 2017. De plus, une version préliminaire de l'article a été présentée sous forme orale au workshop sur l'Argentine qui s'est tenu à Rimouski en mars 2017, au congrès de l'ACFAS qui a eu lieu à McGill en mai 2017, au congrès annuel de Québec Océan qui s'est déroulé à Rivière du Loup en novembre 2017 et enfin au congrès annuel du Géotop qui a eu lieu à Malbaie en mars 2018.

1.3 RÉSUMÉ EN ANGLAIS DU PREMIER ARTICLE

The presence of upwelling systems and oceanic fronts makes the Southwest Atlantic Ocean a region of high primary productivity. These same conditions are present in San Jorge Gulf (SJG) along the southern Argentinian coast, where dinoflagellates and diatoms dominate primary production. The distribution of these microorganisms, including the cysts produced by some dinoflagellates during their life cycles, is controlled in marine environments by oceanographic parameters that include salinity, surface water temperature, ice cover duration, and productivity. The objective of this study is to document the modern distribution of dinoflagellate cyst assemblages in surface sediments so that the environmental preferences of each taxon can be inferred and used to reconstruct paleoenvironmental conditions. The dinoflagellate cyst (dinocyst) assemblages of 52 surface samples collected in 2014 aboard R/V *Coriolis II* in the SJG were described and compared to surface oceanographic conditions and grain size data. The results indicate dinocyst concentrations vary between 64 cysts g^{-1} and 45,848 cysts g^{-1} dry sediment, with *Spiniferites ramosus* and *Operculodinium centrocarpum* the dominant species, accompanied by *Spiniferites mirabilis*, *Dubridinium* sp., cysts of *Polykrikos kofoidii*, and cysts of *Brigantedinium simplex*, *Brigantedinium auranteum*, and *Brigantedinium* spp. We have defined two spatial domains based on the distribution of dinocysts in and near the SJG: northern/southern-central gulf and offshore domains. We found an increase in dinocyst concentrations along a north-south gradient in the SJG and minimum concentrations at offshore sites. In addition, multivariate analyses reveal the relationships among the relative abundances of dinocysts, fine grain size data (<63 μm; silts and clays), and primary productivity, as well as offshore upwelling, which appear to control most of the distribution of dinocysts.

1.4 INTRODUCTION

The Southwest Atlantic is an area of high primary productivity, where upwellings and oceanic fronts control the intensity of organic production (Gregg et al., 2005; Rivas et al., 2006). Along the Argentinian coasts, dinoflagellates and diatoms dominate the primary production (e.g., Lutz and Carreto, 1991; Segura et al., 2013; Krock et al., 2015). These microorganisms represent the bottom link in the food web and are essential for marine ecosystems.

Dinoflagellates are unicellular biflagellate organisms that thrive in both freshwater and marine environments. They display a wide range of morphologies, live in a variety of habitats (Evitt, 1985; Taylor et al., 2008), and are found at all latitudes, though they are particularly abundant in coastal waters (Zonneveld et al., 2013). Most dinoflagellates are autotrophic and/or mixotrophic (50%), but some are either heterotrophic, parasitic, or symbiotic (Stoecker, 1999). Autotrophic dinoflagellates form part of the primary production, while heterotrophic species feed primarily on diatoms, nanoflagellates, bacteria, or other dinoflagellates (Jacobson and Anderson, 1986; Hansen, 1992; Jeong et al., 2010). Most dinoflagellates have a cellulosic theca (~89%) that degrades rapidly following cell death. In addition, about 13% to 16% of the species produce a diploid cell surrounded by a resistant organic membrane (cyst) that allows the organism to survive during dormancy (Head, 1996). The organic membrane is composed of dinosporin and appears carbohydrate-based (Versteegh et al., 2012). Those produced by phototrophs are composed of a cellulose- like glucan, while those of heterotrophs are composed of nitrogen-rich glycan (Bogus et al. 2014). During the dormancy phase, the cyst is preserved in the sediments until the environmental conditions become favorable for excystment. During this stage, the diploid cell extrudes from the cyst and may develop (or not, e.g., Gymnodiniales) a theca with characteristics specific to each species.

Dinoflagellate cysts (dinocysts) are used in many studies as paleoceanographic proxies for the reconstruction of environmental parameters such as salinity, surface water temperature, ice cover duration, and productivity (e.g., Durantou et al., 2012; de Vernal et

al., 2013). However, most studies are located in the North Atlantic (e.g., de Vernal et al., 2013; Zonneveld et al., 2013). In the South Atlantic, the surface distribution of dinocysts is limited to only a few studies (e.g., Wall et al., 1977; Orozco and Carreto, 1989; Esper and Zonneveld, 2002; Candel et al., 2012, Krock et al., 2015). Only one (Krock et al., 2015) is located in San Jorge Gulf (SJG), but it is based on the analysis of five surface sediment samples and thus does not provide a precise distribution of dinocysts in the gulf. In addition, the relationships between cyst assemblages and sea surface conditions were not assessed.

Here, we present the first detailed study of modern dinoflagellate cyst assemblages in surface sediments from the SJG. The objectives are to analyze dinoflagellate cyst assemblages from 52 surface sediment samples and to establish the surface distribution of each taxon and the relationships between cyst assemblages and sea surface parameters. These modern assemblages will serve as paleoenvironmental indicators of sea surface conditions (temperature, salinity, and productivity) in the gulf and at the offshore upwelling area from the sedimentary record for the Late Pleistocene and the Holocene.

1.5 REGIONAL SETTING

The SJG is a shallow oceanic basin (mean depth 70 m) located in the center of Patagonia in the Southwest Atlantic Ocean between 45°S (Cape Dos Bahias) and 47°S (Cape Tres Puntas). It is about 250 km wide and encompasses a total area of 39,000 km^2 (Figure 8, Glembocki et al., 2015).

Atmospheric circulation in the Patagonia region is strongly influenced by westerlies (Aravena and Luckman, 2009). This area lies between the semipermanent subtropical high pressure belt and the subpolar low pressure belt. The small differences in atmospheric pressure between these belts control the intensity and direction of winds that influence, among other phenomena, the oceanic circulation on the southwestern continental shelf of Patagonia (Mayr et al., 2007; Palma et al., 2008).

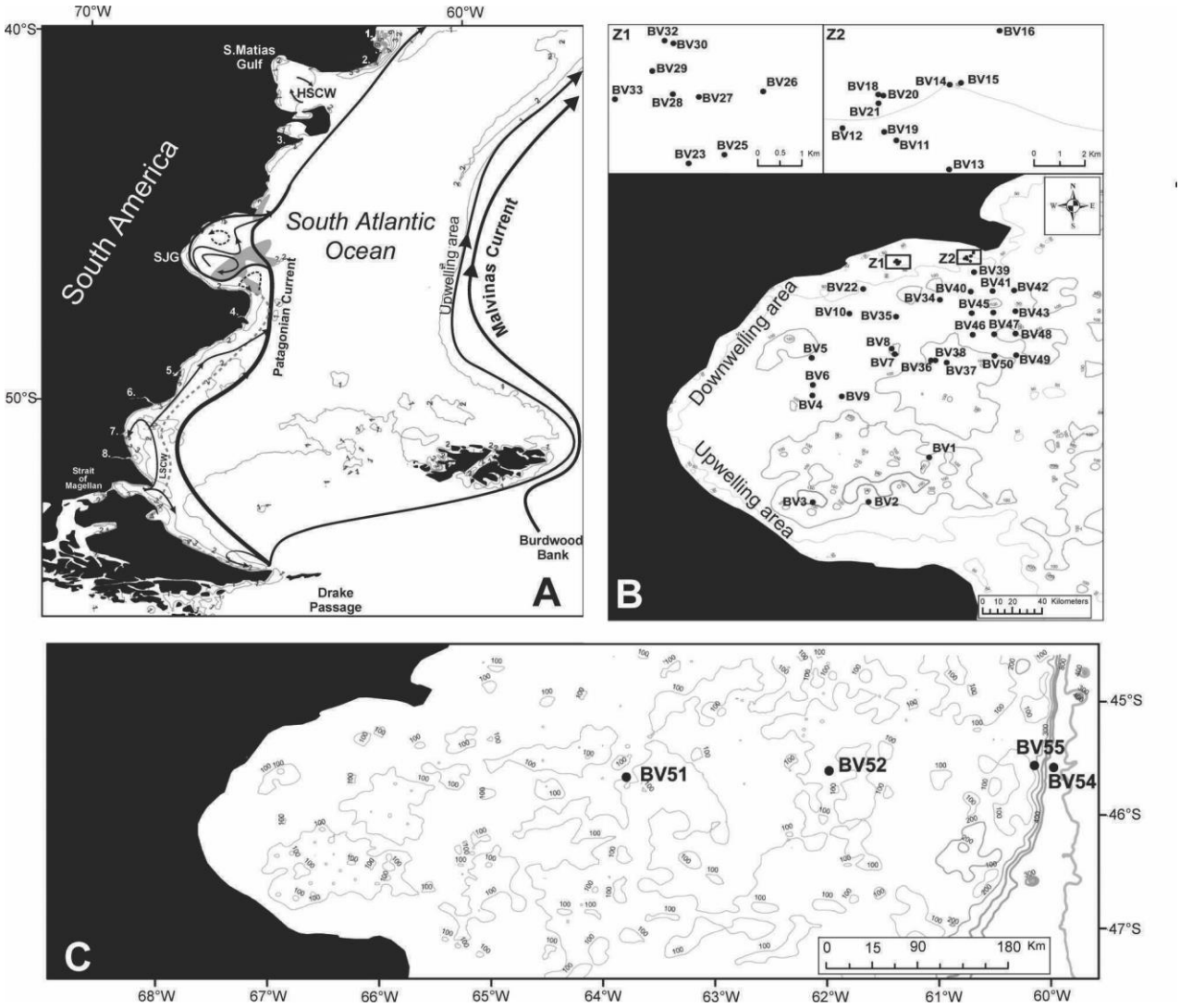

Figure 8. (A) Schematic representation of southwestern Atlantic circulation and summer circulation pattern in San Jorge Gulf (SJG; adapted from Matano et al., 2010, and Matano and Palma, 2018), showing the Malvinas Current, the Patagonia Current, Low Salinity Coastal Water (LSCW), the Magellan discharge (dashed line), and the High Salinity Coastal Water (HSCW), with a focus on tidal coastal fronts (gray zones) in the SJG. The isolines represent the annual climatological chlorophyll *a* concentrations (mg m^{-3}, Rivas et al., 2006). The Patagonian rivers are indicated: 1. Colorado. 2. Negro. 3. Chubut. 4. Deseado. 5. San Julian. 6. Chico. 7. Coig. 8. Gallegos. (B and C). Maps of the SJG illustrating the locations

of surface samples analyzed in this study. Isobaths are from the General Bathymetric Chart of the Oceans (GEBCO).

The general ocean circulation in the Southwest Atlantic is characterized by the Malvinas Current (MC), a branch of the Antarctic Circumpolar Current. It flows northward along the edge of the continental slope from Drake Passage (55°S) to 38°S (Palma et al., 2008; Piola et al., 2009; Matano et al., 2010) and transports cold, salty (>34) nutrient-rich subantarctic waters (Piola et al., 2009). On the continental shelf, water masses have much lower salinity (<34) than MC water masses because of the influence of freshwater discharges by rivers (Deseado, San Julian, Coig, and Gallegos) and low salinity waters carried through the Strait of Magellan located south of the SJG (Bianchi et al., 2005; Rivas et al., 2006; Figure 8A). The latter are responsible for the presence on the Patagonian shelf of low-salinity coastal waters (<33.4), which extend into the SJG (Bianchi and al., 2005) and generate an intense seasonal thermohaline front in the gulf (Krock et al., 2015). There are also high-salinity coastal waters (~34) near San Matias due to intense evaporation (Bianchi et al., 2005; Figure 8A). Interactions of these different water masses on the Patagonian shelf are particularly important for understanding the characteristics of water masses within the SJG.

According to Krock et al. (2015), SJG water masses are strongly influenced by the high salinity coastal water in the north and the low-salinity coastal water in the south. The general circulation in the SJG is seasonally variable, exhibiting two distinct patterns, austral summer and winter modes (Matano and Palma, 2018). The summer mode, which reflects annual mean patterns, is characterized by a cyclonic gyre that is bound to the west by coastal currents and to the east by the Patagonia Current (PC, Matano et al., 2018). The PC is composed mainly of low-salinity, subantarctic waters from the Strait of Magellan (Brandhorst and Castello, 1971). According to Matano and Palma (2018), the summer mode is characterized by maximum intrusion of the PC into the gulf, and the cyclonic gyres weaken significantly during the winter mode. Strong winter mode westerlies generate two anticyclonic subgyres, the larger of which is situated in the southwestern gulf and characterized by a southward-

flowing coastal current (Matano and Palma, 2018). The surface circulation pattern suggests that winds, heat fluxes, the topographic depression in the central part of the gulf, and the seasonal development of tidal fronts control hydrodynamics in the area (Krock et al., 2015; Matano and Palma, 2018).

In the interior of the gulf, the waters are highly stratified (Krock et al., 2015), and warming during austral spring and summer induces thermal fronts that delimit stratified waters (Rivas et al., 2006). This phenomenon is associated with strong tidal currents, which can inhibit the seasonal development of the thermocline, and which generate tidal fronts at the 200 m isobath (Figure 8A; Rivas et al. 2006; Carbajal et al., 2018) that are characterized by areas of high primary production (Sabatini and Martos, 2002). Based on the numerical simulations of Tonini et al. (2006), there is a downwelling system along the northern coastal region and wind-driven upwelling within the south-southwest gulf. We also note the presence along the 200 m isobath of offshore upwelling zones (Matano et al., 2010), whose mechanisms are poorly understood. Some authors have hypothesized that internal friction created by the lateral diffusion of the MC on the continental shelf could cause this upwelling, rather than external forcings such as winds and tides (Matano et al., 2010). Thus, the cold, nutrient-rich subantarctic waters transported by the MC would be shifted toward the coast from below and then raised to the surface by vertical mixing and returned northward by Ekman transport generated by westerlies (Matano and al., 2010).

Surface sediments in most of the SJG are dominated by silt and clay and are associated with a low energy depositional environment, although coarse sand and energetic erosive environments prevail in the northern gulf (Fernandez et al., 2003; Desiage et al., 2018).

1.6 MATERIALS AND METHODS

1.6.1 Sampling

Collection of 52 surface samples was carried out from R/V *Coriolis II* from February 17 to March 4, 2014, during the MARGES (marine geology, sedimentology, stratigraphy, basin architecture and paleoceanography of San Jorge Gulf) oceanographic survey using a

Van Veen grab (Figure 8B and C; Table 3). The upper centimeter was subsampled (~1 cm) and shows good preservation of the sediment/ water interface with minimal bioturbation. Note that these samples may represent different time intervals, depending on their location in the gulf. For example, the sedimentation rates (AMS-^{14}C ages) measured in two sediment cores collected in the gulf have been estimated between 14 cm kyr^{-1} and 24 cm kyr^{-1} (Desiage et al., 2016). As a result, the first centimeter could represent between 40 years and 70 years of sedimentation. Thus, we consider that all sediments deposited during the last ~70 years are representative of "modern" conditions.

1.6.2 Palynological sample preparation

The protocol described by Rochon et al. (1999) was used for palynological preparations. A volume of 5 cm^3 was collected by displacement of an equal volume of distilled water in a graduated cylinder and weighed using a Mettler PE 160 precision balance. A small amount of sediment was air-dried and weighed to measure the sediment water content. Two tablets of *Lycopodium clavatum* (concentration per tablet 12,100 ± 1,892, Batch 414831, University of Lund) were added to the sediment prior to chemical treatment to determine palynomorph concentrations. The sediment was then sieved at 100 µm and 10 µm using Nitex membranes to remove coarse sands, fine silts, and clays. The fraction between 100 µm and 10 µm was treated alternately with warm hydrochloric acid (HCl, 10%) and warm hydrofluoric acid (HF, 49%) to remove the carbonates and the siliceous fraction, respectively. These warm 10-minute HCl and HF (~45°C) treatments were repeated alternately three times, with the exception of one of the HF treatments, which was done overnight (~8 hours). A fourth and final treatment with warm HCl was performed at the end to dissolve the fluorosilicate gels produced during the acid treatments. The final residue was sieved at 10 µm to remove fine particles, and then transferred to a 15 ml conical bottom tube. For mounting the slides, the 15 ml tubes were centrifuged at ~ 2,500 rpm for 10 minutes. The supernatant was removed and the residue homogenized for a few seconds on a vortimixer. A drop was then extracted and mounted between a slide and a coverslip in glycerine gelatin for

observation under a microscope. Finally, a drop of phenol was added to the palynological residue, which was then stored at 4°C.

1.6.3 Palynomorph counts

The counts were performed using a transmitted light microscope (Nikon Eclipse 80i) at ×400 magnification. Palynomorph concentrations are expressed per dry weight (cysts g^{-1}) to eliminate the influence of sediment water content (Dale, 2001), and the relative abundance of taxa is estimated in each sample (% dinocyst sp.). A minimum of 300 dinocysts or marker grains (*Lycopodium clavatum*) was counted to obtain the best statistical representation of the different species present in the samples (Table 3). All dinocysts were identified at the species level except for *Dubridinium* sp. and *Echinidinium* sp. because of morphological similarities that often prevent identification of these brown spiny cysts to the species level. The brown spiny cysts found were named *Echinidium* sp.C and sp.D in the expectation of further study (Figures 32 and 33). *Brigantedinium* spp. includes all cysts of *Brigantedinium* where the cyst orientation did not permit clear observation of the archeopyle. Cysts of *Polykrikos kofoidii/schwartzii* were identified following Rochon et al. (1999). We also distinguished *Operculodinium centrocarpum sensu* Wall and Dale (1966) and *Operculodinium centrocapum* short processes. Pollen grains and spores, pre-Quaternary (reworked) palynomorphs (dinocyst, pollen grains, and spores), *Halodinium*, and organic linings of foraminifers were counted.

1.6.4 Statistical analyses

Sampling sites were arranged in a hierarchical cluster using the relative abundance of each taxon (% dinocyst sp.) to determine dinocyst assemblage zones. The analyses were run on Past for Windows software (version 3.18) using the UPGMA (Unweighted Pair-Group average) function. Clusters are joined based on the Euclidean distance between all sites. Redundancy analyses (RDA) were performed to quantify trends in the abundance of dinocysts in relation to oceanic parameters and grain size data. These multivariate analyses are based on transformed data on the relative abundance and concentrations of dinocysts. Hellinger transformations ($\sqrt{\%}$) are done to decrease the variations between rare and

dominant taxa (Legendre and Gallagher, 2001). The analyses were run using R software for Windows (R version 3.4.2). Environmental variables significantly influence species distribution when $p < 0.05$.

1.6.5 Environmental and grain size data

Temperature and salinity data, as well as phosphate, silicate, and nitrate (μmol L^{-1}) concentrations, covering the period 1955–2012, were collected from the 2013 World Ocean Atlas database (World Ocean Atlas 2013: WOA13) from the National Oceanographic Data Center (https://www.nodc. noaa.gov/ OC5/woa13/ woa13data.html, Table 3). The data were collected on a grid of 0.25° (temperature and salinity) or 1° (phosphate, silicate, and nitrate). When there were no data at or near our sites, the inverse distance weighted (IDW) interpolation method with ArcGIS software was used to calculate weighted averages from the values of a number of neighboring points.

Data on chlorophyll-*a* concentrations (mg m^{-3}) were extracted from Rivas et al. (2006). They were estimated from SeaWiFS processed data and correspond to the period January 1998 to December 2003 (six years). These data come from the Distributed Active Archive Center (DAAC) of the Goddard Space Flight Center (Table 3). For more information on data processing, see Rivas et al. (2006).

Particle size analysis was carried out using a Beckman Coulter Particle Size Analyzer LS 13 320 at ISMER. Prior to analysis, the samples were treated with 10 ml of hydrogen peroxide (H_20_2; 30%) and 10 ml of hydrochloric acid (HCl; 0.5 M) to remove organic matter and carbonates. Samples were deflocculated by successive washing with distilled water, and put in an overhead shaker for 12 hours (overnight) before measurement (Desiage et al., 2018).

1.7 RESULTS

Palynomorph preservation was good to excellent in most samples. Although some taxa (e.g., *Brigantedinium* sp., *Echinidinium* sp.) can be very sensitive to oxidation (Zonneveld et

al., 2001b), none of the oxidation-sensitive taxa present in the samples showed signs of degradation. In addition, the low abundance of reworked palynomorphs suggests that there were few allochthonous sediment inputs. This indicates that the cysts found in our samples represent local productivity and that long-distance transport of dinocysts did not significantly affect the composition of the assemblages described below.

Dinocyst concentrations in the study area varied between 64 cysts g^{-1} and 45,848 cysts g^{-1}, with an average of 12,858 cysts g^{-1}. These concentrations increased along a north south gradient in the gulf, and minimum concentrations were recorded at offshore sites (BV52, 54, 55; Figures 9 and 10). The ratio of autotrophic to heterotrophic dinocysts varied between 20.97 and 0.37, with an average of 3.84, revealing the overall dominance of autotrophic dinocysts in the SJG. The maximum abundances of heterotrophic dinocysts were recorded in the northern part of the SJG and at offshore sites (Figure 11).

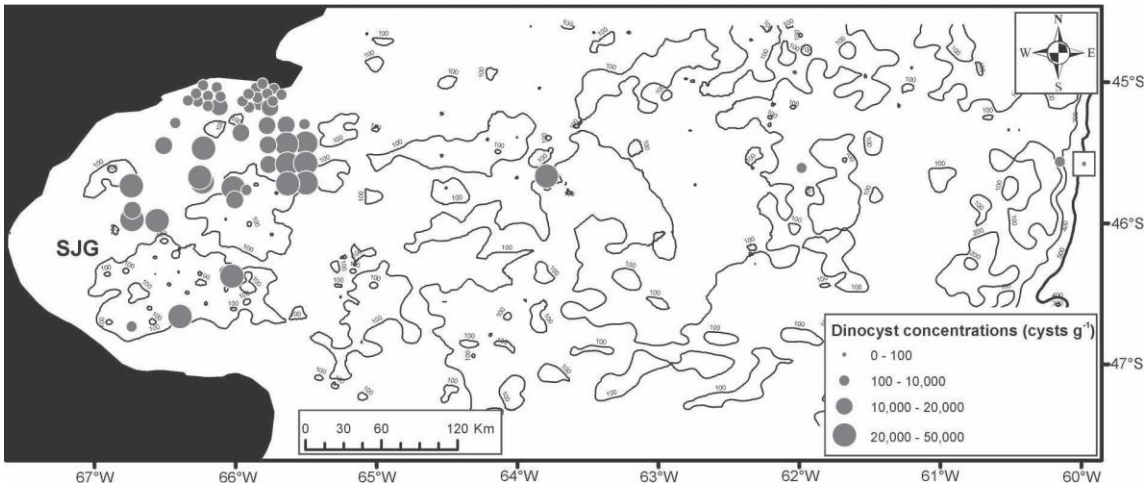

Figure 9. Distribution map of dinocyst concentrations (cysts g^{-1}).

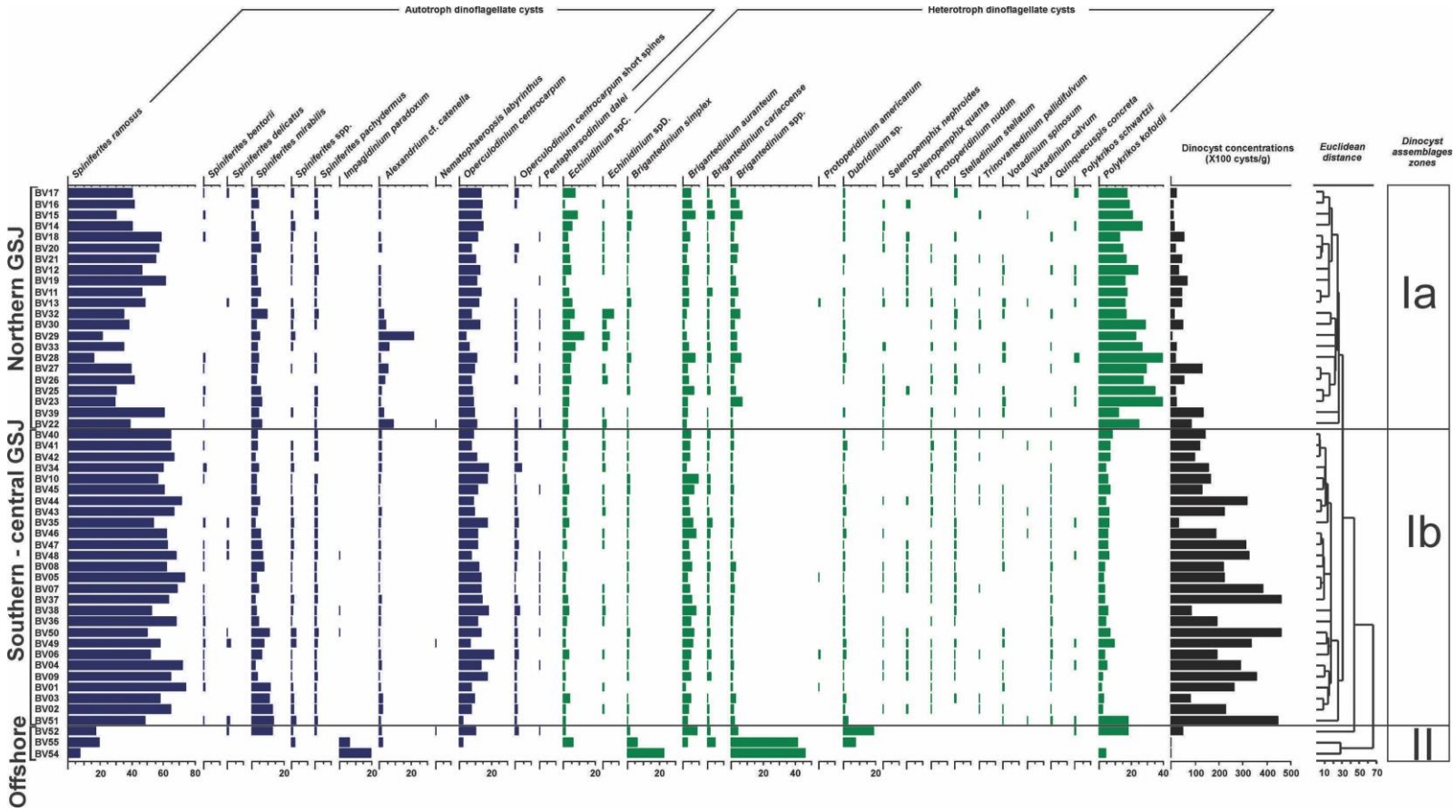

Figure 10. Relative abundance of major dinocyst taxa in the study area and hierarchical clustering of surface sediment samples used to determine dinocyst assemblages.

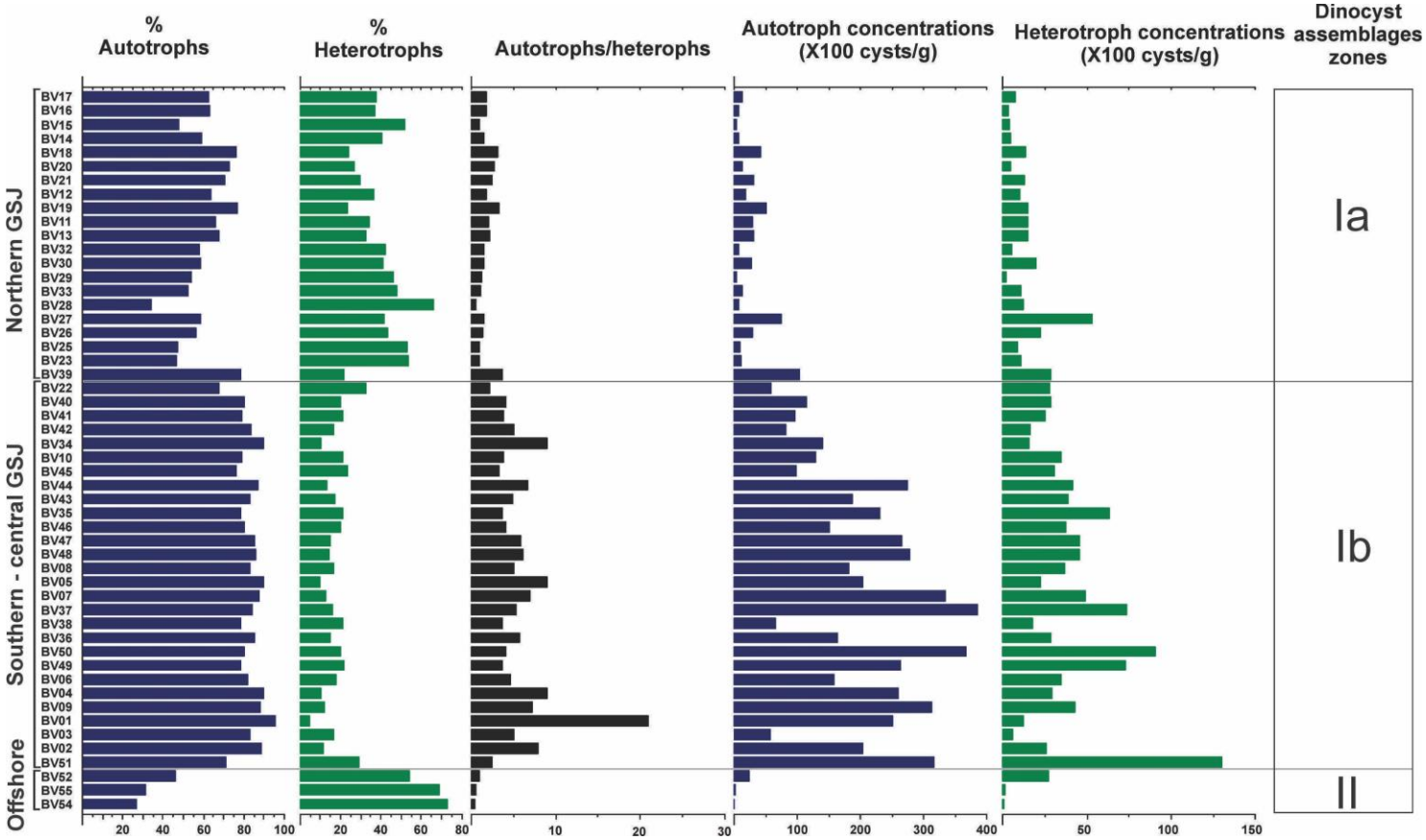

Figure 11. Relative abundances and ratios for autotrophic and heterotrophic dinocysts.

Concentrations of reworked palynomorphs are low in the SJG, with an average of 135 cells g^{-1}. Maximum concentrations (~1,053 cells g^{-1}) are found at the gulf's outer limit (sites BV50 and BV51), and then gradually decrease offshore. Concentrations of organic linings of foraminifera are high in the inner part of the gulf, reaching 2,018 g^{-1}, with an overall average of 748 linings g^{-1}. *Halodinium* sp., described originally as an acritarch (Bujak, 1984) and now confirmed as the resting cyst of an estuarine ciliate (Gurdebeke et al., 2018), are more abundant in the central and southern SJG, with a maximum value of 102 cells g^{-1} at site BV50, and low concentrations in the northern part of the gulf and offshore. This taxon suggests freshwater inputs to in our study area. The high concentrations of *Halodinium* sp. in central and southern SJG are correlated with the influence of freshwater discharge by the rivers located south of the gulf and carried into the SJG by coastal currents (Figure 8A). The abundance of this palynomorph in the gulf would therefore be a good proxy for documenting the fluctuations of freshwater inputs in paleoceanographic reconstructions.

In total, 30 dinocyst taxa were identified and 11 taxa dominate the assemblages by more than 90%: *Spiniferites ramosus, Spiniferites mirabilis, Operculodinium centrocarpum, Alexandrium* cf. *catenella, Impagidinium paradoxum, Echinidinium* sp.C*, Brigantedinium simplex, Brigantedinium auranteum, Brigantedinium* spp., *Dubridinium* sp., and cysts of *Polykrikos kofoidii* (Tables 4 and 5, Figures 31 and 32).

Cluster statistical analysis performed with Past indicates the presence of two dinocyst assemblage zones (Figure 10). Zone I includes stations situated in the SJG that are then divided into two subassemblages, Ia and Ib. Dinocyst subassemblage zone Ia is located in the northern part of the SJG near the coast (31-90 m water depth). The concentrations in this assemblage vary between 480 cysts g^{-1} and 13,160 cysts g^{-1}, with an average of 3,924 cysts g–1, and *Spiniferites ramosus* (16%-60%) and *O. centrocarpum* (3%-14%) are the dominant species. The heterotrophic dinocysts, such as those of *Polykrikos kofoidii* (11%-39%), *Echinidinium* sp.C (0.6%-12%), and *Brigantedinium auranteum* (1.8%-6.9%), are also relatively abundant in this assemblage (Figures 10 and 11).

It is interesting to note that the relative abundance of cysts of the toxin producing species *Alexandrium* cf. *catenella* (Fabro et al., 2018) can reach as high as 21% in this

assemblage zone (Ia). The toxic dinoflagellate responsible for paralytic shellfish poisoning in the Argentinean Sea was originally described as *Alexandrium excavata*, then changed to *Alexandrium tamarense,* and more recently to *Alexandrium catenella*, based on phylogenetic reconstructions of rDNA (Fabro et al., 2017, 2018; Krock et al.,2018). However, *Alexandrium* cysts may have been confused with the organic linings of *Scrippsiella trifida* in previous palynological investigations (Head et al., 2006). Indeed, all *Alexandrium* cysts have similar morphology and poor fossilization potential, and are virtually absent from geological records. In addition, the acids used in standard palynological treatments can damage their cell walls (Head et al., 2006). In the present study, we observed several sediment samples prior to chemical treatments and found numerous cysts of *Alexandrium* cf. *catenella*, the majority with cellular content (Figure 31, panels 7–10). In the processed samples, we also observed cysts of *A.* cf. *catenella*, sometimes with cellular content, but their abundance may have been underestimated because of the problems mentioned earlier.

Subassemblage zone Ib includes stations located in the central and southern part of the SJG (80-100 m water depth). Dinocyst concentrations are maximum and range between 8,268 cysts g^{-1} and 45,848 cysts g^{-1}. The dominant taxa are *S. ramosus* (49%-74%), *O. centrocarpum* (6%-21%), and *S. mirabilis* (2%-12%). Autotrophic dinocysts dominate this subassemblage, and heterotrophic dinocysts are relatively lower in abundance. The most abundant heterotrophic dinocysts are those of *P. kofoidii* (1%-9%) and the *Echinidium* sp.C (0.5%–3.9%; Figures 10 and 11).

Assemblage zone II regroups the four samples located offshore (108-647 m water depth). Concentrations are relatively low, ranging from 64 cysts g^{-1} to 5,026 cysts g^{-1}, in contrast to assemblage zone I. Heterotrophic dinocysts dominate this assemblage and are represented by *Brigantedinium* spp. (4%-46%), cysts of *P. kofoidii* (0%-17%), and *Dubridinium* sp. (0%-18%). The oceanic species *Impagidinium paradoxum* also appears here and can reach a maximum of 19%. In addition, the relative abundance of autotrophic dinocysts is low compared to assemblage I (Figures 10 and 11): *S. ramosus* registers at 7%-19%, *O. centrocarpum* at 0%-10%, and *S. mirabilis* at 0%-12%.

RDA analyses were performed with all variables and with single explanatory variables for relative abundance and concentration data. The RDA results reveal the same sample groupings as those from the cluster analyses. Many environmental variables are statically significant (p <0.05) when they are used as sole explanatory variables or together (Table 6, Figure 12).

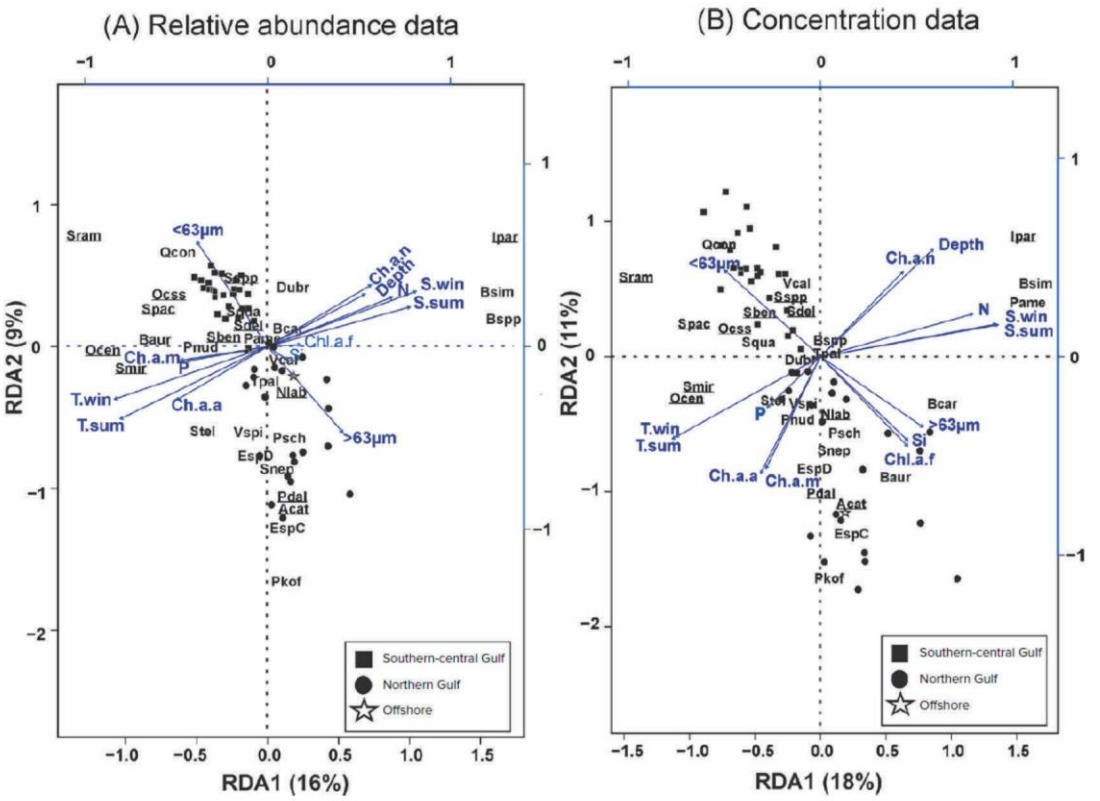

Figure 12. Correlation biplot based on redundancy analysis (RDA) for dinocyst assemblages, sea surface parameters, grain size data (fraction > 63 µm and < 63 µm) and depth. Winter and summer temperature (T.win, T.sum), summer salinity (S.sum), nitrate (N), phosphate (P) concentrations, and chlorophyll-*a* concentrations (February = Ch.a.f, May = Ch.a.m, August = Ch.a.a, November = Ch.a.n). RDA run with (A) relative abundance of cysts, and (B)

concentration data. A variable is statically significant if $p < 0.05$. Variable axes are in blue. Autotrophic dinocysts are underlined.

For relative abundance (%) analyses, chlorophyll-*a* concentrations in March (ch.a.m, austral autumn), August (Ch.a.a, austral winter), and November (Ch.a.n, austral spring); temperature and salinity in winter and summer (T.win, T.sum, S.win, S.sum); and annual concentrations of nitrate (N) and phosphate (P) all contribute significantly to defining assemblage compositions (p <0.05). Northern SJG sites (subassemblage Ia) correlate with heterotrophic dinocysts (cysts of *P. kofoidii* and *P. schwartzii*, *Echinidinium* sp.C, *Echinidinium* sp.D, *Selenopemphix nephroides*, *Trinovantedinium pallidifulvum* and *Votadinium spinosum*). However, sites located in the central and southern SJG (subassemblage zone Ib) do not seem to be associated with any environmental variable (in the two RDA analyses), but correlate with autotrophic dinocysts and with fine particle size (> 63 μm) in surface sediments (Figure 11A).

In concentration analysis, we find the same patterns: the northern sites (subassemblage zone Ia) are associated with Ch.a.f (1.7 mg m^{-3} on average), Ch.a.m (1.6 mg m^{-3} on average), Ch.a.a (1.2 mg m^{-3} on average), Si (34. 9 μmol L^{-1}), and surface temperature (~ 8.5°C during austral winter and 14.9° C during austral summer). Salinity (~ 33.4) in the SJG seems to have a weak influence on the distribution of dinocysts. The main finding in this analysis is a negative correlation between Si and southern-central sites (Figure 11B). It is also noted in the two RDA triplots that round brown cysts (*Brigantedinium simplex and Brigantedinium* spp.) and *I. paradoxum* correlate with water depth (Figure 12).

1.8 DISCUSSION

Relatively high dinocyst concentrations (maximum 45,848 cysts g^{-1} and average 12,858 cysts g^{-1}) can be related to fine particle size in surface sediments in the southern-central gulf (Figures 11 and 12). Indeed, dinocysts are the same size as silt particles and

exhibit similar hydrodynamic behavior, so they tend to be concentrated with fine sediments (e.g., Dale, 1976). In general, two spatial domains emerge from the distribution of dinocysts in the SJG (northern/south-central gulf and offshore domains). Autotrophic dinocysts dominate the assemblages because of the high primary productivity that characterizes the Southwest Atlantic Ocean (Figure 8A). The increase in dinoflagellate cyst concentrations along a north-south gradient in the SJG is most likely due to the input of nutrient rich subantarctic waters via the Patagonia Current (Figure 8A), which promotes the development of dinoflagellate species in southern-central SJG (subassemblage zone Ib). The production of dinocysts appears to be controlled in the north by productivity during austral summer (Ch.a.f), autumn (Ch.a.m), and winter (Ch.a.a), and by surface temperatures (Figure 12).

The high relative abundance of heterotrophic dinocysts in subassemblage Ia in the northern SJG may be related to the presence of diatoms found in the northern part of the gulf (Krock et al., 2015; Latorre, 2018). Indeed, diatoms are the main prey for some heterotrophic dinoflagellates (Jacobson and Anderson, 1986; Hansen, 1992; Jeong and al., 2010). This concept is supported by the relatively high Si concentrations (40.5–41.5 μmol L^{-1}) found at stations BV11, 14, 13, 15, 16, 19, and 20, which could promote the development of diatoms (e.g., Dugdale and Wilkerson, 2001). In addition, Smayda (1997) showed that the presence of diatoms is more important than that of dinoflagellates in turbulent zones (such as in the northern gulf) because their cell structures are adapted to this type of environment, and also because of their competitiveness in the battle for nutrients. Regarding the food web structure in the northern gulf, the high abundance of cysts of *Polykrikos kofoidii* (11%-39%) is interesting because this species is known to feed on a large variety of prey, including other SJG dinoflagellates such as *Gonyaulax spinifera* and *Alexandrium* species (Matsuoka et al., 2000). Diatoms and dinoflagellates could therefore be a food source for heterotrophic dinoflagellates.

The high abundance of dinocysts in the central and southern SJG may be due to the stratified nature of the water column in the central part of the basin (e.g., Krock et al., 2015) and the presence of a tidal front in the area (Figure 7A; Rivas et al., 2006, Carbajal et al.,

2018). Stratified waters favor the development of dinoflagellates, whose two flagella allow them to migrate vertically and obtain the nutrients necessary for their survival at depth (Smayda et al., 1997). The high abundance of autotrophic dinocysts in this subassemblage could be explained by the decreasing trend of Si from north to south, which would favor the development of autotrophic dinoflagellates over diatoms (e.g., Smayda, 1990). The low abundance of dinocysts at offshore sites (assemblage zone II) is similar to other observations of dinocyst distributions in the global ocean (Zonneveld et al., 2013). The ubiquitous genera *Spiniferites* and *Operculodinium*, which are the major contributors to northern and southern-central assemblages, are found preferentially in nutrient-rich coastal waters. In addition, high offshore concentrations of heterotrophic dinocysts are associated with the upwelling around the 200 m isobath (Matano et al., 2010) that promotes high biological productivity and permits the development of primary producers such as diatoms that serve as prey for heterotrophic dinoflagellates. This is corroborated by the high abundance at the offshore sites (BV54, BV55) of round brown cysts (*Brigantedinium* spp., *Brigantedinium simplex*), whose presence is an indicator of high productivity areas such as upwelling zones (e.g., Zonneveld et al., 2001a, Pospelova et al., 2008). The presence of *Impagidinium paradoxum* is strongly correlated to water depth (Figure 12). This taxon is considered to be an oceanic species (Zonneveld et al., 2013).

1.9 CONCLUSION

This study, based on the analysis of 52 surface sediment samples, provides the first detailed description of the distribution of modern dinoflagellate cyst assemblages in the SJG. Two assemblage zones were identified from the relative abundances of dinocysts and from hierarchical clustering and RDA analyses. The distribution of dinocysts appears to be primarily controlled by local primary productivity and offshore upwelling. Dinocyst concentrations are high in the southern-central gulf, where we note the fine particle size of surface sediments. The concentrations of dinocysts increase along a north-south gradient in the SJG, with minimum concentrations at offshore sites (outside the gulf). The high

concentrations of dinocysts in the southern-central gulf are associated with the input of nutrient-rich subantarctic water, water column stratification, and tidal fronts in the southern part of the gulf. The presence of heterotrophic dinocysts in the northern SJG and offshore is related to prey availability and upwelling (Figure 13). Dinocysts are an important part of the organic carbon preserved in SJG sediments, and thus represent an important indicator of primary paleo-productivity that can be used in paleoceanographic reconstructions.

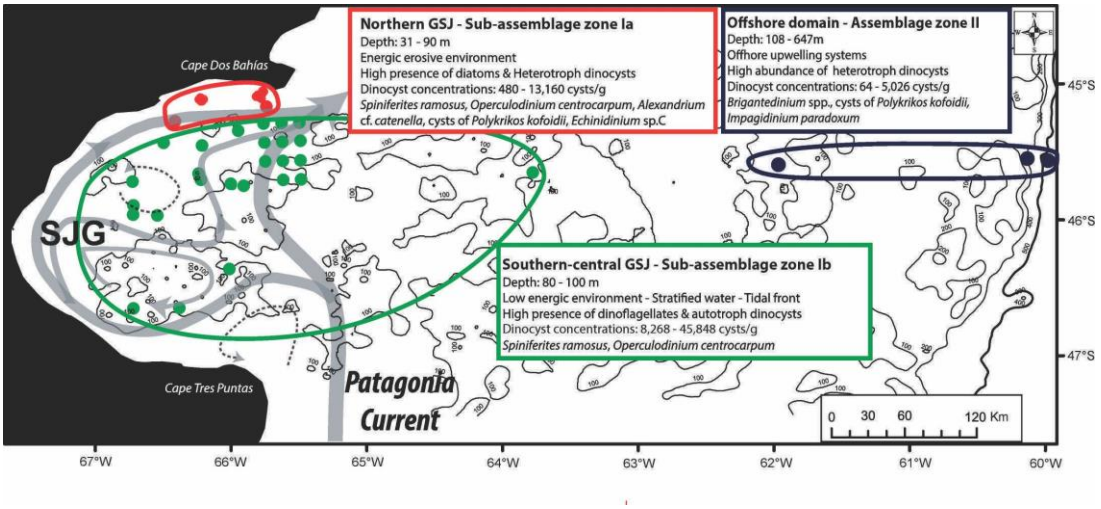

Figure 13. Spatial distribution of dinocyst assemblages in the SJG.

1.10 ACKOWLEDGMENTS

The authors are grateful to the captain, officers, crew, and scientists of the MARGES expedition on board R/V *Coriolis II*. We are grateful for the financial support of the Ministerio de Cienca, Tecnologia e Innovacion Productiva (MINCyT), Provincia de Chubut and the Consejo Nacional de Investigaciones Cientificas Tecnicas (CONICET) for the MARES and MARGES expeditions. Special thanks to A. Rivas and Pierre-Arnaud Desiage, who provided chlorophyll-*a* and grain size data, respectively. We also thank the reviewers for their comments that helped improve this manuscript. This work was carried out with the

financial support of FRQNT (Fonds de recherche du Quebec – Nature et technologies) to G. St-Onge and A. Rochon and NSERC Discovery grants to A. Rochon and G. St-Onge.

1.11 REFERENCES

Aravena, J-C., and B.H. Luckman. 2009. Spatiotemporal rainfall patterns in Southern South America. *International Journal of Climatology* 29(14):2,106–2,120, https://doi.org/10.1002/joc.1761.

Bianchi, A.A. 2005. Vertical stratification and airsea CO2 fluxes in the Patagonian shelf. *Journal of Geophysical Research* 110(C7), https://doi.org/ 10.1029/2004JC002488.

Bogus, K., K.N. Mertens, J. Lauwaert, I.C. Harding, H. Vrielinck, K.A. Zonneveld, and G.J. Versteegh. 2014. Differences in the chemical composition of organic-walled dinoflagellate resting cysts from phototrophic and heterotrophic dinoflagellates. *Journal of Phycology* 50(2):254 266, https://doi.org/ 10.1111/jpy.12170.

Brandhorst, W., and J.P. Castello. 1971. *Evaluación de los Recursos de Anchoíta (*Engraulis anchoita*) frente a la Argentina y Uruguay*. Serie de Informaciones Tecnicas 29, Proy. Des. Pesquero (FAO), 63 pp. Bujak, J.P. 1984. Cenozoic dinoflagellate cysts and acritarchs from the Bering Sea and northern North Pacific, DSDP Leg 19. *Micropaleontology* 30(2):180–212.

Candel, M.S., T. Radi, A. de Vernal, and G. Bujalesky. 2012. Distribution of dinoflagellate cysts and other aquatic palynomorphs in surface sediments from the Beagle Channel, Southern Argentina. *Marine Micropaleontology* 96–97:1–12, https://doi.org/10.1016/j.marmicro.2012.06.009.

Carbajal, J.C., A.L. Rivas, and C. Chavanne. 2018. High-frequency frontal displacements south of San Jorge Gulf during a tidal cycle near spring and neap phases: Biological implications between tidal states. *Oceanography* 31(4):60–69, https://doi.org/10.5670/oceanog.2018.411.

Dale, B. 1976. Cyst formation, sedimentation, and preservation: Factors affecting dinoflagellate assemblages in recent sediment from Trondheimsfjord, Norway. *Review of Palaeobotany and Palynology* 22(1):39–60, https://doi.org/10.1016/0034-6667(76)90010-5.

Dale, B. 2001. Marine dinoflagellate cysts as indicators of eutrophication and industrial pollution: A discussion. *Science of the Total Environment* 264(3):235–240, https://doi.org/10.1016/S0048-9697(00)00719-1.

Desiage, P.-A., J.-C. Montero-Serrano, G. St-Onge, A.C. Crespi-Abril, E. Giarratano, M.N. Gil, and M.J. Haller. 2018. Quantifying sources and transport pathways of surface sediments in the Gulf of San Jorge, central Patagonia (Argentina). *Oceanography* 31(4):92–103, https://doi.org/10.5670/oceanog.2018.401.

Desiage, P-A., G. St-Onge, J-C. Montero-Serrano, M.J. Duchesne, and M. Haller. 2016. Late Pleistocene and Holocene sea-level variations and post-glacial sedimentation in the Gulf of San Jorge (Argentina, Central Patagonia). Poster session presented at the Fall Meeting of the American Geophysical Union.

de Vernal, A., A. Rochon, B. Frechette, M. Henry, T. Radi, and S. Solignac. 2013. Reconstructing past sea ice cover of the Northern Hemisphere from dinocyst assemblages: Status of the approach. *Quaternary Science Reviews* 79:122–134, https://doi.org/10.1016/j.quascirev.2013.06.022.

Dugdale, R.C., and F.P. Wilkerson. 2001. Sources and fates of silicon in the ocean: The role of diatoms in the climate and glacial cycles. *Scientia Marina* 65(S2):141–152, https://doi.org/10.3989/scimar.2001.65s2141.

Durantou, L., A. Rochon, D. Ledu, G. Masse, S. Schmidt, and M. Babin. 2012. Quantitative reconstruction of sea-surface conditions over the last 150 yr in the Beaufort Sea based on dinoflagellate cyst assemblages: The role of large-scale atmospheric circulation patterns. *Biogeosciences* 9(12):5,391–5,406, https://doi.org/10.5194/bg-9-5391-2012.

Esper, O., and K.A.F. Zonneveld. 2002. Distribution of organic-walled dinoflagellate cysts in surface sediments of the Southern Ocean (eastern Atlantic sector) between the Subtropical Front and the Weddell Gyre. *Marine Micropaleontology* 46(1):177–208, https://doi.org/10.1016/S0377-8398(02)00041-5.

Evitt, W.R. 1985. *Sporopollenin Dinoflagellate Cysts: Their Morphology and Interpretation*. American Association of Stratigraphic Palynologists Foundation, Dallas, 333 pp.

Fabro, E., G.O. Almandoz, M. Ferrario, U. John, U. Tillmann, K. Toebe, B. Krock, and A. Cembella. 2017. Morphological, molecular, and toxin analysis of field populations of *Alexandrium* genus from the Argentine Sea. *Journal of Phycology* 53(6):1,206–1,222, https://doi.org/10.1111/jpy.12574.

Fabro, E., B. Krock, A.I. Torres, F.E. Paparazzo, I.R. Schloss, G.A. Ferreyra, and G.O. Almandoz. 2018. Toxigenic dinoflagellates and associated toxins in San Jorge Gulf, Argentina. *Oceanography* 31(4):145–153, https://doi.org/10.5670/oceanog.2018.417.

Fernandez, M., A. Roux, E. Fernandez, J. Calo, A. Marcos, and H. Aldacur. 2003. Grainsize analysis of surficial sediments from Golfo San Jorge, Argentina. *Journal of the Marine Biological Association of the United Kingdom* 83(6):1,193–1,197, https://doi.org/10.1017/ S0025315403008488.

Glembocki, N.G., G.N. Williams, M.E. Gongora, D.A. Gagliardini, and J.M. (Lobo) Orensanz. 2015. Synoptic oceanography of San Jorge Gulf (Argentina): A template for Patagonian red shrimp (*Pleoticus muelleri*) spatial dynamics. *Journal of Sea Research* 95:22–35, https://doi.org/10.1016/j.seares.2014.10.011.

Gregg, W.W. 2005. Recent trends in global ocean chlorophyll. *Geophysical Research Letters* 32(3), https://doi.org/10.1029/2004GL021808.

Gurdebeke, P.R., K.N. Mertens, Y. Takano, A. Yamaguchi, K. Bogus, M. Dunthom, K. Matsuoka, H. Vrielinck, and S. Louwye. 2018. The affiliation of *Hexasterias problematica* and *Halodinium verrucatum* sp. nov. to ciliate cysts based on molecular phylogeny and cyst wall composition. *European Journal of Protistology* 66:115–135, https://doi.org/10.1016/j.ejop.2018.09.002.

Hansen, P.J. 1992. Prey size selection, feeding rates and growth dynamics of heterotrophic dinoflagellates with special emphasis on *Gyrodinium spirale*. *Marine Biology* 114(2):327–334, https://doi.org/10.1007/BF00349535.

Head, M.J. 1996. Modern dinoflagellate cysts and their biological affinities. Pp. 1,197–1,248 in *Palynology Principles and Applications*, vol. 3. J. Jansonius and D.C. McGregor, eds, American Association of Stratigraphic Palynologists Foundation, Dallas, TX.

Head, M.J., J. Lewis, and A. de Vernal. 2006. The cyst of the calcareous dinoflagellate *Scrippsiella trifida*: Resolving the fossil record of its organic wall with that of *Alexandrium tamarense*. *Journal of Paleontology* 80(1):1–18, https://doi.org/10.1666/0022-3360 (2006) 080[0001:TCOTCD]2.0.CO;2.

Jacobson, D.M., and D.M. Anderson. 1986. Thecate heterophic dinoflagellates: Feeding behavior and mechanisms. *Journal of Phycology* 22(3):249–258, https://doi.org/10.1111/j.1529-8817.1986.tb00021.x.

Jeong, H.J., Y.D. Yoo, J.S. Kim, K.A. Seong, N.S. Kang, and T.H. Kim. 2010. Growth, feeding and ecological roles of the mixotrophic and heterotrophic dinoflagellates in marine planktonic food webs. *Ocean Science Journal* 45(2):65–91, https://doi.org/ 10.1007/s12601-010-0007-2.

Krock, B., C.M. Borel, F. Barrera, U. Tillmann, E. Fabro, G.O. Almandoz, M. Ferrario, J.E. Garzon Cardona, B.P. Koch, C. Alonso, and R. Lara. 2015. Analysis of the hydrographic conditions and cyst beds in the San Jorge Gulf, Argentina, that favor dinoflagellate population development including toxigenic species and their toxins. *Journal of Marine Systems* 148:86–100, https://doi.org/10.1016/j.jmarsys.2015.01.006.

Krock, B., M.E. Ferrario, R. Akselman, and N.G. Montoya. 2018. Occurrence of marine biotoxins and shellfish poisoning events and their causative organisms in Argentine marine waters. *Oceanography* 31(4):132–144, https://doi.org/10.5670/oceanog.2018.403.

Latorre, M.P. 2018. *Contrôle de la Structure et de la Distribution de la Communauté Microbienne dans le Golfe de San Jorge, Argentine*. Maitrise, Universite du Quebec a Rimouski, 104 pp.

Legendre, P., and E.D. Gallagher. 2001. Ecologically meaningful transformations for ordination of species data. *Oecologia* 129(2):271–280, https://doi.org/ 10.1007/s004420100716.

Lutz, V.A., and J. Carreto. 1991. A new spectrofluorometric method for the determination of chlorophylls and degradation products and its application in two frontal areas of the Argentine Sea. *Continental Shelf Research* 11:433–451, https://doi.org/ 10.1016/0278-4343(91)90052-8.

Matano, R.P., and E.D. Palma. 2018. Seasonal variability of the oceanic circulation in the Gulf of San Jorge, Argentina. *Oceanography* 31(4):16–24, https://doi.org/ 10.5670/oceanog.2018.402.

Matano, R.P., E.D. Palma, and A.R. Piola. 2010. The influence of the Brazil and Malvinas Currents on the Southwestern Atlantic Shelf circulation. *Ocean Science* 6(4):983–995, https://doi.org/10.5194/os-6-983-2010.

Matsuoka, K., H.J. Cho, and D.M. Jacobson. 2000. Observations of the feeding behavior and growth rates of the heterotrophic dinoflagellate *Polykrikos kofoidii* (Polykrikaceae, Dinophyceae). *Phycologia* 39(1):82–86, https://doi.org/10.2216/i0031-8884-39-1-82.1.

Mayr, C., M. Wille, T. Haberzettl, M. Fey, S. Janssen, A. Lucke, C. Ohlendorf, G. Oliva, F. Schabitz, and G. Schleser. 2007. Holocene variability of the Southern Hemisphere westerlies in Argentinean Patagonia (52°S). *Quaternary Science Reviews* 26(5–6):579–584, https://doi.org/10.1016/j.quascirev.2006.11.013.

Orozco, F.E., and J.I. Carreto. 1989. Distribution of *Alexandrium excavatum* resting cysts in a patagonic shelf area (Argentina). Pp. 309–312 in *Red Tides: Biology, Environmental Science and Toxicology*. T. Okaichi, D.M. Anderson, and T. Nemoro, eds, Elsevier Science Publishing.

Palma, E.D., R.P. Matano, and A.R. Piola. 2008. A numerical study of the Southwestern Atlantic Shelf circulation: Stratified ocean response to local and offshore forcing. *Journal of Geophysical Research* 113(C11), https://doi.org/ 10.1029/2007JC004720.

Piola, A.R., N.M. Avellaneda, R.A. Guerrero, F.P. Jardon, E.D. Palma, and S.I. Romero. 2009. Malvinas-slope water intrusions on the northern Patagonia continental shelf. *Ocean Science Discussions* 6(4):345–359, https://doi.org/10.5194/os-6-345-2010.

Pospelova, V., A. de Vernal, and T.F. Pedersen. 2008. Distribution of dinoflagellate cysts in surface sediments from the northeastern Pacific Ocean (43–25°N) in relation to sea-surface temperature, salinity, productivity and coastal upwelling. *Marine Micropaleontology* 68(1–2):21–48, https://doi.org/10.1016/j.marmicro.2008.01.008.

Rivas, A.L., A.I. Dogliotti, and D.A. Gagliardini. 2006. Seasonal variability in satellite-measured surface chlorophyll in the Patagonian Shelf. *Continental Shelf Research* 26(6):703–720, https://doi.org/10.1016/j.csr.2006.01.013.

Rochon, A., A.D. Vernal, J.L. Turon, J. Matthiessen, and M.J. Head. 1999. Distribution of recent dinoflagellate cysts in surface sediments from the North Atlantic Ocean and adjacent seas in relation to sea-surface parameters. *American Association of Stratigraphic Palynologists Contribution Series* 35:1–146.

Sabatini, M., and P. Martos. 2002. Mesozooplankton features in a frontal area off northern Patagonia (Argentina) during spring 1995 and 1998. *Scientia Marina* 66:215–232, https://doi.org/10.3989/scimar.2002.66n3215.

Segura, V., V. Lutz, A. Dogliotti, R. Silva, R. Negri, R. Akselman, and H. Benavides. 2013. Phytoplankton types and primary production in the Argentine Sea. *Marine Ecology Progress Series* 491:15–31, https://doi.org/10.3354/meps10461.

Smayda, T.J. 1990. Novel and nuisance phytoplankton blooms in the sea: Evidence for a global epidemic. Pp. 29–40 in *Toxic Marine Phytoplankton*. E. Graneli, B. Sundstrom, L. Edler, and D.M. Anderson, eds, Elsevier.

Smayda, T.J. 1997. Harmful algal blooms: Their ecophysiology and general relevance to phytoplankton blooms in the sea. *Limnology and Oceanography* 42(5, part2):1,137–1,153, https://doi.org/ 10.4319/lo.1997.42.5_part_2.1137. Stoecker, D.K. 1999. Mixotrophy among

dinoflagellates. *Journal of Eukaryotic Microbiology* 46(4):397–401, https://doi.org/10.1111/j.1550-7408.1999.tb04619.x.

Taylor, F.J.R., M. Hoppenrath, and J.F. Saldarriaga. 2008. Dinoflagellate diversity and distribution. *Biodiversity and Conservation* 17(2):407–418, https://doi.org/10.1007/s10531-007-9258-3.

Tonini, M.H., E.D. Palma, and A. Rivas. 2006. Modelo de alta resolucion de los golfos norpatagonicos. *Mecánica Computacional* XXV:1,441–1,460.

Versteegh, G.J.M., P. Blokker, K.A. Bogus, I.C. Harding, J. Lewis, S. Oltmanns, A. Rochon, and K.A.F. Zonneveld. 2012. Infra red spectroscopy, flash pyrolysis, thermally assisted hydrolysis and methylation (THM) in the presence of tetramethylammonium hydroxide (TMAH) of cultured and sediment-derived *Lingulodinium polyedrum* (Dinoflagellata) cyst walls. *Organic Geochemistry* 43:92–102, https://doi.org/10.1016/j.orggeochem.2011.10.007.

Wall, D., B. Dale, G.P. Lohmann, and W.K. Smith. 1977. The environmental and climatic distribution of dinoflagellate cysts in modern marine sediments from regions in the North and South Atlantic Ocean and adjacent seas. *Marine Micropaleontolology* 2:121–200, https://doi.org/ 10.1016/0377-8398(77)90008-1.

Zonneveld, K.A., R.P. Hoek, H. Brinkhuis, and H. Willems. 2001b. Geographical distributions of organic-walled dinoflagellate cysts in surficial sediments of the Benguela upwelling region and their relationship to upper ocean conditions. *Progress in Oceanography* 48(1):25–72, https://doi.org/10.1016/S0079-6611(00)00047-1.

Zonneveld, K.A.F., F. Marret, G.J.M. Versteegh, K. Bogus, S. Bonnet, I. Bouimetarhan, E. Crouch, A. de Vernal, R. Elshanawany, L. Edwards, and others. 2013. Atlas of modern dinoflagellate cyst distribution based on 2405 data points. *Review of Palaeobotany and Palynology* 191:1–197, https://doi.org/ 10.1016/j.revpalbo.2012.08.003.

Zonneveld, K.A.F., G.J.M. Versteegh, and G.J. De Lange. 2001a. Palaeoproductivity and postdepositional aerobic organic matter decay reflected by dinoflagellate cyst assemblages of the Eastern Mediterranean S1 sapropel. *Marine Geology* 172(3):181–195, https://doi.org/10.1016/S0025-3227(00)00134-1.

ARTICLE 2

POLLEN DISPERSAL PATTERNS IN MARINE SURFACE SEDIMENTS FROM THE SAN JORGE GULF, SE PATAGONIA (ARGENTINA)

2.1 RÉSUMÉ EN FRANÇAIS DU DEUXIÈME ARTICLE

Cet article analyse les patrons de distribution des assemblages de pollen et de spores dans les sédiments de surface du GSJ et des sites situés en offshore en relation avec l'emplacement des différentes provinces phytogéographiques entourant le GSJ. Les résultats révèlent que les spectres de pollen sont dominés par les Chenopodiaceae-Amaranthaceae, Poaceae, Asteraceae subf. Asteroideae, *Colliguaja integerrima* et *Ephedra* sp. qui représentent la végétation adjacente au GSJ. Dans l'ensemble, la distribution du pollen dans les sédiments de surface reflète l'emplacement des différentes provinces phytogéographiques et pourrait être utilisée comme analogue moderne aux fins de documenter l'histoire de la végétation autour du golfe. Les assemblages de pollen révèlent une légère augmentation du pollen des plantes herbacées et une diminution des arbustes hauts (e.g. *Colliguaja integerrima)* vers la partie centrale et sud du GSJ. De plus, nous avons identifié deux taxons provenant de la forêt subantarctique (*Nothofagus* et *Podocarpus*) qui pourraient être utilisés comme indicateurs dans l'étude de la dynamique et des variations passées de la ceinture de vent d'ouest dans le GSJ au cours du Pléistocène supérieur et de l'Holocène. Les fortes

concentrations de pollen sont enregistrées dans la partie centrale du GSJ (480 - 8080 grains/g), tandis que de faibles concentrations sont mesurées dans les parties nord et sud du golfe, ainsi que sur des sites situés au large (26 - 1806 grains/g). Les résultats révèlent que la distribution du pollen dans la zone d'étude est régie par la ceinture des vents d'ouest.

Cet article, intitulé «*Pollen dispersal patterns in marine surface sediments from San Jorge Gulf, SE Patagonia (Argentina)*», a été rédigé par moi-même sous la supervision de mon directeur André Rochon (UQAR-ISMER), de mon co-directeur Guillaume St-Onge (UQAR-ISMER) et de mon superviseur de stage en Argentine Isabel Vilanova (CONICET-MACN). Il a été accepté pour publication dans sa version finale le 11 juin 2020 par l'editeur de la revue *Palaeogeography, Palaeoclimatology, Palaeoecology*. Les résulats de ces travaux ont été présentés sous forme d'affiches au congrès annuel du Géotop qui s'est déroulé à Orford en mars 2019.

2.2 RÉSUMÉ EN ANGLAIS DU DEUXIÈME ARTICLE

This paper analyzes the distribution patterns of pollen and spore assemblages in modern surface sediments recovered from the bottom of the San Jorge Gulf (SJG) and from offshore sites, in relation to the location of different phytogeographic provinces surrounding the SJG, including the distant forest from southwestern Patagonia. Results reveal that pollen spectra are dominated by Chenopodiaceae-Amaranthaceae, Poaceae, Asteraceae subf. Asteroideae, *Colliguaja integerrima* and *Ephedra* sp.; which represents the vegetation adjacent to the SJG. Overall, the pollen distribution in surface sediments reflects the location of the different phytogeographic provinces and will be used as modern-analogues to document vegetation history around the SJG. Pollen assemblages also reveal the latitudinal variation of vegetation taxa in the Patagonian steppe, which is characterized by a slight increase in herbaceous pollen and a decrease in high shrubs (e.g. *Colliguaja integerrima*) towards the southern-central part of the SJG. Furthermore, we identified two pollen taxa from the southwestern Patagonian forest, *Nothofagus* and *Podocarpus* that could be used as indicators of past dynamics and variations of the Southern Westerly Wind Belt (SWWB) in the SJG during the Late Pleistocene and Holocene. High pollen concentrations are recorded at the central part of the SJG (480-8080 grains/g), while low concentrations are measured in the northern and southern parts of the Gulf, as well as at offshore sites (26-1806 grains/g). The pollen distribution in the study area is most likely governed by the SWWB in combination with the marine sediment composition and surface currents flowing through the SJG.

2.3 INTRODUCTION

Atmospheric circulation in the Southern Hemisphere is mainly controlled by the strong Southern Westerly Wind Belt (SWWB). These strong winds have a significant influence on ocean circulation in the South Atlantic and South Pacific Oceans (Strub et al., 1998, Matano et al., 2010; Matano et al., 2018). Studies have shown that the SWWB plays a key role in global climate (Anderson et al., 2009, Toggweiler, 2009). Indeed, the SWWB controls the strength of the Antarctic Circumpolar Current (ACC), which modulates the release of CO_2 from the deep ocean to the atmosphere, especially during interglacial phases (Anderson et al., 2009; Denton et al., 2010). The Patagonian region (southern tip of South America) is the only continental mass intercepting the core of the SWWB, and thus represents a key region for studying the dynamics and past variations of the SWWB (Moreno et al., 2018; Lisé-Pronovost et al. 2015). In addition, Patagonia has been identified as the major source of dust in the Southern Hemisphere due to strong winds (Bullard et al., 2016). The organic fraction of this dust contains pollen and spores produced by the local vegetation. Wind-borne pollen, incorporated into coastal marine sediments, may reflect seasonal variations from the adjacent continental sector and can be used to describe the fluxes of terrigenous inputs into the ocean and wind dynamics (Heusser, 1983; Melia, 1984; Dupont and Wyputta, 2003; Hooghiemstra et al., 2006). Moreover, pollen is contemporaneous with other microorganisms present in the marine environment (Heusser, 1983); therefore, it represents a powerful tool for exploring ocean - atmosphere interactions by correlating terrestrial inputs with ocean conditions. However, it is essential to know about pollen distribution in modern sediments in order to achieve a more precise interpretation of marine records (Heusser, 1988).

Previous studies carried out in continental sectors of the Patagonian region have successfully shown the coherent relationship between vegetation and surface soil pollen distribution (e.g. Markgraf et al., 1981; Mancini, 1993; Paez et al., 2001; Burry et al., 2005; Mancini et al., 2012). In these studies the surface pollen spectra were useful proxy-data for interpreting climatic conditions in Patagonia (Paez et al., 2001). Nevertheless, there are no

similar studies from surface sediments and marine records, except for one study in sediments offshore Argentina (Groot et al., 1965). The SJG, located in southeastern Patagonia (45° and 47°S), offers a unique opportunity to study the pollen fluxes in the Southwestern Atlantic Ocean and the relationship with the core of the SWWB (30° and 60°S, Bertrand et al., 2014). In this context, the main objective of this investigation is to describe the dispersal patterns of pollen and spores in modern surface sediments of the SJG related to the SWWB and marine currents in order to establish a baseline to study vegetation changes adjacent to the SJG and the past variations of the SWWB.

2.4 REGIONAL SETTING

2.4.1 Location and description of the Study area

The Patagonian region extends over 900,000 km^2, it is a wide area located between 39° and 55°S in South America (Bullard et al., 2016, Figure 14). One of the main features of this region is the Andes Cordillera with high relief (~1500 m above sea level in Chilean Patagonia) at the west, and low relief (100-200 m above sea level) and plains towards the east of this range, up to the Atlantic coast (Garreaud et al., 2013).

Our study area, the SJG, is located in the Argentinian Continental shelf (Southwestern Atlantic coast). The SJG forms a shallow ocean basin (average depth 70m) that stretches between latitudes 45°S and 47°S, being about 250 km wide, and encompassing an area of 39,000 km^2 (Glembocki et al., 2015, Figure 14).

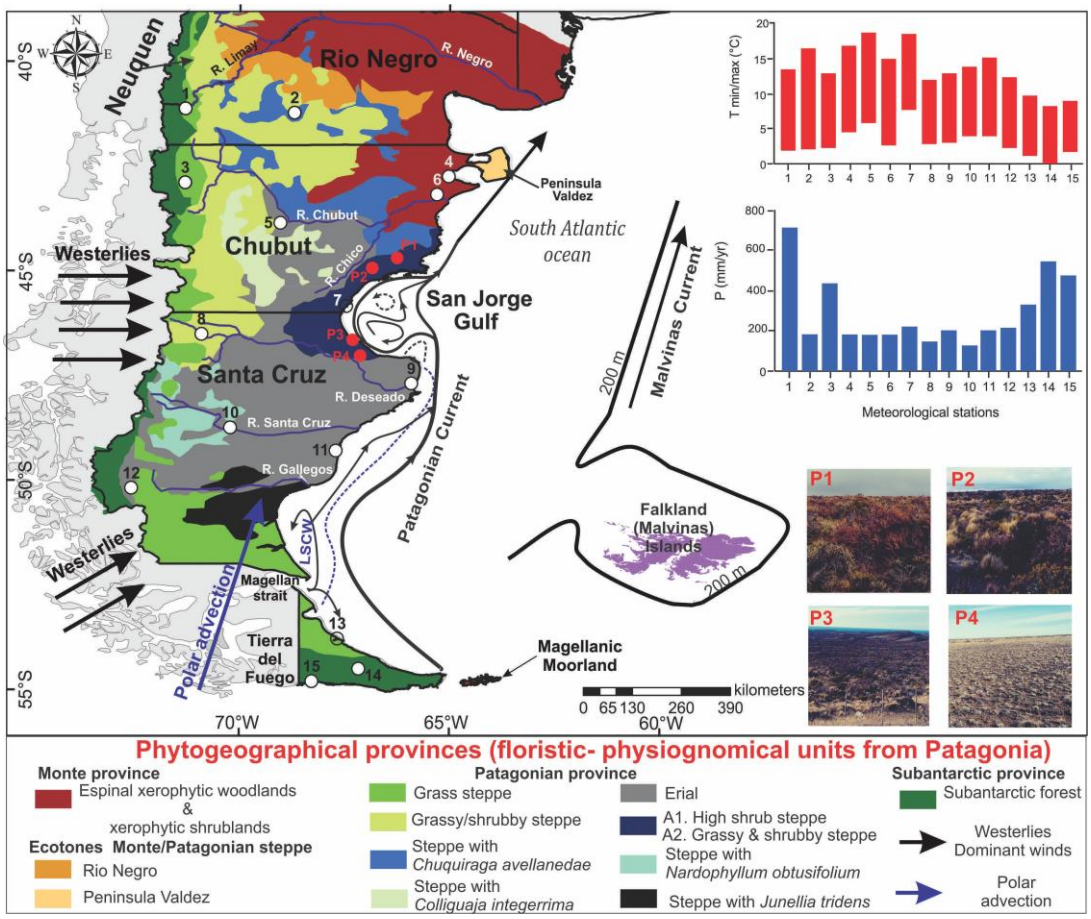

Figure 14. Modern vegetation distribution in Patagonia (adapted from León et al., 1998; Arana et al., 2017) with main ocean currents in Southwestern Atlantic and prevailing winds (adapted from Matano et al., 2010; Matano and Palma, 2018), showing the Malvinas Current, the Patagonia Current, the Low Salinity Coastal Waters (LSCW), westerlies and southwesterlies. (B) Average of annual precipitation and maximum and minimum temperatures along meteorological stations in Patagonia covering the period from 1988 to 2018 (data from National Meteorological Service of Argentina). The white dot are the meteorological stations and the red dot represent the locations of the pictures.

2.4.2 Ocean circulation

The general ocean circulation in the Argentinian continental shelf is characterized by the northward flowing Patagonian Current (PC, Matano et al., 2010; Matano and Palma, 2018), which is mainly composed of subantarctic low saline waters from the Strait of Magellan entering into SJG from the south (Brandhorst and Castello, 1971). The general circulation in the gulf consists of two distinct patterns (austral summer and winter modes) that drive seasonal circulation variability (Matano and Palma, 2018). The summer mode is characterized by a cyclonic gyre and a maximum intrusion of PC; while in the winter mode the cyclonic gyre weaken significantly (Matano and Palma, 2018). Along the edge of the continental slope, the Malvinas Current transports cold, salty (> 34) and nutrient-rich subantarctic waters (Piola et al., 2009, Figure 13).

2.3.3 Atmospheric circulation and climate

The regional climate in Patagonia is controlled by the SWWB (Garreaud et al., 2013). Indeed, this zone lies between the semi-permanent subtropical high pressure belt (South Pacific and South Atlantic Oceans, 30 °S) and the subpolar low pressure belt (60° and 70°S, Paruelo et al., 1995). According to Compagnucci (2011), the small variations in these high-pressure centers control the intensity and direction of the winds. During the austral winter, westerlies become weaker due to the migration of the subtropical high pressure belt to the north. During this period, the continent (35° S) is marked by the formation of a thermal high pressure cell that determines the predominant western direction of the winds (Del valle et al., 1995, Figure 14). Conversely, during the austral summer, wind speeds are above annual averages due to a displacement of the subtropical high pressure belt to the south (Paruelo et al., 1998). On the mainland, oceanic anticyclones are separated by a low pressure system that affects the airflow over the Andes (Del Valle et al., 1995). The Pacific anticyclone gets closer to the coast and goes much further south than the Atlantic anticyclone and generates southwesterly winds sector (Del Valle et al., 1995; Paruelo et al., 1998, Figure 14). The average annual wind velocity is estimated at 32 km/h in the low plains of *Pampa del Castillo* (adjacent to the SJG), which may increase by 23% due to the channelization of the air flows

towards the coastal Atlantic valleys (*Cañadones*) nearby the study area (Labraga, 1994). It has been shown that during the spring-summer transition (November and December) winds can reach 90 km/h, which is marked on the continent by the transition of the high-pressure center to a low-pressure center (Labraga 1994).

Precipitations are controlled by the SWWB, but also by the Andean mountains. Indeed, the Andean Cordillera interrupts the SWWB that brings humid air from the Pacific. This causes shadow rainfall in the western Andes while the eastern part remains dry, with a strong annual precipitation gradient that varies between 7000 and 2000 mm in the west and 200 mm in the east (Coronato et al., 2008; Aravena and Luckman, 2009; Garreaud, 2009). This precipitation gradient is one of the most marked in the world, associated with annual temperatures ranging from 18 to 8 °C (Comodoro Rivadavia, station 7, Figure 14) in the east, and from 12 to 3 °C in the west (Perito Moreno, station 8, Figure 13). This is why Eastern Patagonia is characterized by a semi-arid climate, whereas Western Patagonia has a very humid climate subjected to oceanic influences of the Pacific Ocean (Borromei and Musotto, 2016). On the Atlantic fringe, precipitations are controlled by trade winds associated with the high-pressure subtropical center that brings intense rainfall to central Patagonia (Mancini, 2009; Agosta et al., 2015).

2.4.4 Vegetation

The vegetation distribution in Patagonia is mainly controlled by climatic, edaphic (pH, soil moisture) and geomorphological conditions (Mancini et al., 2005). This situation is subjected to altitudinal and latitudinal variations (Borromei and Musotto, 2016). According to León et al. (1998), which is based on Cabrera (1947, 1976); Soriano (1956); and Arana et al. (2017), different vegetation types develop in Patagonia that can be classified as phytogeographical provinces (Figure 14).

(I) **The Andean Patagonian / Subantarctic forest** extends over the humid temperate sector of western Patagonia and the eastern fringe of the Andes where precipitations are higher than 1000 mm/year (Figure 14). Vegetation is dominated by *Nothofagus* (*N. pumilio*, *N.*

antarctica, N. dombeyi) with other arboreal species, such as *Podocarpus nubigena*, *Saxegothea conspicua*, *Pilgerodendron uviferum*, *Fitzroya cupressoides* and *Drimys winteri* (Borromei and Musotto, 2016). (II) **The Monte** is characterized by xerophytic woodland and a shrub steppe, in a region located northwest of *Rio Negro* where the rainfall is lower than 200 mm (Figure 14). The xerophytic woodland is composed by *Prosopis* sp. and *Larrea* sp. (III) **The Patagonian steppe** encompasses a large extension of the extra-Andean Patagonia, stretching from the limit of the subantarctic forest at the West, and to the Atlantic coast at the East (Figure 14). The climate is semi-arid and precipitations vary between 100 and 300 mm. The vegetation is represented by a shrubby to herbaceous steppe, with several physio-floristic units that have been highlighted based on the digital analysis of satellite images and a compilation of previous investigations (Paruelo et al., 1998; León et al., 1998):

(1) Herbaceous steppe dominated by *Festuca pallescens* in contact with the subantarctic forest;

(2) Shrub steppe characterized by *Chuquiraga avellanedae*;

(3) Shrub steppe with *Colliguaja integerrima*, associated with other shrubby species such as *Verbena tridens, Schinus polygama, Lycium chilense*;

(4) Steppe with *Nardophyllum obtusifolium* and *Junellia tridens*;

(5) Patagonian semi-desert steppe or *Erial*, represented by *Nassauvia* (*N. glomerulosa*, *N.axillaris*), *Chuquiraga aurea*, *Ephedra frustillata*, *Acantholippia seriphiodes*, *Acaena caespitosa*, *Schinus polygamus*, *Lycium ameghinoi*, *Verbena lugustrina* and *Prosopis denudans* with herbaceous cover dominated by *Stipa humilis*;

(6) Around the SJG between alluvial plains, rocky slopes and valleys (*Cañadones*), there are a high shrub and a grassy shrub steppes. The high shrub steppe is dominated by *Colliguaja integerrima* associated with *Trevoa patagonica*, *Anarthrophyllum rigidum*, *Mulinum spinosum Asteraceae* (*Senecio filaginoides*, *Nardophyllum obtusifolium, Grindelia chilense, Baccharis darwinii*, *Perezia recurvata, Nassauvia ulcinata*) with a herbaceous component dominated by Poaceae (*Stipa, Festuca, Poa*) and *Erodium cicutarium*. The grassy shrub steppe is dominated by *Festuca pallescens* and *F. argentina* associated with *Mulinum spinosum, M. halei, Adesmia campestris, Verbena thymifolia, Acaena platyacantha,*

Nassauvia darwinii, *Perezia patagonica* and *Azorella*. The high shrub steppe is located in hills and slopes areas (*Cañadones*) oriented towards to the gulf, whereas grassy & shrubby steppes are found in the flat areas at the SW of Pico Salamanca and towards the south of San Jorge Gulf (León et al., 1998; Oyarzabal et al., 2018; Figure 14). We also note the presence of ecotones, which characterize the transition of the Patagonian steppe and the Monte formations, marked by a mix of floristic species of the two provinces (León et al., 1995).
The human impact on the vegetation is marked by the introduction of exotic taxa such as Pinaceae in the Chilean Patagonia (Teillier et al., 2003) and *Erodium cicutarium*, which was naturalized in the district of San Jorge Gulf (Cabrera et al., 1971). Some taxa (Brassicaceae, *Rumex acetosella*, Asteraceae subf. Cichorioideae) can be abundant due to the effect of intensive grazing by domesticated animals in the Patagonian steppe (Bustamante and Simonetti, 2005, Mancini et al., 2008).

2.5 MATERIALS AND METHODS

A total of 52 surface sediment samples were recovered from the bottom of the SJG by using a Van Veen grab on board of the R/V Coriolis II (Table 7 in supplementary material). This oceanographic expedition was carried out within the framework of the MARGES oceanographic survey (*MARINE GEOLOGY, sedimentology, stratigraphy, basin architecture and paleoceanography of San Jorge* Gulf) from February 17 to March 4, 2014 (Figure 15, St-Onge and Ferreyra, 2018). The sediment samples were collected from the upper first centimeter (~ 1 cm), which represents between 40 and 70 years of sedimentation (Faye et al., 2018). The sampling followed longitudinal and latitudinal transects in the SJG and along the continental shelf. The samples show a good preservation of the sediment/water interface with minimal bioturbation.

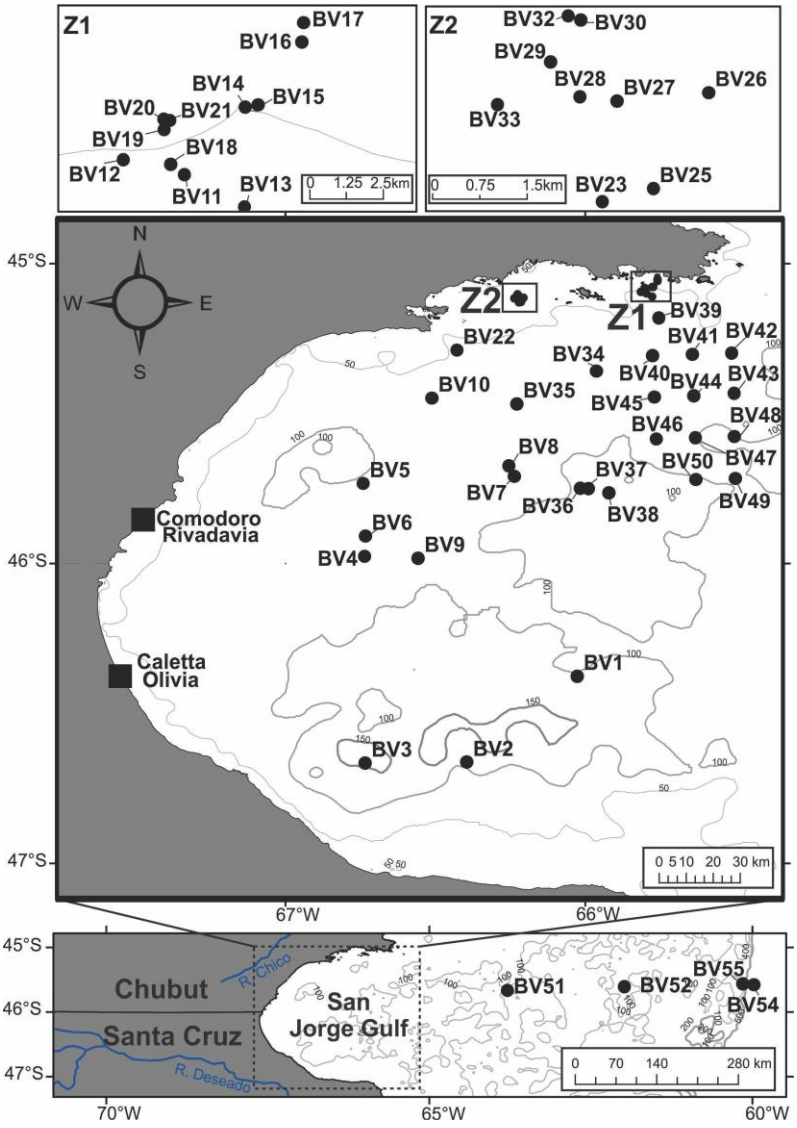

Figure 15. Map of SJG illustrating the location of surface samples analysed in this study. Isobaths are from General Bathymetric Chart of the Oceans (GEBCO).

All sediments were treated alternately with warm hydrochloric acid (HCl, 10%) and warm hydrofluoric acid (HF, 49%) following the protocol described by Rochon et al. (1999) at ISMER. The final residue was sieved at 10 μm and centrifuged at ~ 2500 rpm for 10 min. A drop was then taken and mounted between slide and coverslip in glycerine gelatin for observation under a microscope. Two tablets of *Lycopodium clavatum* (concentration per tablet 12,100 ± 1892, Batch 414,831, University of Lund) were added to the sediment prior to the chemical treatments to determine the palynomorph concentrations. The counts were performed using a transmitted light microscope (Nikon Eclipse 80i) at × 400 magnification. Some pollen grains were identified at the species level and several at the genus level using reference atlases (Heusser, 1971 and Markgraf and D'Antoni, 1978). In some cases, the family or taxonomic group was given based on morphological criteria (e.g. Asteraceae subf. Asteroideae /Mutisieae: spines, wall, apertures). Palynomorph concentrations are expressed per dry weight (palynomorphs/g) and the relative abundance of taxa is estimated in each sample (pollen %). Exotic floristic taxa (e.g. Pinaceae) and spores were excluded from the pollen sum. Samples with less than 100 pollen grains were considered less reliable in pollen analysis. Isopoll contours were drawn on the basis of percentage with ArcGIS software.

Sampling sites were arranged in a hierarchical cluster using the stratigraphic analysis program (*Tilia*, version 2.0.41) developed by Eric Grimm. The analysis (CONISS, Constrained Incremental Sum-of-Square) were run on non-transformed data.

2.6 RESULTS

A total of 33 taxa were recognized, but only 12 dominated the assemblages: *Nothofagus* sp., *Podocarpus* sp., *Colliguaja integerrima*, Asteraceae subf Asteroideae, *Nassauvia* sp., *Chuquiraga* sp., *Ephedra* sp., Apiaceae type, Poaceae, Chenopodiaceae / Amaranthaceae (Cheno-am), Caryophyllaceae and Brassicaceae; altogether reaching values of more than 90 %. The spores are in low proportions and are mainly represented by bryophytes (*Phaeoceros* sp.), fungal spores and Pteridophytes (*Lycopodium* sp.). Other palynomorphs recorded were

dinoflagellate cysts, organic linings of foraminifera, marine and freshwater palynomorphs, (Faye et al., 2018). The palynomorph preservation was good in all the samples, suggesting that oxidation had little or no effect at all over the palynomorph assemblages.

Pollen zones

According to the Constrained Incremental Sum-of-Squares (CONISS) analysis of the relative abundances, 4 pollen zones were identified: Ia, Ib, Ic and Id (Figure 16).

The pollen spectra from zones Ia and Ib correspond to sediment samples located near the coast (avg. 55 m depth) in the northern area of the SJG. These two zones are relatively similar in composition and are marked by low pollen concentrations ranging from 39 to 1806 grains/g (avg. 476 grains/g) and low spore concentrations 0-17 spores/g (avg. 7 spores/g). The most abundant taxa are Cheno-am (15-37%), Poaceae (5-22%), Asteraceae, subf. Asteroideae (5-16%), *Colliguaja integerrima* (2-17%) and *Ephedra* sp. (0-8%). Herbaceous pollen dominates with 60% on average in these subzones. The main difference between the two subzones is the low abundance of *Ephedra* and slightly higher mean abundance of *Colliguaja integerrima* in subzone Ib (Figures 16 and 20).

The pollen spectra from zone Ic come from sediment samples located in the central and southern part of the SJG (avg. 92 m depth). It is marked by maximum concentration values of both pollen and spores, which vary between 480 and 8080 grains/g (avg. 2559 grains/g) and 0-146 spores/g (avg. 31 spores/g), respectively. Herbaceous taxa dominate this zone (avg. 61%), such as Cheno-am (9-33%) and Poaceae (8-24%). The shrubby taxa in this zone are represented by Asteraceae subf. Asteroideae (9-30%), *Colliguaja integerrima* (0.7-15%) and *Ephedra* sp. (1.7-8%).

The zone Id pollen spectra regroups all four samples (BV51, 52, 55, 54) located offshore (avg. 247 m depth). Concentrations are relatively low and range from 26 to 871 grains/g (avg. 360 grains/g) for pollen, and 6 to 49 spores/g (avg.19 spores/g) for spores. The taxa of herbaceous plants constitute more than 58% of the pollen content.

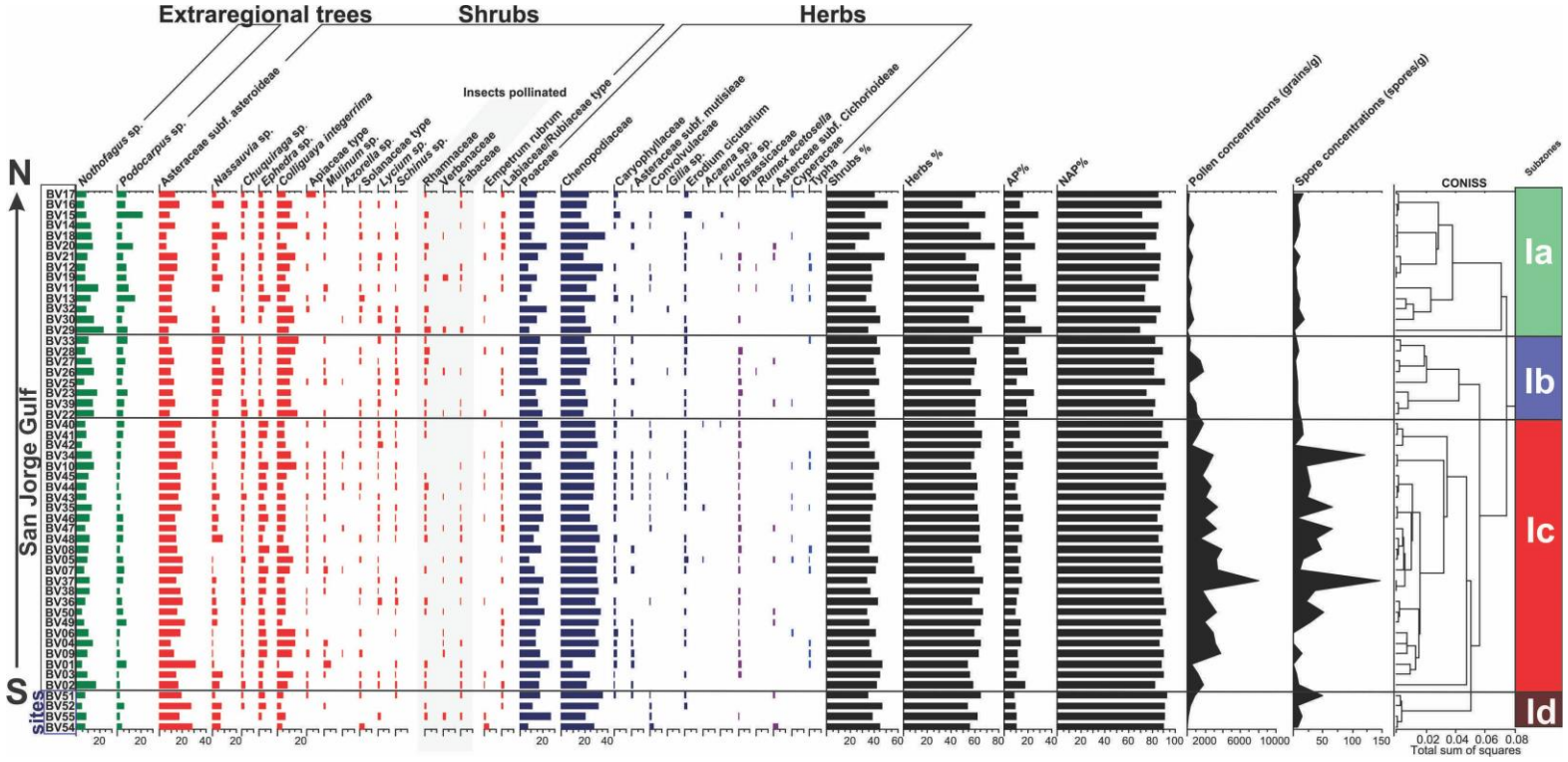

Figure 16. Relative abundance of major pollen taxa in modern surface sediments in SJG and hierarchical clustering of surface sediment samples used to determine pollen assemblages. Note the slight increase of Cheno-am, Poaceae and Asteraceae subf. Asteroideae in southern SJG (subzones Ic and Id).

In general, pollen and spores concentrations range from 26 to 8056 grains/g (avg. 1505 grains/g), and from 0 to 146 spores/g (avg. 20 spores/g), respectively (Figure 17a). High pollen (> 2000 grains/g) and spores concentrations (> 60 spores/g), were recorded in the central area of the SJG, whereas low concentrations were registered in the north and south areas of the Gulf (> 1000 grains/g for pollen and > 20 spores/g for spores, Figures 17a, b).

2.7 DISCUSSION

2.7.1 Pollen-vegetation relationship

This investigation constitutes the first in the SJG that explores the relationship between vegetation and pollen distribution patterns from sediment samples recovered from the bottom surface of the gulf. We found pollen of extra-regional taxa (*Nothofagus* sp. and *Podocarpus* sp.) that represent the arboreal pollen (AP) from forest mainly located in western Patagonia; which are transported for long distances by the westerly winds, ~ over 350 km away from the source. Non Arboreal pollen (NAP), corresponding to shrubby taxa from the Patagonian steppe, mainly represented by Asteraceae (Asteraceae subf. Asteroideae, *Chuquiraga* sp., *Nassauvia* sp.), *Colliguaja integerrima*, *Ephedra* sp., Apiaceae (e.g. *Mulinum* sp., *Azorella* sp.), Solanaceae (*Lycium* sp., Solanaceae type), Anarcadiaceae (*Schinus* sp.), Fabaceae, Verbenaceae and Rhamnaceae. Pollen from other shrubs (*Empetrum rubrum*, Labiaceae / Rubiaceae type) are also present, but their relative abundances are very low. NAP corresponding to herbaceous taxa is mainly represent Chenopodiaceae / Amaranthaceae (Cheno-am), Poaceae and Asteraceae subf. Mutisieae. There is also a low proportion of pollen from other herbaceous taxa (*Gilia* sp., Convolvulaceae, *Erodium cicutarium* and *Acaena* sp., *Fuchsia* sp.), as well as others that are indicators of human impact (Brassicaceae, *Rumex acetosella*, Asteraceae subf. Cichorioideae. (Mancini et al., 2008), and pollen representing semi-aquatic and/or paludal taxa (Cyperaceae, *Typha*).

2.7.2 Modern distribution patterns

The highest relative abundance of arboreal pollen (AP), mainly represented by pollen from *Nothofagus* and *Podocarpus*, occurred in the northern and southern parts of the SJG (Figures 17c-d and 18a-b). The pollen of these taxa are transported over long-distances by westerly winds jet streams high in the troposphere. Hence, both taxa are mostly anemophilous (wind pollinated), having high pollen production, which explains their almost uniform presence over the entire SJG. Their maximum abundances in the northern and southern parts of the SJG could be related to the principal jet stream trajectories (Figures 14 and 18a-b). Therefore, the high abundance of these pollen types will be used to test/assess the intensity of the SWWB at the latitude of the SJG.

The distribution pattern of pollen from herbaceous plants (~ 60%) with high abundances in the central part of the SJG (Figure 17f). Most of the pollen from herbaceaous plants in the SJG belong to Cheno-am (9-37%) and Poaceae (6-25%) taxa and dominate the assemblages. The former shows high relative abundance in the center of the SJG, and the latter to the southern-central part of the gulf (Figure 18c-d). Indeed, the Poaceae are widely distributed in the Patagonian steppe with relative high abundance in flat areas located SW of the SJG (e.g. León et al., 1998); Cheno-am are observed in salt-rich soil in Patagonia, such as the salt marsh, endorheic basin, valleys in hill and coastal lagoon areas along the Argentine coast (León et al., 1998; Paez et al., 2001; Stutz et al., 2006; Marcos and Mancini, 2012). The marine surface distribution patterns of these taxa echo the location of high values of Poaceae and Cheno-am pollen found in the continental surface samples adjacent to the gulf (Paez et al., 2001). Therefore, the distribution patterns of these taxa in the marine surface sediments reflect the occurrence of these plant taxa in the Patagonian steppe controlled by topography and edaphic conditions around the SJG (León et al., 1998; Burry et al., 2005).

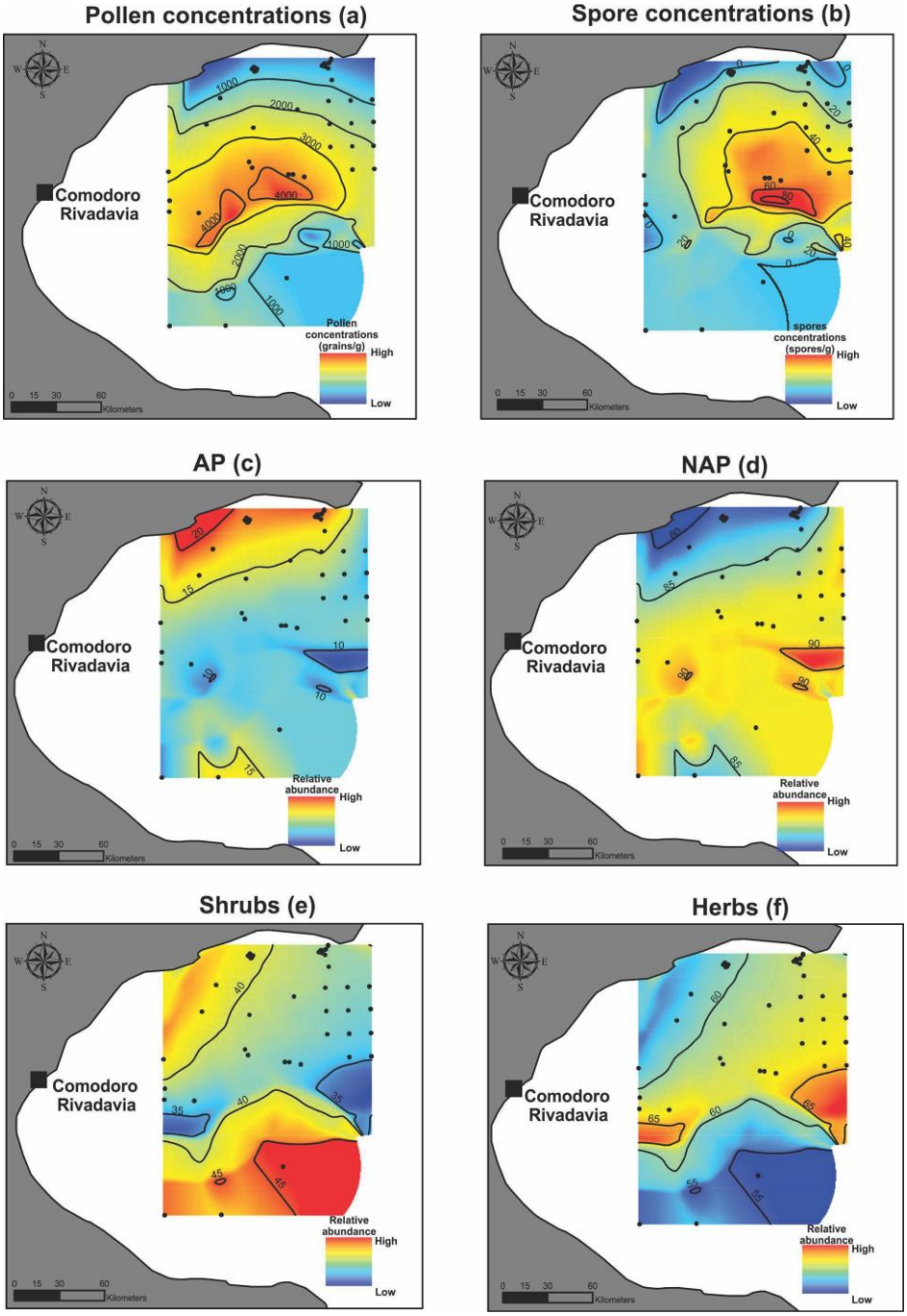

Figure 17. Isopollen map of pollen (a) & spore (b) concentrations with relative abundance distribution of arboreal pollen (AP,c), non-arboreal pollen (NAP, d), shrub (e) and herb (f) taxa.

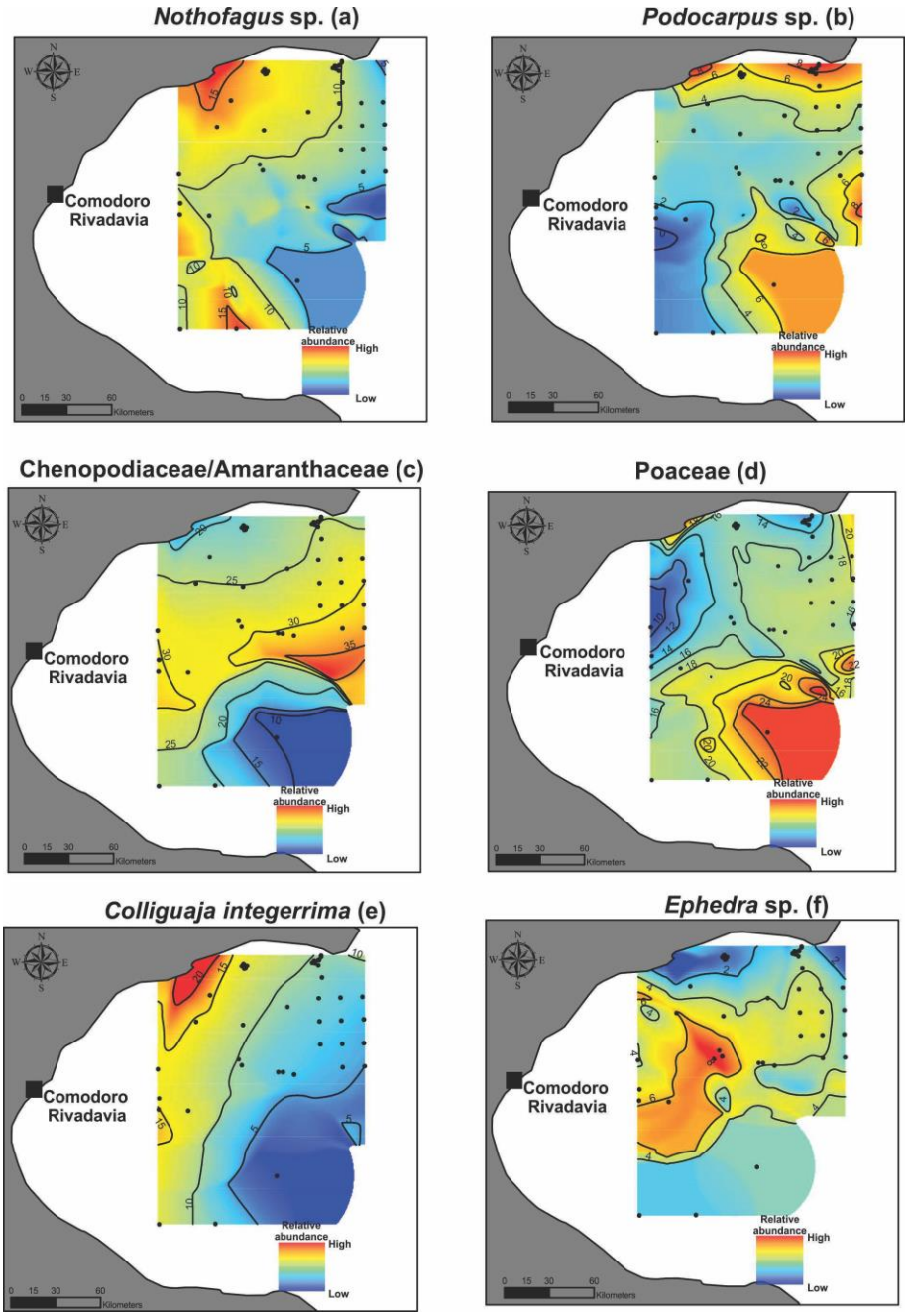

Figure 18. Isopollen map of *Nothofagus* sp. (a), *Podocarpus* sp. (b), Chenopodiaceae /Amaranthaceae (c), Poaceae (d), *Colliguaja integerrima* (e) and *Ephedra* sp. (f).

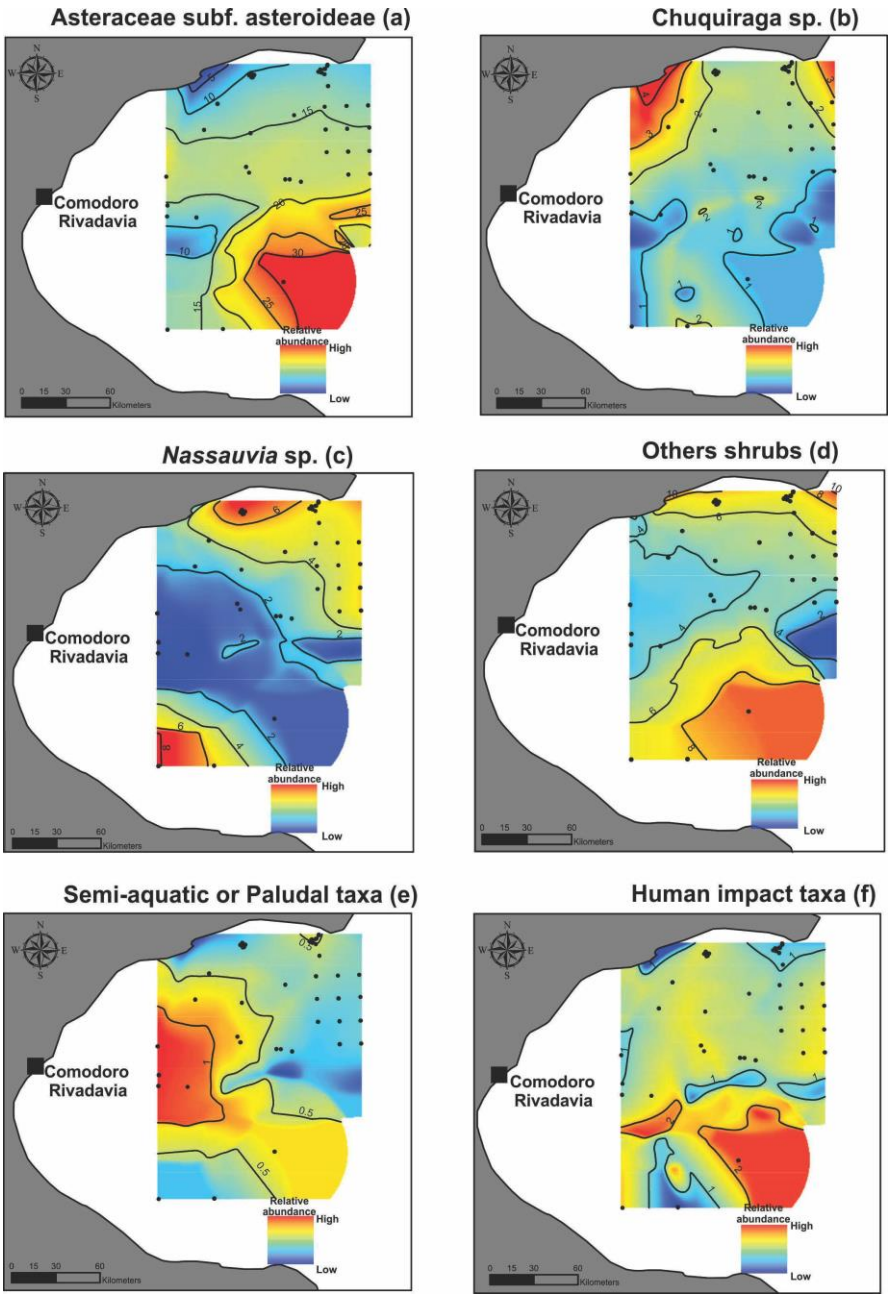

Figure 19. Isopollen map of Asteraceae subf. Asteroideae (a), *Nassauvia* sp. (b), *Chuquiraga* sp. (c), others shrubs (d), semi-aquatic / paludal taxa (Typha and Cyperaceae) (e) and human impact taxa (*Rumex acetosella*, Brassicaceae, Asteraceae subf. Asteroideae) (f).

Low pollen abundance of shrubby plants was found in surface samples, with the exception of *Colliguaja integerrima*, *Ephedra* sp. and Asteraceae. In fact, a large number of the shrub taxa present in the vegetation adjacent to the SJG (Verbenaceae, Rhamnaceae, Fabaceae) release little amounts of pollen because they are entomophilous (insect-pollinated) (e.g. Mancini, 1993; Cross et al., 1966; Medan and Arce, 1999). As a result, they are underrepresented in the surface marine sediments; nevertheless, their relatively high abundances in the northern and southern parts of the gulf are consistent with the presence of these taxa along the coastline of the SJG (Figure 19d). *Colliguaja integerrima* shows maximum pollen abundance to the north and decreases towards the southern-central part of the SJG, while *Ephedra* sp. is abundant in the central part of the SJG (Figure 18e-f). The maximum abundance of *Colliguaja integerrima* in surface samples from the north of the SJG corresponds to those found on continental areas north of the SJG (e.g. Paez et al., 2001). The distribution pattern of this species in marine surface sediment is consistent with the occurrence of *Colliguaja* in the adjacent continent (Figure 14). Asteraceae include several species (*Senecio filaginoides*, *Nardophyllum obtusifolium*, *Grindelia chilense*, *Baccharis darwinii*, *Perezia recurvata*) from the Patagonian steppe, which show an increase in the southern part of the SJG (Figure 19a). The distribution pattern of other species from Asteraceae, such as *Nassauvia* sp. and *Chuquiraga* sp., shows high abundance, the former in the northern and southern parts of the SJG, and the latter in the northern part only. The high abundance of *Chuquiraga* sp. shrubs in the north and northeast of the SJG is in agreement with high values of *Chuquiraga* pollen found in continental samples located northeast of the gulf (Paez et al., 2001; Figure 14).

We noticed a strong correspondence between marine surface patterns and continental/terrestrial surface pollen patterns of certain taxa (e.g. *Colliguaja integerrima*, *Chuquiraga* sp., Chenopodiaceae and Poaceae) with the location of their vegetation source, which shows that the marine pollen dispersal patterns are reflecting the vegetation adjacent to the SJG. It is important, to note that we are not compared our samples with top core samples in the Groot et al. study because those deep sea cores are too distant from the SJG.

Furthermore the top core samples from such cores might not represent modern conditions because piston coring usually disrupts the water-sediment interface.

Semi-aquatic or paludal taxa (Cyperaceae and *Typha*) are recorded in low percentages along the SJG probably due to the absence of major river input in the gulf (Figure 19e). Also, according to Mancini et al. (2008), the poor representation (low pollen values) of pollen types indicating human impact (Brassicaceae, *Rumex acetosella*, Asteraceae subf. Cichorioideae) suggest lesser effect in the Patagonian steppe than in the grass steppe of extra-Andean regions (Figure 19f).

2.7.3 Vegetation changes along SJG

To document the latitudinal changes in pollen assemblages from the SJG in relation to the adjacent Patagonian phytogeographical provinces, the sediment samples were arranged from north to south along the gulf (Figures 16 and 20). The vegetation around the SJG is characterized by some latitudinal variations with a high shrub steppe dominated by *Colliguaja integerrima* in the northern part of the gulf, and grassy shrub steppe dominated by low shrub (Asteraceae, Apiaceae, Fabaceae, Verbenaceae etc.), with an increase of herbaceous component (Poaceae, Cheno-am) towards the southern-central part of the gulf (Figure 14). The pollen spectra echo these changes with a slight increase of Asteraceae pollen, low shrubs and herbaceous pollen (Cheno-am and Poaceae) in the southern-central part of the SJG, as opposed to the strong presence of high shrub pollen (*Colliguaja integerrima*.) in the northern part of the SJG (Figure 20).

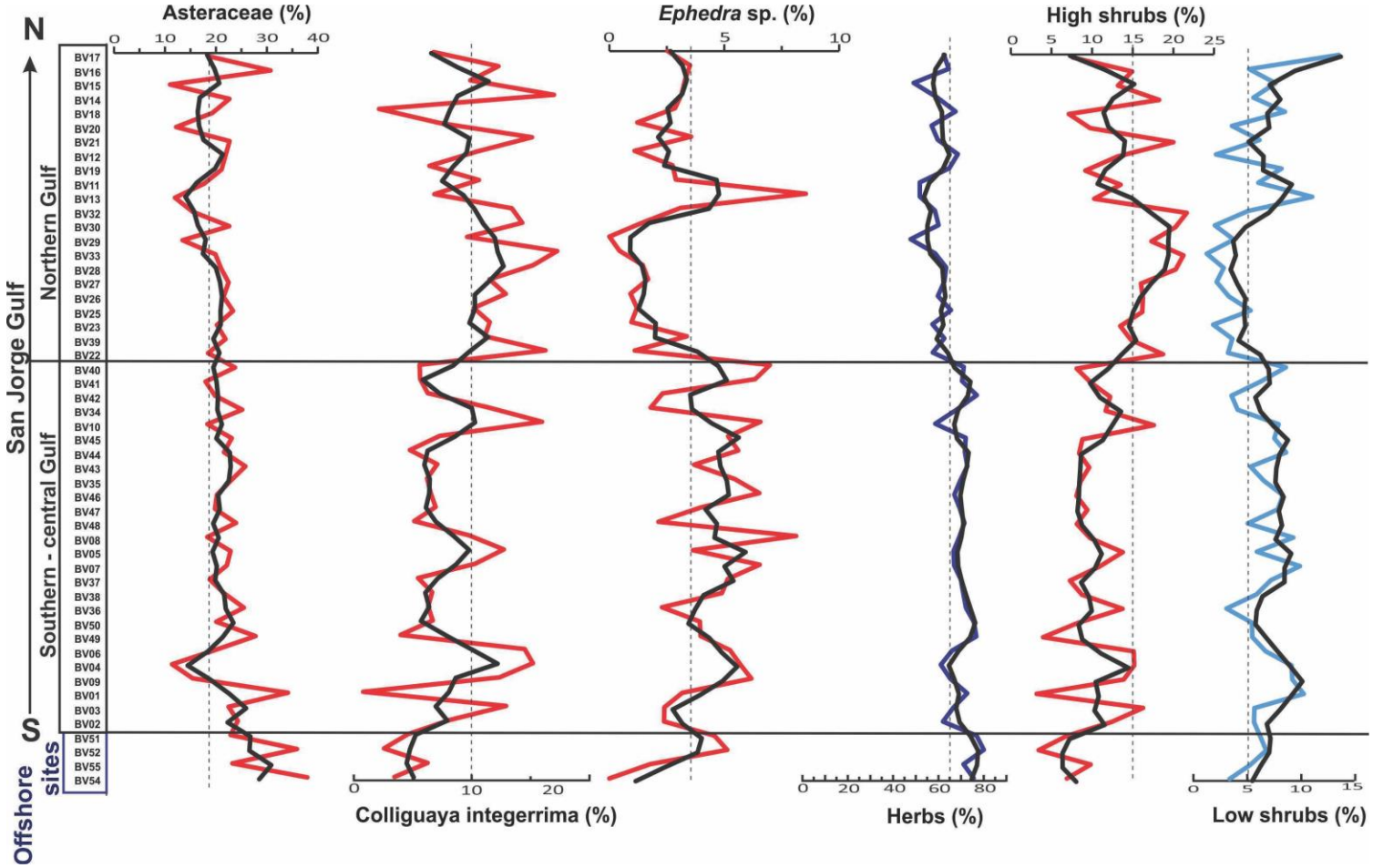

Figure 20. Relative abundance of selected pollen taxa in modern surface sediments in the SJG. Note that Asteraceae = Asteraceae subf. Asteroideae + *Chuquiraga* sp. + *Nassauvia* sp. and High shrub (*Colliguaja integerrima* + Rhamnaceae + *Schinus* sp. + Solanaceae type. + *Lycium* sp.).

To understand the ecological significance of the minor vegetation changes along the SJG, we investigated the ecological requirements of herbs and shrubs in semiarid ecosystems. Patagonian steppe shrubs and herbs have two different root patterns and compete for water and nutrients in the upper layer of the soil (Soriano and Sala, 1984, Sala et al., 2012). According to Soriano and Sala (1984), the herbs are opportunistic species with shallow root systems and can grow rapidly with water availability, while shrubs have a deep root systems and therefore have access to water in lower soil layers. On this basis, the main factor that could explain the increase of herbs and the decrease of high shrubs (e.g. *Colliguaya integerrima*) towards the central and southern continental areas around the SJG could be soil moisture related to others edaphic factors (e.g. substrate variability, altitude, slope orientations, runoff, organic matter, etc.; León et al., 1998; Mancini et a., 2012).

2.7.4 Transport pathway of pollen in SJG

We note that the pollen of Asteraceae (e.g. Asteraceae subf. Asteroideae, *Nassauvia* sp.) and herbaceous plants (e.g. Poaceae and Cheno-am) are transported further offshore (Figure 20). Indeed, most of these plants (Poaceae, Cheno-am, *Senecio* sp., *Baccharis* sp. *Nassauvia* sp.) are anemophilous and the pollen they produce is transported preferentially by the wind far from the coast (e.g., cross et al., 1966; Arroyo et al., 1982; Forcone, 2008; Velásquez et al., 2015). The decrease of pollen concentrations in offshore sites (Figure 16) is consistent with previous studies where wind is the major vector of pollen transport (Melia, 1984). In the absence of major river inputs in the SJG, the pollen is mainly transported by westerly winds, which are the main vectors of transport of pollen in modern sediments. Otherwise, pollen transported by rivers located south of the SJG can then be carried to the SJG by coastal currents. However, the low concentrations of ciliate estuarine palynomorphs (e.g. *Halodinium*) from mixing boundary between those rivers and Atlantic Ocean reflect minor effect of river inputs in the southern-central part of the SJG (Faye et al., 2018). In addition, freshwater palynomorphs (*Pediastrum*) are almost absent (except BV15) from marine surface sediment in the SJG (e.g. Evitt, 1963). Therefore, we conclude that river / marine inputs have little effect in pollen assemblages in the SJG. Thereby, the pollen assemblages found in surface sediments mainly reflect the dynamic processes in the

atmosphere. The high pollen concentrations in the central part of the SJG are similar to that of dinocyst assemblages from the same samples (Faye et al., 2018) and are correlated with the fine particle size of the sediments in the central part of the gulf (Figure 21). This suggests that marine transport is superimposed over the wind transport. Indeed, pollen grains and dinocysts have the same size as silts and tend to be remobilized by ocean currents before being concentrated, preferably with the fine grain sediments (e.g., Cross et al., 1966; Heusser, 1983).

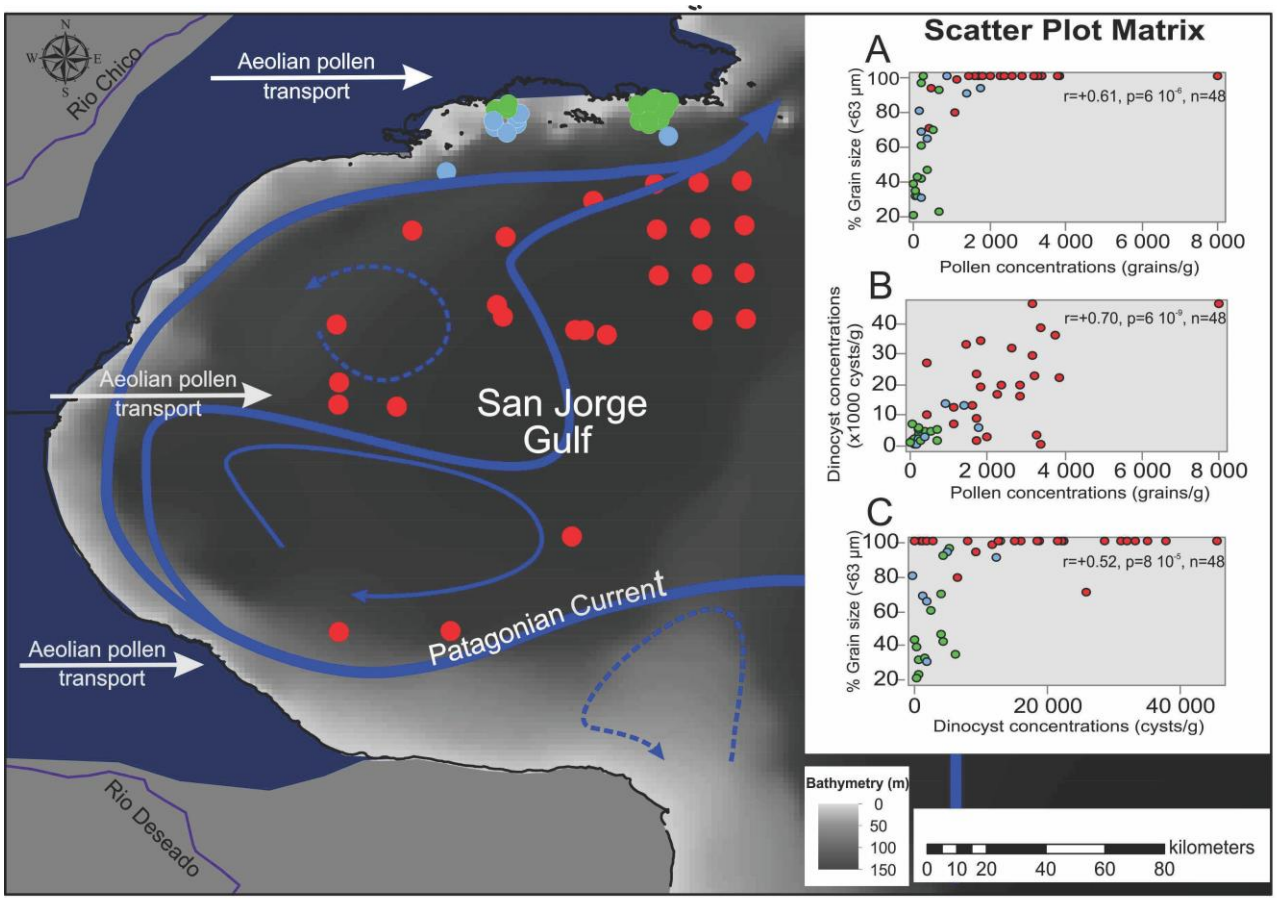

Figure 21. Spatial distribution of pollen zones with the color code used in Fig. 15 and bivariate correlations (r = correlation coefficient) showing positive correlation of fine grain size and high pollen concentrations (A), positive high correlation of high dinocyst and pollen concentrations (B) and positive correlation of fine grain size and high dinocyst concentrations (C). The blue on the continent represent the delimitation of the SJG phytogeographical unit.

2.8 CONCLUSION

In summary, the pollen distribution patterns indicate high pollen concentrations in the central part of the SJG, and low pollen concentrations in the northern and southern part of the gulf, as well as at offshore sites. Due to the wide distribution of several taxa in the Patagonian steppe, we noted some latitudinal variations in pollen dispersal pattern along the SJG marked by a slight increase of herbs and low shrubs pollen towards the southern-central part of the Gulf with a strong presence of high shrub pollen (e.g. *Colliguaja*) in the northern part of the SJG. This change echoes the vegetation around the SJG and some of the patterns described here depict a relatively good correspondence with continental modern pollen patterns:

- The highest abundance of *Colliguaja integerrima* and *Chuquiraga* sp. in the north of the SJG echo their corresponding continental pollen patterns around the SJG. Therefore, their distribution is consistent with the abundance of these species around the SJG;
- The high abundances of Poaceae and Chenopodiaceae pollen in the Southern-central part of the gulf emphasizes the adjacent continental pollen distribution patterns and are correlated with the occurrence of these taxa around the SJG;
- Overall, the pollen distribution patterns from surface sediments samples reflect the vegetation around the SJG and will be used as modern-analogues to document past variations of the vegetation around the SJG.

Pollen transport in the SJG appears to be controlled mainly by the SWWB in combination with surface currents flowing through the SJG. The abundance of *Nothofagus* and *Podocarpus* transported over long distances by wind will be used as wind-intensity proxy to test/assess the efficiency of the SWWB at the latitude of the SJG and to document the dynamics of the Andean Patagonian /subantarctic forest in response to climate change during the Late Pleistocene and Holocene.

2.9 ACKNOWLEGEMENTS

This research was supported by the financial support of the FRQNT (*Fonds de recherche du Québec – Nature et technologies* to G. St-Onge and A. Rochon), and NSERC Discovery grants to A. Rochon and G. St-Onge. The first author benefited from scholarships from ISMER-UQAR and GEOTOP. I also wish to thank the Réseau Québec maritime (RQM) and the FRQNT for funding my internship for learning palynological techniques in Argentina at the *Museo Argentino de Ciencias Naturales BR*. Special thanks to Cynthia Gonzales and Magdalena Llorens (*Herbarium of Universidad Nacional de la Patagonia San Juan Bosco*) who provided pollen material to establish our reference slides. We thank Cristina Telleria for her help in the distinctions of *Chuquiraga* and *Nassauvia* taxa. We thank the Meteorological National Service of Argentina for meteorological data. We wish to thank the anonymous reviewers for their comments, which help improving the manuscript. We are grateful to the captain, officers, crew and scientists of the MARGES expedition on board the R/V Coriolis II. Finally, we wish to thank the *Ministerio de Ciencia, Tecnología e Innovación Productiva,* MINCyT,the Province of Chubut and the *Consejo Nacional de Investigaciones Científicas Técnicas*, CONICET) for the MARGES and MARES expeditions.

2.10 REFERENCES

Agosta, E., Compagnucci, R., Ariztegui, D., 2015. Precipitation linked to Atlantic moisture transport: clues to interpret Patagonian palaeoclimate. Clim. Res. 62 (3), 219–240.

Anderson, R.F., Ali, S., Bradtmiller, L.I., Nielsen, S.H.H., Fleisher, M.Q., Anderson, B.E., Burckle, L.H., 2009. Wind-driven upwelling in the Southern Ocean and the deglacial rise in atmospheric CO2. Science 323, 1443–1448. https://doi.org/10.1126/science.
1167441.

Arana, M.D., Martínez, G.A., Oggero, A.J., Natale, E.S., Morrone, J.J., 2017. Map and shapefile of the biogeographic provinces of Argentina. Zootaxa 4341, 420. Doi:10.11646/zootaxa.4341.3.6.

Aravena, J.-C., Luckman, B.H., 2009. Spatio-temporal rainfall patterns in Southern South America. Int. J. Climatol. 29, 2106–2120. https://doi.org/10.1002/joc.1761.

Arroyo, M.T.K., Primack, R., Armesto, J., 1982. Community studies in pollination ecology in the high temperate Andes of Central Chile. I. Pollination mechanisms and altitudinal variation. Am. J. Botany 69 (1), 82–97.

Bertrand, S., Hughen, K., Sepúlveda, J., Pantoja, S., 2014. Late Holocene covariability of the southern westerlies and sea surface temperature in northern Chilean Patagonia. Quat. Sci. Rev. 105, 195–208.

Borromei, A.M., Musotto, L.L., 2016. Vegetation and Climate in Southern South America during Marine Isotope Stage 3 (MIS 3): An Overview of Existing Terrestrial Pollen Records. Springer, Berlin Heidelberg, New York, NY.

Brandhorst, W., Castello, J.P., 1971. Evaluación de los recursos de anchoíta (Engraulis anchoita) frente a la Argentina y Uruguay. Serie de Informaciones Técnicas.

Bullard, J.E., Baddock, M., Bradwell, T., Crusius, J., Darlington, E., Gaiero, D., Gassó, S., Gisladottir, G., Hodgkins, R., McCulloch, R., McKenna-Neuman, C., Mockford, T., Stewart, H., Thorsteinsson, T., 2016. High-latitude dust in the Earth system: High-Latitude Dust in the Earth System. Rev. Geophys. 54, 447–485. https://doi.org/10.1002/2016RG000518.

Burry, L.S., D'Antoni, H.L., Frangi, J.L., 2005. Polen y vegetación en la Patagonia extraandina argentina a 45° S. In: Anales del Jardín Botánico de Madrid (Vol. 62, No. 2,pp. 143-152).

Bustamante, R.O., Simonetti, J.A., 2005. Is Pinus radiata invading the native vegetation in Central Chile? Demographic responses in a fragmented forest. Biol. Invasions 7, 243–249. https://doi.org/10.1007/s10530-004-0740-5.

Cabrera, A.L., 1947. La estepa Patagónica en Geogràfía de la republica Argentina. In: Ton VIII : 249–276. Geografica. GAEA con Editorial BS.AS, Sociedad Argentina de Estudios.

Cabrera, A.L., 1971. Fitogeografía de la República Argentina. Boletín de la Sociedad Argentina de Botánica. 14 (1-2), 1–50.

Cabrera, A.L., 1976. Regiones Fitogeograficas Argentinas. In Enciclopedia Argentina de Agricultura y Jardineria. II Editorial ACME, Buenos Aires.

Compagnucci, R.H., 2011. Atmospheric circulation over Patagonia from the Jurassic to present: a review through proxy data and climatic modelling scenarios: Patagonian paleo-atmospheric circulation. Biol. J. Linn. Soc. 103, 229–249. https://doi.org/10.1111/j.1095-8312.2011.01655.x.

Coronato, A.M.J., Coronato, F., Mazzoni, E., Vázquez, M., 2008. The physical geography of patagonia and tierra del fuego. In: Developments in Quaternary Sciences. Elsevier, pp. 13–55. https://doi.org/10.1016/S1571-0866(07)10003-8.

Cross, A.T., Thompson, G.G., Zaitzeff, J.B., 1966. Source and distribution of palynomorphs in bottom sediments, southern part of Gulf of California. Mar. Geol. 4 (6),
467–524.

Del Valle, H.F., Labraga, J.C., Goergen, J., 1995. Biozonas de la región Patagónica. Evaluación del estado actual de la desertificación en áreas representativas de la Patagonia: Informe Final de la Fase I. INTAGTZ 37–55.

Denton, G.H., Anderson, R.F., Toggweiler, J.R., Edwards, R.L., Schaefer, J.M., Putnam, A.E., 2010. The last Glacial termination. Science 328, 1652–1656. https://doi.org/10.1126/science.1184119.

Dupont, L., Wyputta, U., 2003. Reconstructing pathways of aeolian pollen transport to the marine sediments along the coastline of SW Africa. Quat. Sci. Rev. 22, 157–174. https://doi.org/10.1016/S0277-3791(02)00032-X.

Evitt, W.R., 1963. Occurrence of freshwater alga Pediastrum in Cretaceous marine sediments. Am. J. Sci. 261 (9), 890–893.

Faye, S., Rochon, A., St-Onge, G., 2018. Distribution of modern dinoflagellate cyst assemblages in surface sediments of the Gulf of San Jorge (Patagonia, Argentina) in relation to sea surface conditions. Oceanography 31 (4), 122–131. https://doi.org/10.5670/oceanog.2018.416.

Forcone, A., 2008. Pollen analysis of honey from Chubut (Argentinean Patagonia). Grana 47 (2), 147–158.

Garreaud, R., Lopez, P., Minvielle, M., Rojas, M., 2013. Large-scale control on the Patagonian climate. J. Clim. 26 (1), 215–230.

Garreaud, R.D., 2009. The Andes climate and weather. Adv. Geosci. 22, 3–11. https://doi.org/10.5194/adgeo-22-3-2009.

Glembocki, N.G., Williams, G.N., Góngora, M.E., Gagliardini, D.A., Orensanz, J.M.L., 2015. Synoptic oceanography of San Jorge Gulf (Argentina): a template for

Patagonian red shrimp (Pleoticus muelleri) spatial dynamics. J. Sea Res. 95, 22–35.

Groot, J.J., Groot, C.R., Ewing, M., Burckle, L., Conolly, J.R., 1965. Spores, pollen, diatoms and provenance of the Agentine basin sediments. Prog. Oceanogr. 4, 179–217.

Heusser, C.J., 1971. Pollen and Spores of Chile. University of Arizona Press.

Heusser, L.E., 1983. Pollen distribution in the bottom sediments of the western North Atlantic Ocean. Mar. Micropaleontol. 8, 77–88. https://doi.org/10.1016/0377-8398(83)90006-3.

Heusser, L.E., 1988. Pollen distribution in marine sediments on the continental margin off northern California. Mar. Geol. 80, 131–147. https://doi.org/10.1016/0025-3227(88)90076-X.

Hooghiemstra, H., Lézine, A.-M., Leroy, S.A.G., Dupont, L., Marret, F., 2006. Late Quaternary palynology in marine sediments: a synthesis of the understanding of pollen distribution patterns in the NW African setting. Quat. Int. 148, 29–44. https://doi.org/10.1016/j.quaint.2005.11.005.

Labraga, J.C., 1994. Extreme winds in the Pampa del Castillo Plateau, Patagonia, Argentina, with reference to wind farm settlement. J. Appl. Meteorol. 33 (1), 85–95.

León, R.J.C., Bran, D., Collantes, M., Paruelo, J.M., 1995. Grandes unidades de vegetación de la Patagonia extra andina. Ecologia Austral 8, 125–144.

León, R.J.C., Bran, D., Collantes, M., Paruelo, J.M., 1998. Grandes unidades de vegetación de la Patagonia extra andina. Ecología Austral 8, 125–144.

Lisé-Pronovost, A., St-Onge, G., Gogorza, C., Haberzettl, T., Jouve, G., Francus, P., Ohlendorf, C., Gebhardt, C., Zolitschka, B., 2015. Rock-magnetic proxies of wind intensity and dust since 51,200 cal BP from lacustrine sediments of Laguna Potrok Aike, southeastern Patagonia. Earth Planet. Sci. Lett. 411, 72–86. https://doi.org/10.1016/j.epsl.2014.11.007.

Mancini, M.V., 1993. Recent pollen spectra from forest and steppe of South Argentina: a comparison with vegetation and climate data. Rev. Palaeobot. Palynol. 77, 129–142. https://doi.org/10.1016/0034-6667(93)90061-X.

Mancini, M.V., 2009. Holocene vegetation and climate changes from a peat pollen record of the forest – steppe ecotone, Southwest of Patagonia (Argentina). Quat. Sci. Rev. 28, 1490–1497. https://doi.org/10.1016/j.quascirev.2009.01.017.

Mancini, M.V., Paez, M.M., Prieto, A.R., Stutz, S., Tonello, M., Vilanova, I., 2005. Mid-Holocene climatic variability reconstruction from pollen records (32°–52°S, Argentina). Quat. Int. 132, 47–59. https://doi.org/10.1016/j.quaint.2004.07.013.

Mancini, M.V., Prieto, A.R., Paez, M.M., Schäbitz, F., 2008. Late quaternary vegetation and climate of Patagonia. In: Developments in Quaternary Sciences. Elsevier, pp. 351–367. https://doi.org/10.1016/S1571-0866(07)10017-8.

Mancini, M.V., de Porras, M.E., Bamonte, F.P., 2012. Southernmost South America steppes: vegetation and its modern pollen-assemblages representation. In: Steppe

Ecosystems: Dynamics, Land Use and Conservation. Nova Science Publishers, Inc., New York, USA.

Marcos, M.A., Mancini, M.V., 2012. Modern pollen and vegetation relationships in northeastern Patagonia (Golfo San Matías, Río Negro). Rev. Palaeobot. Palynol. 171, 19–26. https://doi.org/10.1016/j.revpalbo.2011.11.007.

Markgraf, V., D'Antoni, H.L., 1978. Pollen Flora of Argentina. Arizona, University of Arizona Press, Tucson 208p.

Markgraf, V., D'Antoni, H.L., Ager, T.A., 1981. Modern pollen dispersal in Argentina. Palynology 5 (1), 43–63.

Matano, R., Palma, E., 2018. Seasonal Variability of the Oceanic Circulation in the Gulf of San Jorge. Argentina. Oceanography 31. https://doi.org/10.5670/oceanog.2018. 402.

Matano, R.P., Palma, E.D., Piola, A.R., 2010. The influence of the Brazil and Malvinas Currents on the Southwestern Atlantic Shelf circulation. Ocean Sci. 6, 983–995. https://doi.org/10.5194/os-6-983-2010.

Medan, D., Arce, M.E., 1999. Reproductive biology of the Andean-disjunct genus Retanilla (Rhamnaceae). Plant Syst. Evol. 218 (3–4), 281–298.

Melia, M.B., 1984. The distribution and relationship between palynomorphs in aerosols and deep-sea sediments of the coast off Northwest Africa. Mar. Geol. 58, 345–371. https://doi.org/10.1016/0025-3227(84)90208-1.

Moreno, P.I., Vilanova, I., Villa-Martínez, R., Dunbar, R.B., Mucciarone, D.A., Kaplan, M.R., Garreaud, R.D., Rojas, M., Moy, C.M., De Pol-Holz, R., Lambert, F., 2018. Onset and Evolution of Southern Annular Mode-like changes at Centennial Timescale. Sci. Rep. 8. https://doi.org/10.1038/s41598-018-21836-6.

Paez, M.M., Schäbitz, F., Stutz, S., 2001. Modern pollen–vegetation and isopoll maps in southern Argentina. J. Biogeogr. 28 (8), 997–1021.

Paruelo, J.M., Beltrán, A., Jobbágy, E., Sala, O.E., Golluscio, R.A., 1998. The climate of Patagonia: general patterns and controls on biotic processes. Ecol. Austral 8 (2), 85–101.

Piola, A.R., Avellaneda, N.M., Guerrero, R.A., Romero, S.I., 2009. Malvinas-slope water intrusions 36.

Rochon, A., Vernal, A.D., Turon, J.L., Matthiessen, J., Head, M.J., 1999. Distribution of recent dinoflagellate cysts in surface sediments from the North Atlantic Ocean and adjacent seas in relation to sea-surface parameters. Am. Assoc. Stratigraphic Palynologists Contribution Series 35, 1–146.

Sala, O.E., Golluscio, R.A., Lauenroth, W.K., Roset, P.A., 2012. Contrasting nutrientcapture strategies in shrubs and grasses of a Patagonian arid ecosystem. J. Arid Environ. 82, 130–135.

Soriano, A., 1956. Astectos ecológicos y pasturiles de la vegetación Patagónica relacionados con su estado y capacidad de recuperación. Revista de Investigacions Agropecuarias 10, 349–372.

Soriano, A., Sala, O., 1984. Ecological strategies in a Patagonian arid steppe. Vegetatio 56 (1), 9–15.

St-Onge, G., Ferreyra, G.A., 2018. Introduction to the Special Issue on the Gulf of San Jorge. Patagonia, Argentina.

Strub, P.T., Mesias, J.M., Montecio, V., Ruttlant, J., Salinas, S., 1998. Coastal Ocean Circulation of Western South America. The Global Coastal Ocean-Regional Studies and Syntheses.

Stutz, S., Prieto, A.R., Isla, F.I., 2006. Holocene evolution of the Mar Chiquita coastal lagoon area (Argentina) indicated by pollen analysis. J. Quat. Sci. 21, 17–28. https:// doi.org/10.1002/jqs.952. Tellier, S., Rodriguez, R., Serra, M.T., 2003. Lista preliminar aloctonas asilvestradas en chile Continental. Chloris: Revista chilena de flora y vegetacion 6 (2). http://www. chlorischile.cl.

Toggweiler, J.R., 2009. Climate change: Shifting Westerlies. Science 323, 1434–1435. https://doi.org/10.1126/science.1169823.

Velázquez, N.J., Burry, L.S., Fugassa, M.H., 2015. Palynological analysis of extinct herbivore dung from Patagonia, Argentina. Quat. Int. 377, 140–147.

ARTICLE 3

SOUTHERN WESTERLY WINDS AND PALAEO-OCEANOGRAPHY RELATIONSHIP IN THE SAN JORGE GULF (SW-ATLANTIC OCEAN, ARGENTINA) DURING LATE PLEISTOCENE AND HOLOCENE

3.1 RÉSUMÉ EN FRANÇAIS DU DEUXIÈME ARTICLE

La circulation atmosphérique dans l'hémisphère Sud est principalement contrôlée par les forts vents de la ceinture de vent d'ouest. Ces vents ont une influence significative sur la circulation océanique dans l'Atlantique Sud et le Pacifique Sud. Cependant, on connait peu de choses sur les changements de la ceinture des vents d'ouest et ses relations avec les conditions océaniques dans l'Atlantique Sud-Ouest. Ici, nous utilisons des assemblages de pollen et de kystes dinoflagellés enregistrés dans trois séquences sédimentaires prélévées dans le GSJ (Golfe de san Jorge) afin d'étudier l'histoire de la végétation dans la Patagonie orientale/extra-andine et les variations latitudinales de la ceinture des vents d'ouest liées aux changements océaniques dans le GSJ au cours du Pléistocène supérieur et de l'Holocène. Nos résultats suggèrent qu'avant 14 cal ka BP, le GSJ était caractérisé par un environnement subaérien. Durant cette période, la végétation était dominée par des taxons halophytes

probablement en milieu côtier dans des conditions arides. Après cette période, le spectre pollinique suggère des conditions semi-arides avec le développement de plantes arbustives et herbacées caractéristiques de la steppe patagonienne. Le pollen de *Nothofagus* sp., transporté par les vents d'ouest sur de longues distances est utilisé ici pour tester / évaluer l'efficacité de transport et l'intensité des vents d'ouest dans le GSJ . À cet égard, nous avons constaté de fortes abondances de pollen de *Nothofagus* au début de l'ACR (14 cal ka BP) révélant de forts vents d'ouest suivis d'un affaiblissement progressif au cours du Pléistocène supérieur. L'analyse des données palynologiques (assemblages de kystes de dinoflagellés) montre une immersion du GSJ après 14 ka BP marquée par l'apparition de palynomorphes marins. Durant cette période, les assemblages de kystes de dinoflagellés sont dominés par *Operculodinium centrocarpum* (~ 82%) et *Spiniferites mirabilis* (~ 8%). La codominance de ces deux taxons suggère des conditions tempérées durant la dernière terminaison glaciaire et le début de l'Holocène. Ensuite de l'Holocène inférieur à moyen, le GSJ est marqué par un changement drastique dans le réseau trophique mis en évidence par une augmentation des taxons hétérotrophes tels que *Brigantedinium* spp., *Echinidinium* sp. *Dubridinium* sp. et *Polykrikos kofoidii*. On note au cours de cette période, une intensification des vents d'ouest à la latitude du GSJ synchrone avec l'augmentation de la productivité primaire dans le golfe en raison la fertilisation du GSJ par les flux terrigènes. Au début de la Néoglaciation (après 4 cal ka BP), nous observons une diminution de l'intensité de la ceinture des vents d'ouest en corrélation avec les avancées glaciaires en Patagonie et les conditions tempérées chaudes dans le GSJ marquées par une augmentation de l'abondance de *Spiniferites mirabilis*.

Ce troisième article, intitulé «*Southern Westerly Winds and palaeo-oceanography relationship in San Jorge Gulf (SW-Atlantic Ocean, Argentina) during Late Pleistocene and Holocene*», a été rédigé par moi-même sous la supervision de mon directeur André Rochon (UQAR-ISMER), de mon co-directeur Guillaume St-Onge (UQAR-ISMER) et de mon superviseur de stage en Argentine Isabel Vilanova (CONICET-MACN). Le modèle d'âge et la description lithologique des carottes ont été effectués par Pierre-Arnaud Desiage. L'article sera soumis prochainement dans *Quaternary Science Reviews*. Une version préliminaire de l'article a été présentée sous forme orale au congrès de l'AGU en décembre 2019.

3.2 RÉSUMÉ EN ANGLAIS DU DEUXIÈME ARTICLE

Atmospheric circulation in the Southern Hemisphere is mainly controlled by the strong winds of the Southern Westerly Wind Belt (SWWB). These winds have a significant influence on ocean circulation in the South Atlantic and South Pacific Oceans. However, little is known about SWWB shifts and relationships with oceanic conditions in the South-west Atlantic Ocean. Here, we use pollen and dinoflagellate cyst assemblages recorded in three sedimentary sequences from the San Jorge Gulf (SJG) in order to study the vegetation history in the extra-Andean/eastern Patagonia (Argentina), and the latitudinal variations of the SWWB related to oceanic changes in the SJG during the Late Pleistocene and Holocene. Our results suggest that prior to 14 cal ka BP, the SJG was characterized by a subaerial environment and the vegetation was dominated by halophytic taxa probably under arid conditions in coastal environments. After this period, the pollen spectra suggest semi-arid environments with the development of shrubs and herbaceous in the Patagonian steppe. *Nothofagus* sp. pollen, transported by the westerly winds over long distances is used here to test/assess its efficiency as an indicator of the intensity of the SWWB. In this regard, we found that *Nothofagus* pollen abundances seem to reveal strong westerlies at the beginning of the Antarctic Cold Reversal (14 cal ka BP) followed by a gradual weakening during the Late Pleistocene. We also recorded a relative high sea level in the SJG after 14 cal ka BP, as reflected by the dominance of *Operculodinium centrocarpum* (~ 82%) and *Spiniferites mirabilis* (~ 8%) in the South Atlantic Ocean. The codominance of these two taxa suggests temperate conditions during the Last Glacial termination and Early Holocene. During the Early and Mid-Holocene, the SJG is marked by a drastic shift in the food web in South Atlantic Ocean, highlighted by an increase of heterotrophic taxa such as *Brigantedinium* spp., *Echinidinium* sp. *Dubridinium* sp. and cysts of *Polykrikos kofoidii*. We note during this period high intensity of the westerly winds at the latitude of the SJG, coeval with high primary productivity in the gulf. At the beginning of the Neoglaciation (after 4 cal kyr BP), we observe a decrease in the SWWB intensity that correlates with glacier advances in

Patagonia and warm temperate conditions in the SJG, as indicated by an increase of *Spiniferites mirabilis* abundance.

3.3 INTRODUCTION

The Southern Westerlies Wind Belt (SWWB) controls the atmospheric circulation in the southern mid-latitudes and plays a key role in the global climate (e.g., Anderson and 2009; Denton et al., 2010). These winds exhibit an equatorward/poleward shift (up to 10° of latitude) during glacial/interglacial timescales respectively (Toggweiler et al., 2006). Studies have shown that at the end of the last glacial period, the poleward position of the SWWB induced enhancement of the Antarctic Circumpolar Current (ACC), wind driven-upwellings in the South Atlantic, CO_2 ventilation from the deep ocean to the atmosphere, and increased warming (Anderson and 2009; Denton et al., 2010). The present-day seasonal variations of these winds vary according to the surface temperature changes of the Southern Ocean that control the position of the subtropical high pressure belt. During the austral winter, the SWWB extends northward, while during the austral summer the SWWB contracts and intensifies in the south due to the southward shift of the subtropical high pressure belt (Lamy et al., 2010). The seasonal variations of the SWWB are also influenced by some phenomena (e.g., Southern Annular Mode: SAM, El Niño Southern-Oscillation: ENSO, Antarctic Oscillation: AAO), which influence temperature variations in the Southern Ocean at inter-annual timescales (Moy et al., 2009, Moreno et al., 2018).

Southern South America (Patagonia, 39-55°S) is the only continental mass intercepting the core of the SWWB and constitutes a key region for documenting the latitudinal shifts of these winds (Lamy and Kilian, 2012; Moreno et al., 2018). The latitudinal variations of the SWWB are relatively well documented during the glacial/interglacial phases (Toggweiler et al., 2006). In contrast, studies during the present interglacial (Holocene) are sometimes contradictory and have been discussed in the literature (e.g., Heusser, 1989; Markgraf, 1989, Lamy et al., 2010; Moreno et al., 2010, Fletcher and Moreno 2011). These divergences are due to the fact that several paleo-wind studies were based on precipitation/moisture proxies, relying on a single site along the core of the SWWB, which prevented accurate reconstructions of the latitudinal position of these winds (Bertrand et al., 2014). To overcome

this limitation, some authors used palaeo-wind proxies at several sites located along the northern/southern path of the SWWB (Moreno et al., 2010, Lamy et al., 2010), correlated with palaeo-temperature reconstructions to obtain a synoptic view of past latitudinal variations of the SWWB (Lamy et al., 2010). However, even with this innovative methodology, the contradictions remain especially for the Early Holocene (Fletcher and Moreno 2011). These apparent contradictions may be due to some proxies that could be affected by sedimentary processes, palaeohydrological changes and sea level variations (Fletcher and Moreno 2011; Kilian and Lamy, 2012). In addition, the non-linear shifts of moisture - SWWB shifts relationship, and the paucity of robust dated archives and reservoir effect on age models can complicate the interpretations (Moreno et al., 2010; Kilian and Lamy, 2012).

Various studies in Patagonia overview the latitudinal shifts of the SWWB during the Holocene, but the major part of palaeo-wind records were derived from precipitation/moisture proxies, mostly obtained from lakes and fjords located along the western slope of the Andes Cordillera, where precipitations are strongly correlated with the SWWB (e.g., Kilian and Lamy, 2012; Moreno et al., 2018). On the contrary, along the eastern slope of the Andes (eastern-Patagonian steppe) precipitations display a negative correlation with the SWWB (e.g., Mayr et al., 2007; Lisé-Pronovost et al., 2014; Moreno et al., 2018). In addition, the reconstructions of the Pacific Ocean sea surface temperatures were established in relation to the westerlies position covering nearly 10° of latitude in the South Pacific, which has made possible to follow the oceanic evolution in relation to the position of the SWWB (Bertrand et al., 2014), whereas, there is no record of palaeo-wind intensities in the Argentine Continental Shelf (ACS) area.

In this regard, here we used three sedimentary sequences (06PC, 08PC, 11PC) collected from the SJG (45 and 47°S, on the ACS) located in the path of the SWWB to overcome these disparities in order to investigate the variation of the SWWB and its influence on the oceanic conditions and productivity changes in the South Atlantic since the Last Glacial termination. In this study, we used dinoflagellate cysts (dinocysts), sedimentological data and pollen

records to explore the SWWB/Southern Ocean coupled system. More specifically, we use pollen record to document the vegetation history adjacent to the gulf and dinocyst assemblages to document the evolution of ecological changes in the gulf in relation to stratigraphical/geochronological data and sea level variations in the SJG. In particular, we used *Nothofagus* pollen, transported over 350 km from southwestern Patagonian forests to the SJG to document the evolution of these forests and testing/assessing its efficiency as a wind intensity proxies (e.g., Faye et al., 2020). Finally, we compared our paleo-records to paleoclimate archives and glacier history in Patagonia to document the latitudinal shifts of the SWWB since the Last Glacial Termination.

3.4 STUDY AREA

The Patagonia region is located between 39° and 55° S over the southern tip of South America. The Andes Cordillera constitutes the main feature of this zone and it is characterized by high relief (~ 1500 m above sea level, in Chilean Patagonia) to the west and low relief and plains towards the east of this range, up to the Atlantic coast (Garreaud et al., 2013, Figure 22A). The Patagonian region supports three major icefields (North Patagonian Icefield, South Patagonian Icefield, Darwin Cordillera Icefield) which are sensitive to precipitations (Rignot et al., 2003) and glacial/interglacial cycles (e.g., Rabassa, 2008). During the LGM, these icefields formed a single ice sheet close to 2500 km in length along western Patagonia (36°S and 56°S, Rabassa et al., 2008, Figure 22A). During glacial cycles, Patagonia constituted a source of dust in Antarctica (e.g., Basile et al., 1997; Delmonte et al., 2010) and probably fertilized the Southwest Atlantic Ocean (e.g., Paparazzo et al., 2018). Indeed, the Southwest Atlantic Ocean constitutes nowadays the largest HNLC (High Nitrate low chlorophyll) zone in the world (NASA) and the primary production is limited by iron (Fe) in this area (Johnson et al., 2011; Gledhill and Buck, 2012). Patagonia represents the only source of Fe by aeolian inputs, including volcanic ash (e.g., Simonella et al., 2015;

Johnson et al., 2011; Crespi-Abril et al., 2018). As a result, the Southwest Atlantic is ideal to trace the strengthening/weakening of the SWWB related to palaeoproductivity.

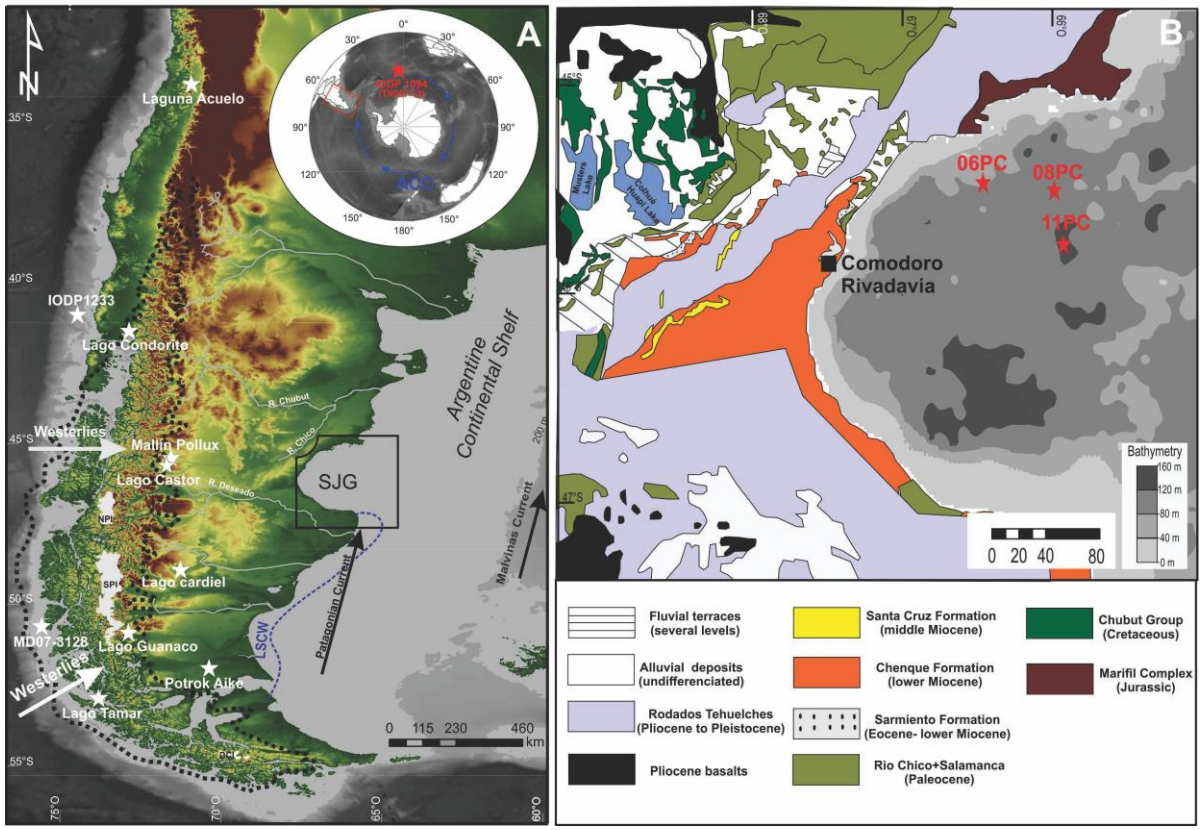

Figure 22. (A) Map of southern Patagonia and ocean circulation on the Argentine Continental Shelf illustrating the Malvinas Current, Patagonia Current and Low Salinity Coastal Water (LSCW in blue dashed line), the limits of the Last Glacial Maximum icefield in black dashed line (Hulton et al., 1994), Northern Patagonian Icefield (NPI), Southern Patagonian Icefield (SPI), Darwin Cordillera Icefield (DCI), Southern westerly wind belt (SWWB) and site locations used in the text. (B) Simplified geological map of the SJG (modified after Foix et al., 2013 and Paredes et al., 2015).

Our study area, the San Jorge Gulf (SJG), is located along the central part of Patagonia between latitude 45°S and 47°S on the Argentine Continental Shelf (ACS, Southwest Atlantic coast, Figure 22). The SJG is an extensional basin related to the fragmentation of the Gondwana supercontinent during the Late Jurassic and Early Cretaceous (Fitzgerald et al., 1990; Foix et al., 2013; Paredes et al., 2015). The early stage of the rift is represented by the Marifill Complex composed of volcanic rocks (Foix et al., 2013). After this period, the basin was filled by sedimentary formations representing various depositional settings related to sea level fluctuations and extensional tectonics, and with an outcrop in the adjacent continent around the SJG (Foix et al., 2013; Paredes, 20015, Figure 22B). The uppermost Jurassic and Lower Cretaceous are composed of lacustrine sedimentary rocks (Las Heras Group) followed by Cretaceous continental sediments of the Chubut group. From the Paleocene to the Pliocene, the sedimentation in the SJG basin is represented by a succession of sedimentary formations, which suggest estuarine (e.g. Salamanca Formation), fluvial (e.g. Rio Chico), pyroclastic (Sarmiento Formation), shallow marine (Chenque Formation) and fluvial/aeolian (e.g. Santa Cruz formation) depositional contexts (Nullo and Combina, 2002; Paredes, 2002; Foix et al., 2013). The late Quaternary deposits suggest that during the Last Glacial period the SJG was exposed and eroded by a palaeofluvial network (Desiage, 2020). This drainage system incised channels and valleys filled with a possible succession of fluvial and lagoonal/estuarine deposits, which were overlain by hemipelagic deposits during the Late Pleistocene and Holocene (Desiage, 2020).

The general ocean circulation on the ACS is characterized by the northward flowing Malvinas Current (MC) along the edge of the continental slope, and the Patagonian Current (PC) on the continental shelf (Matano et al., 2010; Matano and Palma, 2018). The MC transports cold salty (> 34) and nutrient-rich subantarctic waters (Piola et al., 2009), while the PC is mainly composed of subantarctic low saline waters from the Strait of Magellan, which enters into the SJG from the south (Brandhorst and Castello, 1971). In the gulf, the ocean circulation consists of two distinct patterns (austral summer and winter modes) that drive seasonal circulation variability (Matano and Palma, 2018) with a maximum intrusion

of PC in summer due to the strengthening of the SWWB southward (Matano and Palma, 2018).

The SWWB and Andean Cordillera strongly influence the climate and control the latitudinal distribution of rainfall in Patagonia (Garreaud et al., 2013). Indeed, the Andean Cordillera interrupts the SWWB that brings humid air from the Pacific. This causes shadow rainfall (> 1000 mm/year) in the western Andes, while the eastern part remains dry (< 200 mm/year, Coronato et al., 2008; Aravena and Luckman, 2009; Garreaud, 2009). This is why eastern Patagonia is characterized by a semi-arid climate, whereas western Patagonia has a very humid climate subjected to the oceanic influence from the Pacific (Borromei and Musotto, 2016). On the Atlantic fringe, precipitations are controlled by trade winds that bring intense rainfalls to central Patagonia (Agosta et al., 2015).

The vegetation of Patagonia is subjected to altitudinal and latitudinal variations, which are reflected by different vegetation units: (I) **The Andean Patagonian/Subantarctic forest,** which extends over the humid temperate (>1000 mm/year) section of the western and the eastern fringe of the Andes. This vegetation unit is dominated by species of the genus *Nothofagus* (*N. pumilio, N. antarctica, N. dombeyi*), along with *Podocarpus nubigena, Pilgerodendron uviferum* and *Drimys winteri* (Borromei and Musotto, 2016). (II) **The Monte,** is characterized by xerophytic woodlands and a shrub steppe of *Prosopi*s and *Larrea* (> 200 mm/year), located in northwestern Patagonia (León et al., 1998). (III) **The Patagonian steppe** occurs in semi-arid environments (100-300 mm/year). The vegetation is represented by a shrubby to herbaceous steppe, with several physio-floristic species: *Festuca pallescens, Nassauvia* spp., *Chuquiraga aurea, Ephedra frustillata, Chuquiraga avellanedae, Colliguaja integerrima, Verbena tridens, Schinus polygamous* and *Lycium chilense* (León et al., 1998). Around the SJG, there are high shrub dominated by *Colliguaja integerrima* and grassy shrub steppes dominated by Poaceae (León et al., 1998).

3.5 MATERIAL AND METHODS

3.4.1 Coring and sampling

This study is part of the large PROMESSe (*PROgrama Multidisciplinario para el Estudio del ecosistema y la geología marina del golfo San Jorge y las costas de las provincias de Chubut y Santa Cruz*) multidisciplinary program. In the framework of this program, the MARGES (*MARINE GEOLOGY, sedimentology, stratigraphy, basin architecture and paleoceanography of San Jorge* Gulf) oceanographic survey was carried out from February 17 to March 4, 2014 (St-Onge and Ferreyra, 2018). During this expedition, the SJG was sampled at five sites using a piston corer from the R/V Coriolis II. Three piston cores (06PC, 08PC, 11PC), from the coast to offshore, were selected based on the continuity of the sedimentary record (without major disturbances and hiatuses) and the consistence of the radiocarbon ages.

3.4.2 Imaging and XRF analysis

Sedimentological records were processed in the laboratory. Prior to sub-sampling, X-ray images, photography, diffuse spectral reflectance, semi-quantitative minor/major (Ti, Mn, Fe, Zn, Rb, Sr, Al, Si, S, k, Ca etc.) elements by X-ray fluorescence (XRF) were performed on the cores (for more information see Desiage, 2020). We analyzed the XRF Ti data because this element reflects the aeolian inputs in coastal environment and it is generally associated to coarser sediment (Peterson et al., 2000; Croudace and Rothwell, 2015; Faye et al., 2019). Other analyzed elements (Al, Si, K, and Rb) are related to siliclastic inputs and terrigenous fraction abundance (Jansen et al., 2000; Croudace and Rothwell, 2015), whereas Sr represent the biogenic fraction (e.g. Croudace and Rothwell, 2015; Desiage, 2020). In addition, Ca could depict marine carbonates (Desiage, 2020). However, the co-variance of Sr and Ca in the records (06PC, 08 PC and 11PC) suggest that Ca could reflect mostly biogenic fraction (Croudace and Rothwell, 2015). As a result Ti/Ca and Al+Si+K+Ti+Rb/Ca+Sr ratios were used to differentiate marine/biogenic from lithogenic/siliclastic inputs.

3.4.2 Chronology

The chronology of the three sedimentary records (06PC, 08PC, 11PC) is based on 13 samples of bivalve shells (complete or fragments) dated at the W. M. Keck Carbon Cycle AMS laboratory (University of California, Irvine). In addition, 2 micro-fragments of wood and algae (08PC) were dated by AMS ^{14}C at the LSCE (Laboratoire des sciences du climat et de l'environment, CNRS-CEA-UVSQ, Desiage, 2020). The age model was calibrated using the software CALIB version 7.1 (Stuiver and Reimer, 1993) and the Marine13 calibration curve (Reimer et al., 2013) with age reservoir correction ($\Delta R = 0$, Desiage, 2020). The age model was built by Desiage (2020) using the Bayesian age model (BACON v2.2 package) on R software (Blaauw and Christen, 2011, Figure 23).

3.4.2 Grain-size analysis

The particle size analyses (0.04-2000 µm) were carried out on the samples using a Beckman Coulter Particle Size Analyzer LS 13 320 (Desiage, 2020). Prior to analysis, the samples were processed with chemical pre-treatment to remove organic matter (H_2O_2, 30%) and carbonates (HCl, 0.5 M). From the results, we used the median (D50) and 90th percentiles (D90). Additionally, a distribution map of grain-size (sand, coarse silt, medium silt, fine silt and clay) was made along the cores (Figure 24).

3.4.3 Lithostratigraphy

Four lithological units were defined on the basis of visual description, imaging, XRF data, grain-size analysis and radiocarbon ages (Figure 23, Desiage, 2020). The lowermost unit (**U1**) is recorded only in core 06 PC, for which we do not have any radiocarbon ages prior to 14 cal ka BP. This sequence is composed of grayish brown silt (U1a), olive gray silty clay (U1b), light olive gray clayed silt with planar laminations at the top (Uc) and grayish brown clayed silt (U1d). Unit **U2** was identified only in core 08PC. There is no radiocarbon age for this sequence, but it is older than 12.7 cal yr BP. This section is composed by indurated grayish brown (U2a)/olive (U2c) gray clayey silt with planar laminations up to the top interbedded with grayish brown gravelly mud (U2b). The Holocene hemipelagic units

(U3 and U4) are recorded in all cores (06PC, 08PC, 11PC). Unit **U3** corresponds to light olive gray clayey silt with intact and fragmented bivalve shells, which are present sometimes as shell beds (U3c). This highly bioturbated unit overlays U1 in 06 PC and U2 in 08 PC. In core 08PC, the base of U3 presents sandy layers (U3a) and sharp erosional sandy layer contacts with gravels (U3b). Unit U3 is capped by a slightly bioturbated unit (**U4**) which is characterized by olive gray silty clay with some intact and fragmented bivalve shells. Unit U3 exhibits high sedimentation rates at the bottom of 06PC (∼150 cm/kyr), which gradually decrease towards the top of the unit (6-27 cm/kyr, in 06PC and 08PC) and in the uppermost part of U4 (Desiage, 2020). The sedimentation rates in U4 vary between 8-25 cm/kyr in the proximal cores (06 and 08PC) and reach exceptionally 50 cm/kyr in the distal core 11PC (Figure 22, Desiage, 2020).

Three sedimentary records (06PC, 08PC and 11PC) were correlated to constrain the stratigraphy. The XRF data and grain size analyses altogether support the correlations and lithological identification of the four units, in spite that all units were not recovered in every core, the presence of lateral variations in the thickness of the units and the lack of radiocarbon ages at the base of all cores (Figure 23). Unit U1 (06 PC) yielded relatively low values of Ti/Ca and Al+Si+K+Ti+Rb/Ca+Sr ratios, whereas high values were recorded in U2 (08PC). These ratios are relatively low in U3 and slightly increase upward (U4). The grain-size data in units U1 and U3 exhibit a pluricentrimetric variations of the D90 (avg. 26 µm in U1 and avg. 29 µm in U2) and relative constant median (D50) values (avg. 6 µm in U1 and avg. 9 µm in U2). In U3 and U4, the median is relatively constant (avg. 6 µm in 06 PC-08 PC and 5 µm in11 PC) except for some sandy levels (e.g., 212-224 cm in 08PC), whereas the D90 highlights pluricentimetric variations in U3 (avg. 25 µm in 06PC, 56 µm in 08PC and 18 µm in 11PC), and relative constant values in U4 (avg. 21 µm in 06PC, 20 µm in 08PC and 17 µm in 11 PC, Figure 23).

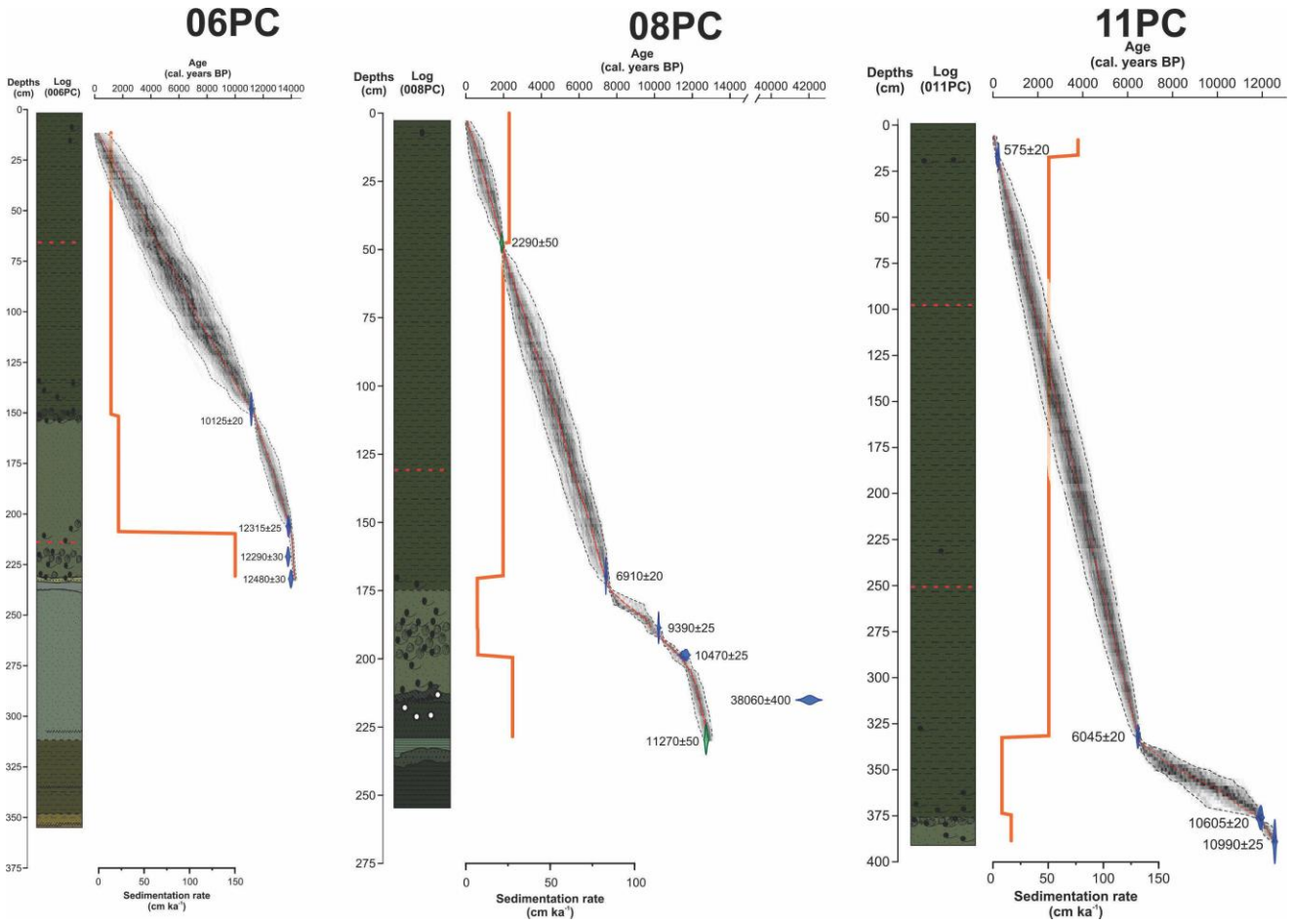

Figure 23. Age-depth relation for cores 06PC, 08PC and 11PC with sedimentation rates. The age model was based on 15 ^{14}C-AMS and was built by Desiage (2020) using the Bayesian age model (BACON v2.2 package) on R software (Blaauw and Christen, 2011) (Desiage, 2020).

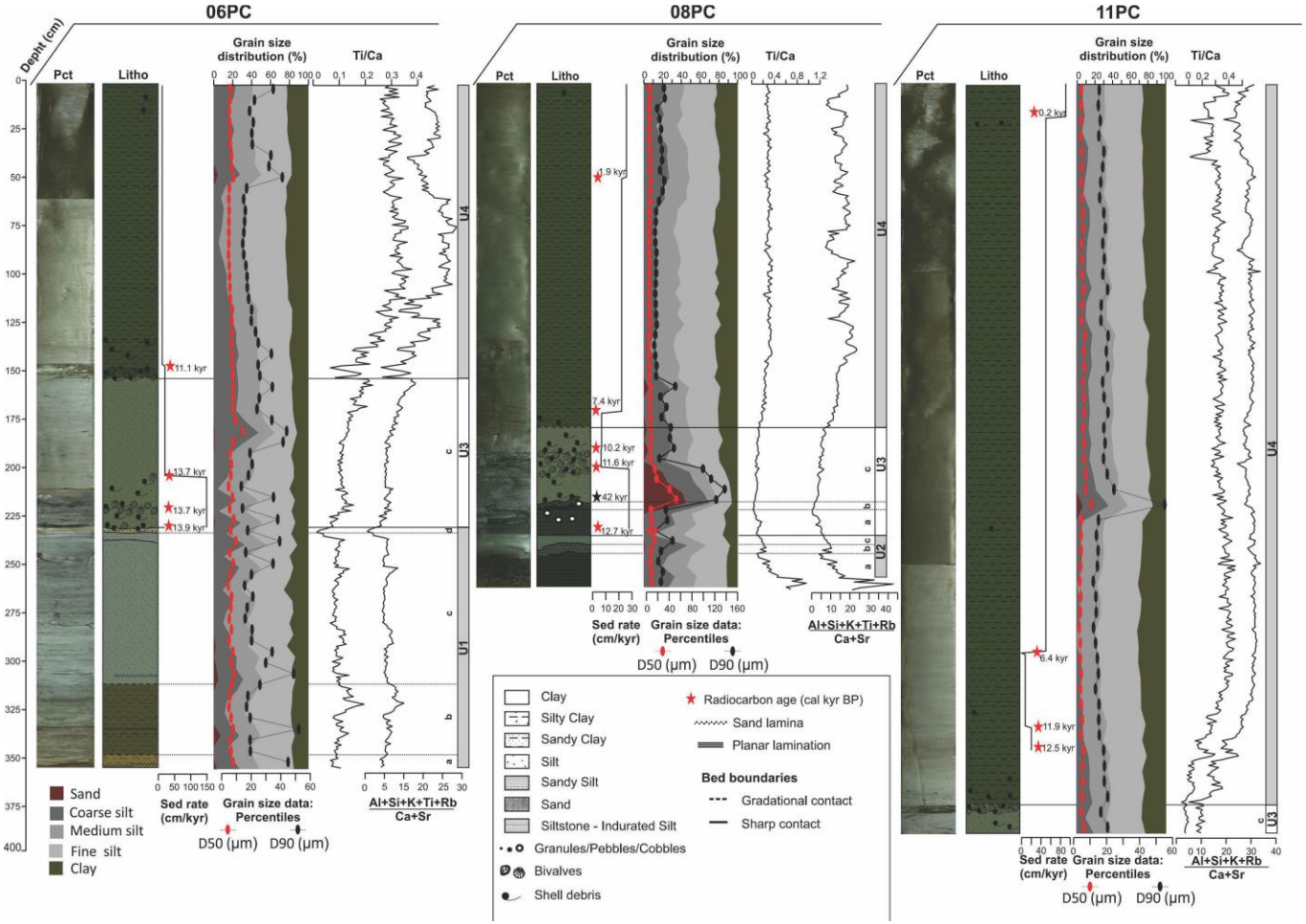

Figure 24. Schematic lithological descriptions and core to core correlations between 06PC, 08PC and 11PC using grain size data (distribution map of percentages of various fractions, D50 and D90) and XRF ratios. The Lithological descriptions is from Desiage (2020).

3.4.4 Palynological sample preparation

One hundred forty-seven subsamples were taken from the three sedimentary sequences representing a resolution between ∼100 yr and ∼300 yr records (06PC, 08PC, 11PC). Standard palynological preparations were used in all samples to recover dinocysts and pollen & spores (Rochon et al., 1999). A volume between 3 and 5 cm^3 of sediment was then sieved at 100 µm and 10 µm using Nitex membrane to remove coarse sands, fine silts and clays. The fraction between 100 µm and 10 µm was treated alternatively with cold hydrochloric acid (HCl, 10%) and hydrofluoric acid (HF, 40%) to remove the carbonates and siliceous fraction, respectively. The treatment was performed twice for HCl (10 min.) and once for HF (overnight, ~8 hours). The residue was rinsed with distillated water between treatments. The final residue was then sieved at 10 µm and centrifuged at ~2500 rpm for 10 minutes. A drop was then taken and mounted between slide and coverslip in glycerine gelatin for observation under microscope. Prior to the Chemical treatments, two tablets of *Lycopodium clavatum* (concentration per tablet 12,100 ± 1,892, Batch 414831, University of Lund) were added to the sediment to determine the palynomorph concentrations. The concentrations were combined to sedimentation rates to calculate palynomorph fluxes (palynomorph cm^{-2} yr^{-1}). The counts were performed using a transmitted light microscope (Nikon Eclipse 80i) at × 400 magnification.

3.4.5 Palynomorph counts

For dinocysts, a minimum of 300 specimens or marker grains were counted in each sample and the relative abundance of each taxa were estimated (% cysts). The dinocyst counts vary between 86 and 4150 cysts (avg. 796 cysts) and 22 taxa were recognized. Most dinoflagellate species are autotrophic and/or mixotrophic, but some are either heterotrophic, parasitic (e.g. *Hematodinium* sp., *Amoebophrya ceratii*) or symbiotic (Stoeker, 1999). The heterotrophic species are related to the availability of prey (diatoms, bacteria and others dinoflagellates) and are common in high productivity areas such as upwelling zones (Faye et al., 2018). As a result, the ratio autotrophic/heterotrophic taxa has been calculated to depict the food web structure along the records. In addition, some taxa were grouped together

according to modern dinoflagellate cyst distribution (Faye et al., 2018) and palaecological significance for each taxa based on numerous studies (Zonneveld et al., 2012; Pospelova et al., 2008). *Brigantedinium* spp. includes *B. simplex. B. auranteum, B. cariacoense, B.* sp and *Echinidinium* sp. is represented by *Echinidinium* Sp. C and *Echinidium*. sp. D (Faye et al., 2018). All heterotrophic dinoflagellate cysts less than 2% are grouped together and named as other heterotrophic taxa (Figure 25).

The pollen counts on the three cores range between 23 and 404 grains (avg. 257 grains). The lowest counts (<100 grains) are found at these depths: 312, 336, 344, 352 cm in 06PC and 196, 204, 212, 236 cm in 08PC. As a result, these sections are considered less reliable for pollen analysis. The pollen percentages were calculated against the sum of all pollen taxa, including arboreal pollen (AP = *Nothofagus* sp., *Podocarpus* sp., *Drymis* sp.) and non-arboreal pollen (NAP = shrubs and herbs). The spores were excluded from the pollen sum. Some pollen taxa have been grouped according to the interpretation of pollen dispersal patterns in modern surface sediment of SJG (Faye et al., 2020). The high shrub taxa regroups pollen of *Colliguaja integerrima,* Rhamanceae, *Schinus* sp., *Solanaceae* type, *Lycium* sp., while the low shrub taxa include other shrub pollen (e.g., Faye et al., 2020). The high abundance of shrub taxa is interpreted as an increase of humidity in the Patagonian steppe (Faye et al., 2018). All pollen from shrubs and herbs with less than 2% are grouped together and named as other shrubs and herbs, respectively. Paludal taxa are represented by Cyperaceae and *Typha* sp. pollen (Figure 26).

The one hundred forty-seven subsamples collected from the three sedimentary cores were analyzed at 8 and 6 cm intervals, which yielded centennial to multi-centennial resolutions (06PC, 08PC and 11PC). Pollen, spores and dinocyst taxa were identified to the lowest rank possible using the transmitted light microscope mentioned above, and pollen atlases (e.g. Heusser, 1971 and Markgraf and D'Antoni, 1978).

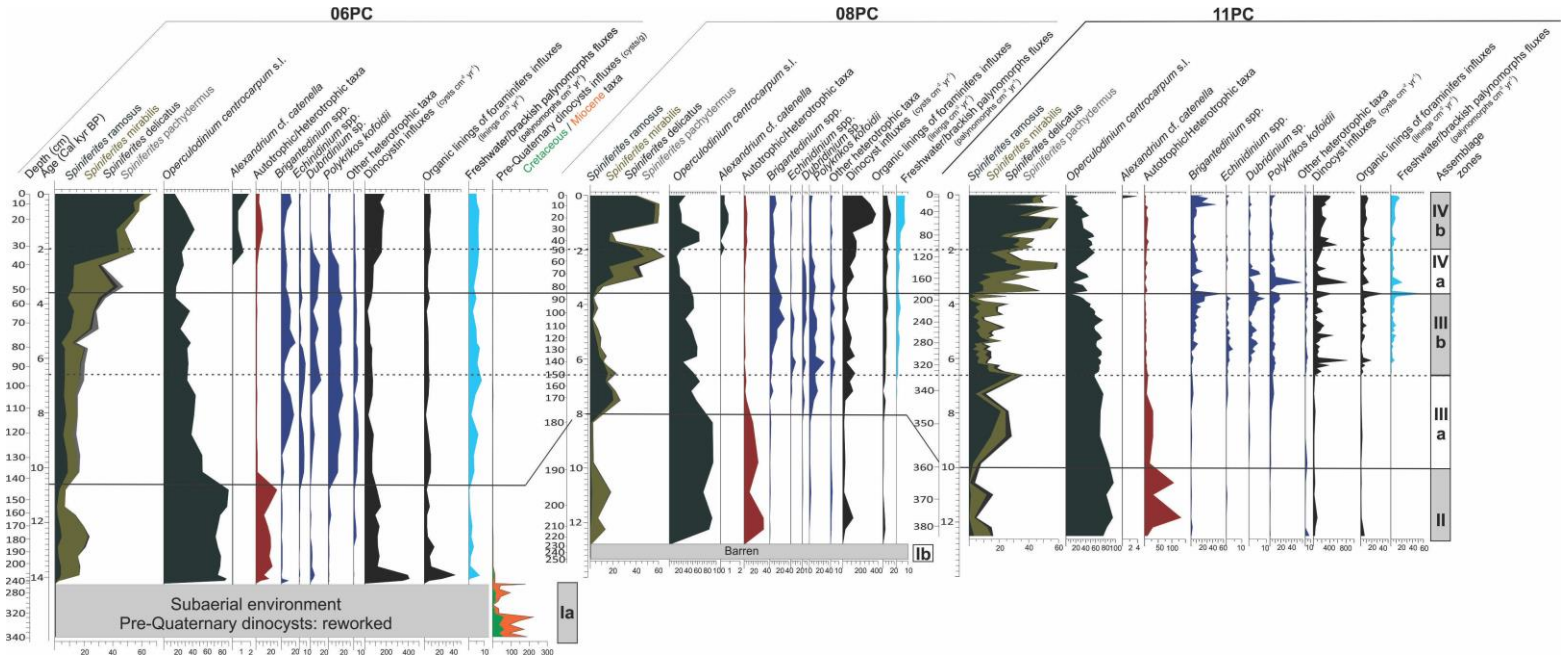

Figure 25. Relative abundances of the main dinocyst taxa and palynomorph concentrations and influxes in the three cores analyzed in this study.

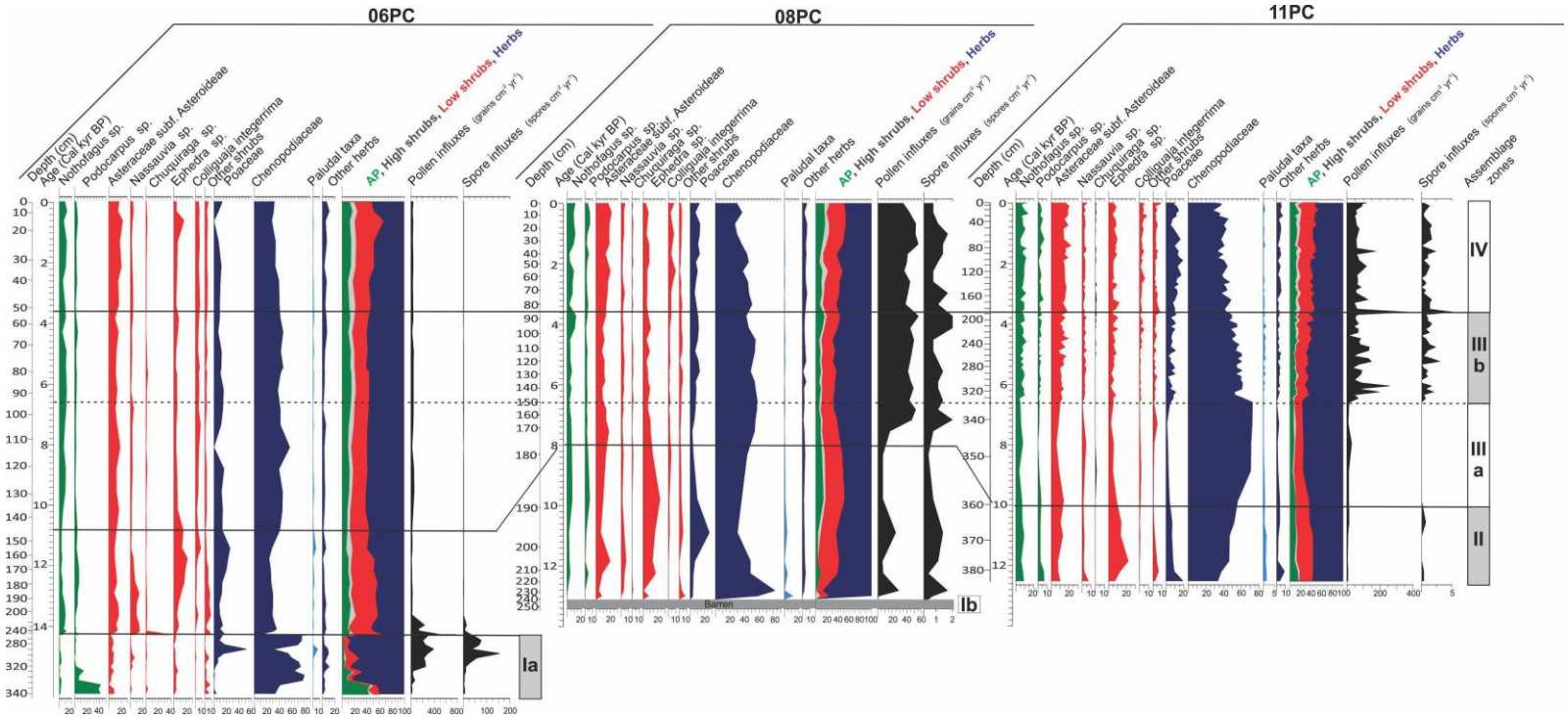

Figure 26. Relative abundances of the main pollen taxa and palynomorph concentrations and influxes in the three cores analyzed in this study.

The pollen/dinocysts ratio (P:D ratio) was calculated on the basis of all contemporary (non-reworked) pollen + spores influxes (palynomorph cm^{-2} yr^{-1}) *versus* autochthonous dinoflagellates influxes (cyts cm^{-2} yr^{-1}) that reflect the terrigenous influxes in the SJG (e.g., McCarthy and Mudie, 1998).

3.4.6 Diagrams and statistical analyses

The diagrams were performed with the stratigraphic analysis program *Tilia* (version 2.0.41) on the basis of percentage data. Principal Component Analysis (PCA) was performed using the relative abundance of palynomorph groups (dinocysts/pollen) from cores 06PC, 08PC, 11PC, and those from modern surface samples (Faye et al., 2018, Figures 25 and 26). Prior to the analysis, Detrended Correspondence Analysis (DCA, SD = 0.3272 for dinocysts and SD = 0.08582 for pollen) was performed, and shows that linear ordination such as PCA is more suitable (length of the first axis < 2 SD, ter Braak and Smilauer, 1998). The palynomorph (dinocysts/pollen) assemblage zones were defined using PCA sample scores (Figure 34).

3.6 RESULTS

3.6.1 Palynology

3.6.1.1 Pollen & spores and dinoflagellate cyst assemblages

We defined four assemblage zones in the three cores on the basis of the percentage of all dinocysts and pollen taxa preserved in the sediments. These assemblage zones were correlated between all cores with relative precision despite multi-millenial/centennial differences between the records, which could be due to the spatial variations of pollen and dinocysts taxa or the distinct age model of each core.

Assemblage Zone I (prior to 14 cal ka BP)

This assemblage zone is found in 06 PC (352-224 cm) and 08PC (248-228 cm) and it is divided in two sub-zones (Ia and Ib). The sub-zone Ia is characterized by the absence of modern dinocysts with high Pre-Quaternary dinocysts and pollen & spores influxes. The Pre-Quaternary dinocyst influxes vary between 1-224 cysts cm^{-2} yr^{-1} (avg. 89 cysts cm^{-2} yr^{-1}) and the species are represented by Cretaceous (e.g. *Hafniasphaera* sp., *Cordosphaeridium-Damasadinium* Complex etc.) and Miocene (e.g. *Emmetrocysta urnaformis*, *Cleistosphaeridium placacanthum*, *Daspilidinium pseudocolligerum*, *O. centrocarpum*, Deflandre and Cookson, 1995) taxa (Figure 25).

The pollen & spores influxes fluctuate between 12-772 grains cm^{-2} yr^{-1} (avg. 227 grains cm^{-2} yr^{-1}) and 2-155 grains cm^{-2} yr^{-1} (avg. 34 spores cm^{-2} yr^{-1}). Fungal spores (*Glomus* sp.) represent more than 70% on average in the spore assemblages. The cumulative sum (Σ) of the most abundant pollen taxa (Chenopodiaceae, Poaceae, *Podocarpus*, Asteraceae subf. Asteroideae) reached 83%. The herb pollen (Chenopodiaceae and Poaceae) dominate this sub-zone (avg. 72%), accompanied by Asteraceae subf. Asteroideae (avg. 5%) and *Podocarpus* (avg. 10%), which reach high percentages at the base of this section (up to 41%). The subzone Ib is characterized by an indurated clayey silt and is devoid of pollen grains (248-240 cm) and dinocysts (248-228 cm) (Figure 26).

Assemblage Zone II (∼14 to 8 cal ka BP)

This zone is well correlated in the three sedimentary sequences (224-136 cm in 06PC, 228-172 cm in 08PC and 389-359 cm in 11PC) and the main features are the appearance of modern dinocysts, organic linings of foraminifers and freshwater/brackish palynomophs (*Halodinium* sp., *Pediastrum* sp. and Tintinids). The dinocyst influxes vary between 14-409 cysts cm^{-2} yr^{-1} (avg. 194 cysts cm^{-2} yr^{-1} in 06PC, 40 cysts cm^{-2} yr^{-1} in 08PC and 41 cysts cm^{-2} yr^{-1} in 11PC), whereas organic linings of foraminifers and freshwater/brackish palynomorphs fluctuate respectively between <1-42 cell cm^{-2} yr^{-1} (avg. 11 cell cm^{-2} yr^{-1} in

06PC, 1.6 cell cm^{-2} yr^{-1} in 08PC and 2 cell cm^{-2} yr^{-1} in 11PC) and 0-6 cells cm^{-2} yr^{-1} (avg. 1.7 cells cm^{-2} yr^{-1} in 06PC, <1 cells cm^{-2} yr^{-1} in 08PC and 0.03 cells cm^{-2} yr^{-1} in 11PC). The most abundant dinocyst taxa reach a cumulative sum (Σ) of 91.2 % (Figure 25) and are represented by autotrophs, such as *O. centrocarpum* s.l. (*O. centrocarpum sensu* Wall and Dale (1966) and *O. centrocapum* short processes, avg. 79% in 06PC, 86% in 08PC and 11PC) and *Spiniferites mirabilis* (avg. 10% in 06PC, 7% in 08PC and 6% in 11PC).

The pollen & spores influxes decrease drastically in this zone compare to assemblage zone I. The fluxes vary between 0-234 grains cm^{-2} yr^{-1} (avg. 62 grains cm^{-2} yr^{-1} in 06PC, 12 grains cm^{-2} yr^{-1} in 08PC and 8.6 grains cm^{-2} yr^{-1} in 11PC) and 0-5.9 spores cm^{-2} yr^{-1} (avg. 3.8 spores cm^{-2} yr^{-1} in 06PC, <1 spore cm^{-2} yr^{-1} in 08PC and 11PC). The pollen assemblage is dominated by Asteraceae subf. Asteroideae, *Nassauvia* sp. *Chuquiraga* sp. and *Ephedra* sp., Chenopodiaceae and Poaceae, which reach an average cumulative sum (Σ) of 80.6 % (77.7% in 06PC, 84.7% in 08PC and in 79.6 % in 11PC). This assemblage zone is characterized by high percentages of low shrub pollen (Asteraceae subf. Asteroideae, *Nassauvia* sp. *Chuquiraga* sp. and *Ephedra* sp. etc.), which reach a mean value of 29.3%, and a decrease of herb taxa (57.8%) compare to sub-zone Ia. Arboreal pollen is represented by *Nothofagus* sp. (avg. 5.6%) and *Podocarpus* sp. (avg. 3.2%) and depict a successive increase in this section (Figure 26).

Assemblage Zone III (8 to 4 cal ka BP)

For dinocyst assemblages, this zone is divided in two sub-zones (IIIa and IIIb). The assemblage zones for both (dinocysts and pollen) are well correlated between the three records (136- 40 cm in 06PC, 172- 80 cm in 08PC and 359-186 cm in 11PC, Figures 25 and 26).

The dinocyst influxes are depicting a relatively stable in 06PC (25-83 cysts cm^{-2} yr^{-1}, avg. 59 cysts cm^{-2} yr^{-1}) and a progressive increase in 08PC (27-135 cysts cm^{-2} yr^{-1}, avg. 71

cysts cm^{-2} yr^{-1}) and 11PC (22-830 cysts cm^{-2} yr^{-1}, avg. 182 cysts cm^{-2} yr^{-1}). The freshwater/brackish palynomorphs are marked by a slight increase and vary between < 1-57 cells cm^{-2} yr^{-1} (avg. 5 cells cm^{-2} yr^{-1} in 06PC, 2 cells cm^{-2} yr^{-1} in 08PC, 7 cells cm^{-2} yr^{-1} in 11PC), whereas organic linings of foraminifers are relatively constant (avg. 6 cells cm^{-2} yr^{-1} in 06PC, 6 cells cm^{-2} yr^{-1} in 08PC, 7 cells cm^{-2} yr^{-1} in 11PC) in this assemblage zone. The main feature of this assemblage is the relative increase of heterotrophic dinocysts (*Brigantedinium* spp., *Echinidinium* sp. *Dubridinium* sp., cyst of *Polykrikos kofoidii*) compared to assemblage zone II. Heterotrophic dinocysts, accompanied by *O. centrocapum* s.l., dominate this assemblage zone and reach an average cumulative sum (Σ) of 82% (avg. 76 in 06PC, 88% in 08PC and 82% in 11PC). The main differences between sub-zones IIIa and IIIb are the progressive decrease of *O. centrocarpum* s.l. and the steady increase of heterotrophic dinocysts up to the top of sub-zone IIIb (Figure 25).

The pollen & spore influxes show a significant increase compared to assemblage zone II and fluctuate between 11-365 grains cm^{-2} yr^{-1} (avg. 60 grains cm^{-2} yr^{-1} in 06PC, 46 grains cm^{-2} yr^{-1} in 08PC and 95 grains cm^{-2} yr^{-1} in 11PC) and 0-57 spores cm^{-2} yr^{-1} (avg. 41 spores cm^{-2} yr^{-1} in 06PC, 9 spores cm^{-2} yr^{-1} in 08PC and 1 spore cm^{-2} yr^{-1} in 11PC). Asteraceae subf. Asteroideae, *Colliguaja integerrima*, Poaceae and Chenopodiaceae dominate this assemblage and reach an average cumulative sum of 75% (avg. 73% in 06PC, 75% in 08PC and 77% in 11PC). Compare to assemblage zone II, this zone is marked by a decrease of *Nassauvia* sp and *Ephedra* sp., and a slight increase of Chenopodiaceae. The herb taxa represent on average 63% of pollen assemblages and the abundance of high shrub taxa (4%) and low shrub taxa (22%) are relatively stable. The sub-zones IIIa and IIIb display slight differences with an increase of pollen and spores influxes up to the top of this assemblages (Figure 26). In this zone, *Nothofagus* (avg. 7%) and *Podocarpus* pollen (avg. 7%) exhibit a slight increase compare to assemblage zone II (Figure 26).

Assemblage Zone IV (4 to 0 cal ka BP)

Assemblage zone IV is well correlated among the records (40-0 cm in 06PC, 80-0 cm in 08PC and 186-0 cm in 11PC) and are observed at the top of each sedimentary sequence.

Dinocyst assemblages were separated into two subzones, while only one pollen assemblage zone was identified in this portion of the cores (Figures 25 and 26).

The dinocysts, organic linings of foraminifers and freshwater/brackish palynomorph influxes depict a progressive increase up to the top of this zone. The dinocyst influxes vary between 61-570 cysts cm^{-2} yr^{-1} (avg. 130 cysts cm^{-2} yr^{-1} in 06PC, 202 cysts cm^{-2} yr^{-1} in 08PC and 282 cysts cm^{-2} yr^{-1} in 11PC), whereas organic linings of foraminifers and freshwater/brackish palynomorphs vary respectively between 3-15 cells cm^{-2} yr^{-1} (avg. 7 cells cm^{-2} yr^{-1} in 06PC, 9 cells cm^{-2} yr^{-1} in 08PC and 8 cells cm^{-2} yr^{-1} in 11P) and 2-15 cells cm^{-2} yr^{-1} (avg. 5 cells cm^{-2} yr^{-1} in 06PC, 5 cells cm^{-2} yr^{-1} in 08PC and 7 cells cm^{-2} yr^{-1} in 11PC). The dinocyst assemblages are dominated by *Spiniferites ramosus*, *S. mirabilis, O. centrocarpum* s.l., and heterotrophic taxa (*Brigantedinium* spp. *Dubridinium* sp. and cyst of *P. kofoidii*), which together reach a cumulative sum (Σ) of 97%. Subzone IVa (2 to 4 cal yr BP) exhibits a moderately high relative abundance of *S. mirabilis* and heterotrophic taxa compare to subzone IVb (0 to 2 cal yr BP), which is marked by a steady increase of *S. ramosus*, a decrease of the heterotrophic taxa (*Echinidium* sp. and cyst of *P. kofoidii*) and the appearance of the toxic taxa *Alexandrium* cf. *catenella* (avg. 0.6%).

The pollen & spore influxes fluctuate between 28-172 grains cm^{-2} yr^{-1} (36 grains cm^{-2} yr^{-1} in 06PC, 44 grains cm^{-2} yr^{-1} in 08PC and 78 grains cm^{-2} yr^{-1} in 11PC) and 0.1-2.4 spores cm^{-2} yr^{-1} (~1 spore cm^{-2} yr^{-1} in each core). These assemblages are dominated by *Nothofagus* sp., Asteraceae subf. Asteroideae, *Colliguaja integerrima*, Poaceae and Chenopodiaceae, which reach a cumulative sum of 85% (avg. 78 in 06PC, 98 in 08PC and 79 in 11PC). The herb pollen (avg. 54%) depicts a steady decrease up to the top of this zone, whereas pollen from shrubs (avg. 27% and 7% respectively) exhibit a progressive increase compared to the underlying zone III. The arboreal pollen depict a slight increase for *Nothofagus* sp. (avg. 9%) and a decreasing trend for *Podocarpus* sp. (~3%) in comparison with zone III (Figure 26).

3.6.1.1 Principal component analysis

For dinocysts, the first axis explains 76 % of the variance of the dataset, while the second axis represents 15% (Figure 27A). The first axis is mainly driven by autotrophic dinocysts (*S. ramosus* in the negative values and *O. centrocarpum* s.l. in the positive values). These two species are found in a wide variety of environments (sub-polar to equatorial). However, *S. ramosus* occur preferentially in nutrient-rich coastal waters (Zonneveld et al., 2013) while *O. centrocarpum* s.l. (>85 %) occurs in high abundances in temperate environments of the North Atlantic Ocean (Dodge et Harland, 1991; Zonneveld et al., 2013). Therefore, the positive values of the first axis seem to be related to temperate environments and negative values to nutrient rich coastal waters. The heterotrophic species (*Brigantedinium* spp., *Dubridinium* sp., and cyst of *P. kofoidii*) depict a positive correlation with axis 2 and some samples from zone IV and III. These heterotrophic species in SJG and in many studies prevail in high productivity areas and are related to the availability of preys, such as diatoms (Pospelova et al., 2008; Zonneveld et al., 2013; Faye et al., 2018). Therefore, we interpret axis 2 in terms of primary productivity.

For pollen, the first and second axis explain respectively 74 % and 7% of the variance in the dataset (Figure 27B). The first axis is mainly represented by halophytic species (Chenopodiaceae), which are mainly growing in depressions with salt-rich soils in Patagonia, such as the salt marsh and coastal lagoon areas along the Argentine coast (Leon et al., 1998; Stutz et al., 2006; Marcos and Mancini, 2011). According to Groot et al. (1965), the occurrence of Chenopodiaceae and *Ephedra* during the Late Pleistocene in the Argentinian Basin suggests arid conditions. Therefore, the positive values of the first axis seem to be related to coastal lagoon environments under arid conditions, which correlate with samples from pollen assemblages of zones I and III. The pollen assemblages from zone IV, and some samples from zone II, depict a relative good correlation with modern vegetation distribution, as well as with several taxa (Poaceae, Asteraceae subf. Asteroideae and *Colliguaja integerrima*.) that are characteristic of the present Patagonian steppe.

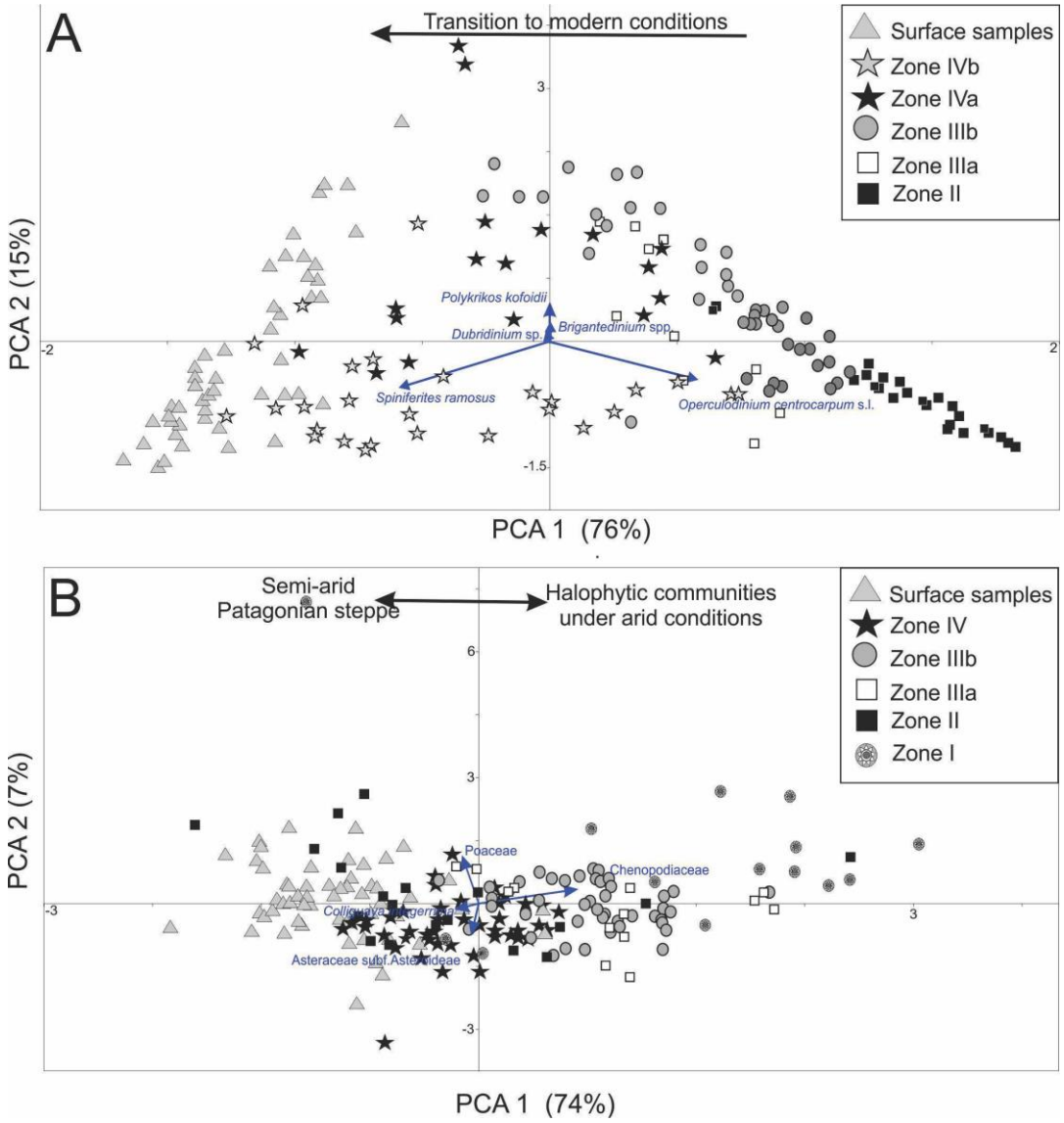

Figure 27. Correlation biplot based on principal component analysis (PCA) for dinocyst (A) and pollen taxa (B) of the three cores analyzed in this study.

3.7 DISCUSSION

3.7.1 Paleoenvironmental history from marine records 06 PC, 08PC and 11PC

- **Late Glacial? (Prior to 14 cal ka BP)**

Assemblage zone I is recorded only in 06PC and is devoided of modern dinocysts. However, we found reworked Pre-Quaternary dinocysts from Cretaceous and Miocene formations adjacent to the SJG that were most likely eroded and subsequently transported to the core location (e.g. Paredes et al., 2015). The exact age of this assemblage is uncertain, but it was deposited prior to 14 cal ka BP. This assemblage suggests a subaerial environment in the SJG and possibly a coastal lagoonal environment. The silty clay sedimentation (U1) depicts shallow water depositional environments supplied by a possible erosive drainage system of Miocene and Cretaceous formations (Figures 23 and 24). This interpretation is consistent with sea level variations in the ACS, which was at 80 m below present sea level around 14 cal ka BP (Violante and Parker, 2004), which suggests that the SJG was exposed before this period (Figure 28H). Geophysical and sedimentological data confirm this interpretation and indicate the presence of a drainage system in the SJG during the last glacial period (Desiage, 2020). The high occurrence of *Glomus* sp. spores, which are abundant in postglacial deposits, could indicate soil erosion (Cook et al., 2011). This suggests that this assemblage may also reflect late glacial sediments within an erosional context (Figure 26). The pollen content is well preserved and depicts that the assemblage could be contemporary with the deposits. The relatively high values of Chenopodiaceae in this assemblage indicate the development of halophytic communities around the SJG under arid conditions (Figure 26). The low values of *Nothofagus* and *Podocapus* pollen at the top of this assemblage zone are in agreement with previous work in western Patagonian forests where low arboreal taxa and the development of erythermal taxa were identified in late glacial records (Mancini et al., 2009, Figure 26). The base of assemblage zone I (06PC, Figure 25) is marked by the occurrence of cold resistant hygrophilous conifers (*Podocarpus* sp.), which indicates cold

and wet conditions in western Patagonian forests (Moreno and Videla, 2016). However, we do not have an analogy of this observation in the western Patagonian forest records (after 19 cal ka BP).

- **End of the Late Glacial – Early Holocene (∼14 to 10/8 cal ka BP)**

Assemblage zone II is correlated among the three records and marked the installation of oceanic conditions in the SJG (appearance of modern dinocysts, organic linings of foraminifers and freshwater/brackish palynomorphs) with hemipelagic sedimentation (U3) (Figures 23 and 24). This assemblage suggests marine invasion in SJG with high dominance of autotrophic taxa (*O. centrocarpum* s.l., 83% and *S. mirabilis*, 7% on average in 06 PC, 08PC and 11PC). High abundances of *O. centrocarpum* s.l. (up to 85%) are found in temperate environments of the North Atlantic Ocean (Dodge et Harland, 1991; Zonneveld et al., 2013), and *S. mirabilis* shows preferences for warm temperate water and high salinity environments (de Vernal et al., 2018). Therefore, the codominance of these two species suggests temperate conditions in SJG during the Last Glacial termination and Early Holocene. On the adjacent continent, the Patagonian steppe was developing and characterized by halophytic (Chenopodiaceae) and psammophytic (Poaeae, Asteraceae, *Ephedra*) communities, which is characteristic of present day vegetation and suggests the establishment of semi-arid conditions similar to modern ones around the SJG (Figures 26 and 27B). In this assemblage, the arboreal taxa (*Nothofagus* and *Podocarpus*) depict low values with slight successive increases in agreement with several pollen records on both sides of the Andes (e.g., Bennett et al., 2000; Mancini et al., 2008; Vilanova et al., 2019) and suggest cold conditions in the southern Patagonian forest (Figure 26).

Early– Middle Holocene (10/ 8 to 4 cal ka BP)

Assemblage zone III highlights the onset of a drastic change in the food web in the SJG, with the increase in the abundance of heterotrophic dinocyts (*Brigantedinium* spp., *Echinidinium* sp., *Dubridinium* sp., cysts of *P. kofoidii*, Figure 25). The occurrence of these

taxa suggests a productivity increase, probably linked to the development of diatoms, which constitute the main food source for several heterotrophic dinoflagellates (Pospelova et al., 2008; Zonneveld et al., 2013; Jeong et al., 2010; Faye et al., 2018). The slight increase of freshwater/brackish palynomorph influxes (*Halodinium* sp., *Pediastrum* sp. and Tintinids) from Southern Patagonian rivers and brought into the SJG by the Patagonian Current could indicate an increase of Patagonian river inputs in the south-west Atlantic and/or linked with an increase of the coastal Patagonian current from this period to the present. However, it is important to note that the low influxes of these allochtonous palynomophs in all records (06PC, 08PC, 11PC) suggest that our assemblages mostly describe local conditions. On the continent, we observe an increase in Chenopodiaceae and a decrease of low shrub taxa (*Ephedra* sp. and *Nassauvia* sp.), which suggest drier conditions than in the present-day (Figure 26, Figure 27B). The increase in *Nothofagus* (Figure 26) is in agreement with records from the southern Patagonian forest depicting its expansion during that period in response to an increase in temperature and higher moisture availability (Bennett et al., 2000; Mancini et al., 2008).

- **Late Holocene (4 cal ka BP)**

Assemblage zone IV corresponds to the Late Holocene and is characterized by a transition to modern conditions in the SJG (Figures 26 and 27). The PCA results are consistent with this interpretation in the SJG highlighted by a good correspondence between palynomorph contents (dinocysts and pollen) from modern surface samples and those from assemblage zone IV (Figure 27). However, the beginning of the Late Holocene is marked by a global cooling trend (Neoglacial) leading to glacier advances and surface water cooling recorded in different places in the world (e.g., Jerardino, 1994; Sepúlveda et al., 2009; Aniya et al., 2012, Solomina et al., 2014). This period is coeval in our record with the occurrence of *S. mirabilis*, which is characteristic of warm temperate conditions (de Vernal et al., 2018). However, some studies based on glacier history in the Lago Argentino area show that the onset of the Neoglacial has started much earlier (since 7730 cal ka BP) and leading to successive glacier advance episodes in Patagonia (Strelin et al., 2014; Kaplan et al., 2016).

Our pollen spectra do not record such a cooling trend, but display a slight increase of low shrub and high shrub taxa. These insights suggest a transition to present-day vegetation (Figures 26 and 27B) with a possible slight increase of humidity in Patagonian steppes compare to the Early and Mid-Holocene (Figures 26 and 27B).

3.7.2 Southern Westerly Wind Belt variations related to sea surface conditions in the SJG and vegetation changes

We infer multi-millennial scale changes of the Southern Westerly Wind Belt (SWWB) related to sea surface conditions on the basis of pollen/dinocyst ratio (P:D index), the abundance of *Nothofagus* sp. and palaeoecological qualitative interpretations from PCA analysis (PCA 1 from dinocyst analysis = temperate/warm condition, PCA 2 from dinocyst analysis = high productivity) and some selected taxa (*Brigantedinium* spp.+*Dubridinium* sp. = productivity, Figure 28). *Nothofagus* pollen show a very good correlation with P:D index and pollen record from Mallín Pollux (46 °S, Aisén province, southern Chile) located at the latitude of the SJG (Markgraf et al., 2007). Therefore *Nothofagus* pollen could represent a good proxy to test/assess the intensity of the SWWB (Figure 28D and E). We did not find such correlation with the *Podocarpus* pollen and their abundance describes different patterns along the SJG (Figures 28F and G). Indeed, previous studies have shown that buoyant pollen types (e.g. *Pinus* similar to *Podocarpus*) have long residence time in the water before being deposited in the sediment and their distribution is related to the hydrographic processes rather than to the pollen source (e.g., Traverse and Ginsburg, 1966). The P:D index reflects continental inputs, which are mostly via aeolian transport to the SJG (Figures 28A and D). In this regard, the maximum influence of the SWWB can be deduced from high values of P:D index and the abundance of *Nothofagus* sp. Indeed, *Nothofagus* pollen is an indicator in the of the intensity of the SWWB due to the long distance wind transport from the southwestern Patagonian forest towards the SJG (Mayr et al., 2006). Our results show stronger westerly winds starting at 14 cal ka BP (equivalent in timing to the Antarctic Cold reversal, ACR) supported by the high value of P:D index, and high *Nothofagus* inputs, which

decrease gradually during the Late Pleistocene at the latitude of the SJG (Figures 28A and D). This period is followed by a gradual warming (development of Patagonian steppe) during the Early and Mid-Holocene correlated to westerlies increasing trend, forcing high terrigenous inputs, which leads to increased ocean fertilization and primary productivity in the SJG (Figures 28A, B, D and H, e.g., Simonella et al., 2015; Paparazzo et al., 2018). The Late Holocene is characterized by warm temperate conditions (increase of *S. mirabilis*) in the SJG at the beginning of the Neoglacial (here 4.2 cal kyr BP) correlated with the slightly weakening trend of westerly winds derived from the low relative abundance of *Nothofagus* and terrigenous input (P:D index), coeval with a decrease in primary productivity (Figures 28A, B and D).

The high SWWB intensity leading to dry conditions in eastern Patagonia can be inferred from the occurrence of herb taxa (e.g. Chenopodiaceae), which suggest reduced precipitations on the continent adjacent to the SJG during the Early and Mid-Holocene. Conversely, periods of low SWWB intensity are marked by a humidity increase depicted by a rise in the abundance of shrub taxa (Late Glacial and Late Holocene). Indeed, the eastern side of the Andes is affected by Atlantic moisture transport during weaker intensity wind periods (Agosta et al., 2015).

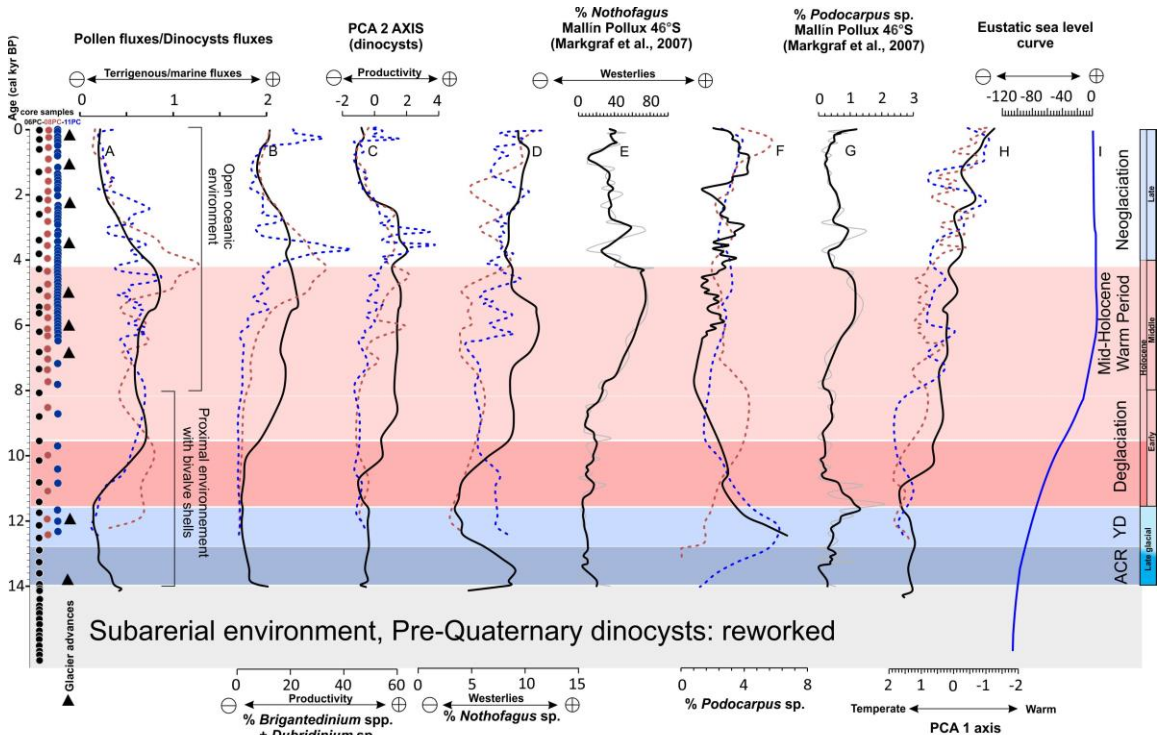

Figure 28. SWWB variations related to sea surface conditions in the SJG. (A) Terrigenous input in the SJG. (B) Relative abundances of *Brigantedinium* spp. and *Dubridinium* sp. related to high productivity. (C) PCA 2 axis from dinocyst analysis associated with primary productivity. (D) Relative abundance of *Nothofagus* sp. used as a wind intensity proxy (this study). (E) Relative abundance of *Nothofagus* sp. in Mallín Pollux (Aisén province, southern Chile) located at the limit of the subantarctic forest (Markgraf et al., 2007). (F) Relative abundance of *Podocarpus* sp (in this study). (G) Relative abundance of *Podocarpus* sp. in Mallín Pollux (Aisén province, Southern Chile) (Markgraf et al., 2007). (H) PCA sample scores for axis 1 in dinocyst analysis of 06PC (in this study). (I) Eustatic sea level curve on the Argentine Continental shelf (Violante and Parker, 2004). The triangles show major glacier advances in Patagonia during the last 14 cal ka BP (Rabassa, 2008; Aniya, 2012; Strelin et al., 2014; Kaplan et al., 2016). The subepoch boundaries for the Holocene are following the subdivision of Walker et al. (2012).

3.7.3 Comparison with other paleowind records in Patagonia

To get an idea of latitudinal variations of the SWWB in different time periods, we first described our records and then compared our interpretation with other paleowind records from Patagonia. We also use the glacier history of this region and sea surface temperature (SST) paleodata from Atlantic and Pacific Oceans derived from alkenone and diatom databases (Bianchi and Gersonde, 2004; Kaiser et al. 2005; Canuipàn et al., 2011, Figure 29).

In the SJG (45 °S), we used the normalized *Nothofagus* sp. (Z scores = (xi-μ)/ σ, μ = mean samples and σ = standard deviation, called *Nothofagus* index) as wind intensity proxy. The results reveal clear trends of the SWWB in the SJG, with positive values (high intensity winds, +0.2) from 14 cal ka BP, which then decrease gradually to negative values (low intensity winds, -0.6) between 14-11.8 cal kyr BP. In the early stage of the Holocene (11.8-9.6 cal ka BP), the decline of SWWB flow (avg. -1.3) persisted over the latitude of the SJG. This period is followed by the intensification of the SWWB (avg. +0.2) between 9.6-8.2 cal ka BP, which reached their highest intensity (avg. +0.5) during the Mid-Holocene (8.2-4.2 cal ka BP). Afterward, our results suggest a weakening phase of the westerly winds (avg. +0.4, Figure 29B).

At approximately the same latitude as the SJG (southwest Patagonia sector), Van Daele et al. (2016) reconstructed low SWWB intensity in Lago Castor (46 °S) between 14-11.8 cal ka BP from low values of (28 μm) wind driven sortable silt (SS' index, bottom current proxy). From 11.8 to 9.6 cal ka BP, low SWWB flow still persisted in Lago Castor (SS' index value of 29.7 μm, Van Daele et al., 2016). After this period (9.6- 8.2 cal ka BP), the increase of SS' index (33.7 μm) marked the intensification of the SWWB which reached their highest intensity (avg. 35.6 μm) in the Mid-Holocene (8.2-4.2 cal ka BP, Van Daele et al., 2016). During late Holocene (after 4.2 cal ka BP), the SS' index (34 μm) shows a weakening of the SWWB flow in Lago Castor (Van Daele et al., 2016, Figure 29C)

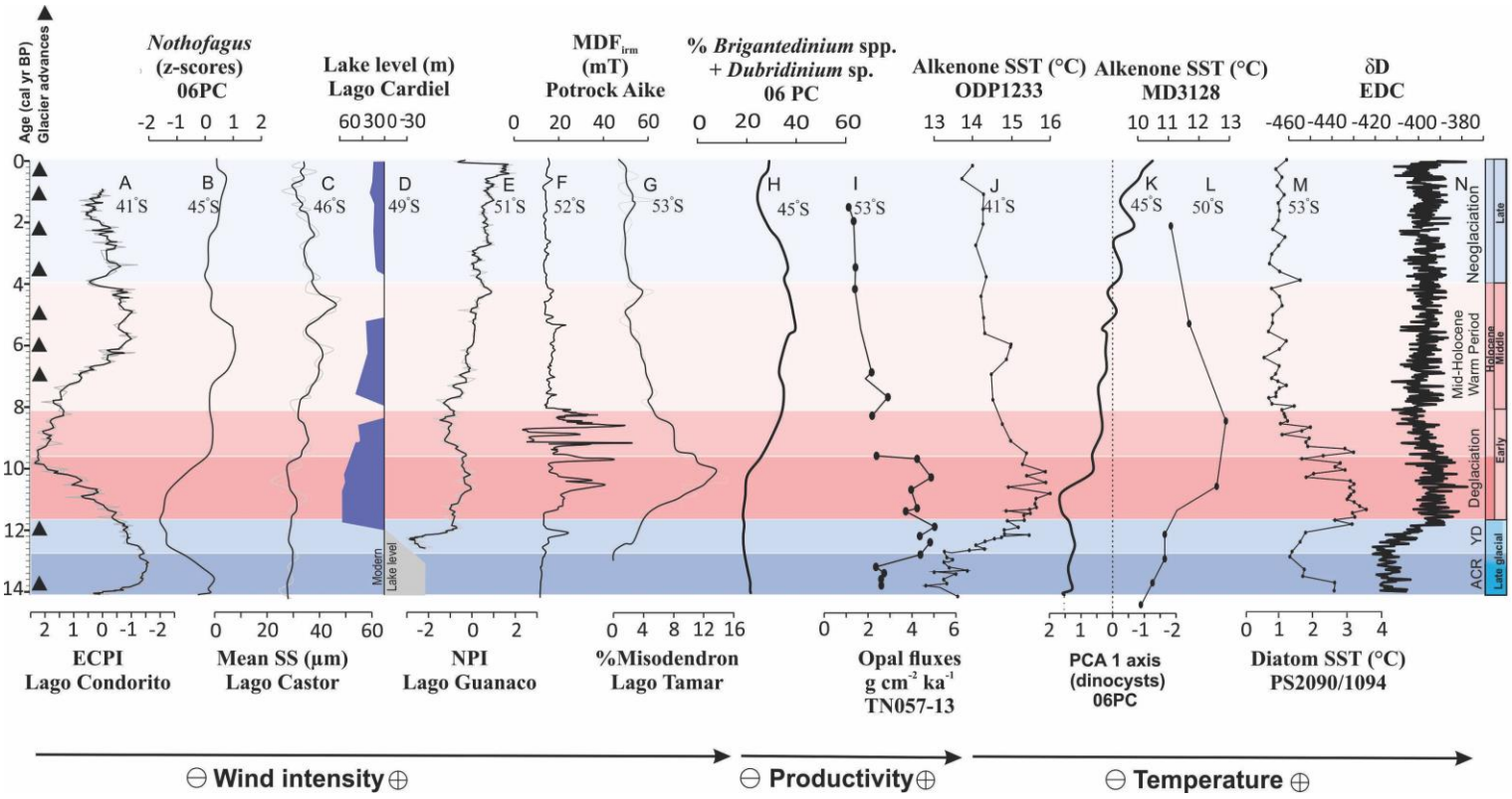
Age (cal yr BP)
Glacier advances
Nothofagus (z-scores) 06PC
Lake level (m) Lago Cardiel
MDF irm (mT) Potrock Aike
% Brigantedinium spp. + Dubridinium sp. 06 PC
Alkenone SST (°C) ODP1233
Alkenone SST (°C) MD3128
δD EDC
A 41°S
B 45°S
C 46°S
D 49°S
E 51°S
F 52°S
G 53°S
H 45°S
I 53°S
J 41°S
K 45°S
L 50°S
M 53°S
N
Modern Lake level
Neoglaciation
Mid-Holocene Warm Period
Deglaciation
YD
ACR
Late
Holocene Middle
Early
Late glacial
ECPI Lago Condorito
Mean SS (µm) Lago Castor
NPI Lago Guanaco
%Misodendron Lago Tamar
Opal fluxes g cm-2 ka-1 TN057-13
PCA 1 axis (dinocysts) 06PC
Diatom SST (°C) PS2090/1094
⊖ Wind intensity ⊕
⊖ Productivity ⊕
⊖ Temperature ⊕

Figure 29. Comparison of Paleo-wind records along northern and southern Patagonia. (A) The normalized index *Eucryphia* + *Caldcluvia*/ Podocarpaceae (EPCI) from Lago Condorito (Moreno et al., 2010). (B) The *Nothofagus* sp. index from the SJG. (C) Mean grain-size value of modified sortable silt (10-125 μm, SS') from Lago Castor (Van Daele et al., 2016). (D) Reconstructed lake level from Lago Cardiel (Quade and Kaplan, 2017). (E) The normalized *Nothofagus*/Poaceae pollen index (NPI) at Lago Guanaco (Moreno et al., 2010). (F) The MDF_{irm} (Median Destructive Field) from Potrok Aike (Lisé-Pronovost et al., 2015). (G) The relative abundance of *Misodendron* in Lago Tamar (Lamy et al., 2009). Productivity derived from relative abundances of *Brigantedinium* spp. and *Dubridinium* sp. in the SJG (H) and opal fluxes in the South Atlantic Ocean (I, Anderson et al., 2009). Paleotemperature reconstructions from the Atlantic Ocean derived from alkenones (J and K) and diatoms (Kaiser et al., 2005; Canuipàn et al., 2011). (L) PCA sample scores for axis 1 in dinocyst analysis. (M) SST reconstructions inferred from diatom assemblages from the South Atlantic Ocean (Bianchi and Gersonde, 2004). (N) Epica-Dome C stable isotope profil (δD) from Antarctica (Parrenin et al., 2013). The triangles show major glacier advances in Patagonia during the last 14 cal ka BP (Rabassa, 2008; Aniya., 2012; Strelin et al., 2014; Kaplan et al., 2016). The subepoch boundaries for the Holocene is following the subdivision of Walker et al. (2012).

Further north at Lago condorito (41 °S, in the Chilean tropical forest), the normalized index *Eucryphia* + *Caldcluvia*/Podocarpaceae (ECPI) was used to study the moisture changes and EPCI positive (negative) reveal weakening (strengthening) of the SWWB (Moreno et al., 2010). This index depicts a multi-millennial pattern with high negative ECPI values (avg. -0.9) between 14-11.8 cal ka BP which suggests intense westerly winds (Moreno et al., 2010). This period is followed a weakening trend SWWB intensities (avg. +1.1) between 11.8 and 8.2 cal ka BP (Moreno et al., 2010). During the Mid-Holocene (8.2-4.2 cal ka BP), the EPCI index (avg. -0.2) depicts an increase trend of the intensity westerly winds (Moreno et al., 2010). Conversely, at the Late Holocene (after 4.2 cal ka BP), the ECPI depict a decrease of the SWWB intensities (avg. +0.03, Moreno et al., 2010, Figure 29A).

Further south, at Lago Cardiel (49 °S, in the Patagonian Steppe), the high lake level (avg. +43 m) between 12 and 8.4 cal ka BP was interpreted as a weakening of the SWWB speed and more influence of the trade winds from the Atlantic Ocean bringing intense rainfall in central Patagonia (Quade and Kaplan, 2017). After this period, the lake level continues to drop with minor fluctuations suggesting more SWWB and/or less trade winds influence (Quade and Kaplan, 2017, Figure 29D).

At Lago Guanaco (51 °S, in the forest-steppe ecotone), the normalized *Nothofagus*/Poaceae pollen index (NPI) was used as a proxy of westerly wind shifts (Moreno et al., 2010). The NPI (avg. -0.6) show an increase between 12 and 9.6 cal kyr BP, with a slight multi-millennial increasing trend after this period (avg. +0.3, Moreno et al., 2010, Figure 29E).

From Laguna Potrok Aike (52 °S, in the Patagonian Steppe), the MDF_{irm} (Median Destructive Field) was interpreted as a proxy of past shifts of westerly winds (Lisé-Pronovost et al., 2015). Between 14 and 11 cal kyr BP, the MDF_{irm} (14.2 mT) indicates weaker winds in Laguna Potrok Aike (Lisé-Pronovost et al., 2015). This period is followed by an increase between 11 and 8 cal kyr BP (24 mT), and thereafter by a plateau with low amplitude changes in MDF_{irm} (15 mT, Lisé-Pronovost et al., 2015, Figure 29F).

At the Lago Tamar site (53 °S, in the Andean forest), the percentage of *Misodendron*, which are hemiparasite infesting *Nothofagus* trees, are used as a proxy of the expansion of *Nothofagus* forests associated with the intensification of the SWWB (Lamy et al., 2010). These taxa show a sharp increase (intense westerly winds) between 12 and 8 cal kyr BP (avg. 6.8 %), which decrease during the Mid and Late Holocene (avg. 2.9 %, Figure 29G).

In summary, we note a coherent anti-phase between the northern/southern sites along Patagonia (Figures 29 and 30), suggesting that the core of the SWWB expands northward during 14 and 11.8 cal ka BP. This period coincides with the timing of the ACR and Younger Dryas (cold interval) leading glacier advances in the Southern Hemisphere (e.g., Rabassa, 2008). This northward expansion of the SWWB is consistent with temperate conditions in the SJG and support the SWWB expansion mechanism postulated by Lamy et al. (2010). Indeed, these authors argued that the northward (southward) position of the SWWB is related to low (high) temperature in South Pacific and Atlantic Oceans (Figure 29J, K, L and M). This period is followed by a southward move of the SWWB core between 11.8 and 9.6 ca ka BP correlated with wind driven-upwellings (high primary productivity marked by increasing opal fluxes) in the South Atlantic Ocean (Anderson et al., 2009) and a temperature increase in the Southern Ocean (Figure 29 J, K, L and M). After 9.6 cal ka BP, the SWWB expands northward (53° - 45 °S) in conjunction with possible ocean fertilization by aeolian inputs driving high primary productivity in the SJG. This SWWB expansion is consistent with the interruption of the wind driven-upwellings in the high latitude of the South Atlantic sector (Figure 28I, e.g. Anderson et al., 2009). Our results do not register the weakening of the entire SWWB core between 41°S and 51°S during the Early Holocene (e.g. Moreno et al., 2010), but high SWWB centered around central Patagonia until Mid-Holocene. This northward migration of the core of the SWWB is consistent with the onset of cold conditions in Southern South America with leading successive glacier advances since 7730 cal ka BP (Strelin et al., 2014; Kaplan et al., 2016). During the Late Holocene (Neoglacial, here after 4.2 cal ka BP), we record a weakening of the SWWB intensities in all Patagonian sector with minor differences in the SWWB intensity between the records on multi-millennial scales (Figure 29). The weakening of the SWWB is consistent with glacier advances in Patagonia

(Strelin et al., 2014; Kaplan et al., 2016). In the SJG, this period is coeval with the marine primary productivity decrease and *S. mirabilis* increase in early Late Holocene (4.2-2 cal ka BP*)*, which suggest warm temperate conditions in the SJG (Figure 25). This observation suggests a more northward position of the SWWB and is consistent with high lake levels in Laguna Aculeo (34°S, at the northern edge of the SWWB core) at 3 cal ka BP, where the lake recharge is related to westerly winds (Jenny et al., 2008). To explain the differences between paleowind records during the late Holocene, some authors suggest more frequents ENSO events since 5 cal kyr BP to the present, which break the zonal wind symmetry of the SWWB (Fletcher and Moreno, 2011).

3.8 CONCLUSION

The pollen versus dinoflagellate cyst records in the SJG provide novel insights regarding the SWWB/Southern Ocean system and vegetation changes around the SJG. Our results suggest that prior to 14 cal ka BP, a subaerial environment is observed in the SJG with a possible coastal lagoonal environment under arid conditions. Following this period, the SJG is characterized by a relative high sea level marked by the appearance of marine palynomorphs. On the continent adjacent to the SJG, the progressive establishment of modern Patagonian steppe communities suggests semi-arid conditions. The *Nothofagus* sp. index compared to some multi-millennial westerly records derived from precipitation-moisture, and an independent moisture proxy (MDF_{irm}) reveal opposite patterns along the northern/southern Patagonian sites since 14 cal ka BP (Figure 29). The results reveal a northern position of the SWWB during the Late Pleistocene followed by a southward shift of the SWWB during the early stage of the Early Holocene, coeval with wind driven-upwellings (high productivity) in the South Atlantic Ocean. This period is followed by high intensity westerly winds centered in the central part of Patagonia (Lago Condorito, SJG) during the transition from the Early- to the Mid-Holocene. This intensification of the SWWB

is synchronous with high primary productivity in the SJG and the interruption of the wind driven-upwelling further south, suggesting a progressive migration of the SWWB towards the North. During the Neoglacial (here after 4 cal ka BP), we observe weakening phases of the westerly intensity in all Patagonian sectors correlated with glacier advances in Patagonia and warm temperate conditions in the SJG (increase of *S. mirabilis*) that suggest a more northern position of the SWWB.

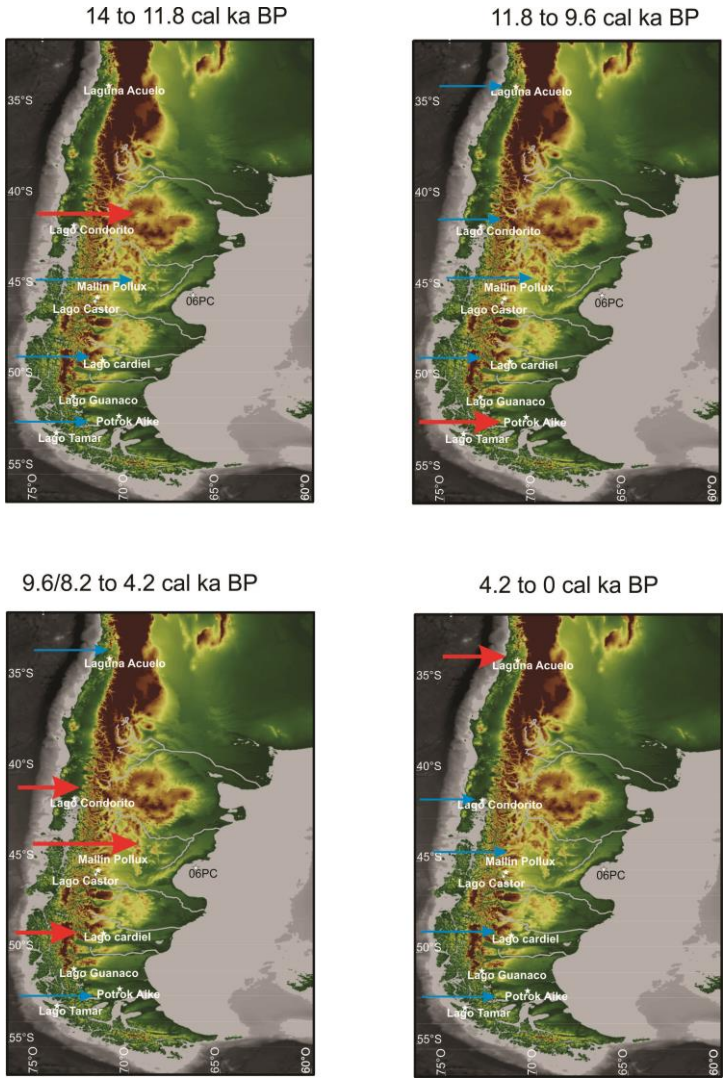

Figure 30. Schematic map showing the migration of the SWWB during the last 14 cal ka BP. The red (blue) arrows depict the intensification (weakening) of the SWWB flow.

3.9 ACKNOWLEDGEMENTS

This research was funded by the FRQNT (*Fonds de recherche du Québec – Nature et technologies* grant to G. St-Onge and A. Rochon) and NSERC (Natural Sciences and Engineering Research Council of Canada) Discovery grants to A. Rochon and G. St-Onge. The first author received various financial support (for scholarships, congress and internship) from ISMER-UQAR, GEOTOP, Québec-Océan and the Réseau Québec maritime. We thank Raquel Guerstein for her help in the identification of Cretaceous and Miocene dinocysts. We are grateful to the captain, officers, crew and scientists of the MARGES expedition on board the R/V Coriolis II. Finally, we thank the *Ministerio de Ciencia, Tecnología e Innovación Productiva,* MINCyT, the Province of Chubut and the *Consejo Nacional de Investigaciones Científicas Técnicas,* CONICET) for the MARGES and MARES expeditions.

3.10 REFERENCES

Agosta, E., Compagnucci, R., Ariztegui, D., 2015. Precipitation linked to Atlantic moisture transport: clues to interpret Patagonian palaeoclimate. Climate Research, 62(3), 219-240.

Anderson, R.F., Ali, S., Bradtmiller, L.I., Nielsen, S.H.H., Fleisher, M.Q., Anderson, B.E., Burckle, L.H., 2009. Wind-Driven Upwelling in the Southern Ocean and the Deglacial Rise in Atmospheric CO2. Science, 323, 1443–1448. https://doi.org/10.1126/science.1167441.s

Aniya, M., 2012. Holocene glaciations of Hielo Patagónico (Patagonia Icefield), South America: A brief review 9.

Aravena, J.-C., Luckman, B.H., 2009. Spatio-temporal rainfall patterns in Southern South America. International Journal of Climatology, 29, 2106–2120. https://doi.org/10.1002/joc.1761.

Ariztegui, D., Gilli, A., Anselmetti, F.S., Goñi, R.A., Belardi, J.B., Espinosa, S., 2010. Lake-level changes in central Patagonia (Argentina): crossing environmental thresholds for Lateglacial and Holocene human occupation. Journal of Quaternary Science, 25, 1092–1099. https://doi.org/10.1002/jqs.1352.

Basile, I., Grousset, F.E., Revel, M., Petit, J.R., Biscaye, P.E., Barkov, N.I., 1997. Patagonian origin of glacial dust deposited in East Antarctica (Vostok and Dome C) during glacial stages 2, 4 and 6. Earth and Planetary Science Letters, 146(3-4), 573-589.

Bennett, K.D., Haberle, S.G., Lumley, S.H., 2000. The last glacial-Holocene transition in southern Chile. Science, 290(5490), 325-328.

Bianchi, C., Gersonde, R., 2004. Climate evolution at the last deglaciation: the role of the Southern Ocean. Earth and Planetary Science Letters, 228, 407–424. https://doi.org/10.1016/j.epsl.2004.10.003.

Blaauw, M., Christen, J.A., 2011. Flexible paleoclimate age-depth models using an autoregressive gamma process. Bayesian Analysis, 6, 457–474. https://doi.org/10.1214/11-BA618.

Brandhorst, W., Castello, J.P., 1971. Evaluación de los recursos de anchoíta (Engraulis anchoita) frente a la Argentina y Uruguay. Serie de Informaciones Técnicas.

Caniupán, M., Lamy, F., Lange, C.B., Kaiser, J., Arz, H., Kilian, R., Baeza Urrea, O., Aracena, C., Hebbeln, D., Kissel, C., Laj, C., Mollenhauer, G., Tiedemann, R., 2011. Millennial-scale sea surface temperature and Patagonian Ice Sheet changes off southernmost Chile (53°S) over the past ~60 kyr: SST CHANGES OFF SOUTHERN CHILE. Paleoceanography, 26, n/a-n/a. https://doi.org/10.1029/2010PA002049.

Cavallotto, J., 2004. Sea-level fluctuations during the last 8600 years in the de la Plata River (Argentina). Quaternary International, 114, 155–165. https://doi.org/10.1016/S1040-6182(03)00050-8.

Cook, E.J., van Geel, B., van der Kaars, S., van Arkel, J., 2011. A review of the use of non-pollen palynomorphs in palaeoecology with examples from Australia. Palynology, 35, 155–178. https://doi.org/10.1080/01916122.2010.545515.

Coronato, A.M.J., Coronato, F., Mazzoni, E., Vázquez, M., 2008. The Physical Geography of Patagonia and Tierra del Fuego, in: Developments in Quaternary Sciences. Elsevier, pp. 13–55. https://doi.org/10.1016/S1571-0866(07)10003-8.

Croudace, I. W., Rothwell, R. G. 2015. Micro-XRF Studies of Sediment Cores: Applications of a non-destructive tool for the environmental sciences (Vol. 17). Springer.

de Vernal, A., Eynaud, F., Henry, M., Limoges, A., Londeix, L., Matthiessen, J., Marret, F., Pospelova, V., Radi, T., Rochon, A., Van Nieuwenhove, N., Zaragosi, S., 2018. Distribution and (palaeo)ecological affinities of the main *Spiniferites* taxa in the mid-

high latitudes of the Northern Hemisphere. Palynology, 42, 182–202. https://doi.org/10.1080/01916122.2018.1465730.

Delmonte, B., Baroni, C., Andersson, P.S., Schoberg, H., Hansson, M., Aciego, S., Petit, J.-R., Albani, S., Mazzola, C., Maggi, V., Frezzotti, M., 2010. Aeolian dust in the Talos Dome ice core (East Antarctica, Pacific/Ross Sea sector): Victoria Land versus remote sources over the last two climate cycles. Journal of Quaternary Science, 25, 1327–1337. https://doi.org/10.1002/jqs.1418.

Denton, G.H., Anderson, R.F., Toggweiler, J.R., Edwards, R.L., Schaefer, J.M., Putnam, A.E., 2010. The Last Glacial Termination. Science, 328, 1652–1656. https://doi.org/10.1126/science.1184119.

Desiage, P-A., 2020. Dynamique sédimentaire, stratigraphie et paléomagnétisme de la région du golfe de San Jorge, Patagonie, Argentine, depuis la dernière déglaciation. Doctoral dissertation, Université du Québec à Rimouski, 231 p.

Dodge, J.D., Harland, R., 1991. The distribution of planktonic dinoflagellates and their cysts in the eastern and northeastern Atlantic Ocean. New Phytologist, 118, 593–603. https://doi.org/10.1111/j.1469-8137.1991.tb01000.x.

Faye, S., Rochon, A., St-Onge, G., 2018. Distribution of Modern Dinoflagellate Cyst Assemblages in Surface Sediments of San Jorge Gulf (Patagonia, Argentina). Oceanography, 31, 122–131. https://doi.org/10.5670/oceanog.2018.416.

Faye, S., Eynaud, F., Bosq, M., Lambert, C., Verdin, F., Vequaud, P., Lodyga, O., Dériennic, H., Lebleu, P., Bujan, S., Billy, I., Martin, B., Roussot-Larroque(†), J., 2019. Holocene palaeoenvironmental evolution of the Médoc peninsula (SW France): insights from the sedimentological study of the "Lède du Gurp" archaeological site. Quaternaire, 31–46. https://doi.org/10.4000/quaternaire.11164.

Faye, S., Rochon, A., St-Onge, G., Vilanova, I., 2020. Pollen dispersal patterns in marine surface sediments from the San Jorge Gulf, SE Patagonia (Argentina). Palaeogeography, Palaeoclimatology, Palaeoecology, 109869.

Fletcher, M.-S., Moreno, P.I., 2011. Have the Southern Westerlies changed in a zonally symmetric manner over the last 14,000 years? A hemisphere-wide take on a controversial problem. Quaternary International, 253, 32–46. https://doi.org/10.1016/j.quaint.2011.04.042.

Fitzgerald, M.G., Mitchum Jr, R. M., Uliana, M.A., Biddle, K.T., 1990. Evolution of the san Jorge basin, Argentina. AAPG bulletin, 74(6), 879-920.

Foix, N., Paredes, J.M., Giacosa, R.E., 2013. Fluvial architecture variations linked to changes in accommodation space: Río Chico Formation (late Paleocene), Golfo San Jorge basin, Argentina. Sedimentary Geology, 294, 342-355.

Garreaud, R., Lopez, P., Minvielle, M., Rojas, M., 2013. Large-Scale Control on the Patagonian Climate. Journal of Climate, 26, 215–230. https://doi.org/10.1175/JCLI-D-12-00001.1.

Garreaud, R.D., 2009. The Andes climate and weather. Advances in Geosciences, 22, 3–11. https://doi.org/10.5194/adgeo-22-3-2009.

Gledhill, M., Buck, K.N., 2012. The organic complexation of iron in the marine environment: a review. Frontiers in Microbiology, 3, 69.

Groot, J.J., Groot, C.R., Ewing, M., Burckle, L., Conolly, J. R., 1965. Spores, pollen, diatoms and provenance of the Agentine basin sediments. Progress in oceanography, 4, 179-217.

Guilderson, T.P., Burckle, L., Hemming, S., Peltier, W.R., 2000. Late Pleistocene sea level variations derived from the Argentine Shelf: sea level variations. Geochemistry, Geophysics, Geosystems, 1, n/a-n/a. https://doi.org/10.1029/2000GC000098.

Heusser, C.J., 1971. Pollen and spores of Chile. University of Arizona Press.

Heusser, C.J., 1989. Southern westerlies during the last glacial maximum. Quaternary Research, 31(3), 423-425.

Jansen, J.H.., Van der Gaast, S.., Koster, B., Vaars, A., 1998. CORTEX, a shipboard XRF-scanner for element analyses in split sediment cores. Marine Geology, 151, 143–153. https://doi.org/10.1016/S0025-3227(98)00074-7.

Jenny, B., Wilhelm, D., Valero-Garcés, B., 2003. The Southern Westerlies in Central Chile: Holocene precipitation estimates based on a water balance model for Laguna Aculeo (33°50′S). Climate Dynamics, 20, 269–280. https://doi.org/10.1007/s00382-002-0267-3.

Jerardino, A., 1995. Late Holocene Neoglacial episodes in southern South America and southern Africa: a comparison. The Holocene, 5, 361–368. https://doi.org/10.1177/095968369500500313.

Kaiser, J., Lamy, F., Hebbeln, D., 2005. A 70-kyr sea surface temperature record off southern Chile (Ocean Drilling Program Site 1233): A 70-kyr sst record off southern Chile. Paleoceanography, 20, n/a-n/a. https://doi.org/10.1029/2005PA001146.

Kaplan, M.R., Schaefer, J.M., Strelin, J.A., Denton, G.H., Anderson, R.F., Vandergoes, M. J., Martini, M. A., 2016. Patagonian and southern South Atlantic view of Holocene climate. Quaternary Science Reviews, 141, 112-125.

Kilian, R., Lamy, F., 2012. A review of Glacial and Holocene paleoclimate records from southernmost Patagonia (49–55°S). Quaternary Science Reviews, 53, 1–23. https://doi.org/10.1016/j.quascirev.2012.07.017.

Lamy, F., Kilian, R., Arz, H.W., Francois, J.-P., Kaiser, J., Prange, M., Steinke, T., 2010. Holocene changes in the position and intensity of the southern westerly wind belt. Nature Geoscience, 3, 695–699. https://doi.org/10.1038/ngeo959.

Leckie, R.M., Sigurdsson, H., Acton, G.D., Draper, G., 2000. Proceedings of the Ocean Drilling Program, 165 Scientific Results, Proceedings of the Ocean Drilling Program. Ocean Drilling Program. https://doi.org/10.2973/odp.proc.sr.165.2000.

León, R.J.C., Bran, D., Collantes, M., Paruelo, J.M., 1995. Grandes unidades de vegetación de la Patagonia extra andina. Ecologia Austral, 8 : 125-144.

Lisé-Pronovost, A., St-Onge, G., Gogorza, C., Haberzettl, T., Jouve, G., Francus, P., Ohlendorf, C., Gebhardt, C., Zolitschka, B., 2015. Rock-magnetic proxies of wind intensity and dust since 51,200 cal BP from lacustrine sediments of Laguna Potrok Aike, southeastern Patagonia. Earth and Planetary Science Letters, 411, 72–86. https://doi.org/10.1016/j.epsl.2014.11.007.

Markgraf, V., D'Antoni, H. L., 1978. Pollen flora of Argentina. Tucson: Arizona, University of Arizona Press, 208p.

Markgraf, V., 1989. Reply to CJ Heusser's "Southern westerlies during the last glacial maximum". Quaternary Research, 31(3), 426-432.

Mancini, M. V., Prieto, A. R., Paez, M. M., Schäbitz, F., 2008. Late Quaternary vegetation and climate of Patagonia. Developments in Quaternary Sciences, 11, 351-367.

Marcos, M.A., Mancini, M.V., 2012. Modern pollen and vegetation relationships in northeastern Patagonia (Golfo San Matías, Río Negro). Review of Palaeobotany and Palynology, 171, 19–26. https://doi.org/10.1016/j.revpalbo.2011.11.007.

Matano, R.P., Palma, E.D., Piola, A.R., 2010. The influence of the Brazil and Malvinas Currents on the Southwestern Atlantic Shelf circulation. Ocean Science, 6, 983–995. https://doi.org/10.5194/os-6-983-2010.

Matano, R., Palma, E., 2018. Seasonal Variability of the Oceanic Circulation in the Gulf of San Jorge, Argentina. Oceanography, 31. https://doi.org/10.5670/oceanog.2018.402.

Mayr, C., Wille, M., Haberzettl, T., Fey, M., Janssen, S., Lucke, A., Ohlendorf, C., Oliva, G., Schabitz, F., Schleser, G., 2007. Holocene variability of the Southern Hemisphere westerlies in Argentinean Patagonia (52°S). Quaternary Science Reviews, 26, 579–584. https://doi.org/10.1016/j.quascirev.2006.11.013.

McCarthy, F.M., Mudie, P. J., 1998. Oceanic pollen transport and pollen: dinocyst ratios as markers of late Cenozoic sea level change and sediment transport. Palaeogeography, Palaeoclimatology, Palaeoecology, 138(1-4), 187-206.

Moreno, P.I., Francois, J.P., Moy, C.M., Villa-Martínez, R., 2010. Covariability of the Southern Westerlies and atmospheric CO2 during the Holocene. Geology, 38, 727–730. https://doi.org/10.1130/G30962.1.

Moreno, P.I., Videla, J., 2016. Centennial and millennial-scale hydroclimate changes in northwestern Patagonia since 16,000 yr BP. Quaternary Science Reviews, 149, 326–337. https://doi.org/10.1016/j.quascirev.2016.08.008.

Moreno, P.I., Vilanova, I., Villa-Martínez, R., Dunbar, R.B., Mucciarone, D.A., Kaplan, M.R., Garreaud, R.D., Rojas, M., Moy, C.M., De Pol-Holz, R., Lambert, F., 2018. Onset and Evolution of Southern Annular Mode-Like Changes at Centennial Timescale. Scientific Reports, 8. https://doi.org/10.1038/s41598-018-21836-6.

Moy, C.M., Moreno, P.I., Dunbar, R.B., Kaplan, M.R., Francois, J.-P., Villalba, R., Haberzettl, T., 2009. Climate Change in Southern South America During the Last Two Millennia, in: Vimeux, F., Sylvestre, F., Khodri, M. (Eds.), Past Climate Variability in South America and Surrounding Regions. Springer Netherlands, Dordrecht, pp. 353–393. https://doi.org/10.1007/978-90-481-2672-9_15.

Nullo, F. E., Combina, A. M., 2002. Sedimentitas terciarias continentales. In Congreso Geológico Argentino, 15, pp. 245-258.

Paparazzo, F., Crespi-Abril, A., Gonçalves, R., Barbieri, E., Gracia Villalobos, L., Solís, M., Soria, G., 2018. Patagonian Dust as a Source of Macronutrients in the Southwest Atlantic Ocean. Oceanography, 31, 33–39. https://doi.org/10.5670/oceanog.2018.408.

Paredes, J. M., 2002. Asociaciones de facies y correlación de las sedimentitas de la Formación Chenque (Oligoceno-Mioceno) en los alrededores de Comodoro Rivadavia, Cuenca del Golfo San Jorge, Argentina. *Latin American Journal of Sedimentology and Basin Analysis*, *9*(1), 53-64.

Paredes, J.M., Foix, N., Guerstein, G.R., Guler, M.V., Irigoyen, M., Moscoso, P., Giordano, S., 2015. A late eocene-early Oligocene transgressive event in the Golfo San Jorge basin: Palynological results and stratigraphic implications. Journal of South American Earth Sciences, 63, 293–309. https://doi.org/10.1016/j.jsames.2015.08.009.

Paredes, J. M., Foix, N., Guerstein, G. R., Guler, M. V., Irigoyen, M., Moscoso, P., Giordano, S., 2015. A late eocene-early Oligocene transgressive event in the Golfo San Jorge basin: Palynological results and stratigraphic implications. Journal of South American Earth Sciences, 63, 293-309.

Parrenin, F., Masson-Delmotte, V., Kohler, P., Raynaud, D., Paillard, D., Schwander, J., Barbante, C., Landais, A., Wegner, A., Jouzel, J., 2013. Synchronous Change of Atmospheric CO2 and Antarctic Temperature During the Last Deglacial Warming. Science, 339, 1060–1063. https://doi.org/10.1126/science.1226368.

Piola, A.R., Avellaneda, N.M., Guerrero, R.A., Romero, S.I., 2009. Malvinas-slope water intrusions 36.

Pospelova, V., de Vernal, A., Pedersen, T.F., 2008. Distribution of dinoflagellate cysts in surface sediments from the northeastern Pacific Ocean (43–25°N) in relation to sea-surface temperature, salinity, productivity and coastal upwelling. Marine Micropaleontology, 68, 21–48. https://doi.org/10.1016/j.marmicro.2008.01.008.

Quade, J., Kaplan, M.R., 2017. Lake-level stratigraphy and geochronology revisited at Lago (Lake) Cardiel, Argentina, and changes in the Southern Hemispheric Westerlies over the last 25 ka. Quaternary Science Reviews, 177, 173-188.

Rabassa, J., 2008. Late Cenozoic Glaciations in Patagonia and Tierra del Fuego, in: Developments in Quaternary Sciences. Elsevier, pp. 151–204. https://doi.org/10.1016/S1571-0866(07)10008-7

Rignot, E., 2003. Contribution of the Patagonia Icefields of South America to Sea Level Rise. Science, 302, 434–437. https://doi.org/10.1126/science.1087393.

Rochon, A., Vernal, A.D., Turon, J.L., Matthiessen, J., Head M.J., 1999. Distribution of recent dinoflagellate cysts in surface sediments from the North Atlantic Ocean and adjacent seas in relation to sea-surface parameters. American Association of Stratigraphic Palynologists Contribution Series, 35, 1-146.

Sepúlveda, J., Pantoja, S., Hughen, K.A., Bertrand, S., Figueroa, D., León, T., Drenzek, N.J.,

Lange, C., 2009. Late Holocene sea-surface temperature and precipitation variability in northern Patagonia, Chile (Jacaf Fjord, 44°S). Quaternary Research, 72, 400–409. https://doi.org/10.1016/j.yqres.2009.06.010.

Simonella, L.E., Palomeque, M.E., Croot, P.L., Stein, A., Kupczewski, M., Rosales, A., Montes, M.L., Colombo, F., García, M.G., Villarosa, G., Gaiero, D.M., 2015. Soluble iron inputs to the Southern Ocean through recent andesitic to rhyolitic volcanic ash eruptions from the Patagonian Andes. Global Biogeochemical Cycles, 29, 1125–1144. https://doi.org/10.1002/2015GB005177.

Solomina, O.N., Bradley, R.S., Hodgson, D.A., Ivy-Ochs, S., Jomelli, V., Mackintosh, A.N., Nesje, A., Owen, L.A., Wanner, H., Wiles, G.C., Young, N.E., 2015. Holocene glacier fluctuations. Quaternary Science Reviews, 111, 9–34. https://doi.org/10.1016/j.quascirev.2014.11.018.

St-Onge, G., Ferreyra, G., 2018. Introduction to the Special Issue on the Gulf of San Jorge (Patagonia, Argentina). Oceanography, 31, 14–15. https://doi.org/10.5670/oceanog.2018.406.

Strelin, J. A., Kaplan, M. R., Vandergoes, M. J., Denton, G. H., Schaefer, J. M., 2014. Holocene glacier history of the Lago Argentino basin, southern Patagonian Icefield. Quaternary Science Reviews, 101, 124-145.

Stuiver, M., Reimer, P.J., 1993. Extended ^{14}C Data Base and Revised CALIB 3.0 ^{14}C Age Calibration Program. Radiocarbon, 35, 215–230. https://doi.org/10.1017/S0033822200013904.

Stutz, S., Prieto, A.R., Isla, F.I., 2006. Holocene evolution of the Mar Chiquita coastal lagoon area (Argentina) indicated by pollen analysis. Journal of Quaternary Science, 21, 17–28. https://doi.org/10.1002/jqs.952.

Toggweiler, J.R., Russell, J.L., Carson, S.R., 2006. Midlatitude westerlies, atmospheric CO_2, and climate change during the ice ages: westerlies and CO_2 during ice age. Paleoceanography, 21, n/a-n/a. https://doi.org/10.1029/2005PA001154.

Van Daele, M., Bertrand, S., Meyer, I., Moernaut, J., Vandoorne, W., Siani, G., De Batist, M., 2016. Late Quaternary evolution of Lago Castor (Chile, 45.6 S): Timing of the deglaciation in northern Patagonia and evolution of the southern westerlies during the last 17 kyr. Quaternary Science Reviews, 133, 130-146.

Vilanova, I., Moreno, P.I., Miranda, C.G., Villa-Martínez, R.P., 2019. The last glacial termination in the Coyhaique sector of central Patagonia. Quaternary Science Reviews, 224, 105976.

Violante, R., 2004., The post-last glacial maximum transgression in the de la Plata River and adjacent inner continental shelf, Argentina. Quaternary International, 114, 167–181. https://doi.org/10.1016/S1040-6182(03)00036-3.

Walker, M., Head, M. J., Lowe, J., Berkelhammer, M., BjÖrck, S., Cheng, H., Newnham, R., 2019. Subdividing the Holocene Series/Epoch: formalization of stages/ages and subseries/subepochs, and designation of GSSPs and auxiliary stratotypes. Journal of Quaternary Science, 34(3), 173-186.

Zonneveld, K.A.F., Marret, F., Versteegh, G.J.M., Bogus, K., Bonnet, S., Bouimetarhan, I., Crouch, E., de Vernal, A., Elshanawany, R., Edwards, L., Esper, O., Forke, S., Grøsfjeld, K., Henry, M., Holzwarth, U., Kielt, J.-F., Kim, S.-Y., Ladouceur, S., Ledu, D., Chen, L., Limoges, A., Londeix, L., Lu, S.-H., Mahmoud, M.S., Marino, G., Matsouka, K., Matthiessen, J., Mildenhal, D.C., Mudie, P., Neil, H.L., Pospelova, V., Qi, Y., Radi, T., Richerol, T., Rochon, A., Sangiorgi, F., Solignac, S., Turon, J.-L., Verleye, T., Wang, Y., Wang, Z., Young, M., 2013. Atlas of modern dinoflagellate cyst distribution based on 2405 data points. Review of Palaeobotany and Palynology, 191, 1–197. https://doi.org/10.1016/j.revpalbo.2012.08.003.

CONCLUSION GÉNÉRALE

Cette étude combinant plusieurs approches (analyses palynologiques et sédimentologiques) a permis de répondre à l'objectif général de la thèse qui est de décrire les variations climatiques et de reconstituer les conditions océanographiques dans le GSJ (Patagonie, Argentine) au cours du Pléistocène supérieur et de l'Holocène. Pour y parvenir, la thèse a été divisée en trois objectifs spécifiques lesquels ont permis d'apporter des éléments d'appréciation afin de répondre à l'objectif général. L'ensemble des données obtenues à partir des échantillons de surface et des séquences sédimentaires prélevées dans le GSJ ont permis : (1) d'établir la première distribution spatiale des assemblages modernes de kystes de dinoflagellés en relation avec les conditions modernes de surface du GSJ, (2) de décrire les patrons de dispersion moderne du pollen et de spores en lien avec la végétation adjacente au GSJ, (3) de transcrire l'histoire de la végétation en Patagonie à l'échelle régionale et de retracer la migration latitudinale de la ceinture des vents d'ouest en relation avec les conditions océaniques dans le golfe au cours des 14 000 dernières années.

Distribution moderne des kystes de dinoflagellés

Afin de mieux interpréter les variations des conditions océaniques dans le GSJ, j'ai exploré les liens entre la distribution des kystes de dinoflagellés et les conditions environnementales dans le golfe. Cette étude se basant sur 52 échantillons de surface montre que les assemblages de kystes de dinoflagellés reflètent les paramètres environnementaux dans le GSJ et dans la partie située au large.

Dans le GSJ, les concentrations de kystes de dinoflagellés décrivent un gradient nord-sud avec une augmentation des concentrations dans la partie centrale et sud du GSJ. Ce changement semble être en lien avec la productivité et les processus contrôlant le dépôt des

kystes de dinoflagellés. À partir des abondances de kystes de dinoflagellés, deux sous-assemblages ont été identifié dans le golfe. **Le premier sous assemblage (Ia)**, localisé dans la partie nord du GSJ, est caractérisé par un environnement très dynamique avec une forte abondance d'organismes hétérotrophes (e.g. *Polykrikos kofoidii*, *Echinidinium* sp.). La présence de ces derniers dans le golfe semble être contrôlée par la disponibilité en proies notamment les diatomées. **Le deuxième sous assemblage (Ib)**, situé dans la partie centre et sud du GSJ, est caractérisé par une forte concentration de kystes de dinoflagellés dominés par les organismes autotrophes. Plusieurs éléments tels que la nature des eaux stratifiées au centre du GSJ, la présence de fronts tidaux au sud du golfe et l'apport des eaux subantarctiques riches en nutriments par les courants côtiers pourraient expliquer cette abondance.

Le deuxième assemblage (II), localisé dans la partie au large du golfe, est caractérisé par une abondance de taxons hétérotrophes (e.g. *Brigantedinium* spp., *Polykrikos kofoidii*) et l'apparition d'*Impagidinium paradoxum*. L'abondance de ces organismes hétérotrophes semble être reliée à l'upwelling situé au niveau de l'isobathe 200 m.

Cette étude a permis d'établir les relations entre la distribution des kystes de dinoflagellés avec les conditions océaniques dans le GSJ. Cependant, un échantillonnage supplémentaire dans le sud du golfe et dans l'ensemble de l'Atlantique Sud-Ouest est nécessaire pour dresser un panorama beaucoup plus large de la distribution des kystes de dinoflagellés dans l'hémisphère Sud. Sous ce rapport, une base de données pourrait être établie, à l'instar de celle dans l'hémisphère Nord (https://www.geotop.ca/recherche/donnees/micropaleontologie/dinokystes/n1492) afin de permettre des reconstitutions quantitatives des conditions océaniques de surface dans l'Atlantique Sud.

Patrons de dispersion moderne des assemblages de pollen et de spores

Les analyses polliniques réalisées à partir des mêmes échantillons de surface que l'objectif 1 ont permis d'établir la première étude sur les patrons de dispersions modernes de

pollen et de spores dans l'Atlantique Sud. Les résultats de cette investigation fournissent des informations cruciales pour mieux décrire les changements paléoenvironnementaux sur la partie continentale adjacente au GSJ. Les fortes concentrations retrouvées dans les parties centre et sud du GSJ sont similaires à celles des kystes de dinoflagellés et sont corrélées avec la granulométrie fine des sédiments. En raison d'une distribution étendue des espèces dans la steppe patagonienne, le spectre pollinique montre une faible variation. Les résultats montrent une abondance de pollen de plantes arbustives hautes (e.g. *Colliguaja integerrima*) et de *Chuquiraga* sp. dans les échantillons situés dans la partie nord du GSJ et une faible augmentation des taxons de plantes herbacées (Poaceae, Chenopodiaceae) dans les parties centre et sud du GSJ. Ces changements se reflètent aussi dans les patrons de dispersion issus des échantillons continentaux de surface autour du GSJ (Paez et al., 2001). La forte correspondance entre certains patrons polliniques dans les échantillons continentaux et marins avec la végétation ont permis de montrer que **les patrons de dispersions polliniques dans les sédiments de surface du GSJ reflètent la végétation actuelle sur le continent adjacent au GSJ**. Ainsi, nous avons pu démontrer que les courants marins n'altèrent pas l'image de la végétation, ce qui atteste de l'applicabilité des études polliniques dans notre site d'étude. De plus, nous avons pu démontrer que **les flux polliniques reflètent les processus dynamiques dans l'atmosphère principalement contrôlés par la ceinture des vents d'ouest**. Dans les sédiments de surface du GSJ, les grains de pollen de *Nothofagus* sp. et *Podocarpus* sp., transportés sur de longues distances de la forêt subantarctique vers le GSJ sur près de 350 km, ont été retrouvés. L'abondance de ces taxons dans les archives sédimentaires a été ciblée comme des candidats potentiels pour évaluer l'intensité des vents d'ouest dans le GSJ et les changements de végétation dans la forêt subantarctique.

L'utilisation des reconstitutions quantitatives a été démontré comme étant un excellent outil pour étudier le climat (e.g. Tonello e al., 2009; Richerol, 2014). De ce fait, il est primordial d'avoir une base de données pollinique moderne qui reflète l'image de la végétation. Récemment Flantua et al. (2015) ont compilés les études polliniques sur les échantillons modernes en Amérique du sud. Il serait donc intéressant d'affiner cette base de

données pour la Patagonie en y implémentant les résultats de cette investigation. De plus, d'autres études pourront être menées dans les zones où l'on ne dispose pas de données. Il serait également important d'obtenir des paramètres climatiques actuels avec une haute résolution spatiale afin d'améliorer les modèles de calibration pour les reconstructions quantitatives du climat sur l'étendue de la Patagonie (e.g. Tonello et al., 2009, Schäbitz et al.,2013).

Histoire de la végétation en Patagonie et les variations de la ceinture des vents d'ouest en relation avec les conditions océanographiques dans le GSJ

L'ensemble des données obtenues à partir de l'analyse palynologique et sédimentaire des trois carottes prélevées dans le GSJ a permis de retracer l'histoire de la végétation adjacente au golfe. Cette étude a permis également de décrire les variations de la ceinture des vents d'ouest en lien avec les conditions océaniques dans l'Atlantique Sud-Ouest.

Les assemblages palynologiques montrent que le GSJ est caractérisé par des **conditions subaériennes avant 14 000 cal BP**. Les analyses sédimentologiques et des assemblages fossiles de kystes de dinoflagellés suggèrent un **environnement de dépôt peu profond dans le GSJ avant 14 000 cal BP, possiblement lagunaire, associé à un système de drainage érodant les formations du Crétacé et du Miocène** (e.g. Desiage, 2020). Durant cette période, la végétation autour du GSJ est dominée par des taxons halophytiques sous un climat aride. Après 14 000 cal BP, le **niveau marin augmente progressivement dans l'Atlantique Sud-Ouest et marque l'immersion du GSJ** avec l'apparition de palynomorphes marins. Sur le continent adjacent au GSJ, la steppe patagonienne se développe autour du golfe avec une grande inertie de la végétation marquée de faibles variations au cours Pléistocène supérieur jusqu'à l'actuel. Au Pléistocène supérieur, les assemblages fossiles de pollen montrent une végétation semi-désertique caractérisée par une abondance de taxons arbustifs bas (Asteraceae, *Ephedra* sp.). Durant cette période, l'analyse du contenu pollinique suggère une végétation très similaire à celle moderne autour du GSJ. À l'Holocène inférieur et moyen, le spectre pollinique montre un retour vers des conditions beaucoup plus arides marquées par

une augmentation des taxons halophytiques (e.g. Chenopodiaceae) et une baisse des taxons arbustifs. Cette période est suivie par une transition vers des conditions semi-désertiques modernes à l'Holocène supérieur marquées par une légère augmentation de l'humidité traduite par une faible expansion des taxons d'arbustifs. L'augmentation de l'humidité dans cette partie orientale de la Patagonie (e.g. continent adjacent au GSJ) semble être en lien avec une diminution de l'intensité de la ceinture des vents d'ouest entrainant ainsi des précipitations beaucoup plus importantes provenant de l'Atlantique (e.g. Agosta et al., 2015).

La comparaison de l'analyse palynologique des trois carottes avec d'autres archives paléoclimatiques situées en Patagonie a permis de décrire les variations de la ceinture des vents d'ouest et ses implications dans l'Atlantique Sud-Ouest. **Les résultats montrent une expansion vers le nord de la ceinture des vents d'ouest au Pléistocène supérieur**. Cette expansion est synchrone avec des conditions tempérées dans le GSJ et des conditions beaucoup plus froides dans le Pacifique et l'Atlantique sud (Bianchi et Gersonde, 2004; Caniupàn et al., 2014). **Cette période est suivie d'une migration vers le sud de la ceinture des vents d'ouest au début de l'Holocène inférieur** induisant un upwelling dans les hautes latitudes de l'Atlantique Sud-Ouest (e.g. Anderson et al., 2009). **À la fin de l'Holocène inférieur jusqu'à l'Holocène moyen, les index polliniques montrent une intensification des vents d'ouest au centre de la Patagonie** induisant une fertilisation du GSJ traduit par une augmentation de la productivité primaire. Ce retour progressif vers le nord de la ceinture des vents d'ouest expliquerait l'affaiblissement de l'upwelling induit par les vents d'ouest dans les hautes latitudes de l'Atlantique Sud (e.g. Anderson et al., 2009). **À l'Holocène supérieur, nos résultats indiquent un affaiblissement des vents d'ouest sur le GSJ** et sur l'ensemble des sites situés en Patagonie indiquant ainsi une expansion de la ceinture des vents d'ouest beaucoup plus au nord

Tableau 2. Relation entre la position des westerlies, les conditions océaniques dans le GSJ et l'histoire de la végétation sur le continent adjacent au golfe.La flèche vers le haut (bas) indique une augmentation (diminution).

	Position des *westerlies*	Conditions océaniques dans le GSJ	Histoire de la végétation de la steppe patagonienne
Holocène supérieur	Expansion vers le nord	-%Dinokystes autotrophes (↑) - Productivité (↓) - Transition vers les conditions modernes	- Steppe herbeuse et arbustive - Taxons arbustifs (↑), humidité (↑) - Établissement de la végétation moderne - Conditions semi-arides
4.2 ka			
Holocène moyen	Expansion progressive vers le nord	- Milieu océanique ouvert - Forte présence de dinokystes hétérotrophes (%) - Forte productivité	- Steppe herbeuse et arbustive - Taxons halophytiques (↑), aridité (↑) - Conditions semi-arides
8.2 ka	Augmentation de l'intensité des westerlies à la latitude du GSJ	Fertilisation du GSJ par les westerlies induisant une augmentation de la productivité	
Holocène inférieur	Contraction vers le sud	- Environnement proximal -%Dinokystes hétérotrophes (↑) - Productivité (↑)	
11.8 ka			
Pléistocène supérieur	Expansion vers le nord	- Immersion du GSJ -%Dinokystes autotrophes (↑) - Conditions tempérées - Faible productivité	- Steppe herbeuse et arbustive - Végétation similaire à celle moderne - Conditions semi-arides
14 ka			

Cette étude constitue la première investigation décrivant la variation de la ceinture des vents d'ouest en relation avec les conditions oceanographiques dans l'Atlantique Sud-Ouest. Ainsi, les résultats de ce travail démontrent-il la possiblité d'étudier la dynamique de la ceinture des vents d'ouest dans l'Atlantique Sud. Cela ouvre ainsi des perspectives de recherches. Dans l'avenir, il serait aussi intéressant de prendre des carottes sur une résolution spatiale d'au moins 5° à 10° de latitude de l'Atlantique Sud-Ouest pour tracer la moindre migration de la ceinture des vents d'ouest et ses implications dans l'Atlatique Sud. De plus, en raison de l'absence d'une base de données des kystes de dinoflagellés dans l'hémisphère Sud qui empêche de faire des reconstititutions quantitatives des conditions océaniques dans l'Atlantique Sud, il serait donc intéressant d'investiguer d'autres proxies qui permettront d'en faire (e.g. $\delta^{18}O$ (e.g. Koutavas et Stieglitz, 2003), Ca/Mg ratio (e.g. Cornblad et Malmgren, 1981, Martin et al., 2002), Alkenones (e.g. Canuipán et al., 2011), TEX_{86} (e.g. Schouten et al., 20013). Ainsi, on pourrait suivre les faibles variations de la ceinture des vents en lien avec les variations de température dans l'Atlantique Sud. Pour compléter cette étude, il serait important d'accroître la résolution temporelle de l'analyse palynologique des carottes sédimentaires (06PC, 08PC et 11PC) afin de mieux évaluer les variations séculaires des vents d'ouest. On pourrait également étudier les assemblages de diatomées ou les flux d'opale sur les mêmes carottes sédimentaires pour mieux caractériser la paléo-productivité dans le GSJ (Romero et al., 2006, Anderson et al., 2009). Par ailleurs, il serait pertinent d'obtenir des données d'archives à haute résolution sur la dynamique passée du courant des Malouines et de la paléoproductivité du système d'upwelling situé au niveau de l'isobathe 200 m à partir d'indicateurs biologiques (assemblages fossiles de kystes de dinoflagellés et de diatomées). Cela permettra d'obtenir des connaissances sur les mécanismes et les retroactions mettant en jeu les intéractions océan-atmosphère dans l'Atlantique Sud-Ouest.

SUPPLEMENTARY MATERIAL

Table 3. Samples used in this study with coordinates, water depth, dinocyst counts, cyst concentrations, grain size data (% fraction > 63 μm and < 63 μm), and hydrographic data for each sample. Nitrate (N), silicate (Si), and phosphate (P) concentrations are expressed in μmol L^{-1}. Concentrations of chlorophyll-*a* (February, May, August, November) are expressed in mg m^{-3}. Temperature and salinity are in °C and PSU (Practical Salinity Units).

Sample ID	Longitude (°W)	Latitude (°S)	Lab number	Depth (m)	Dinocyst counts	Concentrations (cysts g^{-1})	Organic linings of foraminifera (cells g^{-1})	*Halodinium* sp. (cells g^{-1})	> 63 μm	< 63 μm	P	Si	Chl.a.f	Ch.a.m	Ch.a.a	Ch.a.n	Tsum	Twin	Ssum	Swin
BV01	-66.0274	-46.3756	476-1	97	2,306	26,296	274	57	30	70	1.02	20.46	1.24	1.10	1.07	1.84	14.23	8.09	33.33	33.34
BV02	-66.3956	-46.6621	436-1	80	1,759	22,846	1,533	26	0	100	1.02	18.66	1.51	1.40	1.15	2.18	14.24	7.97	33.29	33.30
BV03	-66.7345	-46.6651	436-2	84	1,031	8,502	1,088	0	21	79	1.02	18.80	1.35	1.38	1.16	2.71	14.53	8.04	33.31	33.31
BV04	-66.7364	-45.9758	436-3	91	3,870	28,822	477	37	0	100	1.04	27.92	1.12	1.40	1.22	1.64	14.96	8.50	33.41	33.40
BV05	-66.7414	-45.7331	436-4	93	2,793	22,451	563	113	0	100	1.04	32.65	1.09	1.38	1.20	1.84	15.08	8.65	33.44	33.41
BV06	-66.7339	-45.9082	436-5	90	2,589	19,125	465	74	0	100	1.04	29.50	1.25	1.34	1.22	1.61	15.00	8.55	33.42	33.41
BV07	-66.2366	-45.7091	436-6	95	5,015	38,273	1,099	84	0	100	1.04	33.91	0.99	1.50	1.08	1.60	14.85	8.60	33.43	33.41
BV08	-66.2548	-45.6739	438-1	92	2,659	21,794	729	25	0	100	1.05	34.36	0.90	1.48	1.07	1.48	14.88	8.62	33.43	33.41
BV09	-66.5584	-45.982	438-2	95	4,137	35,452	1,620	0	0	100	1.04	28.10	0.86	1.23	1.17	1.54	14.85	8.48	33.41	33.40
BV10	-66.5119	-45.448	438-3	87	1,474	16,333	720	0	0	100	1.05	36.00	0.75	1.35	1.24	1.94	15.05	8.75	33.46	33.43
BV11	-65.7958	-45.0982	441-1	67	9,240	4,336	723	0	54	46	1.07	40.71	1.99	1.17	1.31	1.94	15.17	8.71	33.46	33.40
BV12	-65.8148	-45.0936	441-2	71	5,850	2,868	804	0	40	60	1.07	40.89	1.99	1.17	1.30	1.94	15.15	8.71	33.46	33.40
BV13	-65.7772	-45.1091	438-6	65	881	4,546	475	15	59	41	1.07	40.51	1.80	1.56	1.27	2.00	15.18	8.70	33.47	33.40
BV14	-65.777	-45.0773	455-6	56	167	1,071	257	0	78	22	1.07	41.12	1.99	1.17	1.24	1.94	15.20	8.70	33.47	33.40
BV15	-65.773	-45.0766	439-2	50	169	740	306	4	62	38	1.07	41.12	1.99	1.17	1.23	1.94	15.20	8.70	33.47	33.40
BV16	-65.7594	-45.0571	439-3	42	167	956	246	0	69	31	1.07	41.56	1.63	0.94	0.92	1.19	15.22	8.70	33.47	33.39
BV17	-65.7589	-45.0511	439-4	32	326	1,975	436	6	69	31	1.07	41.56	1.63	0.94	0.81	1.19	15.22	8.70	33.47	33.39
BV18	-65.8004	-45.0814	439-5	71	547	5,519	1,191	0	4	96	1.07	41.10	1.99	1.17	1.31	1.94	15.16	8.71	33.46	33.40
BV19	-65.8001	-45.095	439-6	64	702	6,446	1,543	0	66	34	1.07	40.71	1.99	1.17	1.30	1.94	15.16	8.71	33.46	33.40
BV20	-65.8022	-45.081	476-2	65	321	1,760	576	16	58	42	1.07	41.10	1.99	1.17	1.31	1.94	15.16	8.71	33.46	33.40
BV21	-65.8021	-45.0843	441-3	70	551	4,317	737	0	31	69	1.07	40.90	1.99	1.17	1.30	1.94	15.16	8.71	33.46	33.40
BV22	-66.42833	-45.28861	441-4	46	772	8,542	1,571	0	—	—	1.05	36.75	1.18	1.48	1.42	1.91	15.02	8.77	33.46	33.44
BV23	-66.2214	-45.1284	441-5	49	305	2,076	340	0	70	30	1.06	39.87	2.31	1.64	1.44	1.71	14.94	8.74	33.46	33.45
BV25	-66.2141	-45.1265	441-6	52	364	1,608	305	35	32	68	1.06	39.87	2.31	1.64	1.44	1.71	14.94	8.74	33.46	33.45
BV26	-66.2062	-45.1128	443-1	43	473	5,172	1,334	0	7	93	1.06	40.09	2.31	1.64	1.42	1.71	14.93	8.74	33.46	33.45
BV27	-66.2193	-45.114	476-3	44	1,072	12,726	2,018	36	10	90	1.06	40.07	2.31	1.64	1.45	1.71	14.94	8.74	33.46	33.45
BV28	-66.2246	-45.1134	443-2	45	322	1,800	363	6	20	80	1.06	40.04	2.31	1.64	1.45	1.71	14.94	8.74	33.46	33.45
BV29	-66.2288	-45.1084	443-3	45	159	480	175	3	80	20	1.06	40.04	2.31	1.64	1.47	1.71	14.95	8.74	33.46	33.44
BV30	-66.2245	-45.1024	443-4	40	528	4,685	932	9	8	92	1.06	40.25	2.31	1.64	1.46	1.71	14.94	8.74	33.46	33.45
BV32	-66.2263	-45.1018	443-5	42	222	1,204	678	0	0	100	1.06	40.25	2.31	1.64	1.47	1.71	14.94	8.74	33.46	33.45
BV33	-66.2364	-45.1145	443-6	46	339	2,275	443	0	36	64	1.06	40.02	2.31	1.64	1.47	1.71	14.95	8.74	33.46	33.44
BV34	-65.9627	-45.3581	455-1	93	1,120	15,469	677	0	0	100	1.07	37.62	0.86	1.47	1.06	1.76	15.05	8.76	33.46	33.42
BV35	-66.2287	-45.4674	459-3	87	1,979	29,400	847	30	0	100	1.05	36.31	0.83	1.43	1.10	1.46	14.95	8.70	33.45	33.42
BV36	-65.99	-45.7499	473-4	95	1,113	19,118	258	86	0	100	1.05	31.96	1.45	1.07	1.04	1.84	14.77	8.54	33.42	33.40
BV37	-66.0171	-45.7494	455-3	99	1,878	45,848	1,269	0	0	100	1.05	31.93	1.25	1.22	1.04	1.73	14.78	8.55	33.42	33.40
BV38	-65.9215	-45.7641	455-4	97	673	8,268	233	0	0	100	1.05	31.99	1.61	0.95	1.02	1.77	14.73	8.51	33.42	33.40
BV39	-65.755	-45.1807	459-4	90	1,323	13,161	746	30	0	100	1.07	39.42	1.32	1.34	1.15	1.79	15.18	8.70	33.47	33.40
BV40	-65.7753	-45.3062	476-5	90	1,331	14,170	873	43	0	100	1.07	38.07	0.92	1.30	1.04	1.85	15.09	8.73	33.46	33.41
BV41	-65.6428	-45.3024	456-1	91	1,085	12,087	758	0	2	98	1.08	37.96	1.07	1.23	1.03	1.80	15.11	8.69	33.46	33.40
BV42	-65.5118	-45.298	459-5	92	920	9,649	587	0	7	93	1.08	37.86	1.06	1.31	1.03	1.84	15.12	8.64	33.46	33.39
BV43	-65.5038	-45.4324	456-3	97	1,752	22,450	692	0	0	100	1.08	36.99	1.65	1.14	0.98	2.26	15.02	8.60	33.45	33.39
BV44	-65.6381	-45.4406	456-4	96	2,193	31,506	690	0	0	100	1.08	37.01	1.54	1.18	1.00	2.01	15.05	8.67	33.45	33.40
BV45	-65.7693	-45.4449	456-5	95	1,010	12,808	621	25	0	100	1.07	37.09	1.24	1.23	0.97	1.99	15.02	8.69	33.45	33.41
BV46	-65.7636	-45.5843	456-6	99	1,062	18,806	602	71	0	100	1.07	35.83	1.64	0.90	0.97	1.95	14.89	8.60	33.44	33.40
BV47	-65.633	-45.5807	458-1	98	1,989	31,010	795	0	0	100	1.08	36.55	2.00	0.85	1.01	2.68	14.85	8.56	33.44	33.39
BV48	-65.5033	-45.5766	458-2	95	2,007	32,316	499	81	0	100	1.08	36.89	1.92	0.93	0.99	2.82	14.88	8.54	33.44	33.39
BV49	-65.4993	-45.7161	458-3	94	2,068	33,551	795	81	0	100	1.07	35.85	2.26	0.86	1.02	3.08	14.72	8.45	33.42	33.38
BV50	-65.631	-45.7201	458-4	94	2,231	45,742	1,169	103	0	100	1.07	34.97	1.99	0.86	1.08	2.57	14.75	8.50	33.42	33.39
BV51	-63.7921	-45.6656	458-5	95	3,891	44,616	1,972	0	0	100	1.07	36.92	0.80	1.07	0.53	3.61	15.02	7.89	33.43	33.34
BV52	-61.9825	-45.6089	458-6	108	537	5,026	1,526	0	49	51	1.05	39.73	1.25	0.92	0.44	2.03	14.55	7.05	33.53	33.54
BV54	-59.9773	-45.5792	459-1	647	26	64	138	0	39	61	1.03	41.93	1.78	0.51	0.35	3.09	12.20	5.59	33.87	33.93
BV55	-60.149	-45.5636	459-2	141	51	160	616	0	53	47	1.03	41.84	2.52	0.64	0.42	4.44	12.37	5.72	33.84	33.90

Table 4. List of dinoflagellate taxa present in our samples with code names.

Taxa	Code
Alexandrium cf. *catenella*	Acat
Impagidinium paradoxum	Ipar
Nematosphaeropsis labyrinthus	Nlab
Operculodinium centrocarpum	Ocen
O. centrocarpum short spines	Ocss
Spiniferites delicatus	Sdel
Spiniferites ramosus	Sram
Spiniferites bentorii	Sben
Spiniferites mirabilis	Smir
Spiniferites pachydermus	Spac
Spiniferites spp.	Sspp
Pentapharsodinium dalei	Pdal
Echinidinium sp.C	EspC
Echinidinium sp.D	EspD
Brigantedinium simplex	Bsim
Brigantedinium auranteum	Baur
Brigantedinium cariacoense	Bcar
Brigantedinium spp.	Bspp
Protoperidinium americanum	Pame
Dubridinium sp.	Dubr
Selenopemphix nephroides	Snep
Selenopemphix quanta	Squa
Protoperidinium nudum	Pnud
Stelladinium stellatum	Stel
Trinovantedinium pallidifulvum	Tpal
Votadinium spinosum	Vspi
Votadinium calvum	Vcal
Quinquecuspis concreta	Qcon
Polykrikos schwartzii	Psch
Polykrikos kofoidii	Pkof

Table 5. Relative abundance (%) of dinoflagellate cyst taxa in our samples.

Sample ID	Acat	Ipar	Niab	Ocen	Ocss	Sdel	Sram	Sben	Smir	Spac	Sspp	Pdal	EspC	EspD	Bsim	Baur	Bcar	Bapp	Pame	Dubr	Snep	Squa	Pnud	Stel	Tpal	Vspi	Vcal	Qcon	Psch	Pkof
BV01	0.22	0.00	0.00	7.24	0.56	0.00	74.02	0.65	11.41	0.43	0.91	0.00	0.43	0.26	0.00	1.06	0.00	0.82	0.03	0.04	0.00	0.00	0.22	0.00	0.00	0.22	0.00	0.04	0.00	1.43
BV02	1.53	0.00	0.00	7.11	1.02	0.00	64.70	0.00	12.79	0.57	1.02	0.00	1.31	0.11	0.61	3.29	0.77	1.53	0.00	0.91	0.11	0.11	0.28	0.00	0.06	0.06	0.00	0.23	0.00	1.88
BV03	2.04	0.00	0.00	9.41	0.78	0.00	58.00	0.00	10.96	0.68	1.26	0.00	3.98	0.00	0.12	4.31	0.35	2.79	0.00	1.55	0.00	0.00	0.29	0.19	0.19	0.00	0.00	0.00	0.00	3.10
BV04	1.16	0.00	0.00	13.26	0.49	0.00	71.96	0.13	2.25	0.41	0.18	0.05	0.44	0.00	0.05	2.91	0.22	1.24	0.00	0.26	0.05	0.03	0.03	0.03	0.00	0.03	0.00	0.08	0.08	4.68
BV05	0.18	0.00	0.00	13.28	0.07	0.00	72.93	0.00	2.90	0.50	0.07	0.04	1.00	0.00	0.17	2.79	0.93	1.61	0.08	0.21	0.04	0.07	0.14	0.18	0.00	0.00	0.00	0.25	0.00	2.54
BV06	0.50	0.00	0.00	21.13	2.09	0.00	51.41	0.19	5.99	0.66	0.08	0.00	3.01	0.27	0.71	4.58	2.12	0.35	0.35	1.54	0.00	0.46	0.19	0.08	0.12	0.00	0.00	0.42	0.00	3.75
BV07	0.06	0.00	0.00	13.48	0.08	0.00	68.20	0.16	4.29	0.76	0.20	0.04	1.32	0.08	0.62	3.54	0.80	1.77	0.00	0.14	0.04	0.22	0.06	0.24	0.02	0.00	0.00	0.24	0.00	3.67
BV08	0.15	0.00	0.00	12.03	0.26	0.00	61.98	0.41	7.48	0.56	0.26	0.04	1.65	0.00	0.93	5.29	1.25	2.49	0.00	0.60	0.08	0.08	0.04	0.11	0.00	0.34	0.00	0.56	0.00	3.38
BV09	0.02	0.00	0.00	17.65	0.63	0.00	64.59	0.31	3.50	0.94	0.19	0.00	1.52	0.00	0.57	4.55	1.99	0.43	0.00	0.19	0.07	0.19	0.31	0.07	0.00	0.02	0.00	0.24	0.00	1.98
BV10	0.41	0.00	0.00	17.44	0.07	0.00	56.17	0.14	3.12	1.09	0.27	0.00	1.63	0.00	1.72	8.96	1.89	0.86	0.00	0.07	0.00	0.00	0.14	0.07	0.00	0.00	0.00	0.27	0.00	5.70
BV11	0.22	0.00	0.00	13.20	0.00	0.00	46.43	0.00	5.41	0.54	0.00	0.00	3.46	0.00	1.55	3.11	3.11	4.14	0.00	0.54	0.22	0.32	0.11	0.00	0.11	0.00	0.00	0.00	0.00	17.53
BV12	0.34	0.00	0.00	12.48	0.00	0.00	46.32	0.00	2.74	1.54	0.17	0.00	4.27	0.51	0.39	3.35	0.79	0.59	0.00	0.51	0.00	0.34	0.00	0.17	0.00	0.34	0.00	0.34	0.34	24.44
BV13	0.57	0.00	0.00	12.26	0.79	0.57	48.24	0.00	3.52	0.45	0.91	0.00	5.11	0.00	1.78	3.08	1.14	1.78	0.16	0.11	0.45	0.23	0.45	0.11	0.00	1.02	0.11	0.00	0.68	16.46
BV14	0.00	0.00	0.00	14.97	0.00	0.00	40.12	0.00	2.40	0.00	1.80	0.00	5.39	0.60	1.80	2.10	0.30	1.80	0.00	0.60	0.60	0.00	0.00	0.00	0.00	0.00	0.00	0.00	0.60	26.95
BV15	0.59	0.00	0.00	13.61	0.00	0.00	30.18	0.59	0.59	1.78	0.59	0.00	8.88	0.00	2.59	6.90	4.31	6.90	0.00	0.59	0.00	0.00	0.00	0.00	0.59	0.00	0.59	0.00	0.00	20.71
BV16	0.60	0.00	0.00	14.37	0.60	0.00	41.92	0.00	4.19	1.20	0.00	0.00	0.60	0.60	0.77	5.36	3.06	4.59	0.00	1.20	0.60	1.80	0.00	0.00	0.00	0.00	0.00	0.00	0.00	18.56
BV17	0.31	0.00	0.00	13.50	1.84	0.31	40.49	0.31	3.37	1.23	1.23	0.00	7.06	0.00	0.92	4.60	0.92	2.76	0.00	0.92	0.00	0.00	0.00	0.92	0.00	0.00	0.00	0.00	1.53	17.79
BV18	0.37	0.00	0.00	11.70	0.00	0.00	58.32	0.55	4.02	0.37	0.37	0.18	2.56	0.37	0.45	4.02	0.45	1.12	0.00	0.73	0.18	0.91	0.00	0.37	0.00	0.00	0.00	0.37	0.00	12.61
BV19	0.85	0.00	0.00	10.68	0.00	0.00	60.97	0.00	3.56	0.14	0.28	0.14	1.28	0.00	0.20	2.37	0.20	2.37	0.00	0.00	0.00	0.28	0.00	0.43	0.00	0.14	0.00	0.00	0.14	15.95
BV20	0.93	0.00	0.00	7.17	1.56	0.00	56.70	0.00	5.61	0.62	0.31	0.00	3.12	0.62	0.58	2.30	0.58	4.03	0.00	0.00	0.62	0.31	0.31	0.00	0.00	0.00	0.00	0.00	0.00	14.64
BV21	0.00	0.00	0.00	10.34	0.36	0.00	54.81	0.00	3.09	1.09	0.54	0.00	3.99	0.18	0.59	2.18	0.59	3.17	0.00	0.91	0.00	0.18	0.36	0.18	0.36	0.18	0.00	0.00	0.00	16.88
BV22	8.68	0.00	0.13	10.75	1.04	0.00	38.86	0.13	6.09	0.65	0.00	1.17	2.85	1.55	0.34	2.05	0.17	0.68	0.00	0.00	0.13	0.00	0.13	0.00	0.00	0.00	0.00	0.00	0.00	24.61
BV23	0.66	0.00	0.00	8.52	0.00	0.00	29.84	0.33	6.23	0.98	0.00	0.00	3.28	0.00	0.00	2.50	0.00	6.68	0.00	0.00	0.33	0.00	0.00	0.00	0.00	0.98	0.00	0.00	0.33	39.34
BV25	1.37	0.00	0.00	7.97	0.00	0.00	30.22	0.55	5.77	0.82	0.00	0.27	3.57	0.00	1.69	6.33	1.27	2.53	0.00	0.00	0.82	0.82	0.27	0.27	0.00	0.27	0.00	0.00	0.55	34.62
BV26	3.38	0.00	0.00	7.19	1.06	0.00	41.65	0.00	2.75	0.00	0.00	0.42	4.86	2.33	0.82	3.48	0.82	1.23	0.00	0.42	0.42	0.00	0.42	1.06	0.00	0.00	0.00	0.00	0.00	27.70
BV27	5.41	0.00	0.00	9.14	0.00	0.00	39.46	0.09	3.26	0.37	0.19	0.47	4.01	0.93	0.52	2.35	0.44	1.92	0.00	0.93	0.09	0.00	0.19	0.19	0.28	0.00	0.00	0.09	0.00	29.66
BV28	0.62	0.00	0.00	10.56	0.62	0.00	16.46	0.93	4.35	0.31	0.00	0.00	4.66	0.00	2.17	7.07	2.17	5.98	0.00	1.24	0.00	0.00	0.00	0.00	0.00	0.93	0.00	0.00	2.17	39.75
BV29	21.38	0.00	0.00	3.77	0.63	0.00	21.38	0.00	5.03	0.00	1.89	0.00	12.58	3.77	0.63	1.89	0.63	3.14	0.00	0.63	0.00	0.00	0.00	0.00	0.00	0.00	0.00	0.00	0.00	22.64
BV30	3.60	0.00	0.00	12.50	0.38	0.00	38.07	0.00	3.03	0.19	0.57	0.38	4.17	1.89	0.41	0.83	0.91	1.82	0.00	0.95	0.00	0.00	0.38	0.19	0.76	0.00	0.00	0.00	0.00	28.98
BV32	2.25	0.00	0.00	7.21	0.45	0.00	35.14	0.00	9.46	1.80	1.35	0.45	6.76	6.31	0.90	1.80	0.90	5.41	0.00	0.45	0.00	0.00	0.00	1.35	0.45	0.45	0.00	0.45	0.00	16.67
BV33	5.60	0.00	0.00	5.90	0.88	0.00	35.10	0.00	3.83	0.00	0.59	0.29	7.08	2.06	0.17	3.29	1.39	3.12	0.00	0.29	1.47	0.00	0.59	0.29	0.00	1.18	0.00	0.29	0.00	26.55
BV34	1.25	0.00	0.00	18.04	3.93	0.00	59.82	1.34	4.29	0.00	1.25	0.00	0.54	0.98	0.15	1.85	0.21	0.56	0.00	0.18	0.00	0.00	0.98	0.18	0.00	0.00	0.00	0.18	0.00	4.29
BV35	0.30	0.00	0.00	17.64	1.87	0.40	53.71	0.66	2.07	0.86	1.06	0.00	3.54	0.00	0.85	5.66	3.12	1.13	0.00	0.25	0.00	0.00	0.30	0.25	0.00	0.05	0.00	0.25	0.15	5.86
BV36	0.45	0.00	0.00	11.23	0.72	0.00	67.48	0.72	3.95	0.36	0.18	0.00	1.80	0.36	0.10	4.75	0.95	0.76	0.00	0.63	0.18	0.00	0.36	0.09	0.00	0.00	0.00	0.54	0.00	4.40
BV37	1.33	0.00	0.00	14.06	1.33	0.00	62.73	0.37	2.08	0.75	1.22	0.05	2.50	0.48	0.34	5.04	1.03	1.26	0.00	0.85	0.00	0.00	0.37	0.16	0.00	0.00	0.00	0.69	0.00	3.35
BV38	0.45	0.15	0.00	18.13	2.53	0.00	52.60	0.30	2.82	0.59	0.89	0.15	2.97	0.89	0.26	7.67	1.85	1.06	0.00	0.59	0.00	0.00	0.00	0.30	0.00	0.00	0.00	0.30	0.00	5.50
BV39	2.19	0.00	0.00	9.22	0.38	0.00	60.47	0.00	4.54	0.53	0.83	0.15	2.72	0.53	0.32	2.23	0.53	0.85	0.00	0.76	0.08	0.00	1.06	0.08	0.23	0.30	0.00	0.08	0.00	11.94
BV40	0.90	0.00	0.00	8.94	1.35	0.00	64.54	0.00	3.38	0.98	0.00	0.00	1.58	0.45	0.78	4.67	1.33	1.11	0.00	0.68	0.23	0.00	0.15	0.38	0.15	0.15	0.00	0.00	0.00	8.26
BV41	1.11	0.00	0.00	7.47	1.20	0.00	64.15	0.09	3.32	1.01	0.74	0.00	2.40	1.01	0.39	3.92	0.78	0.98	0.00	2.49	0.18	0.00	1.57	0.28	0.00	0.00	0.09	0.18	0.00	6.64
BV42	0.98	0.00	0.00	10.76	0.98	0.00	66.20	0.00	2.50	1.52	0.33	0.00	1.85	0.22	0.78	3.82	1.04	0.45	0.00	1.20	0.00	0.00	0.11	0.43	0.22	0.00	0.00	0.00	0.00	6.63
BV43	1.37	0.00	0.00	9.25	0.97	0.00	66.21	0.00	3.77	0.86	0.34	0.00	1.88	0.68	0.80	3.54	0.91	0.91	0.00	1.77	0.00	0.00	0.46	0.11	0.00	0.11	0.06	0.17	0.00	5.82
BV44	0.18	0.00	0.00	8.76	0.50	0.00	70.95	0.00	5.11	0.96	0.41	0.00	2.01	0.36	0.46	2.86	0.46	0.29	0.00	1.00	0.05	0.46	0.41	0.09	0.05	0.18	0.00	0.27	0.00	4.20
BV45	0.10	0.00	0.00	11.49	0.69	0.00	60.50	0.00	2.67	0.50	0.30	0.10	3.17	0.40	1.64	6.73	1.64	0.98	0.00	1.78	0.00	0.00	0.10	0.10	0.10	0.10	0.00	0.20	0.00	6.73
BV46	0.09	0.00	0.00	11.39	0.38	0.00	61.49	0.00	5.37	0.75	0.47	0.00	1.32	0.38	0.15	8.12	1.65	0.90	0.00	1.41	0.09	0.00	0.00	0.19	0.00	0.09	0.09	0.09	0.00	5.56
BV47	0.35	0.00	0.00	11.26	1.56	0.45	62.69	0.45	6.13	1.26	1.06	0.00	1.96	0.30	0.79	3.44	1.06	0.13	0.00	0.40	0.00	0.20	0.10	0.20	0.00	0.10	0.00	0.30	0.00	5.78
BV48	0.20	0.10	0.00	7.52	0.90	0.35	67.91	0.35	6.73	1.20	0.60	0.05	0.25	0.00	0.12	4.07	0.96	0.54	0.00	0.95	0.00	0.25	0.05	0.20	0.00	0.20	0.00	0.20	0.05	6.28
BV49	0.15	0.00	0.05	6.38	0.92	1.89	57.74	0.58	7.45	0.73	2.47	0.00	1.45	0.00	0.61	5.70	0.61	0.81	0.00	1.74	0.05	0.15	0.29	0.15	0.00	0.24	0.00	0.53	0.05	9.28
BV50	0.18	0.09	0.00	13.63	1.17	0.18	49.57	0.22	10.71	1.97	2.33	0.09	1.34	0.00	1.10	6.33	1.79	0.55	0.00	0.58	0.04	0.45	0.00	0.00	0.00	0.40	0.00	0.27	0.00	6.99
BV51	0.31	0.00	0.00	2.08	0.77	1.46	48.27	0.39	13.54	1.18	2.78	0.00	1.23	0.00	0.35	2.38	0.98	2.10	0.00	2.70	0.00	0.00	0.00	0.00	0.00	0.13	0.05	0.80	0.51	17.99
BV52	1.49	0.00	0.37	10.24	1.68	0.56	17.88	0.00	12.66	0.37	0.56	0.19	1.49	0.00	1.15	8.64	1.44	4.03	0.00	18.99	0.00	0.00	0.00	0.00	0.00	0.00	0.00	0.00	0.37	17.88
BV54	0.00	19.23	0.00	0.00	0.00	0.00	7.69	0.00	0.00	0.00	0.00	0.00	0.00	0.00	23.08	0.00	0.00	46.15	0.00	0.00	0.00	0.00	0.00	0.00	0.00	0.00	0.00	0.00	0.00	3.85
BV55	1.96	5.88	0.00	1.96	0.00	0.00	19.61	0.00	0.00	0.00	1.96	0.00	5.88	0.00	6.24	2.50	4.99	41.18	0.00	7.84	0.00	0.00	0.00	0.00	0.00	0.00	0.00	0.00	0.00	0.00

Table 6. Summary statistics for Redundancy Analyses (RDA) with marginal and conditional effects.

	Conditional effects				Marginal effects			
	Eigenvalues				With percentage data		With concentration data	
	With percentage data		With concentration data					
	RDA1 4.8	RDA2 2.8	RDA1 5.3	RDA2 3.4				
Variable	P-value	VIF	P-value	VIF	Eigenvalues	P-value	Eigenvalues	P-value
Depth	0.018	4	0.001	4	2	0.015	3.3	0.001
N	0.001	200	0.001	256	3	0.001	3.8	0.001
P	0.001	60	0.014	61	1.6	0.005	1.9	0.023
Si	0.005	26	0.001	21	0.8	0.1	2.1	0.001
Chl.a.f	0.226	13	0.008	12	0.7	0.137	2.2	0.001
Ch.a.m	0.003	7	0.001	7	1.6	0.001	2.3	0.001
Ch.a.a	0.006	20	0.042	21	2.8	0.001	4.7	0.001
Ch.a.n	0.115	5	0.014	6	2.2	0.002	4.4	0.001
Tsum	0.004	57	0.006	76	3.7	0.001	7.6	0.001
Twin	0.015	152	0.114	186	3.9	0.001	7.5	0.001
Ssum	0.001	175	0.002	170	3.3	0.002	8.7	0.001
Swin	0.088	335	0.489	387	3.6	0.002	9.1	0.001
> 63 µm	0.430	8	0.014	8	1.8	0.001	4.8	0.001
< 63 µm	0.072	5	0.078	5	2.1	0.001	4.5	0.001

Table 7. Samples used in this study with coordinates, water depth, pollen sum, spore sum, *Pediastrum* sum, pollen & spores concentrations and grain size data (% fraction> 63µm and < 63µm).

ID samples	Longitude (°W)	Latitude (°S)	Lab number	Depth (m)	Pollen sum	Spore sum	*Pediastrum* sum	Marker grains	Pollen concentrations	spore concentrations	> 63µm	< 63µm
BV01	-66.0274	-46.3756	476-1	97	126	0	0	939	473	0	29.87	70.13
BV02	-66.3956	-46.6621	436-1	80	210	1	0	471	1760	8	0.02	99.98
BV03	-66.7345	-46.6651	436-2	84	209	1	0	353	1152	6	21.32	78.68
BV04	-66.7364	-45.9758	436-3	91	316	0	0	227	3193	0	0	100
BV05	-66.7414	-45.7331	436-4	93	385	2	0	287	3246	17	0.33	99.67
BV06	-66.7339	-45.9082	436-5	90	324	0	0	249	2893	0	0	100
BV07	-66.2366	-45.7091	436-6	95	321	1	0	214	3434	11	0.02	99.98
BV08	-66.2548	-45.6739	438-1	92	246	3	0	159	3906	48	0	100
BV09	-66.5584	-45.982	438-2	95	259	1	0	176	3821	15	0	100
BV10	-66.5119	-45.448	438-3	87	426	4	0	613	2310	22	0.02	99.98
BV11	-65.7958	-45.0982	441-1	67	311	4	0	1082	417	5	54.35	45.65
BV12	-65.8148	-45.0936	441-2	71	183	3	0	1141	248	4	40.42	59.58
BV13	-65.7772	-45.1091	438-6	65	117	5	0	810	238	10	58.51	41.49
BV14	-65.777	-45.0773	455-6	56	318	5	0	1392	721	11	78.36	21.64
BV15	-65.773	-45.0766	439-2	50	91	12	1	4021	66	9	61.84	38.16
BV16	-65.7594	-45.0571	439-3	42	114	9	0	3417	89	7	69.43	30.57
BV17	-65.7589	-45.0511	439-4	32	118	11	0	1929	165	15	68.57	31.43
BV18	-65.8004	-45.0814	439-5	71	140	4	0	1719	260	7	4.02	95.98
BV19	-65.8001	-45.095	439-6	64	109	5	0	2865	113	5	66.06	33.94
BV20	-65.8022	-45.081	476-2	65	82	0	0	1434	161	0	58.08	41.92
BV21	-65.8021	-45.0843	441-3	70	225	4	0	1119	562	10	30.58	69.42
BV22	-66.42833	-45.28861	441-4	46	363	4	0	1290	1043	11		
BV23	-66.2214	-45.1284	441-5	49	104	3	0	1162	257	7	69.89	30.11
BV25	-66.2141	-45.1265	441-6	52	167	5	0	1614	262	8	32.02	67.98
BV26	-66.2062	-45.1128	443-1	43	326	1	0	604	1806	6	6.71	93.29
BV27	-66.2193	-45.114	476-3	44	356	1	0	899	1457	4	9.95	90.05
BV28	-66.2246	-45.1134	443-2	45	138	6	0	1537	217	9	20.38	79.62
BV29	-66.2288	-45.1084	443-3	45	52	2	0	4156	40	2	79.97	20.03
BV30	-66.2245	-45.1024	443-4	40	336	8	0	1443	723	17	8.23	91.77
BV32	-66.2263	-45.1018	443-5	42	97	3	0	820	314	10	0	100
BV33	-66.2364	-45.1145	443-6	46	226	3	0	1712	393	5	35.64	64.36
BV34	-65.9627	-45.3581	455-1	93	334	14	0	496	2883	121	0	100
BV35	-66.2287	-45.4674	459-3	87	257	5	0	335	3419	67	0	100
BV36	-65.99	-45.7499	473-4	95	349	3	0	757	2423	21	0	100
BV37	-66.0171	-45.7494	455-3	99	330	6	0	317	8056	146	0	100
BV38	-65.9215	-45.7641	455-4	97	286	6	0	630	1751	37	0.21	99.79
BV39	-65.755	-45.1807	459-4	90	297	2	0	1070	939	6	0.3	99.7
BV40	-65.7753	-45.3062	476-5	90	358	3	0	741	1774	15	0	100
BV41	-65.6428	-45.3024	456-1	91	284	4	0	824	1186	17	1.65	98.35
BV42	-65.5118	-45.298	459-5	92	303	1	0	1987	496	2	6.73	93.27
BV43	-65.5038	-45.4324	456-3	97	353	4	0	714	2053	23	0	100
BV44	-65.6381	-45.4406	456-4	96	357	4	0	676	2663	30	0.06	99.94
BV45	-65.7693	-45.4449	456-5	95	329	5	0	753	1668	25	0	100
BV46	-65.7636	-45.5843	456-6	99	322	1	0	1010	1880	6	0	100
BV47	-65.633	-45.5807	458-1	98	202	4	0	285	3315	66	0	100
BV48	-65.5033	-45.5766	458-2	95	234	6	0	832	1503	39	0	100
BV49	-65.4993	-45.7161	458-3	94	126	2	0	326	1887	30	0	100
BV50	-65.631	-45.7201	458-4	94	254	4	0	524	3220	51	0	100
BV51	-63.7921	-45.6656	458-5	95	175	10	0	725	872	50	0	100
BV52	-61.9825	-45.6089	458-6	108	117	2	0	897	383	7	49.33	50.67
BV54	-59.9773	-45.5792	459-1	647	29	7	0	2533	26	6	39.13	60.87
BV55	-60.149	-45.5636	459-2	141	112	10	0	2094	160	14	52.93	47.07

Table 8. Relative abundance (%) of pollen taxa in our samples.

ID samples	*Nothofagus* sp.	*Podocarpus* sp.	Pinaceae (excluded)	Asteraceae subf. Asteroideae	Asteraceae subf. Mutisieae	*Nassauvia* sp.	*Chuquiraga* sp.	*Ephedra* sp.	*Colliguaya integerrima*	*Mulinum* sp.	*Azorella* sp.	Apiaceae type	Solanaceae type	*Lycium* sp.	*Schinus* sp.	Rhamnaceae	Verbenaceae	Fabaceae	*Empetrum rubrum*	Labiaceae/Rubiaceae type	Poaceae	Caryophyllaceae	Chenopodiaceae	Convolvulaceae	*Gilia* sp.	*Erodium cicutarium*	*Acaena* sp.	*Fuschia* sp.	Brassicaceae	*Rumex acetosella*	Asteraceae subf. Cichorioideae	Cyperaceae	Typha	Unknown	Shrubs	Herbs	AP	NAP
BV01	4.76	7.14	1.56	30.95	1.59	0.79	0.79	3.17	0.79	5.56	0.00	0.00	0.00	0.00	0.79	1.59	0.00	0.79	0.00	0.79	24.60	1.59	9.52	0.00	0.00	0.00	0.00	0.00	2.38	0.00	0.00	0.00	0.79	1.59	13.49	73.02	11.90	88.10
BV02	16.19	1.43	0.47	15.71	0.48	5.71	2.38	2.38	8.10	0.00	0.00	0.95	0.95	1.43	0.95	0.95	0.00	0.48	0.48	1.43	16.19	0.48	21.43	0.00	0.00	0.00	0.00	0.00	0.00	0.00	0.00	0.00	0.00	1.90	18.10	62.38	17.62	82.38
BV03	9.09	0.96	0.00	13.88	0.00	8.13	0.48	2.39	12.92	0.96	0.00	0.48	0.96	0.96	0.48	0.96	0.00	0.48	1.44	0.00	17.22	0.48	24.40	0.00	0.00	0.48	0.00	0.00	1.91	0.00	0.00	0.00	0.00	0.96	22.01	66.99	10.05	89.95
BV04	13.29	0.63	1.25	9.81	0.32	0.32	0.95	5.70	15.19	1.90	0.00	0.00	0.00	0.00	0.00	0.00	0.63	0.63	0.00	0.32	13.61	1.58	31.65	0.00	0.00	0.32	0.00	0.00	1.58	0.00	0.00	0.00	1.27	0.32	24.37	61.39	13.92	86.08
BV05	9.09	4.16	0.00	19.22	0.00	0.52	2.86	3.64	12.73	0.52	0.00	0.52	0.78	0.26	0.00	0.00	0.26	0.78	0.00	0.26	8.05	1.04	30.39	0.00	0.00	2.34	0.26	0.00	0.78	0.00	0.26	1.04	0.26	0.00	19.74	67.01	13.25	86.75
BV06	9.57	1.85	0.00	17.59	0.62	0.31	1.23	5.25	14.51	0.00	0.00	0.62	0.31	0.00	0.31	0.00	0.31	0.00	0.00	0.62	13.58	2.78	28.40	0.00	0.00	0.31	0.00	0.00	0.31	0.00	0.00	1.23	0.00	0.31	21.91	66.36	11.42	88.58
BV07	6.54	4.98	0.00	19.31	1.87	0.31	0.62	6.54	10.28	2.18	0.31	0.93	0.00	0.31	0.00	0.31	0.00	0.00	0.00	0.00	12.15	0.93	29.60	0.00	0.00	0.31	0.00	0.00	1.56	0.00	0.00	0.00	0.62	0.31	20.87	67.29	11.53	88.47
BV08	9.76	1.22	0.00	15.45	2.03	0.00	0.81	8.13	9.76	0.00	0.00	1.22	0.00	0.00	0.00	0.00	0.00	0.00	0.00	0.00	17.89	0.41	28.46	0.00	0.00	0.41	0.00	0.00	2.44	0.00	0.00	0.00	1.63	0.41	19.11	69.51	10.98	89.02
BV09	8.88	1.54	0.38	12.36	1.16	0.39	1.54	6.18	12.36	0.39	0.39	1.54	1.54	0.00	0.00	0.00	0.77	0.00	0.00	0.00	16.99	1.54	28.96	0.00	0.00	0.00	0.00	0.00	1.54	0.00	0.00	0.00	1.16	0.77	23.17	65.64	10.42	89.58
BV10	14.08	1.41	0.00	15.02	0.70	0.70	1.88	6.57	15.96	0.23	0.23	0.47	0.47	0.23	0.94	0.00	0.00	0.23	0.00	0.23	9.15	1.17	27.46	0.00	0.00	0.23	0.00	0.00	1.41	0.00	0.00	0.23	0.94	0.00	25.59	58.92	15.49	84.51
BV11	18.01	8.36	0.96	10.29	0.00	5.79	1.61	2.89	10.61	1.93	0.00	0.00	0.64	1.29	0.32	0.64	0.00	0.32	0.00	0.96	9.32	1.29	20.90	0.64	0.00	0.64	0.00	0.00	0.64	0.32	0.00	0.32	0.32	1.93	19.61	52.09	26.37	73.63
BV12	7.10	6.56	1.61	15.30	0.00	4.37	2.19	1.09	10.38	0.00	0.00	0.55	0.55	1.64	0.55	0.00	0.00	0.55	0.00	0.00	6.56	1.09	34.97	0.55	0.00	0.55	0.00	0.00	1.09	0.55	0.00	0.00	1.64	2.19	15.30	68.85	13.66	86.34
BV13	11.97	14.53	0.00	10.26	0.85	0.00	0.85	8.55	6.84	0.85	0.00	0.85	3.42	0.00	0.00	0.00	0.00	0.00	0.85	0.00	5.98	2.56	29.06	0.00	0.00	0.85	0.00	0.00	0.00	0.00	0.00	0.85	0.85	0.00	21.37	52.14	26.50	73.50
BV14	11.95	3.46	0.63	13.52	1.26	5.97	1.89	3.14	16.98	1.26	0.00	0.00	0.31	0.00	0.31	0.63	0.00	0.31	0.31	0.63	12.26	0.63	22.96	0.31	0.00	0.00	0.31	0.00	0.63	0.00	0.00	0.00	0.00	0.94	23.90	59.75	15.41	84.59
BV15	7.69	20.88	4.21	8.79	0.00	0.00	2.20	3.30	9.89	0.00	0.00	1.10	1.10	0.00	0.00	2.20	0.00	0.00	0.00	2.20	10.99	4.40	16.48	1.10	0.00	5.49	0.00	0.00	0.00	0.00	0.00	0.00	0.00	1.10	20.88	49.45	28.57	71.43
BV16	6.14	6.14	1.72	16.67	0.00	9.65	4.39	3.51	12.28	0.88	0.00	0.00	0.88	0.88	0.88	0.00	0.00	0.88	0.00	0.00	12.28	0.88	21.05	0.00	0.00	0.00	0.00	0.00	0.00	0.00	0.00	0.00	0.00	2.63	20.18	64.91	12.28	87.72
BV17	8.47	6.78	0.00	13.56	0.00	3.39	1.69	2.54	6.78	0.85	0.00	7.63	0.00	0.00	0.00	0.85	0.00	0.85	0.00	1.69	14.41	2.54	22.88	0.00	0.00	2.54	0.00	0.00	0.85	0.00	0.00	0.85	0.00	0.85	21.19	62.71	15.25	84.75
BV18	12.86	3.57	0.71	5.71	0.00	12.14	1.43	2.86	2.14	0.71	0.00	2.14	1.43	1.43	2.14	0.00	0.71	0.00	0.00	2.14	10.00	0.00	37.14	0.00	0.00	0.71	0.00	0.00	0.00	0.00	0.00	0.71	0.00	0.00	15.71	67.86	16.43	83.57
BV19	7.34	7.34	2.68	11.93	0.00	8.26	0.92	2.75	6.42	0.00	0.00	0.00	0.00	0.00	0.00	2.75	3.67	0.92	0.00	0.92	13.76	0.00	29.36	0.92	0.00	0.00	0.00	0.00	0.00	0.00	0.00	0.00	0.00	2.75	17.43	65.14	14.68	85.32
BV20	13.41	12.20	4.65	6.10	1.22	3.66	0.00	1.22	7.32	0.00	0.00	0.00	0.00	0.00	0.00	2.44	0.00	0.00	0.00	2.44	21.95	0.00	21.95	0.00	0.00	1.22	0.00	0.00	0.00	0.00	1.22	0.00	0.00	3.66	13.41	57.32	25.61	74.39
BV21	9.33	4.00	0.44	15.11	0.00	5.33	1.78	3.56	15.11	0.89	0.00	0.00	0.44	3.11	0.89	0.44	0.00	0.00	0.89	0.44	15.11	0.00	18.67	0.00	0.00	0.44	0.00	0.44	2.22	0.00	0.44	0.00	0.89	0.44	26.22	60.00	13.33	86.67
BV22	14.88	4.41	0.27	8.82	0.55	4.68	4.41	1.10	16.25	0.55	0.00	0.00	0.55	0.83	0.55	0.55	0.28	0.28	1.10	0.00	18.46	0.55	18.73	0.00	0.00	0.28	0.00	0.00	1.38	0.00	0.00	0.00	0.00	0.83	22.04	57.85	19.28	80.72
BV23	17.31	7.69	0.95	11.54	0.00	7.69	0.96	0.96	11.54	0.00	0.00	0.00	0.00	0.96	0.96	0.00	0.00	0.00	0.00	0.96	13.46	0.00	20.19	0.00	0.00	0.96	0.00	0.00	2.88	0.00	0.00	0.00	0.00	1.92	15.38	57.69	25.00	75.00
BV25	6.59	2.99	0.60	11.98	1.20	8.38	1.80	1.20	10.18	1.80	0.60	1.20	0.00	2.40	2.40	1.20	0.00	0.00	0.00	0.60	22.16	2.40	15.57	0.00	0.00	0.00	0.00	0.00	2.40	0.00	0.00	0.00	0.00	2.99	21.56	65.87	9.58	90.42
BV26	14.72	4.29	1.21	9.20	0.00	9.51	2.76	0.92	12.88	0.31	0.00	0.00	0.00	1.23	1.53	0.61	0.92	0.31	0.00	0.92	14.72	0.61	21.17	0.00	0.31	0.31	0.00	0.00	1.23	0.31	0.00	0.00	0.00	1.23	19.63	60.12	19.02	80.98
BV27	12.36	5.90	2.73	12.64	1.12	6.74	1.69	1.69	11.52	0.56	0.00	0.00	0.56	0.56	0.56	2.81	0.00	0.00	0.00	0.00	14.61	0.56	23.60	0.00	0.00	0.56	0.00	0.00	1.12	0.00	0.28	0.00	0.00	0.56	18.26	62.92	18.26	81.74
BV28	7.25	4.35	0.72	10.14	0.00	8.70	2.17	1.45	15.22	0.00	0.00	0.00	0.72	0.00	0.72	3.62	0.00	0.00	0.72	0.72	15.22	0.72	21.74	0.00	0.00	1.45	0.00	0.00	3.62	0.00	0.00	0.00	0.00	1.45	23.19	63.77	11.59	88.41
BV29	23.08	7.69	3.70	7.69	0.00	5.77	0.00	0.00	9.62	0.00	0.00	0.00	0.00	0.00	3.85	3.85	1.92	1.92	0.00	0.00	7.69	0.00	25.00	0.00	0.00	1.92	0.00	0.00	0.00	0.00	0.00	0.00	0.00	0.00	21.15	48.08	30.77	69.23
BV30	14.29	2.98	1.18	14.58	0.00	5.95	2.08	1.49	14.29	0.00	0.30	0.00	0.30	3.57	1.19	0.89	0.00	0.00	0.30	0.00	14.58	1.19	19.94	0.00	0.00	0.30	0.00	0.00	1.79	0.00	0.00	0.00	0.00	0.00	22.32	60.42	17.26	82.74
BV32	8.25	5.15	1.02	10.31	1.03	2.06	2.06	3.09	13.40	0.00	0.00	2.06	2.06	2.06	2.06	2.06	0.00	0.00	0.00	0.00	22.68	0.00	19.59	0.00	1.03	0.00	0.00	0.00	0.00	0.00	0.00	0.00	0.00	1.03	26.80	58.76	13.40	86.60
BV33	9.73	7.96	2.59	7.52	0.88	10.18	1.33	0.44	17.26	0.88	0.00	0.00	0.00	2.65	0.88	0.44	0.00	0.00	0.00	0.00	16.81	0.44	19.47	0.00	0.00	1.33	0.00	0.00	0.00	0.00	0.00	0.00	0.88	22.57	58.85	17.70	82.30
BV34	12.57	2.40	0.30	18.26	0.60	3.89	2.40	1.80	11.38	0.30	1.20	0.00	0.00	0.30	0.00	0.00	0.00	0.00	0.30	0.60	18.26	1.80	21.26	0.60	0.00	0.30	0.00	0.00	0.60	0.00	0.00	0.00	0.60	0.60	15.87	68.56	14.97	85.03
BV35	12.45	1.17	0.77	18.29	0.00	2.72	1.95	5.45	6.23	0.00	0.00	0.39	0.00	1.17	0.78	0.39	0.00	0.39	0.00	0.39	17.51	1.95	23.35	0.78	0.00	0.78	0.00	0.00	1.17	0.00	0.00	0.39	0.39	1.17	15.18	70.04	13.62	86.38
BV36	7.45	2.87	0.57	19.77	0.00	3.44	2.29	2.29	6.30	0.00	0.00	0.29	0.29	3.15	2.29	1.72	0.00	0.29	0.29	0.00	15.19	1.15	28.65	0.57	0.00	0.00	0.00	0.00	1.43	0.00	0.00	0.00	0.00	0.29	16.91	72.49	10.32	89.68
BV37	10.61	3.94	0.30	14.55	0.00	2.73	1.52	5.15	5.45	0.61	0.00	0.00	0.00	0.91	0.91	0.00	0.30	0.61	0.00	0.61	19.70	1.52	30.30	0.00	0.00	0.00	0.00	0.00	0.00	0.00	0.00	0.00	0.00	0.61	14.55	70.30	14.55	85.45
BV38	10.84	1.40	0.35	17.83	0.00	2.10	1.75	4.90	6.64	0.70	0.00	0.35	0.70	0.35	1.05	0.00	0.00	0.00	0.00	0.00	15.73	0.00	31.82	0.00	0.00	0.35	0.00	0.00	1.75	0.00	0.00	0.00	0.00	1.75	14.69	71.33	12.24	87.76
BV39	13.13	4.71	0.34	13.47	0.00	4.71	3.37	3.37	11.11	0.00	0.00	0.00	0.67	2.69	0.00	0.34	0.00	0.34	0.00	0.00	15.49	1.35	22.56	0.00	0.00	0.34	0.00	0.00	1.01	0.00	0.34	0.34	0.00	0.67	18.52	62.96	17.85	82.15
BV40	6.70	4.75	0.56	18.44	0.00	3.35	1.96	6.98	5.59	0.56	0.00	0.84	0.56	1.12	0.56	0.28	0.00	0.00	0.00	0.28	15.08	1.68	28.21	0.28	0.00	0.00	0.56	0.28	1.68	0.00	0.00	0.00	0.00	0.28	16.76	71.51	11.45	88.55
BV41	8.10	4.23	0.70	13.38	0.00	2.11	2.46	6.34	5.63	0.00	0.00	0.00	0.70	2.11	0.35	1.06	0.00	0.00	0.00	0.00	20.07	1.41	28.52	1.06	0.00	0.35	0.00	0.00	1.41	0.00	0.00	0.00	0.00	0.70	16.20	70.77	12.32	87.68
BV42	4.62	2.31	0.33	13.20	0.00	4.29	2.31	2.31	6.27	0.00	0.00	0.66	0.99	4.29	0.66	0.00	0.00	0.00	0.00	0.66	24.09	0.00	30.69	0.00	0.00	0.66	0.00	0.00	1.98	0.00	0.00	0.00	0.00	0.00	15.84	77.23	6.93	93.07
BV43	7.65	2.83	0.00	15.58	0.28	5.95	3.97	3.68	7.08	0.28	0.00	0.57	0.28	1.70	0.00	0.57	0.57	0.00	0.00	0.28	17.56	1.13	26.35	0.28	0.00	0.28	0.00	0.00	1.42	0.00	0.00	0.28	0.00	1.42	15.01	73.09	10.48	89.52
BV44	8.40	0.56	0.00	17.65	0.28	2.80	0.84	5.60	4.76	0.56	0.84	0.00	0.84	0.00	0.56	2.24	0.00	0.28	0.28	1.12	18.77	1.40	27.45	0.56	0.00	1.68	0.00	0.00	0.56	0.00	0.00	0.00	0.00	1.96	17.09	71.99	8.96	91.04
BV45	9.73	1.22	0.00	17.93	0.61	3.34	1.22	5.17	7.29	0.61	0.00	0.61	0.00	0.61	0.30	0.61	0.00	0.00	0.30	0.91	17.93	2.13	27.05	0.30	0.30	0.30	0.00	0.00	1.22	0.00	0.00	0.00	0.00	0.30	16.41	72.34	10.94	89.06
BV46	11.18	4.35	0.00	13.35	0.00	5.28	1.55	6.52	6.52	0.31	0.00	0.31	0.00	0.93	0.31	0.31	0.00	0.31	0.31	0.62	19.88	1.24	24.22	0.62	0.00	0.00	0.00	0.00	1.24	0.00	0.00	0.00	0.00	0.62	16.46	67.39	15.53	84.47
BV47	7.43	3.96	0.00	14.36	0.00	3.96	0.99	3.96	6.93	0.00	0.99	0.50	0.00	0.99	0.99	0.50	0.50	0.50	0.00	1.49	16.34	0.00	30.69	0.99	0.00	0.00	0.00	0.00	1.98	0.00	0.50	0.00	0.00	1.49	17.33	69.80	11.39	88.61
BV48	11.11	3.85	0.00	14.10	0.00	8.55	1.28	2.14	5.13	0.85	0.00	1.28	0.43	0.85	0.43	1.28	0.00	0.43	0.00	0.43	11.11	2.14	32.05	0.00	0.00	0.43	0.00	0.00	1.71	0.00	0.00	0.43	0.00	0.00	13.25	71.79	14.96	85.04
BV49	6.35	7.14	0.00	21.43	0.79	3.97	0.79	3.97	3.97	0.00	0.00	0.00	0.00	0.00	0.00	0.00	0.00	0.00	0.00	1.59	16.67	0.79	30.95	0.00	0.00	0.00	0.00	0.00	0.79	0.00	0.79	0.00	0.00	0.00	9.52	76.98	13.49	86.51
BV50	4.72	3.94	0.00	15.35	0.00	3.54	0.79	3.94	6.69	0.00	0.00	0.39	0.00	0.39	0.39	0.79	0.39	0.00	0.00	0.79	20.47	0.79	33.46	0.00	0.00	0.39	0.00	0.00	0.79	0.00	0.39	0.00	0.00	1.57	13.78	75.98	8.66	91.34
BV51	6.86	1.14	0.57	18.86	0.57	2.29	0.57	4.57	4.57	0.00	0.00	0.57	1.14	0.00	1.14	0.00	0.00	0.57	0.00	0.57	16.57	1.14	35.43	0.57	0.00	0.57	0.00	0.00	0.00	0.00	0.57	0.00	0.00	1.71	13.14	77.14	8.00	92.00
BV52	4.27	5.13	1.68	26.50	0.00	7.69	1.71	5.13	2.56	0.85	0.00	0.00	0.00	0.00	0.00	0.85	0.00	0.00	0.00	0.85	10.26	0.00	31.62	0.85	0.00	1.71	0.00	0.00	0.00	0.00	0.00	0.00	0.00	0.00	10.26	80.34	9.40	90.60
BV54	6.90	3.45	0.00	27.59	0.00	6.90	0.00	0.00	3.45	0.00	0.00	0.00	3.45	0.00	0.00	0.00	0.00	0.00	3.45	0.00	6.90	0.00	27.59	3.45	0.00	0.00	0.00	0.00	0.00	0.00	3.45	0.00	0.00	3.45	10.34	75.86	10.34	89.66
BV55	8.04	1.79	1.75	16.96	0.00	6.25	0.00	1.79	6.25	0.00	0.00	0.00	0.00	1.79	0.00	1.79	1.79	0.89	0.89	0.00	25.89	0.00	20.54	0.89	0.00	0.00	0.00	0.00	0.89	0.00	0.00	0.00	0.00	3.57	15.18	71.43	9.82	90.18

Table 9. Cores used in this study with coordinates.

ID cores	Latitude	longitude
06PC	-66.461	-45.45
08PC	-65.984	-45.486
11PC	-65.924	-45.75

Table 10. Relative abundances of dinocyst taxa, palynomorph influxes, dinocyst counts, marker grains and PCA sample scores for dinocyst analysis in 06PC.

Depth	Age (Cal kyr BP)	*Spiniferites ramosus*	*Spiniferites mirabilis*	*Spiniferites delicatus*	*Spiniferites pachydermus*	Spiniferites sp.	*Operculodinium centrocarpum* s.l.	*Alexandrium* cf. *catenella*	*Brigantedinium* spp.	Echinidinium sp.	*Dubridinium* sp.	*Polykrikos kofoidii*	Other heterophic dinocysts	A/H	Dinocyst influxes (cysts cm^{-2} yr^{-1})	Freshwater/brackish influxes (palynomorphs cm^{-2} yr^{-1})	organic linings of foramifers influxes (linings cm^{-2} yr^{-1})	Reworked palynomorph fluxes (palynomorphs cm^{-2} yr^{-1})	Pre-Quaternary dinocyst influxes (cysts cm^{-2} yr^{-1})	Dinocyst counts	Marker grains	PCA 1	PCA 2
0	-8.8	61.02	4.47	0.08	0.08	0.16	15.29	1.49	12.24	1.65	0	2.51	1.02	4.74	180.68	4.68	7.79	0.57	0	1275	407	-1.27	-0.89
8	300.4	53.61	4.08	0	0.16	0.08	22.37	0.78	14.44	1.10	0	2.28	1.10	4.29	143.80	5.30	7.56	0.34	0	1274	511	-0.96	-0.77
16	608.3	54.69	2.68	0	0.10	0	29.56	0.41	8.14	1.24	0	2.47	0.72	6.96	177.53	6.76	8.59	1.10	0	971	347	-0.81	-1.19
24	1298.3	41.68	5.37	0.07	0.87	0	42.41	0.07	3.56	1.53	0.36	2.03	2.03	9.51	160.77	6.07	6.77	1.05	0	1377	494	-0.24	-1.12
32	2124	43.39	10.16	0.33	0.44	0	25.25	0.66	6.45	1.75	4.37	5.46	1.75	4.06	157.53	6.54	8.78	0.86	0	915	335	-0.68	-0.39
40	2593.8	12.75	16.27	1.57	1.18	0.39	27.65	0	7.84	1.18	13.53	14.51	3.14	1.49	82.97	5.86	5.04	1.95	0	510	300	-0.03	1.32
48	3390.8	12.35	27.41	3.46	3.70	0	17.04	0	6.17	1.73	10.86	14.57	2.72	1.77	76.70	3.22	4.36	0.57	0	405	335	-0.26	1.73
56	3810.4	8.51	21.28	2.43	2.13	0.91	16.72	0	10.64	4.26	10.33	19.15	3.65	1.08	61.21	4.84	7.44	0.93	0.19	329	310	-0.22	2.11
64	4278	12.57	13.35	1.05	1.31	0	36.13	0	13.09	0.26	3.93	14.14	4.19	1.81	25.73	2.56	2.83	0.07	0.07	382	942	0.15	1.04
72	4915.6	10.76	12.79	1.45	4.65	0.29	22.97	0	11.63	2.62	11.34	17.73	3.78	1.12	52.21	4.86	5.31	1.21	0.15	344	418	-0.12	1.72
78	5433.7	4.44	7.51	0.68	1.71	1.02	37.20	0	19.45	0.68	6.48	17.75	3.07	1.11	50.15	5.13	5.82	1.20	0.17	293	337	0.32	1.59
80	5626	6.51	13.02	0.59	2.07	1.18	32.54	0	12.13	4.44	7.40	15.09	5.03	1.27	66.60	6.90	5.91	3.15	0	338	322	0.19	1.49
88	6196	6.69	10.47	0.58	2.33	0	34.01	0	4.65	8.14	10.17	17.15	5.81	1.18	64.42	5.43	5.81	1.69	0.19	344	308	0.22	1.37
96	6820.5	6.37	9.97	0	3.60	0	32.41	0	3.88	7.48	14.96	16.34	4.99	1.10	76.34	8.46	6.56	2.96	0	361	300	0.20	1.43
104	7339.4	5.99	7.81	0.26	1.30	0	44.01	0	12.76	4.43	2.34	20.05	1.04	1.46	69.87	4.18	5.64	2.37	0.55	384	317	0.45	1.21
112	8070.2	7.41	7.61	0	0.41	0.62	42.18	0	17.70	1.85	2.67	13.79	5.76	1.39	32.44	1.74	2.14	0.93	0	486	864	0.38	1.11
120	8793.8	5.19	6.77	0	2.48	0.68	38.15	0	10.84	5.64	6.09	17.38	6.77	1.14	83.23	6.20	5.82	2.82	0.19	443	307	0.34	1.36
128	9546.4	8.26	6.89	0	1.93	0.28	52.89	0	1.10	6.89	3.31	13.22	5.23	2.36	67.54	3.16	8.74	1.86	0	363	310	0.64	0.38
136	10147.2	8.36	6.96	0	1.39	0.28	53.48	0	3.62	6.13	1.95	13.37	4.46	2.39	68.19	3.61	8.93	1.90	0	359	334	0.65	0.40
144	10814	2.80	4.05	0	0.07	0.29	89.47	0	0.29	0.81	0	1.18	1.03	29.18	112.18	0.41	3.06	0.17	0	1358	768	1.62	-1.09
152	11411.6	1.20	5.24	0.18	0.18	0.37	87.49	0	1.56	0.64	0.28	2.02	0.83	17.74	150.03	0.69	7.18	0.55	0	1087	754	1.61	-0.89
160	11744.3	1.80	11.79	0.25	0	0.19	77.90	0	1.74	0.12	1.06	3.85	1.30	11.39	97.92	1.34	3.53	0.30	0.06	1611	1317	1.37	-0.48
168	12131.9	3.46	15.56	0.43	0.04	0.04	74.79	0	0.99	0.22	0.73	0.78	2.94	16.66	134.41	2.21	3.49	0.06	0	2313	1628	1.28	-0.53
176	12520.8	4.24	18.24	0.72	0	0.44	71.63	0	0.39	0.17	0.28	0.61	3.31	20.10	117.83	1.75	4.35	0.06	0.45	1815	1603	1.19	-0.46
184	12895.8	1.88	17.77	0.94	0.13	0	74.70	0	1.48	0.27	2.02	0.81	0	20.85	120.44	3.24	13.62	0.16	0.49	743	642	1.31	-0.43
192	13257.5	2.12	13.24	0.11	0.05	0.26	79.08	0	1.38	0,00	2.65	1.06	0.05	18.46	134.21	1.21	7.46	0.28	0.43	1888	1464	1.40	-0.61
200	13604.5	3.77	12.95	0.13	0	0.82	78.13	0	1.32	0.06	2.14	0.63	0.06	22.75	115.78	1.02	9.61	0.07	0.51	1591	1430	1.35	-0.67
208	13942.5	3.65	12.86	0.16	0.16	0	74.92	0	0.48	0.95	5.71	0.95	0.16	11.12	396.76	6.93	42.83	0	12.60	630	1155	1.28	-0.53
216	14071.3	2.83	4.69	0	0.20	0	87.10	0	0.98	0	3.62	0.49	0.10	18.30	409.09	0.80	24.39	0	10.80	1023	1819	1.57	-0.99
224	14138.4	1.05	1.57	0	0.26	0	84.44	0	9.93	0.39	1.57	0.78	0	6.89	348.66	0	6.84	0	12.31	765	1596	1.52	-0.67
232		0	0	0	0	0	0	0	0	0	0	0	0	0	0	0	0	0	10.07	0	361	-	-
240		0	0	0	0	0	0	0	0	0	0	0	0	0	0	0	0	0	178.38	0	367	-	-
248		0	0	0	0	0	0	0	0	0	0	0	0	0	0	0.95	0	1.90	44.57	0	767	-	-
256		0	0	0	0	0	0	0	0	0	0	0	0	0	0	0	0	0	35.09	0	995	-	-
264		0	0	0	0	0	0	0	0	0	0	0	0	0	0	0	0	0	101.36	0	854	-	-
272		0	0	0	0	0	0	0	0	0	0	0	0	0	0	0	0	0	45.70	0	573	-	-
280		0	0	0	0	0	0	0	0	0	0	0	0	0	0	0	0	0	28.82	0	833	-	-
288		0	0	0	0	0	0	0	0	0	0	0	0	0	0	0	0	0	1.32	0	1004	-	-
296		0	0	0	0	0	0	0	0	0	0	0	0	0	0	0	0	0	36.10	0	947	-	-
304		0	0	0	0	0	0	0	0	0	0	0	0	0	0	0	0	0	36.33	0	901	-	-
312		0	0	0	0	0	0	0	0	0	0	0	0	0	0	0	0	0	224.17	0	1590	-	-
320		0	0	0	0	0	0	0	0	0	0	0	0	0	0	0	0	0	144.73	0	2714	-	-
328		0	0	0	0	0	0	0	0	0	0	0	0	0	0	0	0	0	92.70	0	1441	-	-
336		0	0	0	0	0	0	0	0	0	0	0	0	0	0	0	0	0	172.29	0	1850	-	-
344		0	0	0	0	0	0	0	0	0	0	0	0	0	0	0	0	0	92.29	0	2780	-	-
352		0	0	0	0	0	0	0	0	0	0	0	0	0	0	0	0	0	188.55	0	2361	-	-

Table 11. Relative abundances of dinocyst taxa, palynomorph influxes, dinocyst counts, marker grains and PCA sample scores for dinocyst analysis in 08PC.

Depth	Age (Cal kyr BP)	*Spiniferites ramosus*	*Spiniferites mirabilis*	*Spiniferites delicatus*	*Spiniferites pachydermus*	Spiniferites sp.	*Operculodinium centrocarpum* s.l.	*Alexandrium* cf. *catenella*	*Brigantedinium* spp.	Echinidinium sp.	*Dubridinium* sp.	*Polykrikos kofoidii*	Other heterophic dinocysts	A/H	Dinocyst influxes (cysts cm^{-2} yr^{-1})	Freshwater/brackish influxes (palynomorphs cm^{-2} yr^{-1})	organic linings of foramifers influxes (linings cm^{-2} yr^{-1})	Reworked palynomorph fluxes (palynomorphs cm^{-2} yr^{-1})	Pre-Quaternary dinocyst influxes (cysts cm^{-2} yr^{-1})	Dinocyst counts	Marker grains	PCA 1	PCA 2
0	-10.1	39.08	1.57	0.12	0.24	0.36	33.78	0.36	11.46	3.86	0.84	6.51	1.81	3.08	219.93	7.69	7.43	0	0.53	829	470	-0.42	-0.43
8	302.3	56.61	3.03	0.09	0.18	0.18	20.09	0.46	13.94	0.73	0.37	3.67	0.64	4.17	311.01	7.13	8.85	0	0	1090	437	-1.08	-0.80
16	663.4	56.14	3.40	0.09	0.60	0	25.72	0.98	6.84	1.95	0.14	3.26	0.88	6.65	378.11	7.21	13.72	0	0.35	2150	709	-0.92	-1.11
24	1001.9	55.62	2.66	0.20	0.60	0.10	25.83	0.95	7.87	1.81	0.30	3.41	0.65	6.12	338.37	7.47	13.07	0.17	0	1994	668	-0.91	-1.07
32	1343.1	17.42	0.76	0.15	0.61	0	63.64	0.15	9.55	0.91	0.76	3.64	2.42	4.79	110.91	3.53	10.08	0	0	660	742	0.71	-0.62
40	1657.4	16.76	4.73	0.33	0.83	0.58	63.98	0.08	8.05	0.25	0.41	3.15	0.83	6.88	155.75	3.10	5.82	0	0.26	1205	877	0.74	-0.63
48	1928.2	39.42	12.61	1.51	1.22	0	27.47	0.19	9.78	0.28	1.13	4.99	1.41	4.68	156.67	3.54	9.87	0	0.15	1063	846	-0.55	-0.25
56	2232.8	47.21	16.74	0.43	1.29	0.32	15.56	0	11.05	0.43	0.54	5.26	1.18	4.42	143.60	1.85	6.32	0.15	0.15	932	694	-0.98	-0.14
64	2588	16.19	20.57	5.14	0.57	0.38	21.33	0	15.62	0.76	6.29	11.81	1.33	1.79	80.89	2.62	8.63	0	0.31	525	694	-0.25	1.42
72	2973.3	20.61	21.94	2.06	1.94	1.21	22.67	0	9.94	1.21	7.76	8.61	2.06	2.38	125.31	1.97	5.62	0.30	0.30	825	704	-0.29	0.99
80	3332.4	6.13	3.30	1.18	0.24	0.94	43.40	0	17.22	0.94	8.25	12.97	5.42	1.23	50.27	1.42	5.33	0	0.12	424	902	0.44	1.10
88	3726.2	2.08	0.69	0	0	0	51.39	0	26.39	0	8.33	9.72	1.39	1.18	41.50	2.31	7.78	0	0.86	244	371	0.69	1.06
96	4121.3	3.54	1.57	0	1.97	0.39	51.97	0	19.69	1.57	6.30	7.87	5.12	1.47	66.38	3.66	8.62	0	0	254	372	0.69	0.79
104	4518.5	1.78	0	0	0.44	0	33.78	0	31.56	7.56	8.89	15.56	0.44	0.56	27.59	1.72	5.27	0	0	225	872	0.26	1.98
112	4888.7	3.01	2.81	0.40	0.20	0.40	47.79	0	16.06	6.43	4.42	16.06	2.41	1.20	70.35	1.55	5.93	0	0	498	757	0.59	1.15
120	5229.8	4.94	3.35	0.53	0.88	0.71	53.44	0	15.52	3.70	1.94	10.23	4.76	1.77	99.23	2.80	6.13	0	0.18	567	611	0.70	0.66
128	5558.2	6.59	1.56	0.17	0.69	0.35	59.45	0	9.36	3.12	2.77	13.69	2.25	2.21	79.72	2.49	5.94	0	0.14	577	774	0.81	0.35
136	5904.8	7.77	4.85	0.78	0.97	0.68	58.74	0	4.27	4.08	2.43	12.91	2.52	2.81	135.31	1.58	4.20	0	0.13	1030	814	0.78	0.22
140	6114.5	11.21	0	0	0	0	28.88	0	5.17	10.78	6.90	31.47	5.60	0.67	39.69	1.37	4.45	0	0	232	625	-0.03	1.71
148	6517.7	15.16	5.85	0.30	2.08	0.79	52.23	0	3.67	3.07	2.18	11.89	2.78	3.24	138.86	1.65	4.13	0.14	0.28	1009	777	0.49	0.07
156	6829.8	13.13	0,00	0.42	1.88	1.04	64.79	0	1.88	1.67	0.21	12.92	2.08	4.33	80.20	0.17	3.34	0	0	480	640	0.82	-0.33
164	7163.7	18.99	1.99	0	1.33	0.66	46.48	0	6.91	2.79	2.26	17.53	1.06	2.27	117.21	0.78	0	0	0.16	753	687	0.26	0.30
172	7531.4	20.21	4.79	0	1.67	0.42	57.29	0	0	0.42	4.38	9.58	1.25	5.40	27.58	0	4.31	0	0.06	480	573	0.52	-0.48
180	8327.8	0.97	0.77	0	0.77	0	92.46	0	2.90	0	0	1.55	0.58	18.88	14.72	0.06	0.91	0	0	517	1051	1.72	-1.07
188	9797	0.28	1.53	0.42	0.14	0.70	93.74	0	0.56	0	0.42	0.97	1.25	30.26	28.32	0	0.59	0.04	0	719	836	1.77	-1.14
196	10901.3	1.46	15.69	0.21	0.42	2.09	72.18	0	1.46	0	0.63	3.35	2.51	11.58	14.85	0	0.06	0.03	0	478	908	1.25	-0.27
204	11844.1	0.67	5.56	0	0	0.17	91.25	0	0	0	0.17	1.18	1.01	41.43	118.34	0.20	2.99	0	0.40	594	673	1.71	-1.05
212	12252.2	0	12.79	0	0	0	84.88	0	1.16	0	0	0	1.16	42.00	27.01	0	3.77	0	0	86	427	1.58	-0.77
228	12826.5	0	0	0	0	0	0	0	0	0	0	0	0	0	0	0	0	0	0.22	0	621	-	-
236	13000	0	0	0	0	0	0	0	0	0	0	0	0	0	0	0	0	0	0	0	2669	-	-
240	13100	0	0	0	0	0	0	0	0	0	0	0	0	0	0	0	0	0	0	0	1635	-	-
244	13200	0	0	0	0	0	0	0	0	0	0	0	0	0	0	0	0	0	0	0	2618	-	-
248	13300	0	0	0	0	0	0	0	0	0	0	0	0	0	0	0	0	0	0	0	1741	-	-

Table 12. Relative abundances of dinocyst taxa, palynomorph influxes, dinocyst counts, marker grains and PCA sample scores for dinocyst analysis in 11PC.

Depth	Age (Cal kyr BP)	*Spiniferites ramosus*	*Spiniferites mirabilis*	*Spiniferites delicatus*	*Spiniferites pachydermus*	Spiniferites sp.	*Operculodinium centrocarpum* s.l.	*Alexandrium* cf. *catenella*	*Brigantedinium* spp.	*Echinidinium* sp.	*Dubridinium* sp.	*Polykrikos kofoidii*	Other heterophic dinocysts	A/H	Dinocyst influxes (cysts cm^{-2} yr^{-1})	Freshwater/brackish influxes (palynomorphs cm^{-2} yr^{-1})	organic linings of foraminifers influxes (linings cm^{-2} yr^{-1})	Reworked palynomorph fluxes (palynomorphs cm^{-2} yr^{-1})	Pre-Quaternary dinocyst influxes (cysts cm^{-2} yr^{-1})	Dinocyst counts	Marker grains	PCA 1	PCA 2
1	-14.4	51.21	0	0.29	0.43	0	13.12	1	21.11	1.85	0.14	9.70	1.14	1.95	325.61	5.57	10.68	0	0	1586	701	-1.16	-0.01
6	22.9	45.28	4.01	0.21	0	0.21	23.73	3.80	11.41	1.69	0.42	8.59	0.63	3.40	414.13	13.42	10.50	0	0	2526	1420	-0.78	-0.30
11	88.6	42.62	3.89	0.29	0.37	0.29	14.03	0.37	31.30	0.29	0.22	4.70	1.62	1.62	390.73	15.79	13.49	0	0	2566	1361	-0.97	0.41
21	244	42.59	5.82	0.82	0.31	0.51	24.92	0	18.90	0.92	0.31	3.78	1.12	3.00	270.55	9.40	10.78	0.28	0	1259	979	-0.69	-0.21
26	337.7	23.30	4.11	0.32	0.90	0	18.10	0.13	45.89	0.83	1.41	3.21	1.80	0.88	306.08	9.04	8.25	0	0	1771	1558	-0.52	1.40
30	418.4	52.50	5.41	0.57	0.73	0.57	31.83	0	7.92	0.08	0	0	0.40	10.90	197.61	7.50	7.66	0	0	2543	1238	-0.70	-1.24
35	521.1	46.08	4.00	0.26	1.19	0.77	33.39	0	10.31	0	0.43	3.07	0.51	5.99	202.10	6.71	8.61	0	0	2358	1174	-0.55	-0.87
46	737.5	32.81	4.70	0.39	1.47	0	45.94	0	9.60	0.20	0.78	2.84	1.27	5.81	214.63	7.15	8.83	0	0	1931	1021	0	-0.71
51	842.5	53.62	5.04	0.24	0.87	0.31	31.81	0	5.28	0.16	0.31	1.42	0.94	11.33	315.30	8.19	11.42	0	0	1635	1270	-0.72	-1.29
66	1202	47.62	5.19	0.87	0.87	0	35.64	0	4.91	0.29	0	3.61	1.01	9.19	198.66	2.29	5.16	0	0	1416	693	-0.52	-1.09
76	1401.4	24.86	7.05	1.04	0.46	0	53.53	0	5.55	0.23	0.81	6.13	0.35	6.65	166.55	2.70	5.39	0	0	1807	865	0.34	-0.57
81	1496	20.47	4.94	0.94	0.59	0.24	57.06	0	9.29	0.47	0.47	4.59	0.94	5.34	169.97	3.80	5.60	0	0	1740	850	0.50	-0.49
86	1590.9	33.50	8.99	0.33	0.49	0	43.30	0	6.21	0.16	0.49	5.56	0.98	6.46	372.26	9.12	15.82	0	0	572	612	-0.07	-0.61
91	1690.7	33.31	7.58	0.34	0.55	0	51.33	0	2.94	0	0.27	3.00	0.68	13.50	281.46	5.00	2.69	0	0	1811	1465	0.13	-1.03
97	1805.2	29.09	7.63	0.15	0.08	0.08	53.16	0	5.10	0.15	0.46	3.56	0.54	9.19	570.55	5.25	7.22	0	0	1591	2609	0.25	-0.84
101	1882.1	34.00	7.00	0.67	0	0	46.22	0	6.56	0.44	0.56	3.56	1.00	7.26	232.69	2.33	4.40	0	0	1570	900	-0.01	-0.80
111	2078.6	14.14	10.55	0.63	0.84	0.63	58.02	0	8.65	0.21	0.63	4.43	1.27	5.58	181.83	3.07	3.45	0	0	907	474	0.66	-0.21
126	2382.7	25.10	8.89	0.99	0.20	0.59	39.92	0	12.45	1.19	0.40	8.89	1.38	3.11	101.68	4.22	7.23	0	0	1515	506	0.00	0.12
131	2483.1	24.28	33.70	0	1.09	0	31.16	0	7.25	0	0.36	0.72	1.45	9.22	66.85	2.66	2.91	0	0	1676	276	-0.14	0.26
137	2604.5	34.43	22.49	0.17	2.08	0	20.93	0	9.52	0.35	1.90	6.06	2.08	4.03	130.85	4.53	6.11	0	0	1793	578	-0.60	0.30
141	2680.4	34.17	22.25	1.12	0.66	0.72	20.93	0	9.28	0.46	0.92	8.89	0.59	3.96	297.25	6.65	10.76	0	0	1778	1519	-0.60	0.38
146	2773.6	20.30	13.03	0	1.52	0.61	28.79	0	20.91	0.30	5.45	8.48	0.61	1.80	91.87	3.06	5.29	0	0	1458	330	-0.17	0.92
151	2871.6	8.17	19.44	0.65	2.12	0.65	41.50	0	7.68	0.16	6.70	9.97	2.94	2.64	113.12	3.33	4.25	0	0	1647	612	0.39	0.88
156	2974.9	14.52	24.54	0.10	1.23	0.72	45.71	0	1.33	0.20	0	10.43	1.23	6.58	185.23	3.03	7.39	0	0	1837	978	0.37	0.32
166	3187.9	6.25	12.44	0.31	1.19	0.05	13.27	0	4.49	0.15	2.27	58.47	1.08	0.51	825.04	21.30	14.06	0	0	953	1937	-0.33	3.28
171	3292.1	9.46	23.88	0.16	1.12	0.32	33.71	0	13.96	0	2.89	11.72	2.73	2.20	89.09	4.57	2.43	0	0	2843	624	0.17	1.26
181	3497.7	9.39	35.08	1.93	0	0	43.09	0	6.35	0	3.04	0.28	0.83	8.53	75.32	1.87	3.95	0	0	1951	362	0.43	0.51
186	3595.7	0.76	3.04	0	0.38	0	7.98	0	58.17	0	6.46	18.63	4.56	0.14	458.18	57.49	40.07	0	0	233	263	-0.36	3.51
191	3688.4	4.55	18.38	0.89	0.49	0.40	26.78	0	25.20	0.40	4.74	16.50	1.68	1.06	217.35	10.95	14.39	0	0	1890	1012	0.07	2.06
196	3779.4	0	2.96	0.37	0.37	0	35.19	0	25.19	2.59	9.26	18.89	5.19	0.64	81.61	6.65	5.44	0	0	1343	270	0.34	2.01
201	3881.9	2.30	6.90	0	1.15	0.38	40.61	0	24.14	0.38	4.60	15.71	3.83	1.06	72.71	5.85	5.57	0	0	1457	261	0.43	1.58
206	3981.3	7.89	14.37	1.13	3.10	0	49.86	0	8.45	1.41	3.94	7.61	2.25	3.23	112.67	6.03	6.98	0	0	1279	355	0.59	0.50
211	4077.7	4.21	13.19	0.92	1.10	0.37	47.80	0	18.32	1.10	3.11	6.41	3.48	2.08	78.34	3.01	4.16	0	0	2829	546	0.60	0.88
215	4155.4	5.07	12.44	0.92	0.77	0.31	54.38	0	11.98	1.23	2.76	8.29	1.84	2.83	166.41	7.16	7.67	0	0	1588	651	0.74	0.54
221	4273.7	6.74	10.97	0.38	0.19	0	58.71	0	10.68	0	1.92	9.62	0.77	3.35	228.96	6.17	10.14	0	0	1842	1039	0.80	0.31
226	4371.9	4.31	15.47	1.91	0.32	0.80	57.74	0	8.13	0.48	1.59	7.50	1.75	4.14	22.79	0.87	1.16	0	0	11167	627	0.84	0.36
231	4467.4	2.79	5.03	1.12	0.56	0	64.53	0	13.97	1.12	0	8.66	2.23	2.85	96.75	4.32	4.05	0	0	1502	358	1.01	0.28
236	4566.1	6.17	2.88	0.82	0.41	0	74.07	0	6.17	0.41	0	7.41	1.65	5.39	59.78	3.44	2.95	0	0	1650	243	1.18	-0.41
241	4669.2	5.51	8.27	0.97	0.16	0.32	66.61	0	9.08	1.46	1.62	5.19	0.81	4.51	166.52	5.94	3.78	0	0	1504	617	1.02	-0.09
246	4762.2	6.76	11.15	1.46	1.28	0.18	58.68	0	9.87	1.10	1.65	6.76	1.10	3.88	263.08	9.14	10.10	0	0	844	547	0.81	0.21
251	4862.2	7.24	13.32	2.57	0.47	0	57.01	0	7.24	0	2.80	7.24	2.10	4.16	204.39	3.82	4.30	0	0	850	428	0.77	0.23
256	4961.5	4.76	9.96	1.01	0.14	0	59.60	0	9.67	1.59	4.33	5.92	3.03	3.08	166.75	6.98	3.85	0	0	1687	693	0.87	0.25
261	5050.1	6.23	6.23	1.36	1.56	0	65.56	0	5.45	2.14	1.95	7.39	2.14	4.24	78.17	0.61	1.37	0	0	2669	514	0.98	-0.09
266	5137.9	6.95	7.40	1.25	0.09	0.09	68.98	0	4.37	0.71	1.87	6.68	1.60	5.56	482.46	9.46	7.31	0	0	944	1122	1.05	-0.29
271	5233.8	8.91	2.51	0.28	0	0	72.98	0	4.74	2.51	1.11	5.85	1.11	5.53	172.66	5.77	6.25	0	0	844	359	1.10	-0.56
276	5332.1	13.93	5.57	0.82	1.15	0	62.79	0	3.93	1.80	3.77	5.08	1.15	5.35	142.30	5.37	3.03	0	0	1740	610	0.77	-0.44
281	5439.3	3.33	3.95	1.25	0.42	0	60.91	0	12.27	1.87	4.78	9.77	1.46	2.32	54.86	1.37	1.48	0	0	3559	481	0.91	0.40
286	5536.3	5.39	5.79	2.20	0.60	0.40	61.48	0	8.38	2.59	2.79	8.58	1.80	3.14	152.22	4.25	0.91	0	0	1336	501	0.90	0.18
291	5641.8	2.01	6.59	2.01	0.57	0.57	67.05	0	5.16	4.01	1.72	7.74	2.58	3.72	101.84	1.46	2.04	0	0	1391	349	1.10	0.06
295	5725.3	7.09	5.04	1.49	0.93	0.19	71.83	0	0.75	1.49	3.36	5.04	2.80	6.44	129.05	2.41	1.69	0	0	1686	536	1.12	-0.51
301	5842.8	4.17	6.16	3.26	1.27	0.18	71.74	0	1.99	1.63	0.91	4.89	3.80	6.56	86.25	2.81	2.81	0	0	2598	552	1.18	-0.36
306	5941	6.65	6.39	1.02	0	0.77	63.94	0	4.35	1.79	1.53	8.70	4.86	3.71	118.62	2.73	4.25	0	0	1338	391	0.94	-0.04
311	6043.4	5.74	5.74	0.83	0	0	70.07	0	3.34	1.98	1.46	8.34	2.50	4.67	830.01	6.92	19.04	0	0	469	959	1.10	-0.24
316	6142	5.94	4.38	0.63	0.63	1.56	70.31	0	2.19	0.94	0.63	10.31	2.50	5.04	64.75	0.81	1.21	0	0	2006	320	1.10	-0.24
321	6240.1	12.88	4.07	3.05	0	1.19	66.61	0	0.68	1.02	0	8.64	1.86	7.19	380.75	0.65	7.74	0	0	629	590	0.88	-0.52
326	6337.9	12.52	3.52	1.76	0.59	0.78	67.71	0	0.98	0.78	0.39	8.61	2.35	6.63	73.22	0.72	1.15	0	0	2833	511	0.91	-0.54
331	6450.8	13.66	6.66	2.64	0.57	0.11	66.25	0	1.15	0.92	0.46	6.20	1.38	8.90	192.36	1.33	4.20	0	0	1838	871	0.86	-0.59
335	6579	28.82	4.80	1.26	1.14	0.63	55.75	0	2.02	0.51	0	4.80	0.25	12.18	36.97	0.19	0.56	0	0	1390	791	0.32	-0.96
341	7283.6	4.32	3.17	2.88	0.58	0.29	75.22	0	4.32	1.15	0.29	7.49	0.29	6.38	12.24	0	0.28	0	0	1842	347	1.24	-0.40
347	7928.7	21.24	2.69	1.61	0.54	0.81	69.89	0	0	0.27	0	2.96	0	30	43.23	0	0.93	0.12	0	559	372	0.80	-1.21
353	8843.6	14.75	9.22	3.69	0.69	0	68.43	0	1.61	0	0.23	1.15	0.23	30	17.61	0	2.47	0	0	1601	434	0.90	-0.85
359	9839.9	2.78	3.17	1.39	0.60	0	86.90	0	0	0	0	1.59	3.57	18.38	18.57	0	0.48	0	0	1763	504	1.57	-0.99
365	10558.1	0	0.26	2.51	0	0.13	96.17	0	0.53	0	0	0	0.40	107.29	36.97	0.05	0.88	0	0	1332	758	1.83	-1.25
369	10992.8	1.46	9.84	4.01	0.24	0	81.29	0	1.22	0.61	0	0.73	0.61	30.65	19.27	0.02	0.33	0	0	2775	823	1.47	-0.71
375	11824.9	0.17	2.84	1.11	0.24	0.07	94.82	0	0.27	0	0	0.17	0.31	132.87	92.89	0.02	0.85	0	0.02	2902	4150	1.80	-1.20
381	12175.1	1.83	9.83	2.35	0.44	0	82.25	0	2.70	0.09	0.09	0.35	0.09	29.24	48.79	0.13	4.12	0	0.04	3889	1149	1.48	-0.74
389	12492.8	3.16	11.21	0.86	0.43	0.14	75.14	0	0.86	0	0	0.72	7.47	10.05	30.70	0	6.35	0	0	3744	696	1.29	-0.56

Table 13. Relative abundances of pollen taxa, pollen & spores sum and pollen & spore influxes and PCA sample scores for pollen analysis in 06PC.

Depth	Age (Cal kyr BP)	AP	High shrubs	Low shrubs	Herbs	*Nothofagus* sp.	*Podocarpus* sp.	*Drymis* sp.	Asteraceae subf.asteroideae	*Nassauvia* sp.	*Chuquiraga* sp.	*Ephedra* sp.	*Colliguaya intergerrima*	Other shrubs	Poaceae	Chenopodiaceae	Paludal taxa	other herbs	Pollen fluxes (grains cm^{-2} yr^{-1})	Spore concentration fluxes (spores cm^{-2} yr^{-1})	Pollen counts	Spore counts	Marker grains	PCA 1	PCA 2
0	-8.8	11.96	7.61	28.62	51.81	9.42	2.54	0	17.03	3.99	0.36	4.35	5.07	5.43	13.04	32.25	0	6.52	39.11	0.57	276	4	407	-0.60	-0.35
8	300.4	16.14	8.66	25.98	49.21	12.20	3.94	0	14.57	4.72	1.18	4.33	6.30	3.54	7.09	31.10	0	11.02	28.67	0.56	254	5	511	-0.57	-1.06
16	608.3	12.00	8.50	46.00	33.50	7.00	5.00	0	22.50	3.50	2.00	16.50	5.50	4.50	0	28.50	0.50	4.50	36.57	0.73	200	4	347	-0.65	-3.32
24	1298.3	14.34	8.30	28.68	48.68	12.08	2.26	0	17.74	1.89	1.13	6.04	6.42	3.77	7.17	34.34	0.38	6.79	30.94	0.47	265	4	494	-0.40	-1.31
32	2124	13.50	8.44	29.54	48.52	10.55	2.95	0	20.25	2.95	0.42	5.49	5.06	3.80	11.81	33.76	0	2.95	40.80	1.03	237	6	335	-0.50	-0.84
40	2593.8	9.13	8.17	25.96	56.73	5.77	3.37	0	14.90	3.85	0.48	4.81	5.77	4.33	10.10	39.90	0.48	6.25	33.84	0.81	208	5	300	-0.10	-0.38
48	3390.8	11.00	10.50	24.50	54.00	9.50	1.50	0	16.00	4.00	0.50	3.50	7.00	4.00	9.00	40.50	1.00	3.50	37.88	0.19	200	1	335	-0.07	-0.61
56	3810.4	12.56	7.17	22.87	57.40	10.31	2.24	0	9.87	3.59	0	8.07	5.38	3.14	8.97	42.15	1.35	4.93	41.49	0.56	223	3	310	0.09	-0.03
64	4278	9.83	6.44	23.39	60.34	4.75	5.08	0	15.25	1.69	0	6.44	4.41	2.03	6.44	46.44	0	7.46	19.87	0	295	0	942	0.36	-0.82
72	4915.6	13.76	6.12	21.41	58.72	11.62	2.14	0	12.23	2.75	1.22	3.36	3.98	3.98	11.93	42.81	1.22	2.75	49.63	1.06	327	7	418	0.08	0.35
78	5433.7	12.80	7.20	18.80	61.20	10.40	2.40	0	11.20	2.00	2.00	2.80	6.40	1.60	11.60	46.40	0	3.20	42.79	0.34	250	2	337	0.28	0.52
80	5626	14.29	6.91	22.58	56.22	11.06	3.23	0	11.06	1.84	3.23	5.07	5.07	3.23	10.14	42.40	0.92	2.76	42.76	0.20	217	1	322	0.08	0.16
88	6196	14.89	7.23	21.70	56.17	11.91	2.98	0	13.62	0.85	1.28	5.11	5.96	2.13	15.32	37.87	0.85	2.13	44.01	1.12	235	6	308	-0.27	0.55
96	6820.5	12.98	6.73	23.08	57.21	11.06	1.92	0	10.58	5.29	0.96	5.29	4.81	2.88	14.42	41.83	0	0.96	43.99	1.27	208	6	300	-0.01	0.82
104	7339.4	10.53	8.33	21.93	59.21	8.77	1.75	0	13.16	3.07	0.88	3.95	7.89	1.32	11.40	42.11	0.44	5.26	41.48	0.36	228	2	317	0.01	0.10
112	8070.2	9.03	5.56	25.35	60.07	6.94	2.08	0	18.40	2.78	0	3.47	5.56	0.69	0	57.29	0	2.78	19.23	0	288	0	864	1.06	-1.75
120	8793.8	11.74	6.05	23.13	59.07	10.32	1.42	0	12.10	3.20	1.78	4.98	4.27	2.85	16.01	39.86	0.36	2.85	52.79	0.19	281	1	307	-0.16	0.88
128	9546.4	10.75	5.21	22.48	61.56	9.77	0.98	0	12.38	2.28	0.33	5.86	4.23	2.61	12.05	45.60	1.30	2.61	57.12	0.56	307	3	310	0.25	0.37
136	10147.2	8.07	5.38	24.22	62.33	5.83	2.24	0	16.14	1.79	0	6.28	2.24	3.14	13.90	45.29	0	3.14	42.36	0.38	223	2	334	0.20	0.25
144	10814	8.03	4.82	30.92	56.22	3.61	4.42	0	12.45	2.01	0.80	15.26	4.02	1.20	13.25	41.37	0.40	1.20	20.57	0.66	249	8	768	-0.01	0.22
152	11411.6	6.25	10.80	23.30	59.66	3.41	2.84	0	9.09	0.57	0	13.07	8.52	2.84	25.57	28.41	4.55	1.14	24.29	0.83	176	6	754	-0.97	2.15
160	11744.3	9.95	5.43	37.10	47.51	4.52	4.98	0.45	9.50	4.98	0	22.17	3.17	2.71	22.62	23.98	0,00	0.90	13.43	0.61	221	10	1317	-1.13	1.30
168	12131.9	9.27	4.79	37.06	48.88	2.56	6.71	0	11.18	5.43	0	18.21	1.28	5.75	19.81	26.52	0.96	1.60	18.19	0.81	313	14	1628	-0.95	0.86
176	12520.8	12.10	4.78	40.13	42.99	5.41	6.69	0	13.06	7.64	0.64	16.88	1.59	5.10	13.06	27.07	1.59	1.27	20.38	1.30	314	20	1603	-0.84	-0.33
184	12895.8	9.63	4.81	39.57	45.99	4.81	4.81	0	8.56	13.90	1.07	11.76	1.07	8.02	12.30	29.95	0	3.74	30.31	1.78	187	11	642	-0.66	0.17
192	13257.5	13.29	4.62	37.57	44.51	8.67	4.62	0	15.03	10.12	1.73	7.23	0.87	7.23	8.38	30.35	1.16	4.62	24.59	0.85	346	12	1464	-0.61	-0.95
200	13604.5	11.56	10.54	35.71	42.18	10.20	1.36	0	15.99	9.52	1.70	5.10	4.42	9.52	9.52	28.91	0	3.74	21.40	0.44	294	6	1430	-0.75	-0.93
208	13942.5	9.41	2.15	36.02	52.42	8.60	0.81	0	11.56	13.98	1.08	7.80	1.08	2.69	13.98	33.33	0.81	4.30	234.28	13.23	372	21	1155	-0.50	0.37
216	14071.3	9.01	2.17	37.27	51.55	6.83	2.17	0	13.98	14.29	0.93	6.83	0.62	2.80	9.63	36.02	0.31	5.59	128.76	6.80	322	17	1819	-0.30	-0.47
224	14138.4	11.84	2.80	37.07	48.29	10.90	0.62	0.31	12.77	14.64	0.31	5.30	0	6.85	12.46	31.46	0	4.36	146.30	6.38	321	14	1596	-0.60	-0.03
232	-	9.96	9.96	49.00	31.08	4.78	5.18	0	1.59	7.57	37.85	1.99	0	9.96	17.53	9.56	0	3.98	505.75	32.24	251	16	361	-1.96	1.85
240	-	1.03	0.51	3.59	94.87	0.51	0.51	0	1.79	0.51	0	1.28	0.26	0.26	2.82	89.23	0	2.82	772.99	15.86	390	8	367	3.04	1.42
248	-	0.63	0.63	6.58	92.16	0	0.63	0	3.13	0	0.31	3.13	0	0.63	13.48	76.80	0	1.88	302.53	41.73	319	44	767	2.15	2.56
256	-	2.49	0.36	9.96	87.19	0.71	1.78	0	6.76	0.36	0	2.85	0	0.36	8.19	76.51	0	2.49	205.43	76.76	281	105	995	2.19	1.35
264	-	1.70	0	7.82	90.48	0.68	1.02	0	6.80	0.34	0.68	0	0	0	17.35	70.07	0	3.06	250.42	68.14	294	80	854	1.67	2.67
272	-	1.62	0.32	7.77	90.29	0.32	1.29	0	4.21	1.29	0.32	1.62	0	0.65	51.78	29.77	7.12	1.62	392.26	35.54	309	28	573	-1.19	7.19
280	-	3.04	1.82	14.89	80.24	2.13	0.91	0	7.90	2.43	1.52	2.43	0.30	2.13	15.50	54.71	3.95	6.08	287.29	155.43	329	178	833	0.78	1.79
288	-	2.64	3.52	20.82	73.02	2.64	0	0	6.74	6.45	1.17	2.05	1.17	6.74	6.16	60.12	0.59	6.16	224.60	57.30	341	87	1004	1.21	0.52
296	-	4.28	0.92	12.84	81.96	3.36	0.92	0	7.34	1.53	0	2.45	0	2.45	6.12	71.87	0.31	3.67	251.17	31.49	327	41	947	1.94	0.82
304	-	1.90	0.95	9.52	87.62	0	1.90	0	2.54	3.17	0.32	3.49	0	0.95	2.22	74.60	0.63	10.16	254.31	10.50	315	13	901	2.18	0.76
312	-	15.58	2.60	14.29	67.53	1.30	14.29	0	7.79	0	0	6.49	0	2.60	0	63.64	0	3.90	35.23	10.52	77	23	1590	1.56	-0.51
320	-	7.26	1.61	8.06	83.06	0	7.26	0	4.03	0	0	3.23	0	2.42	0.81	80.65	0	1.61	33.23	4.29	124	16	2714	2.56	0.57
328	-	9.40	1.34	7.38	81.88	3.36	6.04	0	3.36	0	0	3.36	0	2.01	0	77.85	0	4.03	68.38	4.13	149	9	1441	2.41	0.43
336	-	44.44	5.56	5.56	44.44	2.78	41.67	0	0	0	0	2.78	0	8.33	0	41.67	0	2.78	12.87	2.14	36	6	1850	0.34	-0.30
344	-	40.40	1.01	17.17	41.41	2.02	38.38	0	8.08	2.02	3.03	4.04	0	1.01	0	37.37	0	4.04	23.55	5.71	99	24	2780	0.03	-1.18
352	-	42.86	7.14	10.71	39.29	1.79	41.07	0	8.93	0	0	1.79	0	7.14	3.57	33.93	0	1.79	17.25	6.47	56	21	2361	-0.23	-0.84

Table 14. Relative abundances of pollen taxa, pollen & spores sum and pollen & spore influxes and PCA sample scores for pollen analysis in 08PC.

Depth	Age (Cal kyr BP)	AP	High shrubs	Low shrubs	Herbs	*Nothofagus* sp.	*Podocarpus* sp.	*Drymis* sp.	Asteraceae subf.asteroideae	*Nassauvia* sp.	*Chuquiraga* sp.	*Ephedra* sp.	*Colliguaya intergerrima*	Other shrubs	Poaceae	Chenopodiaceae	Paludal taxa	other herbs	Pollen fluxes (grains cm^{-2} yr^{-1})	Spore concentration fluxes (spores cm^{-2} yr^{-1})	Pollen counts	spore counts	Marker grains	PCA 1	PCA 2
0	-10.1	15.15	9.09	27.27	48.49	11.36	3.79	0	16.67	5.30	0.76	3.79	7.58	2.27	12.88	29.54	0	6.06	35.02	0.53	132	2	470	-0.78	-0.40
8	302.3	15.69	3.92	33.99	46.40	9.15	6.54	0	21.57	3.27	0	7.19	2.61	3.27	7.19	36.60	0	2.61	43.66	0.29	153	1	437	-0.25	-1.63
16	663.4	16.50	7.07	30.30	46.13	9.76	6.73	0	18.52	3.37	1.35	6.06	5.05	3.03	13.47	26.60	0	6.06	52.23	0.88	297	5	709	-0.94	-0.61
24	1001.9	14.43	8.85	28.20	48.52	11.48	2.95	0	18.03	3.61	0.66	4.59	7.54	2.62	13.11	29.51	0	5.90	51.76	1.36	305	8	668	-0.78	-0.52
32	1343.1	11.14	7.53	29.82	51.51	9.04	2.11	0	18.37	2.11	0.60	8.13	5.42	2.71	10.84	35.55	0.60	4.52	55.79	1.01	332	6	742	-0.35	-0.79
40	1657.4	8.18	5.03	24.53	62.26	3.14	5.03	0	13.21	2.20	0.31	8.18	3.77	1.89	13.21	43.40	0.63	5.03	41.10	0.90	318	7	877	0.10	0.35
48	1928.2	6.62	6.99	27.94	58.45	4.04	2.57	0	16.18	1.47	1.10	8.46	5.88	1.84	7.72	45.59	0.74	4.41	40.09	0.59	272	4	846	0.27	-0.76
56	2232.8	11.44	10.17	26.69	51.70	9.32	2.12	0	19.92	1.27	0	5.51	9.75	0.42	10.17	37.28	0	4.24	36.36	0.31	236	2	694	-0.28	-0.97
64	2588	9.72	6.60	26.39	57.29	7.64	2.08	0	16.32	2.08	0.69	5.56	5.90	2.43	7.64	44.46	0.69	4.51	44.38	0.46	288	3	694	0.22	-0.76
72	2973.3	10.70	4.06	27.31	57.93	7.75	2.58	0.37	15.87	4.43	0	5.54	3.32	2.21	6.27	45.39	0	6.27	41.16	1.52	271	10	704	0.34	-0.89
80	3332.4	7.17	5.61	24.30	62.92	3.12	4.05	0	14.02	2.49	0.93	4.98	3.74	3.74	8.41	49.85	0.31	4.36	38.05	0.71	321	6	902	0.55	-0.23
88	3726.2	15.46	4.12	24.23	56.19	12.37	3.09	0	13.40	1.55	0	7.22	3.61	2.58	10.82	42.27	0	3.09	55.92	1.73	194	6	371	0.08	-0.06
96	4121.3	11.83	3.55	23.67	60.95	10.65	1.18	0	8.88	2.96	0	10.65	1.78	2.96	11.83	46.15	0.59	2.37	44.16	1.57	169	6	372	0.30	0.59
104	4518.5	5.69	4.46	20.05	69.80	3.96	1.73	0	11.39	2.48	0.25	4.46	1.73	4.21	10.40	54.93	1.24	3.22	49.54	0.49	404	4	872	0.84	0.53
112	4888.7	7.83	4.52	22.29	65.36	4.82	3.01	0	8.13	2.71	1.20	9.34	1.81	3.61	6.93	54.22	0.30	3.92	46.90	0.42	332	3	757	0.87	0.18
120	5229.8	7.09	3.15	21.26	68.50	4.72	2.36	0	11.81	4.33	0.39	4.72	2.36	0.79	11.42	51.20	1.18	4.72	44.45	0.88	254	5	611	0.59	0.55
128	5558.2	9.06	3.36	24.83	62.75	6.71	2.35	0	11.07	3.69	1.34	6.71	1.01	4.36	13.09	48.32	0.34	1.01	41.17	0.97	298	7	774	0.42	0.75
136	5904.8	6.09	4.64	23.77	65.50	3.77	2.32	0	12.46	2.90	0.29	6.96	1.45	4.35	7.54	53.03	0	4.93	45.32	0.66	345	5	814	0.82	-0.14
140	6114.5	8.71	2.79	23.00	65.50	5.92	2.79	0	8.36	3.48	0.35	9.76	0.70	3.14	8.36	55.05	0.35	1.74	49.10	0.68	287	4	625	0.91	0.41
148	6517.7	6.65	4.11	20.57	68.67	3.48	3.16	0	9.49	1.90	1.58	6.96	2.22	2.53	7.91	57.61	0.63	2.53	43.49	0.96	316	7	777	1.04	0.37
156	6829.8	5.79	2.89	24.44	66.88	3.86	1.93	0	14.15	2.89	0.64	6.75	0.64	2.25	7.07	56.93	0.64	2.25	51.96	0.84	311	5	640	1.00	-0.25
164	7163.7	8.70	3.68	25.75	61.87	5.69	3.01	0	13.71	1.34	0.33	10.03	2.01	2.01	5.69	54.84	0	1.34	46.54	1.56	299	10	687	0.90	-0.58
172	7531.4	8.36	2.79	29.62	59.23	5.92	2.44	0	17.77	1.39	0	10.45	1.74	1.05	2.79	54.01	0	2.44	16.49	0.29	287	5	573	0.88	-1.48
180	8327.8	10.88	5.44	31.38	52.30	6.69	4.18	0	13.39	2.93	1.26	13.39	3.77	2.09	4.60	43.51	0.84	3.35	6.81	0.09	239	3	1051	0.24	-1.12
188	9797	13.64	3.98	34.09	48.29	7.39	6.25	0	9.66	1.14	0	23.30	1.14	2.84	9.66	35.78	1.14	1.70	6.93	0.39	176	10	836	-0.21	-0.39
196	10901.3	3.80	5.06	27.85	63.29	2.53	1.27	0	6.33	3.80	0	16.46	1.27	5.06	26.58	30.37	3.80	2.53	24.76	0.94	79	3	908	-0.79	2.61
204	11844.1	3.23	0	38.71	58.06	3.23	0	0	19.35	6.45	0	12.90	0	0	6.45	48.39	0	3.23	6.18	0.80	31	4	673	0.48	-1.28
212	12252.2	8.70	0	30.43	60.87	4.35	4.35	0	8.70	4.35	0	17.39	0	0	4.35	47.81	4.35	4.35	7.22	0	23	0	427	0.57	-0.57
228	12826.5	0.76	0.76	10.61	87.87	0.76	0	0	3.79	3.03	0.76	0.76	0	3.03	3.79	81.81	0	2.27	28.50	1.51	132	7	621	2.57	1.15
236	13000	0	7.69	15.38	76.93	0	0	0	7.69	0	0	7.69	0	7.69	3.85	61.54	11.54	0	1.31	0.50	26	10	2669	1.15	0.01
240	13100	0	0	0	0	0	0	0	0	0	0	0	0	0	0	0	0	0	0	0	0	0	1635	-	-
244	13200	0	0	0	0	0	0	0	0	0	0	0	0	0	0	0	0	0	0	0	0	0	2618	-	-
248	13300	0	0	0	0	0	0	0	0	0	0	0	0	0	0	0	0	0	0	0	0	0	1741	-	-

Table 15. Relative abundances of pollen taxa, pollen & spores sum and pollen & spore influxes and PCA sample scores for pollen analysis in 11PC.

Depth	Age (Cal kyr BP)	AP	High shrubs	Low shrubs	Herbs	*Nothofagus* sp.	*Podocarpus* sp.	*Drymis* sp.	Asteraceae subf.asteroideae	*Nassauvia* sp.	*Chuquiraga* sp.	*Ephedra* sp.	*Colliguaya intergerrima*	Other shrubs	Poaceae	Chenopodiaceae	Paludal taxa	other herbs	Pollen fluxes (grains cm^{-2} yr^{-1})	Spore concentration fluxes (spores cm^{-2} yr^{-1})	Pollen counts	Spore counts	Marker grains	PCA 1	PCA 2
1	-14.4	13.62	10.12	29.57	46.69	11.67	1.95	0	16.73	5.45	0.39	6.23	1.95	8.95	10.89	30.34	0	5.45	119.37	0.46	257	1	701	-0.65	-0.76
6	22.9	8.86	10.13	30.38	50.63	6.96	1.90	0	16.77	4.75	0.95	5.06	5.06	7.91	7.91	37.98	0	4.75	92.16	0.87	316	3	1420	-0.19	-1.00
11	88.6	9.57	4.94	31.79	53.70	6.79	2.78	0	20.06	1.54	0.31	8.33	3.70	2.78	11.42	36.12	0.31	5.86	93.02	1.44	324	5	1361	-0.34	-0.86
21	244	13.92	7.73	31.44	46.91	9.79	4.12	0	18.56	3.61	0.52	7.22	4.64	4.64	14.43	27.83	0.52	4.12	53.61	0.83	194	3	979	-0.88	-0.46
26	337.7	16.50	4.53	26.54	52.43	13.59	2.91	0	18.77	1.29	0.97	4.53	3.24	2.27	11.00	36.25	0	5.18	60.71	0.39	309	2	1558	-0.31	-0.68
30	418.4	8.97	11.30	26.58	53.15	6.31	2.66	0	18.27	2.66	0	4.98	8.31	3.65	11.63	34.55	0	6.98	48.05	0.32	301	2	1238	-0.48	-0.67
35	521.1	12.54	7.07	25.72	54.67	7.40	5.14	0	14.47	2.89	0.64	7.40	4.50	2.89	7.07	45.03	0	2.57	53.54	0.69	311	4	1174	0.27	-0.69
46	737.5	11.03	7.12	31.67	50.18	7.83	3.20	0	18.86	3.56	0	8.54	2.49	5.34	5.34	40.21	0	4.63	59.07	1.68	281	8	1021	0	-1.60
51	842.5	13.16	6.25	23.68	56.91	10.53	2.63	0	13.49	2.30	0.33	5.92	4.28	3.62	8.55	43.09	0.33	4.93	75.47	1.49	304	6	1270	0.14	-0.39
66	1202	11.94	4.48	26.87	56.71	4.98	6.97	0	14.43	2.49	0	9.45	1.99	2.99	15.92	37.30	0	3.48	57.62	1.72	201	6	693	-0.28	0.44
76	1401.4	8.39	5.48	33.87	52.26	5.48	2.90	0	22.26	2.58	0	7.74	2.90	3.87	9.35	40.98	0.65	1.29	59.69	0.19	310	1	865	-0.03	-1.25
81	1496	14.05	4.90	29.08	51.97	11.44	2.61	0	15.69	4.25	0.65	8.17	2.61	2.61	11.44	36.61	0	3.92	61.19	1.00	306	5	850	-0.28	-0.38
86	1590.9	11.27	10.21	27.82	50.70	7.04	4.23	0	16.55	3.87	0.35	6.69	4.93	5.63	14.08	32.40	0	4.23	172.75	2.43	284	4	612	-0.58	-0.18
91	1690.7	11.07	6.19	25.73	57.01	8.14	2.93	0	14.98	0.98	0	9.12	3.26	3.58	12.70	39.42	0	4.89	58.98	0.96	307	5	1465	-0.13	-0.07
97	1805.2	12.97	5.70	29.11	52.22	11.39	1.58	0	18.99	2.53	0.32	6.96	1.27	4.75	15.19	33.54	0	3.48	69.10	1.09	316	5	2609	-0.52	-0.19
101	1882.1	11.27	4.93	23.24	60.56	10.56	0.70	0	13.73	3.17	0.35	5.28	3.17	2.46	19.01	40.16	0	1.41	73.43	0.52	284	2	900	-0.18	1.18
111	2078.6	11.22	3.21	23.72	61.85	9.62	1.60	0	15.06	3.21	0	4.81	0.96	2.88	12.82	44.55	0	4.49	119.68	1.53	312	4	474	0.18	0.22
126	2382.7	12.79	6.23	24.26	56.72	9.18	3.61	0	15.41	2.95	0	5.25	4.26	2.62	17.05	38.03	0	1.64	61.29	0.60	305	3	506	-0.29	0.63
131	2483.1	11.59	7.61	24.28	56.52	8.70	2.90	0	15.22	3.26	0	5.80	5.80	1.81	12.32	40.21	0.36	3.62	66.85	0	276	0	276	-0.11	-0.05
137	2604.5	9.80	5.74	21.62	62.84	8.11	1.69	0	15.54	2.03	0	3.38	3.38	3.04	11.15	46.95	0.34	4.39	67.01	0.68	296	3	578	0.32	-0.01
141	2680.4	11.11	3.49	27.30	58.10	8.25	2.86	0	16.19	0.63	1.27	9.21	1.90	1.59	13.97	39.37	0	4.76	61.64	0.78	315	4	1519	-0.12	0.06
146	2773.6	9.45	6.51	28.01	56.03	6.51	2.93	0	16.94	3.26	0	7.49	2.61	4.23	8.79	42.68	0	4.56	85.47	0	307	0	330	0.11	-0.75
151	2871.6	10.85	4.75	22.37	62.03	7.80	3.05	0	16.61	1.36	0	4.41	2.37	2.37	12.54	43.73	0.34	5.42	54.53	0.74	295	4	612	0.14	0.01
156	2974.9	14.01	6.69	24.84	54.46	11.15	2.87	0	15.92	2.87	0.64	4.46	2.23	5.41	12.74	37.25	0	4.46	59.47	0.38	314	2	978	-0.26	-0.11
166	3187.9	10.60	4.30	25.50	59.60	4.64	5.96	0	15.23	2.32	1.32	5.30	1.32	4.30	10.26	48.36	0.33	0.66	128.63	1.70	302	4	1937	0.44	-0.09
171	3292.1	10.28	5.61	27.10	57.01	9.03	1.25	0	13.08	1.25	0.62	11.84	1.25	4.67	7.48	46.73	0.31	2.49	45.83	1.29	321	9	624	0.41	-0.52
181	3497.7	12.17	7.57	26.97	53.29	9.21	2.96	0	16.45	1.32	0.66	7.57	2.30	6.25	10.20	41.11	0.33	1.64	63.25	1.46	304	7	362	0.01	-0.52
186	3595.7	8.10	9.05	26.67	56.18	6.19	1.90	0	18.10	3.81	0.48	2.38	2.38	8.57	9.52	43.34	0	3.33	365.85	5.23	210	3	263	0.11	-0.64
191	3688.4	12.63	4.10	18.77	64.50	8.53	4.10	0	10.92	1.37	1.02	5.46	0.68	3.41	11.60	49.16	0.68	3.07	62.93	0.86	293	4	1012	0.50	0.60
196	3779.4	8.98	3.59	31.14	56.29	8.98	0	0	15.57	4.79	0	10.18	1.20	2.99	4.79	49.70	0	1.80	50.48	1.21	167	4	270	0.60	-1.07
201	3881.9	13.53	5.31	25.12	56.04	9.66	3.86	0	13.04	2.42	0.97	7.73	2.90	3.38	8.70	45.89	0	1.45	57.67	1.11	207	4	261	0.32	-0.25
206	3981.3	8.00	4.89	18.22	68.89	4.44	3.56	0	9.33	3.11	0	4.89	3.11	2.67	10.67	54.67	0.44	3.11	71.41	1.59	225	5	355	0.82	0.75
211	4077.7	10.30	1.99	22.92	64.79	7.31	2.99	0	12.62	2.66	0.66	5.32	0.66	2.99	4.98	55.49	1.33	2.99	43.19	1.43	301	10	546	0.96	-0.42
215	4155.4	9.82	5.82	25.09	59.27	8.00	1.82	0	12.00	2.18	0	10.18	5.09	1.45	10.18	48.01	0	1.09	70.29	0.77	275	3	651	0.42	0.07
221	4273.7	11.36	4.87	22.73	61.04	8.44	2.92	0	14.94	3.90	0	3.57	2.60	2.60	7.14	51.94	0	1.95	67.87	1.32	308	6	1039	0.68	-0.42
226	4371.9	10.56	4.95	21.78	62.71	6.93	3.63	0	12.87	2.64	0	5.94	0.99	4.29	6.27	54.13	0.66	1.65	11.01	0.22	303	6	627	0.86	-0.33
231	4467.4	9.90	3.19	28.43	58.48	9.27	0.64	0	19.49	1.60	0	6.07	1.60	2.88	5.75	48.86	0.96	2.88	84.59	0.81	313	3	358	0.51	-1.24
236	4566.1	13.59	4.21	21.36	60.84	11.33	2.27	0	10.36	2.91	0.32	7.12	2.59	2.27	7.12	52.10	0.32	1.29	76.02	1.23	309	5	243	0.73	-0.02
241	4669.2	9.63	2.33	21.93	66.11	8.64	1.00	0	12.96	2.99	0.66	5.32	1.33	1.00	5.65	57.46	0.66	2.33	81.24	1.35	301	5	617	1.06	-0.29
246	4762.2	8.74	2.45	24.13	64.68	6.99	1.75	0	15.73	1.75	0	5.94	2.10	1.05	5.59	55.25	0.70	3.15	137.55	2.40	286	5	547	0.91	-0.68
251	4862.2	9.71	2.16	21.58	66.55	8.27	1.44	0	8.27	5.04	0	6.83	0	3.60	10.79	53.60	0.72	1.44	132.76	0.96	278	2	428	0.79	0.83
256	4961.5	6.71	2.01	20.81	70.47	6.04	0.67	0	9.73	1.34	0.67	8.72	1.01	1.34	4.70	60.41	0.34	5.03	71.70	0.72	298	3	693	1.27	-0.12
261	5050.1	7.64	1.04	24.31	67.01	4.51	3.13	0	16.67	2.08	0	5.21	0	1.39	2.43	60.42	0.69	3.47	43.80	0.30	288	2	514	1.27	-1.09
266	5137.9	8.91	1.32	23.76	66.01	8.25	0.66	0	13.86	3.30	0	6.27	0.99	0.66	5.28	55.78	0.99	3.96	130.29	1.72	303	4	1122	0.96	-0.52
271	5233.8	8.39	2.26	22.90	66.45	5.16	3.23	0	12.90	3.87	0	5.16	0.97	2.26	4.52	60.64	0	1.29	149.09	2.89	310	6	359	1.26	-0.39
276	5332.1	10.29	1.61	23.15	64.95	8.04	2.25	0	14.15	2.57	0	6.11	0.64	1.29	7.40	54.66	0	2.89	72.55	0	311	0	610	0.87	-0.26
281	5439.3	7.32	3.18	19.43	70.07	5.73	1.59	0	9.87	3.82	0	5.41	0.32	3.18	9.87	55.43	0.64	4.14	35.81	0.34	314	3	481	0.90	0.60
286	5536.3	9.84	1.97	18.36	69.83	8.20	1.64	0	9.84	4.26	0	4.26	0.98	0.98	5.90	60.99	0	2.95	92.67	1.22	305	4	501	1.28	0.17
291	5641.8	11.30	2.40	17.12	69.18	9.59	1.71	0	10.96	3.08	0	2.74	0.68	2.05	10.27	54.12	1.03	3.77	85.21	0.88	292	3	349	0.81	0.59
295	5725.3	11.33	5.00	18.67	65.00	9.00	2.33	0	11.33	2.67	0	4.33	0.67	4.67	2.00	60.33	0	2.67	72.23	0.96	300	4	536	1.29	-0.64
301	5842.8	11.07	2.68	20.13	66.12	7.72	3.36	0	10.74	2.68	0	5.70	0.67	3.02	4.03	59.40	0	2.68	46.56	0.16	298	1	552	1.22	-0.30
306	5941	7.80	3.05	19.32	69.83	6.10	1.69	0	11.86	2.71	0	4.41	1.36	2.03	4.75	61.70	0.68	2.71	89.50	0	295	0	391	1.32	-0.20
311	6043.4	9.70	1.00	17.73	71.57	6.69	3.01	0	11.37	3.34	0	2.01	0	2.01	6.69	61.20	0	3.68	258.78	1.73	299	2	959	1.28	0.20
316	6142	9.79	2.97	20.77	66.47	8.90	0.89	0	13.95	2.37	0	3.26	1.19	2.97	4.45	60.83	0.30	0.89	68.19	0.61	337	3	320	1.27	-0.46
321	6240.1	11.84	1.64	19.74	66.78	8.55	2.63	0.66	10.53	3.29	0	5.26	0.66	1.64	11.18	52.31	0	3.29	196.18	1.94	304	3	590	0.70	0.66
326	6337.9	11.15	2.87	22.29	63.69	9.87	1.27	0	11.46	2.55	0	7.96	0.96	2.23	8.28	52.87	0	2.55	44.99	0.43	314	3	511	0.77	0.05
331	6450.8	4.47	3.83	19.49	72.21	3.51	0.96	0	12.14	1.92	0	5.11	1.60	2.56	7.99	62.93	0	1.28	69.13	0.66	313	3	871	1.34	0.29
335	6579	6.57	1.04	15.22	77.17	4.84	1.73	0	10.03	0	0	5.19	0	1.04	4.50	72.67	0	0	13.51	0.09	289	2	791	2.00	0.27
341	7283.6	6.51	4.98	12.64	75.87	5.36	1.15	0	8.05	1.92	0	2.30	0.38	4.98	0.77	72.41	0	2.68	9.20	0.14	261	4	347	2.04	-0.10
347	7928.7	7.66	2.30	15.71	74.33	7.66	0	0	5.75	4.21	0	5.75	0.77	1.53	1.92	71.26	0	1.15	30.33	0.12	261	1	372	1.97	0.23
353	8843.6	4.75	2.37	17.29	75.59	3.39	1.36	0	8.81	2.71	1.02	4.75	1.69	0.68	2.71	70.85	0.34	1.69	11.97	0.20	295	5	434	1.90	0.07
359	9839.9	10.64	0.91	24.32	64.13	6.99	3.65	0	13.98	1.22	0	8.81	0.91	0.30	3.95	55.93	0.61	3.65	12.12	0.11	329	3	504	1.00	-0.79
365	10558.3	9.80	1.01	26.35	62.84	7.09	2.70	0	10.47	1.69	0	14.19	0	1.01	6.76	52.03	0.34	3.72	14.44	0.73	296	15	758	0.77	-0.24
369	10992.8	11.78	2.23	29.30	56.69	9.24	2.55	0	13.06	2.23	0	13.38	0.64	2.23	6.37	46.80	1.27	2.23	7.35	0.12	314	5	823	0.45	-0.69
375	11824.9	8.42	3.68	31.58	56.32	5.79	2.63	0	7.37	1.58	0	22.11	0	4.21	7.89	45.79	1.05	1.58	4.25	0.07	190	3	4150	0.44	-0.11
381	12175.3	14.19	3.87	25.16	56.78	7.74	6.45	0	7.74	1.94	0	12.90	0	6.45	9.03	37.43	1.29	9.03	6.58	0.47	155	11	1149	-0.11	-0.04
389	12492.8	15.82	1.90	24.68	57.60	8.86	6.96	0	10.13	6.96	0	6.96	0	2.53	18.99	33.54	1.27	3.80	6.97	0.35	158	8	696	-0.52	1.35

Table 16. Dinocyst counts of surface samples.

ID samples	*Alexandrium* cf. *Catenella*	*Nematosphaeropsis labyrinthus*	*Operculodinium centrocarpum*	*O. centrocarpum short spines*	*Spiniferites delicatus*	*Spiniferites ramosus*	*Spiniferites mirabilis*	*Spiniferites bentorii*	*Spiniferites pachydermus*	*Spiniferites* spp.	*Echinidinium* sp. C	*Echinidinium* sp. D	*Brigantedinium* spp.	*Brigantedinium cariacoense*	*Brigantedinium simplex*	*Bringantedinium auranteum*	*Dubridinium* sp.	*Selenopemphix nephroides*	*Selenopemphix quanta*	*Protoperidinium nudum*	*Stelladinium stellatum*	*Trinovantedinium pallidifulvum*	*Votadinium calvum*	*Votadinium spinosum*	*Quinquecuspis concreta*	*Polykrikos kofoidii*	*Polykrikos schwartzii*
BV01	5	0	167	13	0	1707	263	15	10	21	10	6	0	0	0	0	0	0	0	5	0	0	0	5	1	33	0
BV02	27	0	125	18	0	1138	225	0	10	18	23	2	0	0	0	0	0	2	2	5	0	1	0	1	4	33	0
BV03	21	0	97	8	0	598	113	0	7	13	41	0	0	0	0	0	0	0	0	3	2	2	0	0	0	32	0
BV04	45	0	513	19	0	2785	87	5	16	7	17	0	0	0	0	0	0	2	1	1	1	0	0	1	3	181	3
BV05	5	0	371	2	0	2037	81	0	14	2	28	0	0	0	0	0	1	2	4	5	0	0	0	7	71	0
BV06	13	0	547	54	0	1331	155	5	17	2	78	7	0	0	0	0	0	12	5	2	3	0	0	11	97	0
BV07	3	0	676	4	0	3420	215	8	38	10	66	4	0	0	0	0	0	2	11	3	12	1	0	0	12	184	0
BV08	4	0	320	7	0	1648	199	11	15	7	44	0	0	0	0	0	0	2	2	1	3	0	0	9	15	90	0
BV09	1	0	730	26	0	2672	145	13	39	8	63	0	0	0	0	0	0	3	8	13	3	0	0	1	10	82	0
BV10	6	0	257	1	0	828	46	2	16	4	24	0	0	0	0	0	0	0	0	2	1	0	0	0	4	84	0
BV11	2	0	122		0	429	50	0	5	0	32	0	0	0	0	0	0	2	3	1	0	1	0	0	0	162	0
BV12	2	0	73		0	271	16	0	9	1	25	3	0	0	0	0	0	0	2	0	1	0	0	2	2	143	2
BV13	5	0	108	7	5	425	31	0	4	8	45	0	0	0	0	0	0	4	2	4	1	0	0	9	1	145	6
BV14	0	0	25		0	67	4	0	0	3	9	1	0	0	0	0	0	1	0	0	0	0	0	0	0	45	1
BV15	1	0	23		0	51	1	1	3	1	15	0	0	0	0	0	0	0	0	0	0	1	0	0	1	35	0
BV16	1	0	24	1	0	70	7	0	2	0	1	1	0	0	0	0	0	1	3	0	0	0	0	0	0	31	0
BV17	1	0	44	6	1	132	11	1	4	4	23	0	0	0	0	0	0	0	0	3	0	0	0	0	0	58	5
BV18	2	0	64		0	319	22	3	2	2	14	2	0	0	0	0	0	1	5	0	2	0	0	0	2	69	0
BV19	6	0	75		0	428	25	0	1	2	9	0	0	0	0	0	0	0	2	0	3	0	0	1	0	112	1
BV20	3	0	23	5	0	182	18	0	2	1	10	2	0	0	0	0	0	2	1	1	0	0	0	0	0	47	0
BV21	0	0	57	2	0	302	17	0	6	3	22	1	0	0	0	0	0	0	1	2	1	2	0	1	0	93	0
BV22	67	1	83	8	0	300	47	1	5	0	22	12	0	0	0	0	0	1	0	1	0	0	0	0	0	190	0
BV23	2	0	26		0	91	19	1	3	0	10	0	0	0	0	0	0	1	0	0	0	0	0	3	0	120	1
BV25	5	0	29		0	110	21	2	3	0	13	0	0	0	0	0	0	3	3	1	1	0	0	1	0	126	2
BV26	16	0	34	5	0	197	13	0	0	0	23	11	0	0	0	0	0	2	0	2	5	0	0	0	0	131	0
BV27	58	0	98		0	423	35	1	4	2	43	10	0	0	0	0	0	1	0	2	2	3	0	0	1	318	0
BV28	2	0	34	2	0	53	14	3	1	0	15	0	0	0	0	0	0	0	0	0	0	0	0	3	0	128	7
BV29	34	0	6	1	0	34	8	0	0	3	20	6	0	0	0	0	0	0	0	0	0	0	0	0	0	36	0
BV30	19	0	66	2	0	201	16	0	1	3	22	10	0	0	0	0	0	0	0	2	1	4	0	0	0	153	0
BV32	5	0	16	1	0	78	21	0	4	3	15	14	0	0	0	0	0	0	0	0	3	1	0	1	1	37	0
BV33	19	0	20	3	0	119	13	0	0	2	24	7	0	0	0	0	0	5	0	2	1	0	0	4	1	90	0
BV34	14	0	202	44	0	670	48	15	0	14	6	11	0	0	0	0	0	0	0	11	2	0	0	0	2	48	0
BV35	6	0	349	37	8	1063	41	13	17	21	70	0	0	0	0	0	0	0	0	6	5	0	0	1	5	116	3
BV36	5	0	125	8	0	751	44	8	4	2	20	4	0	0	0	0	0	2	0	4	1	0	0	0	6	49	0
BV37	25	0	264	25	0	1178	39	7	14	23	47	9	0	0	0	0	0	0	0	7	3	0	0	0	13	63	0
BV38	3	0	122	17	0	354	19	2	4	6	20	6	0	0	0	0	0	0	0	0	2	0	0	0	2	37	0
BV39	29	0	122	5	0	800	60	0	7	11	36	7	0	0	0	0	0	1	0	14	1	3	0	4	1	158	0
BV40	12	0	119	18	0	859	45	0	13	0	21	6	0	0	0	0	0	3	0	2	5	2	0	2	0	110	0
BV41	12	0	81	13	0	696	36	1	11	8	26	11	0	0	0	0	0	2	0	17	3	0	0	1	2	72	0
BV42	9	0	99	9	0	609	23	0	14	3	17	2	0	0	0	0	0	0	0	1	4	2	0	0	0	61	0
BV43	24	0	162	17	0	1160	66	0	15	6	33	12	0	0	0	0	0	0	0	8	2	0	0	2	4	102	0
BV44	4	0	192	11	0	1556	112	0	21	9	44	8	0	0	0	0	0	1	10	9	2	1	0	4	6	92	0
BV45	1	0	116	7	0	611	27	0	5	3	32	4	0	0	0	0	0	0	0	1	1	1	0	1	2	68	0
BV46	1	0	121	4	0	653	57	0	8	5	14	4	0	0	0	0	0	1	0	0	2	0	0	1	2	59	0
BV47	7	0	224	31	9	1247	122	9	25	21	39	6	0	0	0	0	0	0	4	2	4	0	1	2	5	115	0
BV48	4	0	151	18	7	1363	135	7	24	12	5	0	0	0	0	0	0	0	5	1	4	0	0	4	4	126	1
BV49	3	1	132	19	39	1194	154	12	15	51	30	0	0	0	0	0	0	1	3	6	3	0	0	5	11	192	1
BV50	4	0	304	26	4	1106	239	5	44	52	30	0	0	0	0	0	0	1	10	0	0	0	0	9	6	156	0
BV51	12	0	81	30	57	1878	527	15	46	108	48	0	0	0	0	0	0	0	0	0	0	0	2	5	31	700	20
BV52	8	2	55	9	3	96	68	0	2	3	8	0	0	0	0	0	0	0	0	0	0	0	0	0	0	96	2
BV54	0	0	0		0	2	0	0	0	0	0	0	0	0	0	0	0	0	0	0	0	0	0	0	0	1	0
BV55	1	0	1		0	10	0	0	0	1	3	0	0	0	0	0	0	0	0	0	0	0	0	0	0	0	0

Table 17. Pollen counts of surface samples.

ID samples	*Nothofagus* sp.	*Podocarpus* sp.	Pinaceae (excluded)	Asteraceae subf. Asteroideae	Asteraceae subf. Mutisieae	*Nassauvia* sp.	*Chuquiraga* sp.	*Ephedra* sp.	*Calliguaya integerrima*	*Mulinum* sp.	*Azorella* sp.	Apiaceae type	Solanaceae type	*Lycium* sp.	*Schinus* sp.	Rhamnaceae	Verbenaceae	Fabaceae	*Empetrum rubrum*	Labiaceae/Rubiaceae type	Poaceae	Caryophyllaceae	Chenopodiaceae	Convolvulaceae	*Gilia* sp.	*Erodium cicutarium*	*Acaena* sp.	*Fuschia* sp.	Brassicaceae	*Rumex acetosella*	Asteraceae subf. Cichorioideae	Cyperaceae	Typha	Unknown	Riccia	Bryophyta	Pteridophyta/Lycopodium	Spores indifferenciés
BV01	6	9	2	39	2	1	1	4	1	7	0	0	0	0	1	2	0	1	0	1	31	2	12	0	0	0	0	0	3	0	0	0	1	2	0	0	0	0
BV02	34	3	1	33	1	12	5	5	17	0	0	2	2	3	2	2	0	1	1	3	34	1	45	0	0	0	0	0	0	0	0	0	0	4	0	1	0	0
BV03	19	2	0	29	0	17	1	5	27	2	0	1	2	2	1	2	0	1	3	0	36	1	51	0	0	1	0	0	4	0	0	0	0	2	0	1	0	0
BV04	42	2	4	31	1	1	3	18	48	6	0	0	0	0	0	0	2	2	0	1	43	5	100	0	0	1	0	0	5	0	0	0	4	1	0	0	0	0
BV05	35	16	0	74	0	2	11	14	49	2	0	2	3	1	0	0	1	3	0	1	31	4	117	0	0	9	1	0	3	0	1	4	1	0	0	2	0	0
BV06	31	6	0	57	2	1	4	17	47	0	0	2	1	0	1	0	1	0	0	2	44	9	92	0	0	1	0	0	1	0	0	4	0	1	0	0	0	0
BV07	21	16	0	62	6	1	2	21	33	7	1	3	0	1	0	1	0	0	0	0	39	3	95	0	0	1	0	0	5	0	0	0	2	1	0	1	0	0
BV08	24	3	0	38	5	0	2	20	24	0	0	3	0	0	0	0	0	0	0	0	44	1	70	0	0	1	0	0	6	0	0	0	4	1	0	2	1	0
BV09	23	4	1	32	3	1	4	16	32	1	1	4	4	0	0	0	2	0	0	0	44	4	75	0	0	0	0	0	4	0	0	0	3	2	0	1	0	0
BV10	60	6	0	64	3	3	8	28	68	1	1	2	2	1	4	0	0	1	0	1	39	5	117	0	0	1	0	0	6	0	0	1	4	0	1	3	0	0
BV11	56	26	3	32	0	18	5	9	33	6	0	0	2	4	1	2	0	1	0	3	29	4	65	2	0	2	0	0	2	1	0	1	1	6	0	4	0	0
BV12	13	12	3	28	0	8	4	2	19	0	0	1	1	3	1	0	0	1	0	0	12	2	64	1	0	1	0	0	2	1	0	0	3	4	0	3	0	0
BV13	14	17	0	12	1	0	1	10	8	1	0	1	4	0	0	0	0	0	1	0	7	3	34	0	0	1	0	0	0	0	0	1	1	0	0	4	0	1
BV14	38	11	2	43	4	19	6	10	54	4	0	0	1	0	1	2	0	1	1	2	39	2	73	1	0	0	1	0	2	0	0	0	0	3	0	4	1	0
BV15	7	19	4	8	0	0	2	3	9	0	0	1	1	0	0	2	0	0	0	2	10	4	15	1	0	5	0	0	0	0	0	0	0	1	0	10	1	1
BV16	7	7	2	19	0	11	5	4	14	1	0	0	1	1	1	0	0	1	0	0	14	1	24	0	0	0	0	0	0	0	0	0	0	3	0	8	0	1
BV17	10	8	0	16	0	4	2	3	8	1	0	9	0	0	0	1	0	1	0	2	17	3	27	0	0	3	0	0	1	0	0	1	0	1	0	9	0	2
BV18	18	5	1	8	0	17	2	4	3	1	0	3	2	2	3	0	1	0	0	3	14	0	52	0	0	1	0	0	0	0	0	1	0	0	1	3	0	0
BV19	8	8	3	13	0	9	1	3	7	0	0	0	0	0	0	3	4	1	0	1	15	0	32	1	0	0	0	0	0	0	0	0	0	3	1	3	0	1
BV20	11	10	4	5	1	3	0	1	6	0	0	0	0	0	0	2	0	0	0	2	18	0	18	0	0	1	0	0	0	0	1	0	0	3	0	0	0	0
BV21	21	9	1	34	0	12	4	8	34	2	0	0	1	7	2	1	0	0	2	1	34	0	42	0	0	1	0	0	5	0	1	0	2	1	0	4	0	0
BV22	54	16	1	32	2	17	16	4	59	2	0	0	2	3	2	2	1	1	4	0	67	2	68	0	0	1	0	0	5	0	0	0	0	3	0	4	0	0
BV23	18	8	1	12	0	8	1	1	12	0	0	0	0	1	1	0	0	0	0	1	14	0	21	0	0	1	0	0	3	0	0	0	0	2	0	3	0	0
BV25	11	5	1	20	2	14	3	2	17	3	1	2	0	4	4	2	0	0	0	1	37	4	26	0	0	0	0	0	4	0	0	0	0	5	0	5	0	0
BV26	48	14	4	30	0	31	9	3	42	1	0	0	0	4	5	2	3	1	0	3	48	2	69	0	1	1	0	0	4	1	0	0	0	4	0	1	0	0
BV27	44	21	10	45	4	24	6	6	41	2	0	0	2	2	2	10	0	0	0	0	52	2	84	0	0	2	0	0	4	0	1	0	0	2	0	1	0	0
BV28	10	6	1	14	0	12	3	2	21	0	0	0	1	0	1	5	0	0	1	1	21	1	30	0	0	2	0	0	5	0	0	0	0	2	0	6	0	0
BV29	12	4	2	4	0	3	0	0	5	0	0	0	0	0	2	2	1	1	0	0	4	0	13	0	0	1	0	0	0	0	0	0	0	0	0	2	0	0
BV30	48	10	4	49	0	20	7	5	48	0	1	0	1	12	4	3	0	0	1	0	49	4	67	0	0	1	0	0	6	0	0	0	0	0	0	8	0	0
BV32	8	5	1	10	1	2	2	3	13	0	0	2	2	2	2	2	0	0	0	0	22	0	19	0	1	0	0	0	0	0	0	0	0	1	0	3	0	0
BV33	22	18	6	17	2	23	3	1	39	2	0	0	0	6	2	1	0	0	0	0	38	1	44	0	0	3	0	0	0	0	0	0	2	2	0	3	0	0
BV34	42	8	1	61	2	13	8	6	38	1	4	0	0	1	0	0	0	0	1	2	61	6	71	2	0	1	0	0	2	0	0	0	2	2	0	8	2	4
BV35	32	3	2	47	0	7	5	14	16	0	0	1	0	3	2	1	0	1	0	1	45	5	60	2	0	2	2	0	3	0	0	1	1	3	0	1	1	3
BV36	26	10	2	69	0	12	8	8	22	0	0	1	1	11	8	6	0	1	1	0	53	4	100	2	0	0	0	0	5	0	0	0	0	1	0	3	0	0
BV37	35	13	1	48	0	9	5	17	18	2	0	0	0	3	3	0	1	2	0	2	65	5	100	0	0	0	0	0	0	0	0	0	0	2	0	6	0	0
BV38	31	4	1	51	0	6	5	14	19	2	0	1	2	1	3	0	0	0	0	0	45	0	91	0	0	1	0	0	5	0	0	0	0	5	0	6	0	0
BV39	39	14	1	40	0	14	10	10	33	0	0	0	2	8	0	1	0	1	0	0	46	4	67	0	0	1	0	0	3	0	1	1	0	2	0	0	1	1
BV40	24	17	2	66	0	12	7	25	20	2	0	3	2	4	2	1	0	0	0	1	54	6	101	1	0	0	2	1	6	0	0	0	0	1	0	2	1	0
BV41	23	12	2	38	0	6	7	18	16	0	0	0	2	6	1	3	0	0	0	0	57	4	81	3	0	1	0	0	4	0	0	0	0	2	0	2	1	1
BV42	14	7	1	40	0	13	7	7	19	0	0	2	3	13	2	0	0	0	0	2	73	0	93	0	0	2	0	0	6	0	0	0	0	0	0	1	0	0
BV43	27	10	0	55	1	21	14	13	25	1	0	2	1	6	0	2	2	0	0	1	62	4	93	1	0	1	0	0	5	0	0	1	0	5	0	3	1	0
BV44	30	2	0	63	1	10	3	20	17	2	3	0	3	0	2	8	0	1	1	4	67	5	98	2	0	6	0	0	2	0	0	0	0	7	0	4	0	0
BV45	32	4	0	59	2	11	4	17	24	2	0	2	0	2	1	2	0	0	1	3	59	7	89	1	1	1	0	0	4	0	0	0	0	1	0	5	0	0
BV46	36	14	0	43	0	17	5	21	21	1	0	1	0	3	1	1	0	1	1	2	64	4	78	2	0	0	0	0	4	0	0	0	0	2	0	1	0	0
BV47	15	8	0	29	0	8	2	8	14	0	2	1	0	2	2	1	1	1	0	3	33	0	62	2	0	0	0	0	4	0	1	0	0	3	0	2	2	0
BV48	26	9	0	33	0	20	3	5	12	2	0	3	1	2	1	3	0	1	0	1	26	5	75	0	0	1	0	0	4	0	0	1	0	0	0	5	1	0
BV49	8	9	0	27	1	5	1	5	5	0	0	0	0	0	0	0	0	0	0	2	21	1	39	0	0	0	0	0	1	0	1	0	0	0	0	2	0	0
BV50	12	10	0	39	0	9	2	10	17	0	0	1	0	1	1	2	1	0	0	2	52	2	85	0	0	1	0	0	2	0	1	0	0	4	0	4	0	0
BV51	12	2	1	33	1	4	1	8	8	0	0	1	2	0	2	0	0	1	0	1	29	2	62	1	0	1	0	0	0	0	1	0	0	3	0	8	2	0
BV52	5	6	2	31	0	9	2	6	3	1	0	0	0	0	0	1	0	0	0	1	12	0	37	1	0	2	0	0	0	0	0	0	0	0	0	2	0	0
BV54	2	1	0	8	0	2	0	0	1	0	0	0	1	0	0	0	0	0	1	0	2	0	8	1	0	0	0	0	0	0	1	0	0	1	0	7	0	0
BV55	9	2	2	19	0	7	0	2	7	0	0	0	0	2	0	2	2	1	1	0	29	0	23	1	0	0	0	0	1	0	0	0	0	3	0	8	2	0

Table 18. Dinocyst counts in core 06PC.

Depth	*Alexandrium* cf. *Catenella*	*Operculodinium centrocarpum*	*O. centrocarpum short spines*	*Spiniferites delicatus*	*Spiniferites ramosus*	*Spiniferites mirabilis*	*Spiniferites pachydermus*	*Spiniferites* spp.	*Echinidinium* sp. C	*Echinidinium* sp. D	*Brigantedinium* spp.	*Brigantedinium cariacoense*	*Brigantedinium simplex*	*Bringantedinium auranteum*	*Dubridinium* sp.	*Selenopemphix nephroides*	*Selenopemphix quanta*	*Protoperidinium nudum*	*Stelladinium stellatum*	*Trinovantedinium pallidifulvum*	*Votadinium calvum*	*Votadinium spinosum*	*Quinquecuspis concreta*	*Polykrikos kofoidii*
0	19	171	24	1	778	57	1	2	13	8	67	3	0	86	0	0	0	0	2	0	6	4	1	32
8	10	263	22	0	683	52	2	1	10	4	89	3	0	92	0	1	0	0	3	0	3	4	3	29
16	4	264	23	0	531	26	1	0	10	2	47	2	0	30	0	1	1	0	1	0	3	1	0	24
24	1	545	39	1	574	74	12	0	16	5	40	0	2	7	5	4	4	1	0	0	17	1	1	28
32	6	222	9	3	397	93	4	0	10	6	39	0	5	15	40	3	1	0	0	0	4	4	4	50
40	0	124	17	8	65	83	6	2	4	2	33	0	5	2	69	0	1	0	0	0	10	5	0	74
48	0	62	7	14	50	111	15	0	5	2	21	0	4	0	44	3	0	1	0	0	6	1	0	59
56	0	52	3	8	28	70	7	3	10	4	28	1	3	3	34	0	0	3	0	0	4	2	3	63
64	0	131	7	4	48	51	5	0	1	0	48	1	1	0	15	3	0	0	0	0	9	0	4	54
72	0	71	8	5	37	44	16	1	5	4	29	5	5	1	39	0	0	4	0	0	2	1	6	61
78	0	98	11	2	13	22	5	3	2	0	50	3	2	2	19	0	2	0	0	0	1	0	6	52
80	0	102	8	2	22	44	7	4	12	3	36	3	2	0	25	2	3	0	0	0	3	7	2	51
88	0	109	8	2	23	36	8	0	20	8	11	4	0	1	35	0	0	1	0	0	9	4	6	59
96	0	109	8	0	23	36	13	0	22	5	11	0	2	1	54	0	0	2	1	0	4	8	3	59
104	0	157	12	1	23	30	5	0	16	1	43	4	2	0	9	0	0	0	0	0	1	1	2	77
112	0	195	10	0	36	37	2	3	7	2	79	2	5	0	13	4	3	2	0	0	9	2	8	67
120	0	157	12	0	23	30	11	3	21	4	43	3	2	0	27	1	1	1	1	1	18	4	3	77
128	0	182	10	0	30	25	7	1	17	8	0	1	2	1	12	0	0	2	2	2	8	1	4	48
136	0	182	10	0	30	25	5	1	19	3	12	1	0	0	7	1	2	3	0	0	5	3	2	48
144	0	1167	48	0	38	55	1	4	9	2	4	0	0	0	0	0	6	0	6	0	1	0	1	16
152	0	861	90	2	13	57	2	4	6	1	16	1	0	0	3	0	5	1	1	0	2	0	0	22
160	0	1202	53	4	29	190	0	3	2	0	23	2	3	0	17	5	2	0	14	0	0	0	0	62
168	0	1658	72	10	80	360	1	1	0	5	18	0	5	0	17	5	0	0	63	0	0	0	0	18
176	0	1258	42	13	77	331	0	8	3	0	6	0	0	1	5	1	0	0	59	0	0	0	0	11
184	0	522	33	7	14	132	1	0	1	1	11	0	0	0	15	0	0	0	0	0	0	0	0	6
192	0	1432	61	2	40	250	1	5	0	0	24	0	2	0	50	1	0	0	0	0	0	0	0	20
200	0	1206	37	2	60	206	0	13	1	0	19	0	2	0	34	0	0	1	0	0	0	0	0	10
208	0	438	34	1	23	81	1	0	4	2	3	0	0	0	36	0	0	1	0	0	0	0	0	6
216	0	861	30	0	29	48	2	0	0	0	10	0	0	0	37	0	0	1	0	0	0	0	0	5
224	0	620	26	0	8	12	2	0	2	1	76	0	0	0	12	0	0	0	0	0	0	0	0	6
232	0	0	0	0	0	0	0	0	0	0	0	0	0	0	0	0	0	0	0	0	0	0	0	0
240	0	0	0	0	0	0	0	0	0	0	0	0	0	0	0	0	0	0	0	0	0	0	0	0
248	0	0	0	0	0	0	0	0	0	0	0	0	0	0	0	0	0	0	0	0	0	0	0	0
256	0	0	0	0	0	0	0	0	0	0	0	0	0	0	0	0	0	0	0	0	0	0	0	0
264	0	0	0	0	0	0	0	0	0	0	0	0	0	0	0	0	0	0	0	0	0	0	0	0
272	0	0	0	0	0	0	0	0	0	0	0	0	0	0	0	0	0	0	0	0	0	0	0	0
280	0	0	0	0	0	0	0	0	0	0	0	0	0	0	0	0	0	0	0	0	0	0	0	0
288	0	0	0	0	0	0	0	0	0	0	0	0	0	0	0	0	0	0	0	0	0	0	0	0
296	0	0	0	0	0	0	0	0	0	0	0	0	0	0	0	0	0	0	0	0	0	0	0	0
304	0	0	0	0	0	0	0	0	0	0	0	0	0	0	0	0	0	0	0	0	0	0	0	0
312	0	0	0	0	0	0	0	0	0	0	0	0	0	0	0	0	0	0	0	0	0	0	0	0
320	0	0	0	0	0	0	0	0	0	0	0	0	0	0	0	0	0	0	0	0	0	0	0	0
328	0	0	0	0	0	0	0	0	0	0	0	0	0	0	0	0	0	0	0	0	0	0	0	0
336	0	0	0	0	0	0	0	0	0	0	0	0	0	0	0	0	0	0	0	0	0	0	0	0
344	0	0	0	0	0	0	0	0	0	0	0	0	0	0	0	0	0	0	0	0	0	0	0	0
352	0	0	0	0	0	0	0	0	0	0	0	0	0	0	0	0	0	0	0	0	0	0	0	0

Table 19. Pollen counts in core 06PC.

Depth	*Nothofagus* sp.	*Podocarpus* sp.	*Drymis* sp.	*Ephedra* sp.	*Colliguaya integerrima*	*Asteraceae* subf. *Asteroideae*	*Nassauvia* sp.	*Chuquiraga* sp.	*Mulinum* sp.	*Azorella* sp.	Apiaceae *type*	Solanaceae *type*	*Lycium* sp.	*Schinus* type	Rhamnaceae	Verbenaceae	Fabaceae	*Prosopis* sp.	*Phacelia* sp.	*Larrea* sp.	*Empetrum rubrum*	*Lobioideae/Rubioideae* type	*Poaceae*	Asteraceae subf. Mutisieae	Caryophyllaceae	Chenopodiaceae	*Gomphrena* sp.	Convolvulaceae	Gilia sp.	Limonium sp.	*Erodium cicutarium*	*Acaena* sp.	Onagraceae/*Fuschia*	Brassicaceae	*Rumex acetosella*	Asteraceae subf. Cichorioideae	Cyperaceae	*Typha* sp.	Unknown	monolete	Bryophyta	Fungal spores	spores triletes	Pteridophyta/Lycopodium
0	26	7	0	12	14	47	11	1	1	1	2	2	3	0	2	0	0	0	0	0	1	3	36	1	7	89	0	0	0	0	2	0	0	8	0	0	0	0	6	0	0	1	1	2
8	31	10	0	11	16	37	12	3	2	0	0	1	4	0	1	0	0	0	0	0	0	1	18	12	11	79	0	0	0	0	0	0	0	1	0	0	0	0	2	0	0	2	2	1
16	14	10	0	33	11	45	7	4	0	0	0	0	5	0	1	0	0	0	0	0	0	3	0	0	3	57	0	0	0	0	0	0	0	6	0	0	1	0	1	0	2	1	1	0
24	32	6	0	16	17	47	5	3	3	0	0	0	2	2	1	0	0	0	0	0	0	2	19	3	5	91	0	0	0	0	0	0	0	10	0	0	1	0	2	0	0	1	3	0
32	25	7	0	13	12	48	7	1	0	0	0	0	6	2	0	0	0	0	0	0	0	1	28	2	2	80	0	0	0	0	0	1	0	2	0	0	0	0	2	0	3	2	1	0
40	12	7	0	10	12	31	8	1	1	0	0	0	4	1	0	1	0	0	0	0	1	1	21	1	4	83	0	0	0	0	0	2	0	6	0	0	1	0	4	0	0	4	1	0
48	19	3	0	7	14	32	8	1	1	0	0	1	4	0	2	0	0	0	0	0	0	0	18	2	3	81	0	1	0	0	0	0	0	1	0	0	2	0	2	0	1	0	0	0
56	23	5	0	18	12	22	8	0	1	0	0	0	3	1	0	0	0	1	0	0	0	1	20	0	4	94	0	2	0	0	0	1	0	4	0	0	3	0	2	0	0	3	0	0
64	14	15	0	19	13	45	5	0	0	0	0	0	2	1	3	0	0	0	0	0	0	0	19	11	5	137	0	0	0	0	0	0	0	6	0	0	0	0	2	0	0	0	0	0
72	38	7	0	11	13	40	9	4	0	0	0	0	3	4	0	1	1	0	0	0	0	4	39	1	4	140	0	0	0	0	0	2	0	2	0	0	4	0	5	0	2	4	0	1
78	26	6	0	7	16	28	5	5	0	0	0	0	1	0	1	0	1	0	0	0	1	0	29	1	4	116	0	1	0	1	0	1	0	0	0	0	0	0	2	0	1	1	0	0
80	24	7	0	11	11	24	4	7	0	0	0	0	2	1	1	0	0	0	0	0	0	3	22	2	3	92	0	0	0	0	0	0	0	1	0	0	2	0	4	0	1	0	0	0
88	28	7	0	12	14	32	2	3	0	0	0	0	3	0	0	0	1	0	0	0	0	1	36	1	3	89	0	0	0	0	1	0	0	0	0	0	2	0	1	0	1	4	0	1
96	23	4	0	11	10	22	11	2	0	0	0	0	4	0	0	0	1	0	0	0	0	1	30	1	1	87	0	0	0	0	0	0	0	0	0	0	0	0	1	0	2	3	1	0
104	20	4	0	9	18	30	7	2	2	0	0	0	0	1	0	0	0	0	0	0	0	0	26	0	6	96	0	0	0	0	1	0	0	5	0	0	1	0	4	0	2	0	0	0
112	20	6	0	10	16	53	8	0	0	0	0	0	0	0	0	0	0	0	0	0	2	0	0	2	4	165	0	0	0	0	0	0	0	2	0	0	0	0	1	0	0	0	0	0
120	29	4	0	14	12	34	9	5	0	0	0	2	2	0	1	1	1	0	0	0	1	0	45	1	7	112	0	0	0	0	0	0	0	0	0	0	1	0	4	0	0	1	0	0
128	30	3	0	18	13	38	7	1	2	0	2	0	0	1	2	0	0	0	0	0	0	1	37	1	6	140	0	0	0	0	0	0	0	1	0	0	4	0	1	0	0	2	0	1
136	13	5	0	14	5	36	4	0	0	0	0	0	2	1	4	0	0	0	0	0	0	0	31	0	5	101	0	0	0	0	0	0	0	2	0	0	0	0	0	0	0	1	0	1
144	9	11	0	38	10	31	5	2	0	0	0	0	0	0	2	0	0	0	0	0	1	0	33	1	2	103	0	0	0	0	0	0	0	0	0	0	1	0	1	0	3	2	0	3
152	6	5	0	23	15	16	1	0	0	0	0	0	0	0	4	0	0	0	0	0	1	0	45	0	2	50	0	0	0	0	0	0	0	0	0	0	8	0	1	0	2	4	0	0
160	10	11	1	49	7	21	11	0	0	0	0	0	3	2	0	0	0	0	0	0	1	0	50	0	0	53	0	0	0	0	0	1	0	1	0	0	0	0	6	0	5	2	2	1
168	8	21	0	57	4	35	17	0	0	0	0	3	3	3	2	0	2	0	0	0	2	3	62	3	2	83	0	0	0	0	0	0	0	0	0	0	3	0	4	0	2	7	2	3
176	17	21	0	53	5	41	24	2	0	0	1	0	4	3	3	0	0	0	0	0	0	5	41	1	1	85	1	0	0	0	0	0	0	1	0	0	5	0	5	0	8	7	2	3
184	9	9	0	22	2	16	26	2	1	0	1	0	3	0	4	0	3	1	0	0	1	1	23	3	3	56	0	1	0	0	0	0	0	0	0	0	0	0	1	0	4	5	2	0
192	30	16	0	25	3	52	35	6	0	0	0	4	2	4	3	0	1	3	1	0	0	7	29	6	5	105	0	4	1	0	0	0	0	0	0	0	4	0	5	0	5	0	1	6
200	30	4	0	15	13	47	28	5	0	0	1	1	4	8	5	3	0	3	0	0	2	1	28	6	5	85	0	0	0	0	0	0	0	0	0	0	0	0	4	0	4	0	1	1
208	32	3	0	29	4	43	52	4	1	0	2	1	0	2	1	0	1	1	0	0	1	0	52	7	3	124	0	0	1	1	0	2	0	2	0	0	2	1	2	3	4	11	1	2
216	22	7	0	22	2	45	46	3	0	1	2	0	0	4	1	1	0	0	0	0	0	0	31	10	4	116	0	0	0	1	1	0	0	2	0	0	1	0	1	0	7	10	0	0
224	35	2	1	17	0	41	47	1	1	0	2	1	1	5	2	2	4	2	0	0	2	0	40	8	1	101	0	0	0	0	0	4	0	1	0	0	0	0	4	1	8	3	1	1
232	12	13	0	5	0	4	19	95	0	0	0	1	4	8	12	0	0	0	0	0	0	0	44	4	4	24	0	0	2	0	0	0	0	0	0	0	0	0	4	0	1	11	3	1
240	2	2	0	5	1	7	2	0	0	0	0	0	0	1	0	0	0	0	0	0	0	0	11	8	3	348	0	0	0	0	0	0	0	0	0	0	0	0	0	0	0	8	0	0
248	0	2	0	10	0	10	0	1	0	0	0	0	0	0	2	0	0	0	0	0	0	0	43	3	2	245	0	0	0	0	0	0	0	1	0	0	0	0	4	0	1	42	0	1
256	2	5	0	8	0	19	1	0	0	0	0	0	0	0	1	0	0	0	0	0	0	0	23	7	0	215	0	0	0	0	0	0	0	0	0	0	0	0	0	0	0	102	2	1
264	2	3	0	0	0	20	1	2	0	0	0	0	0	0	0	0	0	0	0	0	0	0	51	9	0	206	0	0	0	0	0	0	0	0	0	0	0	0	0	0	0	80	0	0
272	1	4	0	5	0	13	4	1	0	0	0	0	0	0	1	0	0	0	0	0	1	0	160	5	0	92	0	0	0	0	0	0	0	0	0	0	22	0	1	0	0	25	2	1
280	7	3	0	8	1	26	8	5	0	0	0	1	0	4	0	0	0	0	0	0	1	1	51	8	11	180	1	0	0	0	0	0	0	0	0	0	13	0	3	0	0	176	2	0
288	9	0	0	7	4	23	22	4	0	0	5	0	2	5	1	4	1	1	0	0	1	3	21	5	14	205	2	0	0	0	0	0	0	0	0	0	2	0	0	0	0	82	1	4
296	11	3	0	8	0	24	5	0	0	0	1	0	0	1	2	0	2	0	0	0	0	2	20	6	6	235	0	0	0	0	0	0	0	0	0	0	1	0	0	0	0	35	3	3
304	0	6	0	11	0	8	10	1	0	0	0	0	0	2	1	0	0	0	0	0	0	0	7	2	30	235	0	0	0	0	0	0	0	0	0	0	2	0	0	0	0	11	2	0
312	1	11	0	5	0	6	0	0	0	0	0	0	0	2	0	0	0	0	0	0	0	0	0	3	0	49	0	0	0	0	0	0	0	0	0	0	0	0	0	0	0	18	5	0
320	0	9	0	4	0	5	0	0	0	0	1	0	0	0	2	0	0	0	0	0	0	0	1	0	2	100	0	0	0	0	0	0	0	0	0	0	0	0	1	0	0	4	12	0
328	5	9	0	5	0	5	0	0	0	0	0	0	0	0	2	0	0	0	0	0	0	1	0	6	0	116	0	0	0	0	0	0	0	0	0	0	0	0	1	0	0	3	6	0
336	1	15	0	1	0	0	0	0	0	0	0	0	0	0	2	0	0	0	0	1	0	0	0	1	0	15	0	0	0	0	0	0	0	0	0	0	0	0	0	0	0	2	4	0
344	2	38	0	4	0	8	2	3	0	0	0	0	0	0	1	0	0	0	0	0	0	0	0	3	0	37	0	0	0	0	0	1	0	0	0	0	0	0	0	0	9	7	8	0
352	1	23	0	1	0	5	0	0	0	0	0	0	0	0	4	0	0	0	0	0	0	0	2	1	0	19	0	0	0	0	0	0	0	0	0	0	0	0	2	0	1	6	14	0

Table 20. Dinocyst counts in core 08PC.

Depth	*Alexandrim* cf. *Catenella*	*Operculodinium centrocarpum*	*O. centrocarpum short spines*	*Spiniferites delicatus*	*Spiniferites ramosus*	*Spiniferites mirabilis*	*Spiniferites pachydermus*	*Spiniferites* spp.	*Echinidinium* sp. C	*Echinidinium* sp. D	*Brigantedinium* spp.	*Brigantedinium cariacoense*	*Brigantedinium simplex*	*Bringantedinium auranteum*	*Dubridinium* sp.	*Selenopemphix nephroides*	*Selenopemphix quanta*	*Protoperidinium nudum*	*Stelladinium stellatum*	*Trinovantedinium pallidifulvum*	*Votadinium calvum*	*Votadinium spinosum*	*Quinquecuspis concreta*	*Polykrikos kofoidii*
0	3	265	15	1	324	13	2	3	32	0	86	1	0	8	7	0	8	0	3	0	4	0	0	54
8	5	211	8	1	617	33	2	2	6	2	147	1	0	4	4	0	0	0	2	0	5	0	0	40
16	21	534	19	2	1207	73	13	0	34	8	119	3	0	25	3	0	5	2	2	0	6	1	3	70
24	19	488	27	4	1109	53	12	2	32	4	125	0	6	26	6	0	1	0	4	0	3	0	5	68
32	1	397	23	1	115	5	4	0	5	1	55	2	4	2	5	2	1	1	0	0	8	0	4	24
40	1	740	31	4	202	57	10	7	3	0	91	1	5	0	5	2	0	0	1	0	4	1	2	38
48	2	285	7	16	419	134	13	0	3	0	98	0	3	3	12	4	3	0	1	0	2	2	3	53
56	0	139	6	4	440	156	12	3	4	0	97	1	4	1	5	1	2	0	1	0	3	1	3	49
64	0	108	4	27	85	108	3	2	2	2	79	2	1	0	33	2	0	0	0	0	4	1	0	62
72	0	178	9	17	170	181	16	10	7	3	76	4	2	0	64	4	0	0	0	0	2	7	4	71
80	0	174	10	5	26	14	1	4	2	2	70	3	0	0	35	0	0	1	1	0	17	1	3	55
88	0	65	9	0	3	1	0	0	0	0	33	2	1	2	12	0	0	0	0	0	0	0	2	14
96	0	121	11	0	9	4	5	1	3	1	48	1	1	0	16	1	2	1	1	0	3	1	4	20
104	0	67	9	0	4	0	1	0	16	1	70	0	1	0	20	0	0	0	1	0	0	0	0	35
112	0	226	12	2	15	14	1	2	32	0	76	4	0	0	22	0	1	0	0	0	6	3	2	80
120	0	290	13	3	28	19	5	4	21	0	84	2	2	0	11	1	1	1	0	0	13	5	6	58
128	0	305	38	1	38	9	4	2	16	2	52	0	1	1	16	1	0	0	2	0	9	0	1	79
136	0	556	49	8	80	50	10	7	39	3	43	1	0	0	25	2	1	0	3	5	5	0	10	133
140	0	50	17	0	26	0	0	0	22	3	11	0	1	0	16	1	1	0	6	3	0	2	0	73
148	0	482	45	3	153	59	21	8	28	3	32	1	4	0	22	2	4	1	10	1	4	3	3	120
156	0	277	34	2	63	0	9	5	8	0	9	0	0	0	1	0	2	1	4	0	0	2	1	62
164	0	317	33	0	143	15	10	5	18	3	46	0	5	1	17	0	1	1	1	0	2	3	0	132
172	0	262	13	0	97	23	8	1	2	0	0	0	0	0	21	0	1	0	5	0	0	0	0	46
180	0	463	15	0	5	4	4	0	0	0	13	1	1	0	0	0	0	0	2	0	0	0	1	8
188	0	640	34	3	2	11	1	5	0	0	4	0	0	0	3	1	1	0	6	0	0	0	1	7
196	0	300	45	1	7	75	2	10	0	0	7	0	0	0	3	0	8	0	2	0	2	0	0	16
204	0	523	19	0	4	33	0	1	0	0	0	0	0	0	1	0	1	0	5	0	0	0	0	7
212	0	70	3	0	0	11	0	0	0	0	1	0	0	0	0	0	0	0	1	0	0	0	0	0
228	0	0	0	0	0	0	0	0	0	0	0	0	0	0	0	0	0	0	0	0	0	0	0	0
236	0	0	0	0	0	0	0	0	0	0	0	0	0	0	0	0	0	0	0	0	0	0	0	0
240	0	0	0	0	0	0	0	0	0	0	0	0	0	0	0	0	0	0	0	0	0	0	0	0
244	0	0	0	0	0	0	0	0	0	0	0	0	0	0	0	0	0	0	0	0	0	0	0	0
248	0	0	0	0	0	0	0	0	0	0	0	0	0	0	0	0	0	0	0	0	0	0	0	0

Table 21. Dinocyst counts in core 08PC.

Depth	*Alexandrim* cf. *Catenella*	*Operculodinium centrocarpum*	*O. centrocarpum short spines*	*Spiniferites delicatus*	*Spiniferites ramosus*	*Spiniferites mirabilis*	*Spiniferites pachydermus*	*Spiniferites* spp.	*Echinidinium* sp. C	*Echinidinium* sp. D	*Brigantedinium* spp.	*Brigantedinium cariacoense*	*Brigantedinium simplex*	*Bringantedinium auranteum*	*Dubridinium* sp.	*Selenopemphix nephroides*	*Selenopemphix quanta*	*Protoperidinium nudum*	*Stelladinium stellatum*	*Trinovantedinium pallidifulvum*	*Votadinium calvum*	*Votadinium spinosum*	*Quinquecuspis concreta*	*Polykrikos kofoidii*
0	3	265	15	1	324	13	2	3	32	0	86	1	0	8	7	0	8	0	3	0	4	0	0	54
8	5	211	8	1	617	33	2	2	6	2	147	1	0	4	4	0	0	0	2	0	5	0	0	40
16	21	534	19	2	1207	73	13	0	34	8	119	3	0	25	3	0	5	2	2	0	6	1	3	70
24	19	488	27	4	1109	53	12	2	32	4	125	0	6	26	6	0	1	0	4	0	3	0	5	68
32	1	397	23	1	115	5	4	0	5	1	55	2	4	2	5	2	1	1	0	0	8	0	4	24
40	1	740	31	4	202	57	10	7	3	0	91	1	5	0	5	2	0	0	1	0	4	1	2	38
48	2	285	7	16	419	134	13	0	3	0	98	0	3	3	12	4	3	0	1	0	2	2	3	53
56	0	139	6	4	440	156	12	3	4	0	97	1	4	1	5	1	2	0	1	0	3	1	3	49
64	0	108	4	27	85	108	3	2	2	2	79	2	1	0	33	2	0	0	0	0	4	1	0	62
72	0	178	9	17	170	181	16	10	7	3	76	4	2	0	64	4	0	0	0	0	2	7	4	71
80	0	174	10	5	26	14	1	4	2	2	70	3	0	0	35	0	0	1	1	0	17	1	3	55
88	0	65	9	0	3	1	0	0	0	0	33	2	1	2	12	0	0	0	0	0	0	0	2	14
96	0	121	11	0	9	4	5	1	3	1	48	1	1	0	16	1	2	1	1	0	3	1	4	20
104	0	67	9	0	4	0	1	0	16	1	70	0	1	0	20	0	0	0	1	0	0	0	0	35
112	0	226	12	2	15	14	1	2	32	0	76	4	0	0	22	0	1	0	0	0	6	3	2	80
120	0	290	13	3	28	19	5	4	21	0	84	2	2	0	11	1	1	1	0	0	13	5	6	58
128	0	305	38	1	38	9	4	2	16	2	52	0	1	1	16	1	0	0	2	0	9	0	1	79
136	0	556	49	8	80	50	10	7	39	3	43	1	0	0	25	2	1	0	3	5	5	0	10	133
140	0	50	17	0	26	0	0	0	22	3	11	0	1	0	16	1	1	0	6	3	0	2	0	73
148	0	482	45	3	153	59	21	8	28	3	32	1	4	0	22	2	4	1	10	1	4	3	3	120
156	0	277	34	2	63	0	9	5	8	0	9	0	0	0	1	0	2	1	4	0	0	2	1	62
164	0	317	33	0	143	15	10	5	18	3	46	0	5	1	17	0	1	1	1	0	2	3	0	132
172	0	262	13	0	97	23	8	1	2	0	0	0	0	0	21	0	1	0	5	0	0	0	0	46
180	0	463	15	0	5	4	4	0	0	0	13	1	1	0	0	0	0	0	2	0	0	0	1	8
188	0	640	34	3	2	11	1	5	0	0	4	0	0	0	3	1	1	0	6	0	0	0	1	7
196	0	300	45	1	7	75	2	10	0	0	7	0	0	0	3	0	8	0	2	0	2	0	0	16
204	0	523	19	0	4	33	0	1	0	0	0	0	0	0	1	0	1	0	5	0	0	0	0	7
212	0	70	3	0	0	11	0	0	0	0	1	0	0	0	0	0	0	0	1	0	0	0	0	0
228	0	0	0	0	0	0	0	0	0	0	0	0	0	0	0	0	0	0	0	0	0	0	0	0
236	0	0	0	0	0	0	0	0	0	0	0	0	0	0	0	0	0	0	0	0	0	0	0	0
240	0	0	0	0	0	0	0	0	0	0	0	0	0	0	0	0	0	0	0	0	0	0	0	0
244	0	0	0	0	0	0	0	0	0	0	0	0	0	0	0	0	0	0	0	0	0	0	0	0
248	0	0	0	0	0	0	0	0	0	0	0	0	0	0	0	0	0	0	0	0	0	0	0	0

Table 22. Pollen counts in core 08PC.

Depth	*Nothofagus* sp.	*Podocarpus* sp.	*Drymis* sp.	*Ephedra* sp.	*Colliguaya integerrima*	*Asteraceae* subf. *Asteroideae*	*Nassauvia* sp.	*Chuquiraga* sp.	*Mulinum* sp.	*Azorella* sp.	Apiaceae *type*	Solanaceae *type*	*Lycium* sp.	*Schinus* type	Rhamnaceae	Verbenaceae	Fabaceae	*Prosopis* sp.	*Phacelia* sp.	*Larrea* sp.	*Empetrum rubrum*	*Labiaceae/Rubiaceae* type	*Poaceae*	Asteraceae subf. Mutisieae	Caryophyllaceae	Chenopodiaceae	*Gomphrena* sp.	Convolvulaceae	Gilia sp.	Limonium sp.	*Erodium cicutarium*	*Acaena* sp.	Onagraceae/Fuschia	Brassicaceae	*Rumex acetosella*	Asterceae subf. Cichorioideae	Cyperaceae	*Typha* sp.	*Gunnera* sp.	Unknown	monolete	Bryophyta	Fungal spores	spores triletes	Pteridophyta/Lycopodium
0	15	5	0	5	10	22	7	1	0	0	0	0	0	2	0	1	0	0	0	0	0	0	17	2	4	39	0	0	1	0	1	0	0	0	0	0	0	0	3	0	2	0	0	0
8	14	10	0	11	4	33	5	0	2	0	0	0	1	1	0	0	0	0	0	0	0	1	11	1	1	56	0	0	0	0	0	0	0	2	0	0	0	0	2	0	0	1	0	0
16	29	20	0	18	15	55	10	4	3	0	0	0	5	1	0	0	0	0	0	0	0	0	40	6	7	79	0	0	0	0	2	0	0	3	0	0	0	0	0	1	0	2	2	1	0
24	35	9	0	14	23	55	11	2	1	0	3	0	3	1	0	0	0	0	0	0	0	0	40	4	6	90	0	0	0	0	0	0	0	8	0	0	0	0	0	3	0	5	2	1	0
32	30	7	0	27	18	61	7	2	0	0	1	0	5	1	1	1	0	0	0	0	0	0	36	2	5	119	0	0	0	0	0	0	0	7	0	0	2	0	1	2	2	2	0	1	1
40	10	16	0	26	12	42	7	1	0	0	2	0	3	0	1	0	0	0	0	0	0	0	42	2	8	138	0	0	0	0	0	0	0	6	0	0	2	0	0	4	2	0	4	1	0
48	11	7	0	23	16	44	4	3	0	1	0	1	0	0	2	0	0	0	0	0	1	0	21	2	6	124	0	0	0	0	0	0	0	4	0	0	2	0	0	5	1	0	0	2	1
56	22	5	0	13	23	47	3	0	0	0	0	0	1	0	0	0	0	0	0	0	0	0	24	2	5	89	0	0	0	0	0	0	0	2	0	0	0	0	1	0	0	1	1	0	0
64	22	6	0	16	17	47	6	2	1	0	0	0	1	0	1	1	1	0	0	0	1	1	22	2	4	129	0	1	0	0	0	0	1	3	0	1	2	0	1	2	3	0	0	0	0
72	21	7	1	15	9	43	12	0	1	0	1	0	0	0	2	1	0	0	0	0	0	1	17	2	5	125	0	0	0	2	0	0	1	5	0	0	0	0	2	0	5	2	3	0	0
80	10	13	0	16	12	45	8	3	0	0	1	0	4	2	0	0	0	0	0	0	0	5	27	4	6	161	0	0	0	0	0	0	0	3	0	0	0	1	1	5	1	1	3	1	0
88	24	6	0	14	7	26	3	0	0	0	1	0	1	0	0	0	0	1	0	0	1	1	21	2	1	82	0	0	0	0	0	0	0	3	0	0	0	0	0	3	2	0	4	0	0
96	18	2	0	18	3	15	5	0	0	0	0	0	3	0	0	1	0	0	0	0	1	0	20	2	1	77	0	0	0	0	0	0	0	1	0	0	1	0	0	2	2	2	1	1	0
104	16	7	0	18	7	46	10	1	1	0	1	0	11	0	0	0	0	0	0	0	1	3	42	2	6	222	0	0	0	0	0	0	0	5	0	0	4	1	0	1	1	1	2	0	0
112	16	10	0	31	6	27	9	4	1	0	0	0	8	1	0	0	0	0	0	1	1	0	23	3	9	180	0	0	0	0	0	0	1	0	0	0	1	0	0	2	2	0	1	0	0
120	12	6	0	12	6	30	11	1	0	0	0	0	2	0	0	0	0	0	0	0	0	0	29	2	9	130	0	0	0	0	0	0	0	1	0	0	3	0	0	0	0	1	4	0	0
128	20	7	0	20	3	33	11	4	0	0	1	0	4	2	1	0	0	2	0	0	1	2	39	2	0	144	0	0	0	0	0	0	0	1	0	0	1	0	0	5	0	2	5	0	0
136	13	8	0	24	5	43	10	1	0	0	1	0	9	2	0	1	0	0	0	0	0	2	26	6	6	186	0	0	0	0	0	0	0	2	0	0	0	0	3	0	0	3	2	0	0
140	17	8	0	28	2	24	10	1	1	0	1	0	4	1	1	0	0	0	0	0	1	0	24	1	4	158	0	0	0	0	0	0	0	0	0	0	0	1	0	2	2	0	2	0	0
148	11	10	0	22	7	30	6	5	1	0	0	0	6	0	0	0	0	0	0	0	1	0	25	2	3	182	0	0	0	0	0	0	0	3	0	0	2	0	0	5	0	3	4	0	0
156	12	6	0	21	2	44	9	2	0	0	0	0	7	0	0	0	0	0	0	0	0	0	22	0	5	177	0	0	0	0	0	1	0	1	0	0	2	0	0	0	0	1	4	0	0
164	17	9	0	30	6	41	4	1	0	0	0	0	4	1	0	0	0	0	0	0	1	0	17	1	2	164	0	0	0	0	0	0	0	1	0	0	0	0	0	5	0	1	8	1	0
172	17	7	0	30	5	51	4	0	0	0	0	0	2	1	0	0	0	0	0	0	0	0	8	3	2	155	0	0	0	0	0	1	0	1	0	0	0	0	0	2	0	3	1	1	0
180	16	10	0	32	9	32	7	3	0	0	0	0	2	1	1	0	0	0	0	0	0	1	11	2	5	104	0	0	0	0	0	0	0	1	0	0	2	0	0	3	1	1	1	0	0
188	13	11	0	41	2	17	2	0	0	0	0	0	3	2	0	0	0	0	0	0	0	0	17	2	1	63	0	0	0	0	0	0	0	0	0	0	2	0	0	2	1	3	5	1	0
196	2	1	0	13	1	5	3	0	0	0	0	0	3	0	0	0	0	0	0	0	1	0	21	0	2	24	0	0	0	0	0	0	0	0	0	0	1	2	0	1	0	1	1	0	1
204	1	0	0	4	0	6	2	0	0	0	0	0	0	0	0	0	0	0	0	0	0	0	2	1	0	15	0	0	0	0	0	0	0	0	0	0	0	0	0	0	0	4	0	0	0
212	1	1	0	4	0	2	1	0	0	0	0	0	0	0	0	0	0	0	0	0	0	0	1	0	1	11	0	0	0	0	0	0	0	0	0	0	0	1	0	2	0	0	0	0	0
228	1	0	0	1	0	5	4	1	2	0	0	0	0	1	0	0	0	0	0	0	1	0	5	2	0	108	0	0	1	0	0	0	0	0	0	0	0	0	0	1	0	0	7	0	0
236	0	0	0	2	0	2	0	0	0	0	0	0	1	0	1	0	0	0	0	0	0	0	1	0	0	15	0	0	0	0	0	0	0	0	0	0	3	0	0	1	0	7	2	1	0
240	0	0	0	0	0	0	0	0	0	0	0	0	0	0	0	0	0	0	0	0	0	0	0	0	0	0	0	0	0	0	0	0	0	0	0	0	0	0	0	0	0	0	0	0	0
244	0	0	0	0	0	0	0	0	0	0	0	0	0	0	0	0	0	0	0	0	0	0	0	0	0	0	0	0	0	0	0	0	0	0	0	0	0	0	0	0	0	0	0	0	0
248	0	0	0	0	0	0	0	0	0	0	0	0	0	0	0	0	0	0	0	0	0	0	0	0	0	0	0	0	0	0	0	0	0	0	0	0	0	0	0	0	0	0	0	0	0

Table 23. Dinocyst counts in core 11PC.

Depth	Alexandrium cf. Catenella	Operculodinium centrocarpum	O. centrocarpum short spines	Spiniferites delicatus	Spiniferites ramosus	Spiniferites mirabilis	Spiniferites pachydermus	Spiniferites spp.	Echinidinium sp. C	Echinidinium sp. D	Brigantedinium spp.	Brigantedinium cariacoense	Brigantedinium simplex	Briangontedinium auronteum	Dubridinium sp.	Selenopemphix nephroides	Selenopemphix quanta	Protoperidinium nudum	Stelladinium stellatum	Trinovantedinium pallidifulvum	Votadinium calvum	Votadinium spinosum	Quinquecuspis concreta	Polykrikos kofoidii
1	7	87	5	2	359	0	3	0	9	4	133	0	0	15	1	1	0	0	5	0	0	0	2	68
6	54	315	22	3	643	57	0	3	23	1	157	2	1	2	6	0	3	0	3	0	0	3	0	122
11	5	182	9	4	580	53	5	4	4	0	413	0	0	13	3	2	0	0	1	0	8	1	10	64
21	0	227	17	8	417	57	3	3	9	0	170	0	0	15	3	0	1	0	0	0	0	0	10	37
26	2	273	9	5	363	64	14	0	13	0	690	0	2	23	22	3	0	0	0	0	5	1	19	50
30	0	376	18	7	650	67	9	7	1	0	97	0	1	0	0	0	0	0	0	0	0	0	5	0
35	0	382	10	3	541	47	14	9	0	0	119	0	1	1	5	0	0	0	0	0	0	1	5	36
46	0	432	37	4	335	48	15	0	2	0	98	0	0	0	8	2	0	0	1	0	1	0	9	29
51	0	387	17	3	681	64	11	4	2	0	67	0	0	0	4	2	0	0	0	0	2	0	8	18
66	0	222	25	6	330	36	6	0	2	0	34	0	0	0	0	1	2	0	0	0	2	0	2	25
76	0	433	30	9	215	61	4	0	2	0	45	0	3	0	7	0	1	0	0	0	0	0	2	53
81	0	453	32	8	174	42	5	2	4	0	76	1	2	0	4	1	0	0	0	0	5	0	2	39
86	0	244	21	2	205	55	3	0	1	0	38	0	0	0	3	1	1	0	0	0	1	0	3	34
91	0	726	26	5	488	111	8	0	0	0	42	0	1	0	4	4	0	0	1	1	2	0	2	44
97	0	1328	59	4	759	199	2	2	4	0	128	0	3	2	12	4	0	0	0	0	1	0	9	93
101	0	388	28	6	306	63	0	0	4	0	57	0	2	0	5	0	3	0	0	1	0	0	5	32
111	0	256	19	3	67	50	4	3	1	0	40	0	1	0	3	2	0	0	0	0	2	0	2	21
126	0	179	23	5	127	45	1	3	4	2	63	0	0	0	2	5	0	0	0	0	2	0	0	45
131	0	85	1	0	67	93	3	0	0	0	20	0	0	0	1	0	1	0	1	0	1	0	1	2
137	0	115	6	1	199	130	12	0	2	0	54	0	1	0	11	1	1	0	3	0	1	0	6	35
141	0	310	8	17	519	338	10	11	7	0	139	0	2	0	14	0	5	0	1	0	1	0	2	135
146	0	94	1	0	67	43	5	2	1	0	69	0	0	0	18	0	0	0	0	0	2	0	0	28
151	0	245	9	4	50	119	13	4	0	1	46	0	1	0	41	3	7	0	1	0	5	0	2	61
156	0	432	15	1	142	240	12	7	2	0	11	1	0	1	0	0	1	0	0	0	3	0	8	102
166	0	251	7	6	121	241	23	1	3	0	83	0	2	2	44	2	2	0	0	0	5	2	10	1132
171	0	205	6	1	59	149	7	2	0	0	87	0	0	0	18	3	1	0	0	0	2	0	11	73
181	0	143	13	7	34	127	0	0	0	0	23	0	0	0	11	0	0	0	0	0	0	0	3	1
186	0	17	4	0	2	8	1	0	0	0	153	0	0	0	17	2	1	0	1	0	1	0	7	49
191	0	252	19	9	46	186	5	4	4	0	254	1	0	0	48	0	0	0	0	0	7	2	8	167
196	0	89	6	1	0	8	1	0	7	0	64	1	3	0	25	0	2	0	1	0	2	3	6	51
201	0	93	13	0	6	18	3	1	1	0	62	0	1	0	12	3	0	0	0	0	4	0	3	41
206	0	163	14	4	28	51	11	0	5	0	30	0	0	0	14	0	0	0	0	0	4	1	3	27
211	0	233	28	5	23	72	6	2	4	2	100	0	0	0	17	2	0	0	0	0	9	1	7	35
215	0	327	27	6	33	81	5	2	8	0	76	0	1	1	18	2	1	0	0	0	2	0	7	54
221	0	562	48	4	70	114	2	0	0	0	111	0	0	0	20	1	0	0	0	0	4	0	3	100
226	0	322	40	12	27	97	2	5	1	2	50	1	0	0	10	0	0	0	0	0	4	4	3	47
231	0	201	30	4	10	18	2	0	2	2	49	0	1	0	0	0	1	0	1	0	4	0	2	31
236	0	159	21	2	15	7	1	0	1	0	15	0	0	0	0	1	0	0	0	0	0	0	3	18
241	0	388	23	6	34	51	1	2	3	6	56	0	0	0	10	1	3	0	0	0	0	0	1	32
246	0	290	31	8	37	61	7	1	5	1	51	1	2	0	9	0	0	0	0	0	4	0	2	37
251	0	218	26	11	31	57	2	0	0	0	31	0	0	0	12	0	1	0	3	0	0	0	5	31
256	0	377	36	7	33	69	1	0	11	0	62	0	5	0	30	2	2	0	0	0	3	0	14	41
261	0	314	23	7	32	32	8	0	10	1	25	0	3	0	10	1	0	0	1	0	4	0	5	38
266	0	728	46	14	78	83	1	1	8	0	47	0	2	0	21	0	3	0	1	0	10	0	4	75
271	0	242	20	1	32	9	0	0	8	1	17	0	0	0	4	0	0	1	0	0	2	1	0	21
276	0	342	41	5	85	34	7	0	10	1	24	0	0	0	23	0	0	0	0	0	6	0	1	31
281	0	263	30	6	16	19	2	0	8	1	52	0	5	2	23	0	0	0	0	1	3	0	3	47
286	0	283	25	11	27	29	3	2	13	0	40	0	2	0	14	1	1	0	1	0	4	0	2	43
291	0	214	20	7	7	23	2	2	14	0	18	0	0	0	6	1	3	0	0	0	2	0	3	27
295	0	360	25	8	38	27	5	1	8	0	0	1	3	0	18	3	0	0	2	0	2	1	7	27
301	0	378	18	18	23	34	7	1	9	0	11	0	0	0	5	2	0	0	0	1	6	1	11	27
306	0	237	13	4	26	25	0	3	5	2	16	0	1	0	6	1	0	0	0	2	6	0	10	34
311	0	620	52	8	55	55	0	0	18	1	30	0	2	0	14	0	1	0	1	0	10	0	12	80
316	0	205	20	2	19	14	2	5	3	0	7	0	0	0	2	0	0	0	0	0	3	0	5	33
321	0	366	27	18	76	24	0	7	2	4	4	0	0	0	0	0	0	0	1	0	4	2	4	51
326	0	325	21	9	64	18	3	4	3	1	5	0	0	0	2	0	2	0	1	3	2	0	4	44
331	0	553	24	23	119	58	5	1	4	4	10	0	0	0	4	0	0	0	2	1	7	0	2	54
335	0	419	22	10	228	38	9	5	3	1	16	0	0	0	0	0	1	0	0	0	1	0	0	38
341	0	260	1	10	15	11	2	1	4	0	15	0	0	0	1	0	0	0	0	0	0	0	1	26
347	0	246	14	6	79	10	2	3	1	0	0	0	0	0	0	0	0	0	0	0	0	0	0	11
353	0	287	10	16	64	40	3	0	0	0	7	0	0	0	1	1	0	0	0	0	0	0	0	5
359	0	416	22	7	14	16	3	0	0	0	0	0	0	0	0	17	0	0	1	0	0	0	0	8
365	0	710	19	19	0	2	0	1	0	0	4	0	0	0	0	0	1	0	2	0	0	0	0	0
369	0	611	58	33	12	81	2	0	5	0	10	0	0	0	0	0	4	0	0	0	0	0	1	6
375	0	3819	116	46	7	118	10	3	0	0	11	0	0	0	0	0	7	0	4	0	2	0	0	7
381	0	916	29	27	21	113	5	0	1	0	29	0	2	0	1	0	1	0	0	0	0	0	0	4
389	0	508	15	6	22	78	3	1	0	0	6	0	0	0	0	3	0	0	49	0	0	0	0	5

Table 24. Pollen counts in core11PC.

Depth	*Nothofagus sp.*	*Podocarpus sp.*	*Drymis sp.*	*Ephedra sp.*	*Calliguaya integerrima*	*Asteraceae subf. Asteroideae*	*Nassauvia sp.*	*Chuquiraga sp.*	*Mulinum sp.*	*Azorella sp.*	*Apiaceae type*	*Solanaceae type*	*Lycium sp.*	*Schinus type*	Rhamnaceae	Verbenaceae	Fabaceae	*Prosopis sp.*	*Phacelia sp.*	*Larrea sp.*	*Empetrum rubrum*	*Labiaceae/Rubiaceae type*	*Poaceae*	Asteraceae subf. Mutisieae	Caryophyllaceae	Chenopodiaceae	*Gomphrena sp.*	Convolvulaceae	Gilia sp.	Limonium sp.	*Erodium cicutarium*	*Acaena sp.*	Onagraceae/Fuschia	Brassicaceae	*Rumex acetosella*	Asterceae subf. Cichorioideae	Cyperaceae	*Typha sp.*	*Gunnera sp.*	Unknown monolete	Bryophyta	Fungal spores	spores trilietes	Pteridophyta/Lycopodium
1	30	5	0	16	5	43	14	1	1	0	0	0	17	2	2	0	0	0	0	0	0	1	28	1	6	78	0	0	0	0	1	0	1	5	0	0	0	0	0	0	1	0	0	0
6	22	6	0	16	16	53	15	3	5	0	0	0	10	6	0	0	1	0	0	0	1	2	25	2	9	120	0	0	0	0	1	1	0	2	0	0	0	0	0	0	3	0	0	0
11	22	9	0	27	12	65	5	1	1	0	2	0	1	3	0	0	1	0	0	0	1	0	37	5	9	117	0	0	0	0	0	0	0	5	0	0	0	1	0	1	0	5	0	0	0
21	19	8	0	14	9	36	7	1	2	0	0	0	2	2	2	0	1	0	0	0	0	0	28	0	3	54	0	1	0	0	0	0	0	4	0	0	0	1	0	0	1	1	1	0
26	42	9	0	14	10	58	4	3	1	0	0	0	4	0	0	1	0	0	0	0	1	0	34	3	8	112	0	0	0	0	0	0	0	4	0	0	0	0	1	0	0	0	2	0
30	19	8	0	15	25	55	8	0	0	0	0	0	4	1	4	0	0	0	0	0	2	0	35	7	9	104	0	0	0	0	1	0	0	4	0	0	0	0	0	4	0	0	1	0	1
35	23	16	0	23	14	45	9	2	1	0	0	0	6	0	2	0	0	0	0	0	0	0	22	3	1	140	0	0	0	0	1	0	0	3	0	0	0	0	1	1	2	1	0	0
46	22	9	0	24	7	53	10	0	2	0	0	0	12	0	1	0	0	0	0	0	0	0	15	2	7	113	0	0	0	0	0	0	0	4	0	0	0	0	0	2	3	5	0	0	0
51	32	8	0	18	13	41	7	1	2	0	1	0	5	1	0	0	0	0	1	0	0	1	26	3	7	131	0	1	0	0	0	0	0	4	0	0	1	0	0	0	0	5	1	0	0
66	10	14	0	19	4	29	5	0	0	0	0	0	4	0	1	0	0	0	0	1	0	0	32	2	4	75	0	0	0	0	0	0	0	1	0	0	0	0	0	1	4	0	0	1
76	17	9	0	24	9	69	8	0	2	0	0	0	3	1	4	1	0	0	0	0	1	0	29	0	2	127	0	0	0	0	0	0	0	2	0	0	2	0	0	1	0	0	0	1	0
81	35	8	0	25	8	48	13	2	0	0	0	0	2	3	2	1	0	0	0	0	0	0	35	2	4	112	0	1	0	0	0	0	0	5	0	0	0	0	0	5	1	4	0	0	0
86	20	12	0	19	14	47	11	1	1	0	0	0	10	3	2	0	0	0	0	0	0	0	40	2	5	93	0	0	0	0	0	1	0	3	0	0	0	0	1	2	0	3	0	1	0
91	25	9	0	28	10	46	3	0	1	0	0	0	6	2	1	1	0	0	0	0	0	0	39	4	6	121	0	0	0	0	0	0	0	5	0	0	0	0	0	1	1	4	0	0	0
97	36	5	0	22	4	60	8	1	0	0	0	0	13	1	0	0	1	0	0	0	0	0	48	3	5	106	0	0	0	0	0	0	0	3	0	0	0	0	0	4	0	5	0	0	0
101	30	2	0	15	9	39	9	1	0	0	1	0	4	1	0	0	0	0	0	0	0	1	54	1	2	114	0	0	0	0	0	1	0	0	0	0	0	0	0	1	0	0	2	0	0
111	30	5	0	15	3	47	10	0	1	0	0	0	5	2	0	0	0	0	0	0	0	1	0	40	2	8	139	0	0	0	0	0	0	2	0	2	0	0	0	0	0	2	1	2	1	0	0
126	28	11	0	16	13	47	9	0	0	0	0	0	4	0	2	0	0	0	0	0	2	0	52	2	1	116	0	0	0	0	0	1	0	1	0	0	0	0	1	0	1	2	0	0
131	24	8	0	16	16	42	9	0	0	0	0	0	3	1	1	0	0	0	0	0	0	0	34	1	4	111	0	0	0	0	0	0	1	4	0	0	0	1	0	1	0	0	0	0	0
137	24	5	0	10	10	46	6	0	1	0	0	0	4	3	0	0	0	0	0	0	0	1	0	33	1	8	139	0	0	0	0	0	0	0	0	4	0	0	1	0	0	2	0	3	0	0	0
141	26	9	0	29	6	51	2	4	0	0	0	1	3	1	0	0	0	0	0	0	0	0	0	44	0	4	125	0	0	0	1	0	2	0	7	0	0	0	0	1	0	0	3	0	0	0	1
146	20	9	0	23	8	52	10	0	1	0	0	0	11	1	0	0	0	0	0	0	0	0	0	27	3	5	131	0	0	0	0	0	1	0	5	0	0	0	0	0	1	0	0	0	0	0	0
151	23	9	0	13	7	49	4	0	0	0	0	0	7	0	0	0	0	0	0	0	0	0	0	37	5	6	130	0	0	0	0	0	0	0	3	0	1	1	0	1	0	0	4	0	0	0
156	35	9	0	14	7	50	9	2	0	0	0	0	10	1	3	1	0	0	0	0	0	2	0	40	1	6	117	0	1	0	0	0	1	0	5	0	0	0	0	0	2	0	2	0	0	0	0
166	14	18	0	16	4	46	7	4	0	0	0	0	7	1	1	0	0	0	0	0	0	2	2	31	2	0	146	0	0	0	0	0	0	0	0	0	1	0	0	0	0	2	2	2	0	0	0
171	29	4	0	38	4	42	4	2	0	0	0	0	13	0	1	0	0	0	0	0	0	0	1	24	4	2	150	0	0	0	0	0	0	0	2	0	0	1	0	0	0	0	7	0	1	1	0
181	28	9	0	23	7	50	4	2	0	0	0	0	12	4	0	0	0	0	0	0	0	2	1	31	1	1	125	0	0	0	0	0	3	0	0	0	0	1	0	0	2	0	7	0	0	0	0
186	13	4	0	5	5	38	8	1	1	0	0	0	11	3	0	0	0	0	0	0	0	1	2	20	2	5	91	0	0	0	0	0	0	0	0	0	0	0	0	0	1	1	1	1	0	0	0
191	25	12	0	16	2	32	4	3	0	0	0	0	9	1	0	0	0	0	0	0	0	0	0	34	2	6	144	0	0	0	0	0	0	0	1	0	0	2	0	0	0	1	3	0	0	0	0
196	15	0	0	17	2	26	8	0	1	0	0	0	3	1	0	0	0	0	0	0	0	0	0	8	0	2	83	0	0	0	0	0	0	0	1	0	0	0	0	0	1	0	2	2	2	0	0
201	20	8	0	16	6	27	5	2	0	0	0	0	4	1	0	1	0	0	0	0	0	1	0	18	2	1	95	0	0	0	0	0	0	0	0	0	0	0	0	0	2	0	2	2	0	0	0
206	10	8	0	11	7	21	7	0	0	0	0	0	4	0	0	0	0	0	0	0	0	1	0	1	24	3	1	123	0	0	0	0	0	1	0	2	0	0	0	0	0	2	3	0	0	0	0
211	22	9	0	16	2	38	8	2	0	0	0	0	3	1	0	0	0	0	0	0	0	3	2	15	2	3	167	0	0	0	0	0	0	0	4	0	0	4	0	0	0	1	4	3	2	0	0
215	22	5	0	28	14	33	6	0	0	0	0	1	1	0	0	0	0	0	0	0	0	1	1	28	0	3	132	0	0	0	0	0	0	0	0	0	0	0	0	0	0	1	1	1	0	0	0
221	26	9	0	11	8	46	12	0	0	0	0	0	6	0	1	0	0	0	0	0	0	1	0	22	1	4	160	0	0	0	0	0	1	0	0	0	0	0	0	0	0	4	2	0	0	0	0
226	21	11	0	18	3	39	8	0	0	0	0	0	5	3	4	0	0	0	0	0	0	0	1	19	5	0	164	0	0	0	0	0	0	0	0	0	0	1	1	0	1	0	4	0	1	1	0
231	29	2	0	19	5	61	5	0	1	0	0	0	4	1	0	0	0	0	0	0	0	1	2	18	2	4	153	0	0	0	0	0	0	1	0	2	0	0	3	0	0	0	0	2	0	0	1
236	35	7	0	22	8	32	9	1	0	0	1	0	4	0	1	0	0	0	0	0	0	1	0	22	2	0	161	0	0	0	0	0	0	0	2	0	0	1	0	0	0	0	2	2	1	0	0
241	26	3	0	16	4	39	9	2	0	0	0	0	2	1	0	0	0	0	0	0	0	0	0	17	2	3	173	0	0	0	0	0	0	1	0	1	0	0	2	0	0	0	3	2	0	0	0
246	20	5	0	17	6	45	5	0	1	0	0	0	1	0	0	0	0	0	0	0	0	0	1	16	1	6	158	0	0	0	0	0	0	1	0	1	0	0	2	0	0	1	0	5	0	0	0
251	23	4	0	19	0	23	14	0	1	0	0	0	5	0	1	0	0	0	0	0	0	2	1	30	2	2	149	0	0	0	0	0	0	0	0	0	0	0	2	0	0	1	0	0	1	1	0
256	18	2	0	26	3	29	4	2	0	0	0	0	2	0	1	1	0	0	0	0	0	0	0	14	6	7	180	0	0	0	0	1	0	0	0	1	0	0	1	0	0	0	2	1	0	0	0
261	13	9	0	15	0	48	6	0	0	0	0	0	3	0	0	0	0	0	0	0	0	1	0	7	5	3	174	0	0	0	0	0	0	0	2	0	0	2	0	0	0	0	2	0	0	0	0
266	25	2	0	19	3	42	10	0	0	0	0	0	1	0	0	0	0	0	0	0	0	1	0	16	3	7	169	0	0	0	0	0	1	0	1	0	0	3	0	0	0	0	3	1	0	0	0
271	16	10	0	16	3	40	12	0	2	0	0	0	4	0	0	0	0	0	0	0	0	1	0	14	1	2	188	0	0	0	0	0	1	0	0	0	0	0	0	0	2	0	5	1	0	0	0
276	25	7	0	19	2	44	8	0	0	0	0	0	3	0	0	0	0	0	0	0	0	1	0	23	2	4	170	0	0	0	0	0	0	0	3	0	0	0	0	0	1	0	0	0	0	0	0
281	18	5	0	17	1	31	12	0	0	0	0	0	7	0	2	0	0	0	0	0	0	1	0	31	4	5	174	0	0	0	0	0	0	0	4	0	0	2	0	0	0	0	3	0	0	0	0
286	25	5	0	13	3	30	13	0	0	0	0	0	2	0	1	0	0	0	0	0	0	0	0	18	1	6	186	0	0	0	0	0	0	0	2	0	0	0	0	0	1	0	4	0	0	0	0
291	28	5	0	8	2	32	9	0	0	0	0	0	4	1	0	0	0	0	0	0	0	1	0	30	4	4	158	0	0	0	0	0	2	0	1	0	0	3	0	0	0	0	1	2	0	0	0
295	27	7	0	13	2	34	8	0	1	0	0	0	13	0	0	0	0	0	0	0	0	0	0	6	2	3	181	0	0	0	0	0	1	0	2	0	0	0	0	0	0	0	3	1	0	0	0
301	23	10	0	17	2	32	8	0	0	0	0	0	5	1	0	0	0	0	0	0	0	1	2	12	3	4	177	0	0	0	0	0	0	0	1	0	0	0	0	0	0	0	1	0	0	0	0
306	18	5	0	13	4	35	8	0	1	0	0	0	5	0	0	0	0	0	0	0	0	0	0	14	2	6	182	0	0	0	0	0	0	0	0	0	0	0	2	0	0	0	0	0	0	0	0
311	20	9	0	6	0	34	10	0	1	0	0	0	3	0	0	0	0	0	0	0	0	1	1	20	6	4	183	0	0	0	0	1	0	0	0	0	0	0	0	0	0	0	2	0	0	0	0
316	30	3	0	11	4	47	8	0	0	0	0	0	6	0	0	0	0	1	0	0	3	0	0	15	0	1	205	0	0	0	0	1	0	0	0	1	0	0	1	0	0	3	0	3	0	0	0
321	26	8	2	16	2	32	10	0	0	0	0	0	2	0	1	0	0	0	0	0	2	0	0	34	2	4	159	0	0	0	0	0	4	0	0	0	0	0	0	0	0	0	3	0	0	0	0
326	31	4	0	25	3	36	8	0	0	0	0	0	5	1	0	0	0	0	0	0	1	0	0	26	3	2	166	0	0	0	0	0	1	0	2	0	0	0	0	0	0	0	2	0	0	1	0
331	11	3	0	16	5	38	6	0	0	0	0	0	6	1	0	0	0	0	0	0	1	0	0	25	3	0	197	0	0	0	0	0	0	0	1	0	0	0	0	0	0	0	3	0	0	0	0
335	14	5	0	15	0	29	0	0	0	0	0	0	3	0	0	0	0	0	0	0	0	0	0	13	0	0	210	0	0	0	0	0	0	0	0	0	0	0	0	0	0	0	2	0	0	0	0
341	14	3	0	6	1	21	5	0	0	0	0	0	9	3	0	0	1	0	0	0	0	0	0	2	3	2	189	0	0	0	0	0	0	0	2	0	0	0	0	0	0	0	4	0	0	0	0
347	20	0	0	15	2	15	11	0	0	0	0	0	3	1	0	0	0	0	0	0	0	0	0	5	1	1	186	0	0	0	0	0	0	0	1	0	0	0	0	0	0	0	1	0	0	0	0
353	10	4	0	14	5	26	8	3	0	0	0	0	1	1	0	0	0	0	0	0	0	0	0	8	2	0	209	0	0	0	0	0	2	0	1	0	0	1	0	0	1	0	5	0	0	0	0
359	23	12	0	29	3	46	4	0	0	0	0	0	0	0	0	0	0	0	0	0	1	0	0	13	2	5	184	0	0	0	0	0	0	0	5	0	0	2	0	0	0	0	2	0	1	0	0
365	21	8	0	42	0	31	5	0	0	0	0	0	2	1	0	0	0	0	0	0	0	0	0	20	6	3	154	0	0	0	0	0	0	0	2	0	0	1	0	0	0	0	9	1	3	2	0
369	29	8	0	42	2	41	7	0	1	0	0	0	5	0	0	0	0	0	0	0	1	0	0	20	0	4	147	0	0	0	0	0	0	0	2	0	1	4	0	0	0	0	0	4	0	1	0
375	11	5	0	42	0	14	3	0	0	1	0	0	2	4	1	0	0	0	0	0	0	0	0	15	2	0	88	0	0	0	0	0	0	0	0	0	0	2	0	1	0	0	2	1	0	0	0
381	12	10	0	20	0	12	3	0	0	1	0	0	3	1	2	0	0	0	0	0	3	0	0	14	4	6	58	0	0	0	0	1	1	1	0	1	0	2	0	0	1	0	9	1	0	1	0
389	14	11	0	11	0	16	11	0	0	0	0	0	1	1	1	0	0	0	0	0	1	0	0	30	3	2	53	0	0	0	0	1	0	0	0	0	0	2	0	0	0	0	7	0	0	1	0

Figure 31. Photomicrographs of dinoflagellate cysts from San Jorge Gulf. Scale bar is 10 µm. 1. *Spiniferites ramosus*. 2. *Spiniferites pachydermus*. 3. *Impagidinium paradoxum*. 4. *Spiniferites mirabilis*. 5. *Operculodinium centrocarpum*. 6. *Operculodinium centrocarpum* short processes. 7. *Alexandrium* cf. *catenella*. 8. *Nematosphaeropsis labyrinthus*. 9. *Quinquecuspis concreta*. 10. *Alexandrium* cf. *catenella*. 11. *Polykrikos kofoidii*. 12. *Polykrikos schwartzii*.

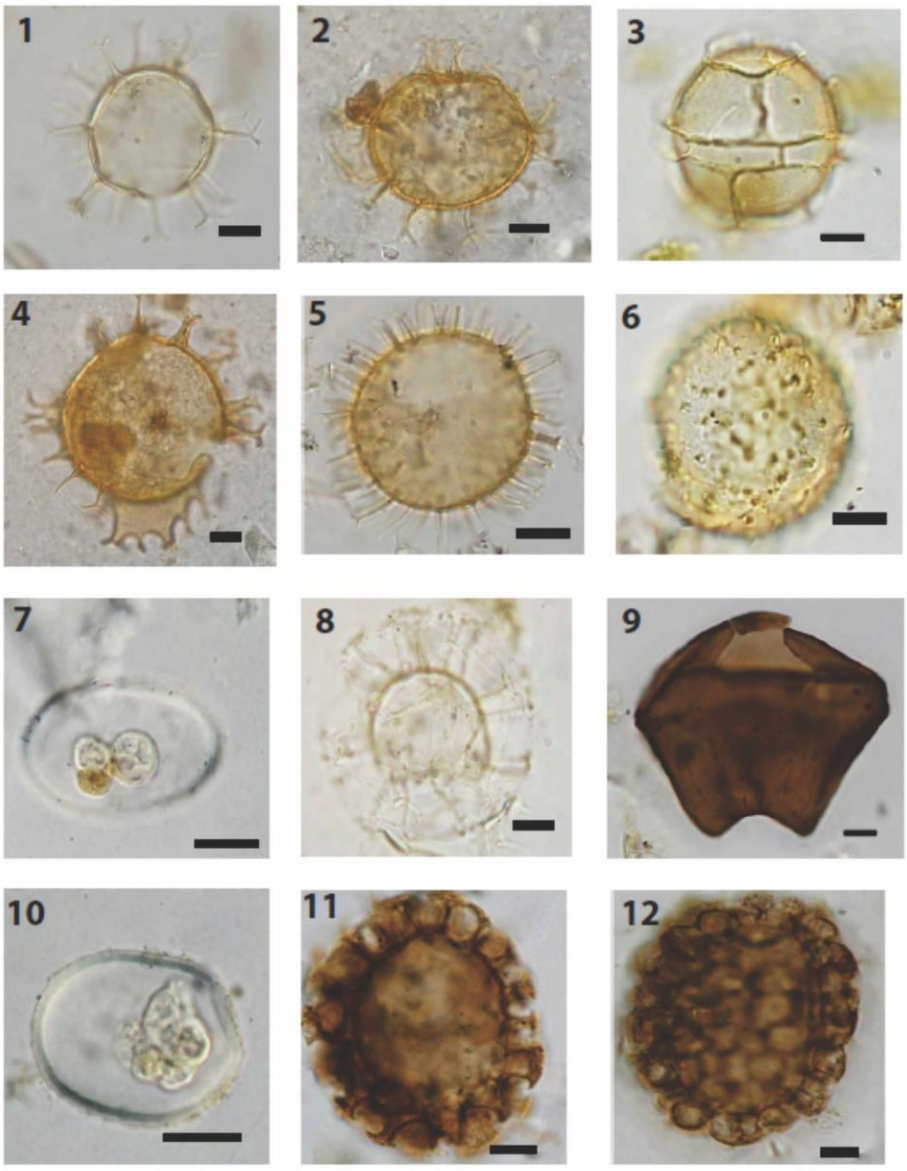

Figure 32. 1. *Trinovantedinium pallidifulvum*. 2. *Brigantedinium auranteum*. 3. *Brigantedinium simplex*. 4. *Dubridinium* sp. 5. *Echinidinium* sp.D. 6. *Echinidinium* sp.C. 7. *Votadinium spinosum*. 8. *Stelladinium stellatum*. 9. *Selenopemphix nephroides*. 10. *Selenopemphix quanta*. 11. *Halodinium* sp. 12. Organic lining of foraminifera.

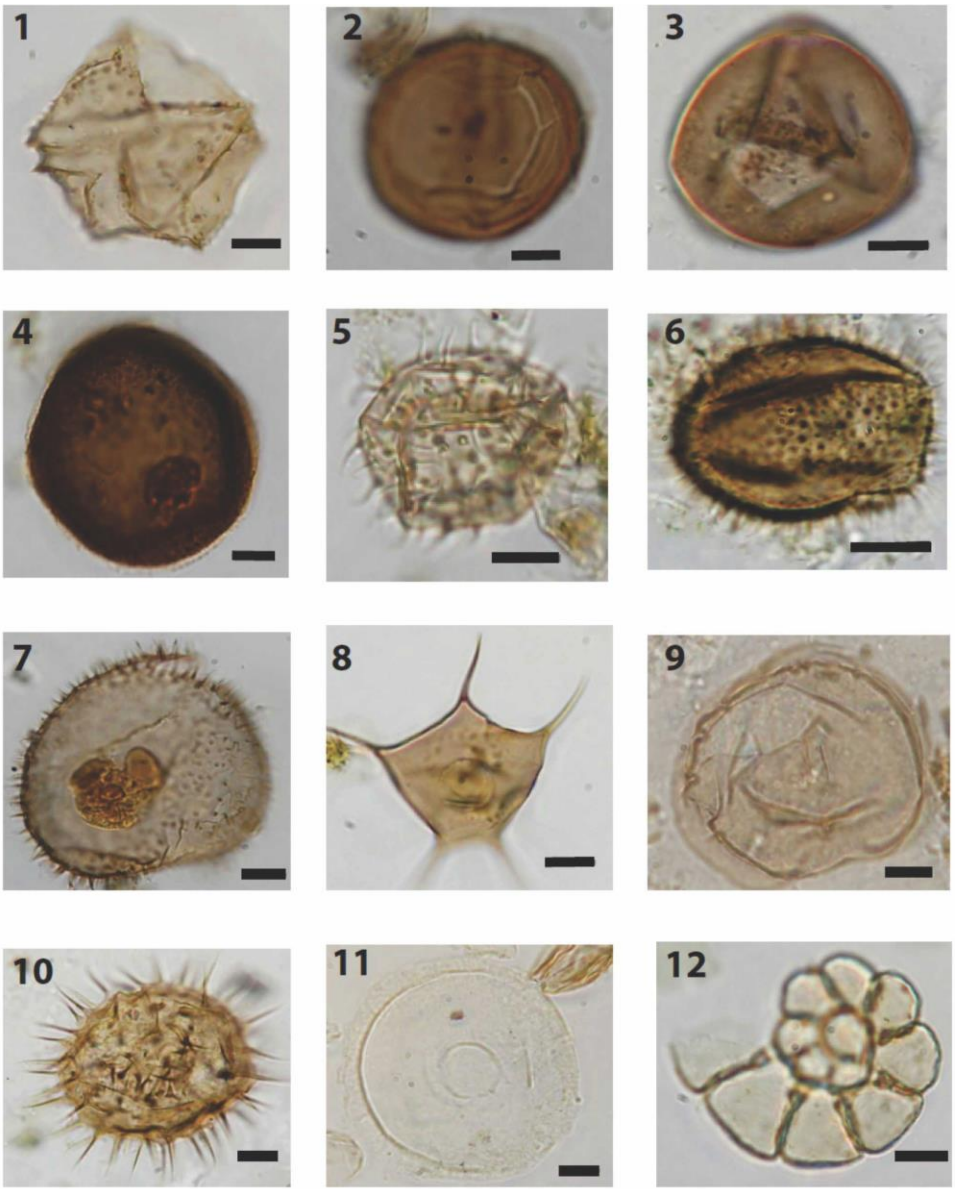

Figure 33. Scanning electron micrographs of dinocysts from San Jorge Gulf. 1. *Brigantedinium auranteum*. 2. *Brigantedinium cariacoense*. 3., 4., and 5. *Echinidinium* sp.D. 6. *Echinidinium* sp.C.

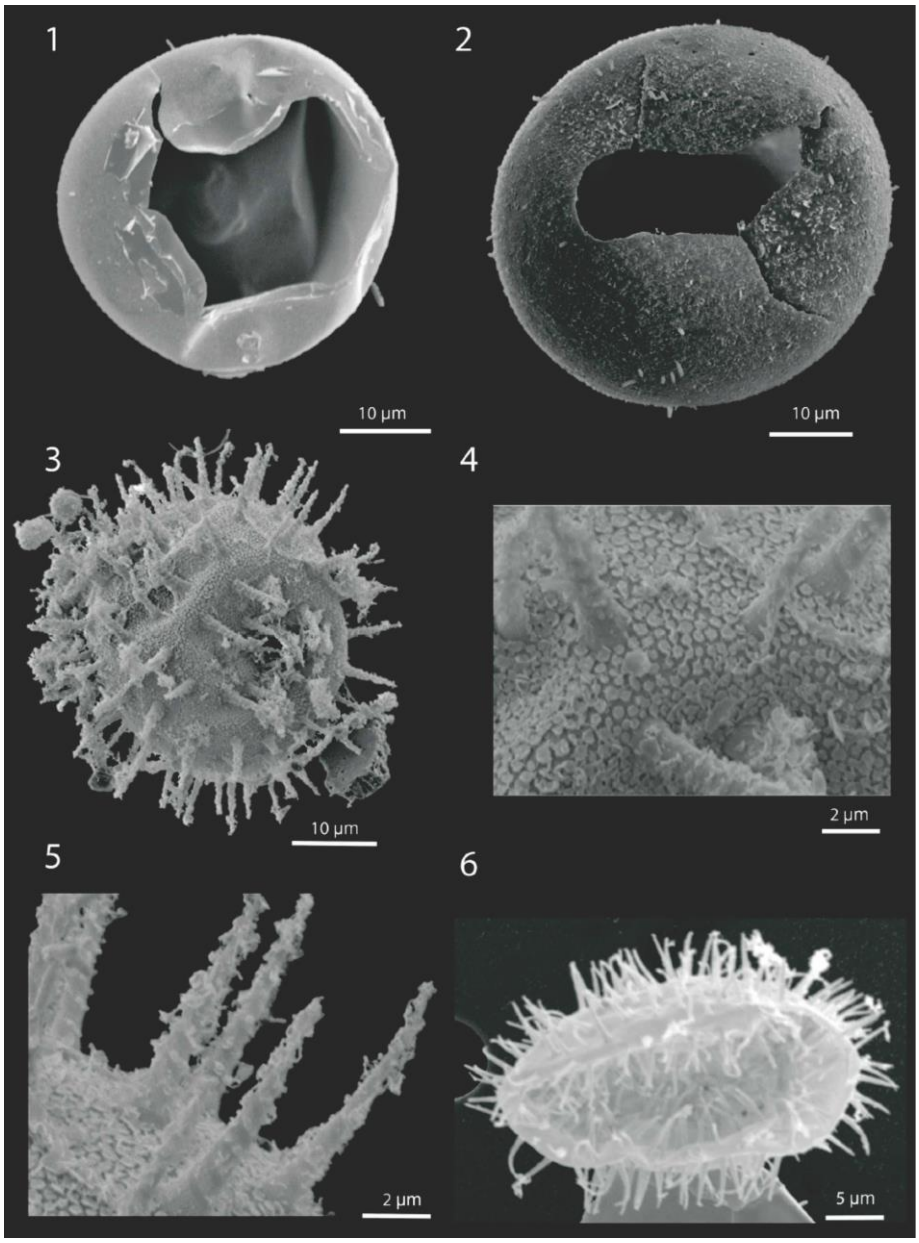

Figure 34. DCA (Dentrented Correspondence Analysis) analysis to show how the samples are group regardless their latitudinal position. The samples located in the northern area of the SJG (subzones Ia and Ib) are relatively similar in composition except some samples and are correlated with *Colliguaja integerrima*, *Chuquiraga* sp. and high shrub taxa. Conversely, samples located in the southern-central gulf (subzone Ic) are grouped together and are correlated with Poaceae taxa.

.

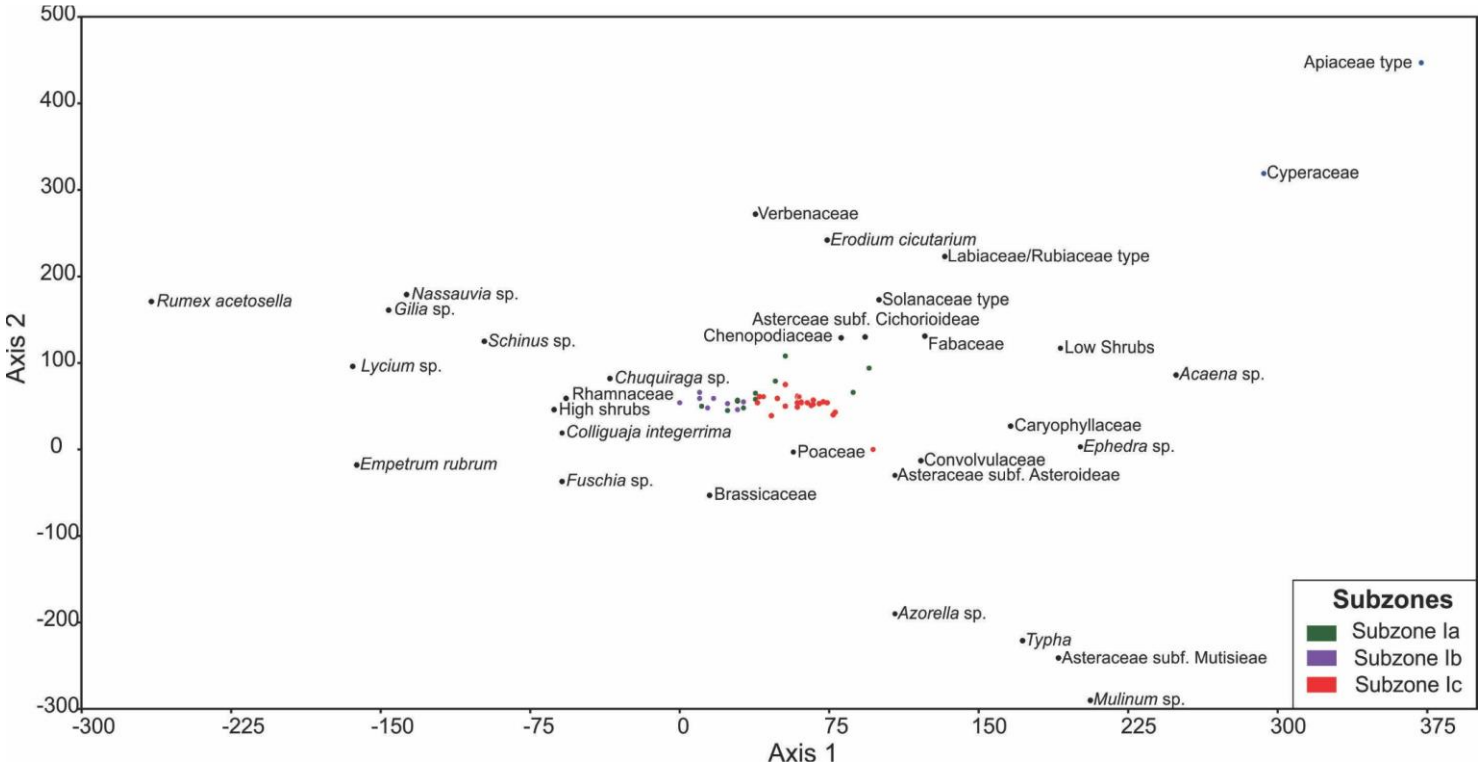

Figure 35. PCA samples scores for axis 1 using pollen (A) and dinocysts (B) data were used to define pollen and dinocysts subzones.

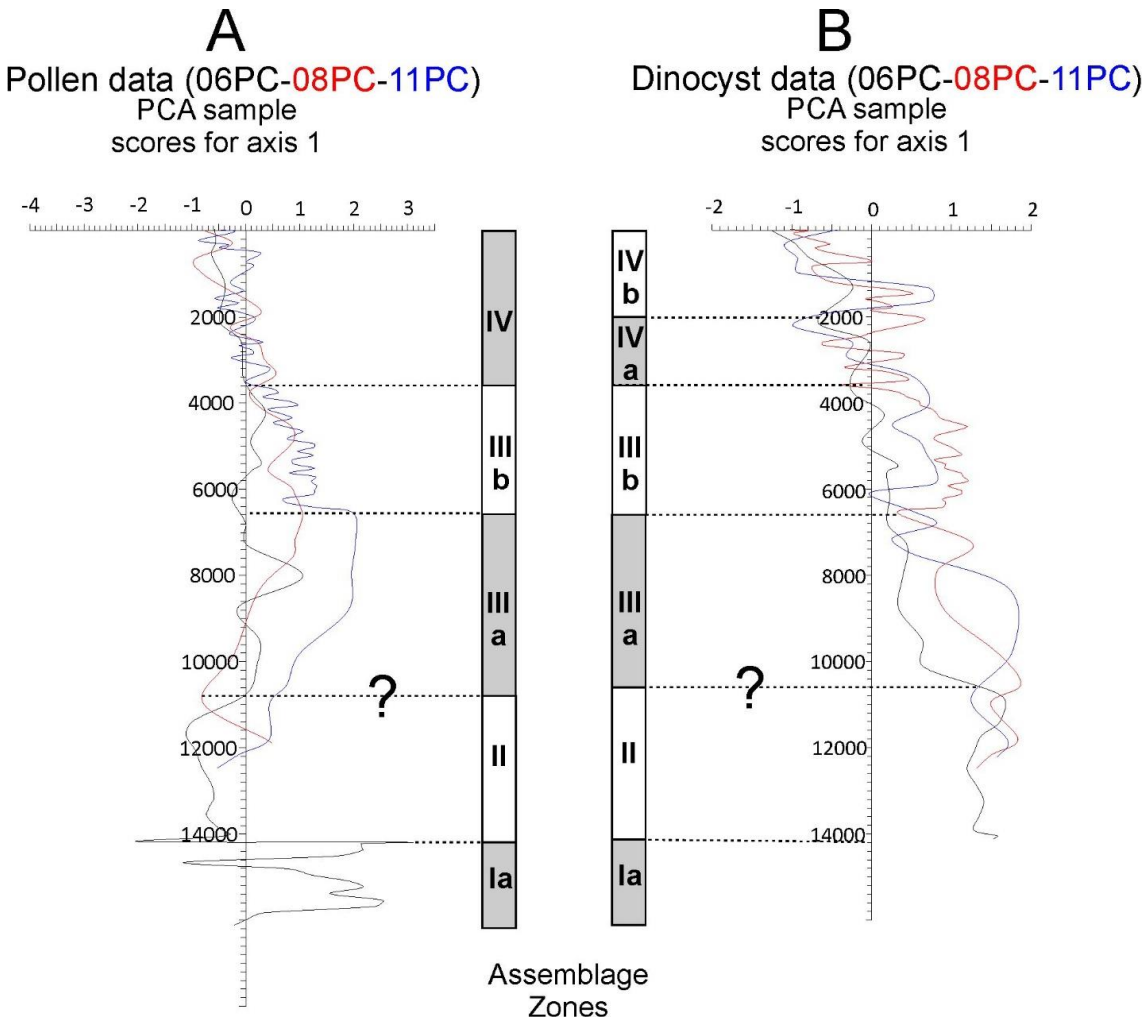

Figure 36. Photomicrographs of Pre-Quaternary dinoflagellate cysts and unknow palynomorphs from San Jorge Gulf. Scale bar is 10 μm. 1A and B. *Emmetrocysta urnaformis*. 2A and B. *Cordosphaeridium-Damassadinium* complex. 3A and B. *Hafniasphaera* sp.

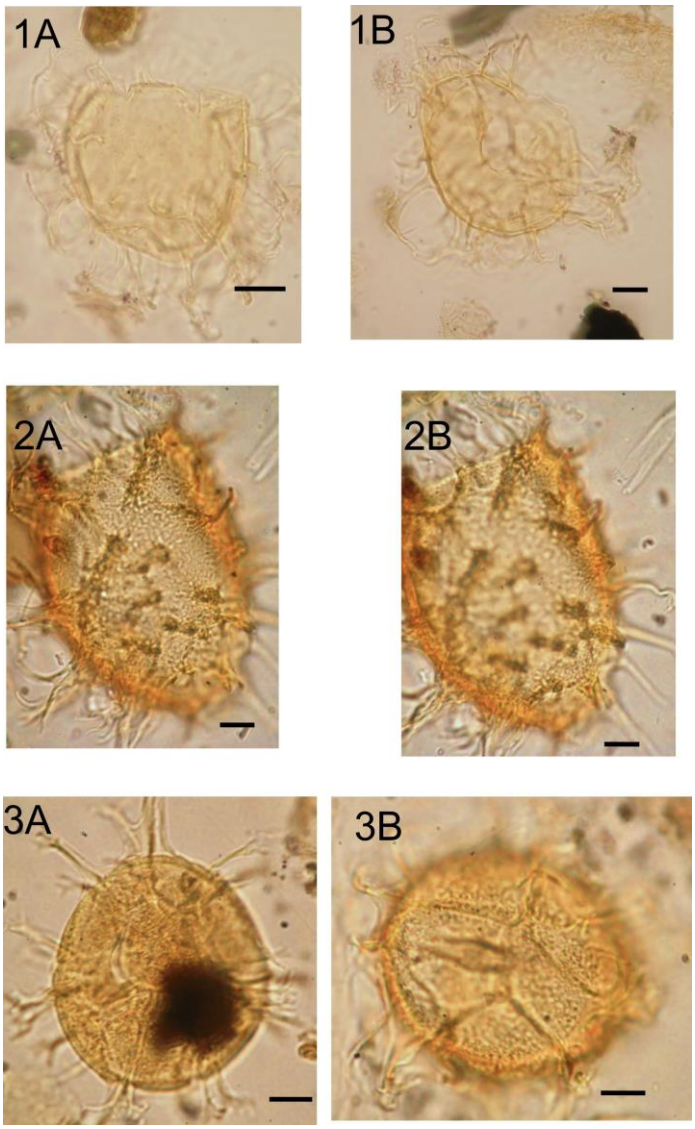

Figure 37. 1A and B. *Operculodinium centrocarpum* (Deflandre and Cookson, 1995). 2A and B. *Cordosphaeridium-Damassadinium* complex. 3A and B. *Hystrichosphaeridum* sp.

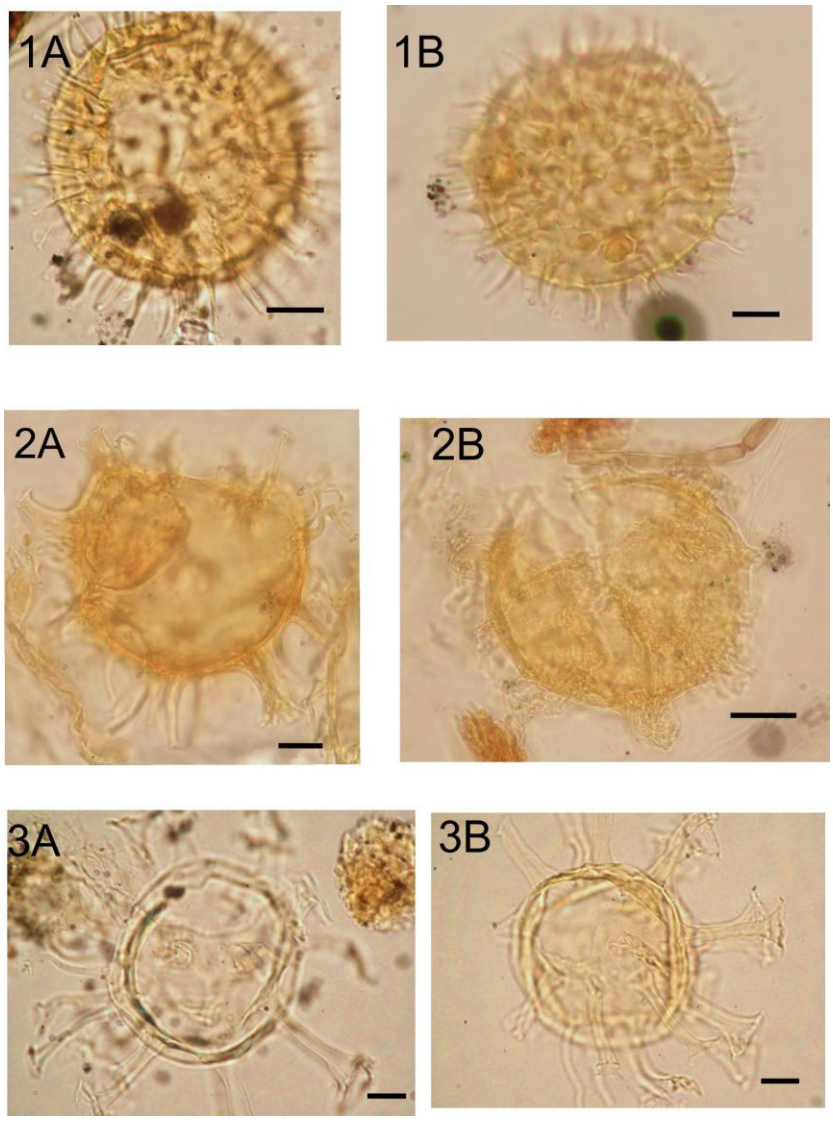

Figure 38. 1A and B. Tanyosphaeridium xanthiopyxides. 2A and B. Palambage? 3A and B. Dapsilidinium pseudocolligerum.

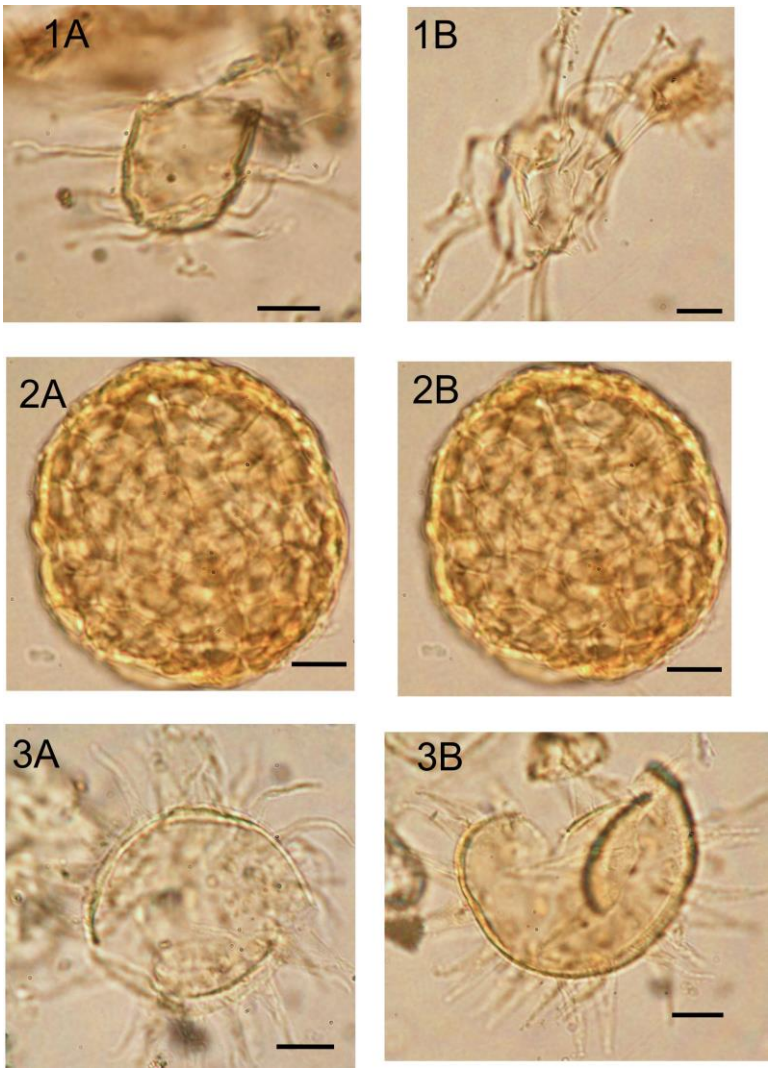

Figure 39. 1A and B. *Cleistosphaeridium placacanthum*. 2.3.4.5. Unknow.

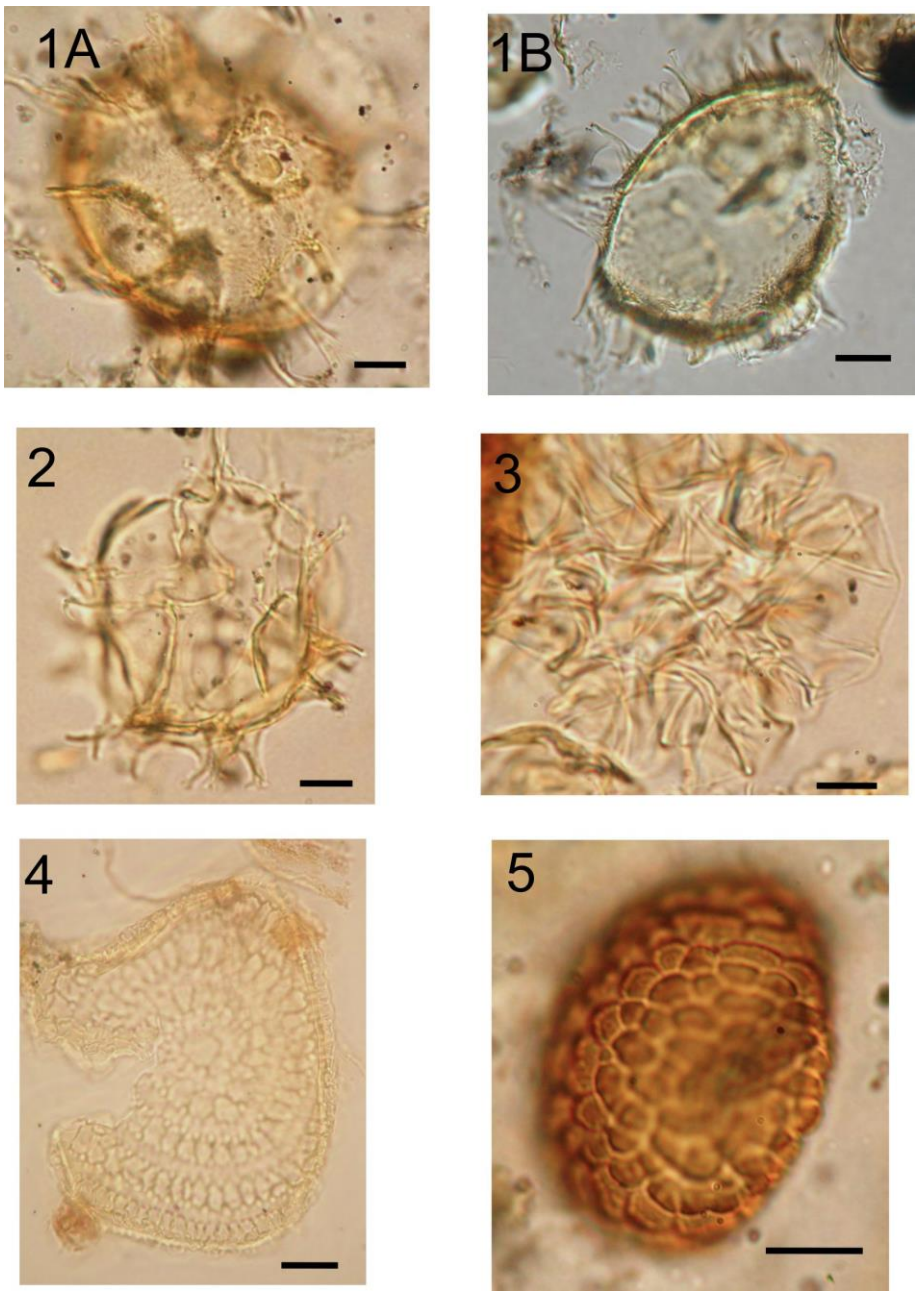

RÉFÉRENCES BIBLIOGRAPHIQUES

Aceituno, P. 1988. On the functioning of the Southern Oscillation in the South American sector. Part I: Surface climate. Monthly Weather Review, 116(3), 505-524.

Agosta, E., Compagnucci, R., Ariztegui, D. 2015. Precipitation linked to Atlantic moisture transport: clues to interpret Patagonian palaeoclimate. Climate Research, 62(3), 219-240.

Akselman, R. 1987. Quistes planctónicos de dinofíceas en áreas de plataforma del Atlántico Sudoccidental, I. Reporte taxonómico de la familia Peridiniaceae Ehrenberg. Bol. Inst. Oceanogr, 35, 17–32.

Akselman, R. 1999. Abundancia y distribución temporal de quistes de reposo de dinoflagelados recientes de una Estación Fija en la plataforma frente a Mar del Plata, Argentina. 3° Congreso Latinoamericano sobre Ciencias del Mar, Trujillo, Perú. Libro de resúmenes ampliados, 1, 323–324 p.

Anderson, R.F., Ali, S., Bradtmiller, L.I., Nielsen, S.H.H., Fleisher, M.Q., Anderson, B.E., Burckle, L. H. 2009. Wind-driven upwelling in the Southern Ocean and the deglacial rise in atmospheric CO2. science, 323(5920), 1443-1448.

Aravena, J.-C., Luckman, B.H. 2009. Spatio-temporal rainfall patterns in Southern South America. International Journal of Climatology, 29, 2106–2120. doi:10.1002/joc.1761

Ariztegui, D., Gilli, A., Anselmetti, F. S., Goñi, R. A., Belardi, J. B., Espinosa, S. 2010. Lake-level changes in central Patagonia (Argentina): crossing environmental thresholds for Lateglacial and Holocene human occupation. Journal of Quaternary Science, 25(7), 1092-1099.

Bertrand, S., Hughen, K., Sepúlveda, J., Pantoja, S. 2014. Late Holocene covariability of the southern westerlies and sea surface temperature in northern Chilean Patagonia. Quaternary Science Reviews, 105, 195-208.

Bianchi, C., Gersonde, R. 2004. Climate evolution at the last deglaciation: the role of the Southern Ocean. Earth and Planetary Science Letters, 228(3), 407-424.

Bianchi, A.A. 2005. Vertical stratification and air-sea CO_2 fluxes in the Patagonian shelf.

Journal of Geophysical Research, 110. doi:10.1029/2004JC002488.

Borel, C.M., Krock, B., Barrera, F.M., Tillmann, U., Gómez, E.A., Lara, R.J. 2012. Registro sedimentario de quistes de dinoflagelados de pared orgánica en EL Rincón, Atlántico Sudoccidental. Argentina. VIII Jornadas Nacionales de Ciencias del Mar - XVI Coloquio de Oceanografía, Comodoro Rivadavia, Argentina.

Borg, M., Twell, D. 2011. Pollen: structure and development. eLS.

Borromei, A.M., Musotto, L.L. 2016. Vegetation and Climate in Southern South America during Marine Isotope Stage 3 (MIS 3): an Overview of Existing Terrestrial Pollen Records, in: Gasparini, G.M., Rabassa, J., Deschamps, C., Tonni, E.P. (Eds.), Marine Isotope Stage 3 in Southern South America, 60 KA B.P.-30 KA B.P. Springer International Publishing, Cham, pp. 279–298. doi:10.1007/978-3-319-40000-6_15.

Broecker, W.S. 1998. Paleocean circulation during the last deglaciation: a bipolar seesaw? Paleoceanography, 13(2), 119-121.

Bullard, J.E., Baddock, M., Bradwell, T., Crusius, J., Darlington, E., Gaiero, D., Gassó, S., Gisladottir, G., Hodgkins, R., McCulloch, R., McKenna-Neuman, C., Mockford, T., Stewart, H., Thorsteinsson, T., 2016. High-latitude dust in the Earth system: High-Latitude Dust in the Earth System. Reviews of Geophysics, 54, 447–485. doi:10.1002/2016RG00051

Burry, L.S., D'Antoni, H.L., Frangi, J.L. 2005. Polen y vegetación en la Patagonia extraandina argentina a 45º S. In Anales del Jardín Botánico de Madrid, (Vol. 62, No. 2, pp. 143-152.

Candel, M.S., Radi, T., de Vernal, A., Bujalesky, G. 2012. Distribution of dinoflagellate cysts and other aquatic palynomorphs in surface sediments from the Beagle Channel, Southern Argentina. Marine Micropaleontology, 96, 1-12.

Caniupán, M., Lamy, F., Lange, C.B., Kaiser, J., Arz, H., Kilian, R., Laj, C. 2011. Millennial-scale sea surface temperature and Patagonian Ice Sheet changes off southernmost Chile (53 S) over the past~ 60 kyr. Paleoceanography, 26(3).

Carbajal, J.C., A.L. Rivas, and C. Chavanne. 2018. High-frequency frontal displacements south of San Jorge Gulf during a tidal cycle near spring and neap phases: Biological implications between tidal states. Oceanography, 31(4):60–69, https://doi.org/10.5670/oceanog.2018.411.

Compagnucci, R.H. 2011. Atmospheric circulation over Patagonia from the Jurassic to present: a review through proxy data and climatic modelling scenarios: Patagonian palaeo-atmospheric circulation. Biological Journal of the Linnean Society, 103, 229–

249. doi:10.1111/j.1095-8312.2011.01655.x.

Cronblad, H.G., Malmgren, B.A. 1981. Climatically controlled variation of Sr and Mg in Quaternary planktonic foraminifera. Nature, 291(5810), 61-64.

Coronato, A.M., Coronato, F., Mazzoni, E., Vázquez, M. 2008. The physical geography of Patagonia and Tierra del Fuego. Developments in Quaternary Sciences, 11, 13-55.

Dale, B. 1976. Cyst formation, sedimentation, and preservation: factors affecting dinoflagellate assemblages in recent sediments from Trondheimsfjord, Norway. Review of Palaeobotany and Palynology, 22(1), 39-60.

de Vernal, A.D., Henry, M., Matthiessen, J., Mudie, P.J., Rochon, A., Boessenkool, K. P., Harland, R. 2001. Dinoflagellate cyst assemblages as tracers of sea-surface conditions in the northern North Atlantic, Arctic and sub-Arctic seas: The new 'n= 677'data base and its application for quantitative palaeoceanographic reconstruction. Journal of Quaternary Science: Published for the Quaternary Research Association, 16(7), 681-698.

de Vernal, A. 2009. Marine palynology and its use for studying nearshore environments. IOP Conference Series: Earth and Environmental Science, 5, 012002. doi:10.1088/1755-1307/5/1/012002.

de Vernal, A., Rochon, A., Fréchette, B., Henry, M., Radi, T., Solignac, S. 2013. Reconstructing past sea ice cover of the Northern Hemisphere from dinocyst assemblages: status of the approach. Quaternary Science Reviews, 79, 122–134. doi:10.1016/j.quascirev.2013.06.022.

Denton, G.H., Anderson, R.F., Toggweiler, J.R., Edwards, R.L., Schaefer, J.M., Putnam, A.E. 2010. The last glacial termination. Science, 328(5986), 1652-1656.

Desiage, P.A. 2020. Sédimentologie, stratigraphie, paléomagnétisme et paléocéanographie du golfe de San Jorge, Patagonie, Argentine, depuis la dernière glaciation. Thèse de doctorat, Université du Québec à Rimouski, 231 p.

Dupont, L., Wyputta, U. 2003. Reconstructing pathways of aeolian pollen transport to the marine sediments along the coastline of SW Africa. Quaternary Science Reviews 22, 157–174. https://doi.org/10.1016/S0277-3791(02)00032-X.

Durantou, L., Rochon, A., Ledu, D., Massé, G., Schmidt, S., Babin, M. 2012. Quantitative reconstruction of sea-surface conditions over the last 150 yr in the Beaufort Sea based on dinoflagellate cyst assemblages: the role of large-scale atmospheric circulation

patterns. Biogeosciences, 9, 5391–5406. doi:10.5194/bg-9-5391-2012.

Esper, O., Zonneveld, K.A. 2002. Distribution of organic-walled dinoflagellate cysts in surface sediments of the Southern Ocean (eastern Atlantic sector) between the Subtropical Front and the Weddell Gyre. Marine Micropaleontology, 46(1-2), 177-208.

Evitt, W.R. 1985. Sporopollenin Dinoflagellate Cysts: Their Morphology and Interpretation. American Association of Stratigraphic Palynologists Foundation, Dallas, 333 p.

Fabro, E., G.O. Almandoz, M. Ferrario, U. John, U. Tillmann, K. Toebe, B. Krock, A. Cembella. 2017. Morphological, molecular, and toxin analysis of field populations of *Alexandrium* genus from the Argentine Sea. Journal of Phycology, 53(6):1,206–1,222, https://doi.org/10.1111/jpy.12574.

Fitzgerald, M.G., Mitchum, R.M., Uliana, M.A. and Biddle, K.T. 1990. Evolution of the san Jorge basin, Argentina. AAPG bulletin, 74(6), pp.879-920.

Flantua, S.G., Hooghiemstra, H., Grimm, E.C., Behling, H., Bush, M.B., González-Arango, C., Prieto, A. R. 2015. Updated site compilation of the Latin American pollen database. Review of Palaeobotany and Palynology, 223, 104-115.

Fletcher, M. S., Moreno, P. I. 2011. Zonally symmetric changes in the strength and position of the Southern Westerlies drove atmospheric CO2 variations over the past 14 ky. Geology, 39(5), 419-422.

Garreaud, R.D. 2009. The Andes climate and weather. Advances in Geosciences, 22, 3.

Garreaud, R., Lopez, P., Minvielle, M., Rojas, M. 2013. Large-scale control on the Patagonian climate. Journal of Climate, 26(1), 215-230.

Gilli, A., Ariztegui, D., Anselmetti, F.S., McKenzie, J.A., Markgraf, V., Hajdas, I., McCulloch, R. D. 2005. Mid-Holocene strengthening of the southern westerlies in South America-sedimentological evidences from Lago Cardiel, Argentina (49 S). Global and Planetary Change, 49(1-2), 75-93.

Gledhill, M., Buck, K.N. 2012. The organic complexation of iron in the marine environment: a review. The microbial ferrous wheel: iron cycling in terrestrial, freshwater, and marine environments, 29.

Glembocki, N.G., Williams, G.N., Góngora, M.E., Gagliardini, D.A., Orensanz, J.M.L., 2015. Synoptic oceanography of San Jorge Gulf (Argentina) : A template for

Patagonian red shrimp (Pleoticus muelleri) spatial dynamics. Journal of Sea Research, 95, 22-35.

Glibert, P.M., Anderson, D.M., Gentien, P., Granéli, E., Sellner, K.G. 2005. The global, complex phenomena of harmful algal blooms. Oceanography, 18 (2), 136-147.

Haberzettl, T., Mayr, C., Wille, M., Zolitschka, B. 2007. Linkages between southern hemisphere westerlies and hydrological changes in semi-arid Patagonia during the last 16,000 years. PAGES news, 15(2), 22-23.

Hansen, P.J. 1992. Prey size selection, feeding rates and growth dynamics of heterotrophic dinoflagellates with special emphasis on *Gyrodinium spirale*. Marine Biology, 114, 327–334. doi:10.1007/BF00349535.

Harland, R., Pudsey, C. J., Howe, J. A., Fitzpatrick, M. E. 1998. Recent dinoflagellate cysts in a transect from the Falkland Trough to the Weddell Sea, Antarctica. Palaeontology, 41(6), 1093-1132.

Head, M.J. 1996. Modern dinoflagellate cysts and their biological affinities. Pp. 1,197–1,248 in Palynology Principles and Applications, vol. 3. J. Jansonius and D.C. McGregor, eds, American Association of Stratigraphic Palynologists Foundation, Dallas, TX.

Heusser, L.E. 1983. Pollen distribution in the bottom sediments of the western North Atlantic Ocean. Marine Micropaleontology 8, 77–88. https://doi.org/10.1016/0377-8398(83)90006-3.

Heusser, C.J. 1989. Southern westerlies during the last glacial maximum. Quaternary Research, 31(3), 423-425.

Hooghiemstra, H., Lézine, A.-M., Leroy, S.A.G., Dupont, L., Marret, F. 2006. Late Quaternary palynology in marine sediments: A synthesis of the understanding of pollen distribution patterns in the NW African setting. Quaternary International 148, 29–44. https://doi.org/10.1016/j.quaint.2005.11.005.

Jacobson, D.M., Anderson, D.M. 1986. Thecate heterophic dinoflagellates: feeding behavior and mechanisms. Journal of Phycology, 22, 249–258.

Jenny, B., Wilhelm, D., Valero-Garcés, B. 2003. The Southern Westerlies in central Chile: Holocene precipitation estimates based on a water balance model for Laguna Aculeo (33 50′ S). Climate Dynamics, 20(2-3), 269-280.

Jeong, H.J., Yoo, Y.D., Kim, J.S., Seong, K.A., Kang, N.S., Kim, T.H. 2010. Growth, feeding and ecological roles of the mixotrophic and heterotrophic dinoflagellates in marine planktonic food webs. Ocean Science Journal, 45, 65–91. doi:10.1007/s12601-010-

0007-2.

Kaiser, J., Lamy, F., Hebbeln, D. 2005. A 70-kyr sea surface temperature record off southern Chile (Ocean Drilling Program Site 1233). Paleoceanography, 20(4).

Kilian, R., Lamy, F. 2012. A review of Glacial and Holocene paleoclimate records from southernmost Patagonia (49–55°S). Quaternary Science Reviews, 53, 1–23. https://doi.org/10.1016/j.quascirev.2012.07.017.

Koutavas, A., Lynch-Stieglitz, J. 2003. Glacial-interglacial dynamics of the eastern equatorial Pacific cold tongue-Intertropical Convergence Zone system reconstructed from oxygen isotope records. Paleoceanography, 18(4).

Krock, B., Borel, C.M., Barrera, F., Tillmann, U., Fabro, E., Almandoz, G.O., Ferrario, M., Garzón Cardona, J.E., Koch, B.P., Alonso, C., Lara, R. 2015. Analysis of the hydrographic conditions and cyst beds in the San Jorge Gulf, Argentina, that favor dinoflagellate population development including toxigenic species and their toxins. Journal of Marine Systems, 148, 86–100. doi:10.1016/j.jmarsys.2015.01.006.

Lamy, F., Rühlemann, C., Hebbeln, D., Wefer, G. 2002. High-and low-latitude climate control on the position of the southern Peru-Chile Current during the Holocene. Paleoceanography, 17(2).

Lamy, F., Kilian, R., Arz, H.W., Francois, J.P., Kaiser, J., Prange, M., Steinke, T. 2010. Holocene changes in the position and intensity of the southern westerly wind belt. Nature Geoscience, 3(10), 695-699.

Ledu, D., 2009. Reconstitutions de la variabilité climatique dans l'axe principal du passage du Nord-Ouest au cours de l'holocène. Thèse de doctorat, Université du Québec à Rimouski, 227 p.

Ledu, D., Rochon, A., de Vernal, A., Barletta, F., St-Onge, G. 2010. Holocene sea ice history and climate variability along the main axis of the Northwest Passage, Canadian Arctic. Paleoceanography, 25(2).

Lisé-Pronovost, A., St-Onge, G., Gogorza, C., Haberzettl, T., Jouve, G., Francus, P., Team, P. S. 2015. Rock-magnetic proxies of wind intensity and dust since 51,200 cal BP from lacustrine sediments of Laguna Potrok Aike, southeastern Patagonia. Earth and Planetary Science Letters, 411, 72-86.

Mancini, M.V. 2009. Holocene vegetation and climate changes from a peat pollen record of the forest – steppe ecotone, Southwest of Patagonia (Argentina). Quaternary Science

Reviews, 28, 1490–1497. doi:10.1016/j.quascirev.2009.01.017.

Mancini, M.V., Prieto, A.R., Paez, M.M., Schäbitz, F. 2008. Late Quaternary Vegetation and Climate of Patagonia, in: Developments in Quaternary Sciences. Elsevier, pp. 351–367. doi:10.1016/S1571-0866(07)10017-8.

Mancini, M.V., de Porras, M.E., Bamonte, F.P. 2012. Southernmost South America steppes: vegetation and its modern pollen-assemblages representation. Steppe Ecosystems: Dynamics, Land Use and Conservation. Nova Science Publishers, Inc., New York, USA.

Markgraf, V., d'Antoni, H.L. 1978. Pollen flora of Argentina. Tucson: Arizona, University of Arizona Press viii, 208p.-Illus., map, keys. Palynology. Geog, 4.

Markgraf, V. 1989. Palaeoclimates in Central and South America since 18,000 BP based on pollen and lake-level records. Quaternary Science Reviews, 8(1), 1-24.

Martin, P.A., Lea, D.W., Rosenthal, Y., Shackleton, N. J., Sarnthein, M., Papenfuss, T. 2002. Quaternary deep sea temperature histories derived from benthic foraminiferal Mg/Ca. Earth and Planetary Science Letters, 198(1-2), 193-209.

Marret, F., Zonneveld, K.A.F. 2003. Atlas of modern organic-walled dinoflagellate cyst distribution. Review of Palaeobotany and Palynology, 125, 1–200. doi:10.1016/S0034-6667(02)00229-4.

Matano, R.P., Palma, E.D. 2008. On the Upwelling of Downwelling Currents. Journal of Physical Oceanography, 38, 2482–2500. doi:10.1175/2008JPO3783.1.

Matano, R.P., Palma, E.D., Piola, A.R. 2010. The influence of the Brazil and Malvinas Currents on the Southwestern Atlantic Shelf circulation. Ocean Science, 6, 983–995. doi:10.5194/os-6-983-2010.

Mayr, C., Wille, M., Haberzettl, T., Fey, M., Janssen, S., Lucke, A., Ohlendorf, C., Oliva, G., Schabitz, F., Schleser, G. 2007. Holocene variability of the Southern Hemisphere westerlies in Argentinean Patagonia (52°S). Quaternary Science Reviews, 26, 579–584. doi:10.1016/j.quascirev.2006.11.013.

Mayr, C., Lücke, A., Wagner, S., Wissel, H., Ohlendorf, C., Haberzettl, T., Zolitschka, B. 2013. Intensified Southern Hemisphere Westerlies regulated atmospheric CO_2 during the last deglaciation. Geology, 41(8), 831-834.

Melia, M.B. 1984. The distribution and relationship between palynomorphs in aerosols and deep-sea sediments of the coast off Northwest Africa. Marine Geology, 58, 345–371.

https://doi.org/10.1016/0025-3227(84)90208-1

Mohtadi, M., Romero, O.E., Kaiser, J., Hebbeln, D. 2007. Cooling of the southern high latitudes during the Medieval Period and its effect on ENSO. Quaternary Science Reviews, 26(7-8), 1055-1066.

Moreno, P.I., Francois, J.P., Moy, C.M., Villa-Martínez, R. 2010. Covariability of the Southern Westerlies and atmospheric CO2 during the Holocene. Geology, 38(8), 727-730.

Moreno, P. I., Videla, J. 2016. Centennial and millennial-scale hydroclimate changes in northwestern Patagonia since 16,000 yr BP. Quaternary Science Reviews, 149, 326-337.

Moy, C.M., Dunbar, R.B., Moreno, P.I., Francois, J.P., Villa-Martínez, R., Mucciarone, D. M., Garreaud, R.D. 2008. Isotopic evidence for hydrologic change related to the westerlies in SW Patagonia, Chile, during the last millennium. Quaternary Science Reviews, 27(13-14), 1335-1349.

Moy, C.M., Moreno, P.I., Dunbar, R.B., Kaplan, M.R., Francois, J.-P., Villalba, R., Haberzettl, T., 2009. Climate Change in Southern South America During the Last Two Millennia, in: Vimeux, F., Sylvestre, F., Khodri, M. (Eds.), Past Climate Variability in South America and Surrounding Regions. Springer Netherlands, Dordrecht, pp. 353–393. doi:10.1007/978-90-481-2672-9_15.

Moy, C. M., Dunbar, R. B., Guilderson, T. P., Waldmann, N., Mucciarone, D. A., Recasens, C., Anselmetti, F. S. 2011. A geochemical and sedimentary record of high southern latitude Holocene climate evolution from Lago Fagnano, Tierra del Fuego. Earth and planetary science letters, 302(1), 1-13.

North Greenland Ice Core Project members. 2004. High-resolution record of Northern Hemisphere climate extending into the last interglacial period. Nature, v.431, No. 7005, pp. 147-151, 9 September 2004.

Orozco, F. E., Carreto, J. I. 1989. Distribution of *Alexandrium excavatum* resting cysts in a patagonic shelf area (Argentina).Distribución de esporas de resistencia de *Alexandrium excavatum* en un area de la plataforma patagónica.

Paez, M. M., Schäbitz, F., Stutz, S. 2001. Modern pollen–vegetation and isopoll maps in southern Argentina. Journal of Biogeography, 28(8), 997-1021.

Palma, E.D., Matano, R.P., Piola, A.R. 2004. A numerical study of the Southwestern Atlantic Shelf circulation: Barotropic response to tidal and wind forcing. Journal of

Geophysical Research: Oceans, 109(C8).

Palma, E.D., Matano, R.P., Piola, A.R. 2008. A numerical study of the Southwestern Atlantic Shelf circulation : Stratified ocean response to local and offshore forcing. Journal of Geophysical Research: Oceans, 113(C11).

Parker, G., Paterlini, M.C. and Violante, R., 1997. El fondo marino.

Parrenin, F., Masson-Delmotte, V., Köhler, P., Raynaud, D., Paillard, D., Schwander, J., Barbante, C., Landais, A., Wegner, A. and Jouzel, J. 2013. Synchronous change of atmospheric CO2 and Antarctic temperature during the last deglacial warming. Science, 339(6123), pp.1060-1063.

Paruelo, J.M., Beltrán, A., Jobbagy, E., Sala, O.E., Golluscio, R.A. 1998. The climate of Patagonia: general patterns and controls on biotic processes. Ecología Austral, 8, 85–101.

Piola, A.R., Avellaneda, N.M., Guerrero, R.A., Jardón, F.P., Palma, E.D., Romero, S.I. 2010. Malvinas-slope water intrusions on the northern Patagonia continental shelf. Ocean Science, 6, 345.

Pittock, A.B. 1980. Patterns of Climatic Variation in Argentina and Chile—I Precipitation, 1931–60. Monthly Weather Review, 108, 1347–1361. doi:10.1175/1520-0493(1980)108<1347:POCVIA>2.0.CO;2.

Ponce, J.F., Rabassa, J., Coronato, A. and Borromei, A.M. 2011. Palaeogeographical evolution of the Atlantic coast of Pampa and Patagonia from the last glacial maximum to the Middle Holocene. Biological Journal of the Linnean Society, 103(2), pp.363-379.

Pons, A. 1958. Le pollen, Armand Pons. Que sais je.

Pospelova, V., de Vernal, A., Pedersen, T.F. 2008. Distribution of dinoflagellate cysts in surface sediments from the northeastern Pacific Ocean (43–25 N) in relation to sea-surface temperature, salinity, productivity and coastal upwelling. Marine Micropaleontology, 68(1), 21-48.

Quade, J., Kaplan, M.R. 2017. Lake-level stratigraphy and geochronology revisited at Lago (Lake) Cardiel, Argentina, and changes in the Southern Hemispheric Westerlies over the last 25 ka. Quaternary Science Reviews, 177, 173-188.

Ray, N., Adams, J. 2001. A GIS-based vegetation map of the world at the last glacial maximum (25,000-15,000 BP). Internet archaeology 11.

Richerol, T. 2014. Climat Holocène du Nunatsiavut inféré à partir des assemblages sédimentaires de pollen et de kystes de dinoflagellés des fjords (Labrador, Canada). Université de Laval, 207 p.

Rivas, A.L., Dogliotti, A.I., Gagliardini, D.A. 2006. Seasonal variability in satellite-measured surface chlorophyll in the Patagonian Shelf. Continental Shelf Research, 26, 703–720. doi:10.1016/j.csr.2006.01.013.

Rochon, A., Vernal, A.D. 1994. Palynomorph distribution in recent sediments from the Labrador Sea. Canadian Journal of Earth Sciences, 31(1), 115-127.

Rochon, A., Vernal, A.D., Turon, J.L., Matthiessen, J., Head, M. J. 1999. Distribution of recent dinoflagellate cysts in surface sediments from the North Atlantic Ocean and adjacent seas in relation to sea-surface parameters. American Association of Stratigraphic Palynologists Contribution Series, 35, 1-146.

Romero, O.E., Kim, J.H., Hebbeln, D. 2006. Paleoproductivity evolution off central Chile from the Last Glacial Maximum to the Early Holocene. Quaternary Research, 65(3), 519-525.

Sabatini, M., Martos, P. 2002. Mesozooplankton features in a frontal area off northern Patagonia (Argentina) during spring 1995 and 1998. Scientia Marina, 66, 215–232.

Schäbitz, F., Wille, M., Francois, J.P., Haberzettl, T., Quintana, F., Mayr, C., Prieto, A.R. 2013. Reconstruction of palaeoprecipitation based on pollen transfer functions–the record of the last 16 ka from Laguna Potrok Aike, southern Patagonia. Quaternary Science Reviews, 71, 175-190.

Schimpf, D., Kilian, R., Kronz, A., Simon, K., Spötl, C., Wörner, G., Mangini, A. 2011. The significance of chemical, isotopic, and detrital components in three coeval stalagmites from the superhumid southernmost Andes (53 S) as high-resolution palaeo-climate proxies. Quaternary Science Reviews, 30(3-4), 443-459.

Schneider, C., Gies, D. 2004. Effects of El Niño–southern oscillation on southernmost South America precipitation at 53°S revealed from NCEP–NCAR reanalyses and weather station data. International Journal of Climatology, 24, 1057–1076. doi:10.1002/joc.1057.

Schouten, S., Hopmans, E.C., Damsté, J.S.S. 2013. The organic geochemistry of glycerol dialkyl glycerol tetraether lipids: a review. Organic geochemistry, 54, 19-61.

Sepúlveda, J., Pantoja, S., Hughen, K. A., Bertrand, S., Figueroa, D., León, T., Lange, C. 2009. Late Holocene sea-surface temperature and precipitation variability in northern

Patagonia, Chile (Jacaf Fjord, 44 S). Quaternary Research, 72(3), 400-409.

Smayda, T.J., Trainer, V.L. 2010. Dinoflagellate blooms in upwelling systems: Seeding, variability, and contrasts with diatom bloom behaviour. Progress in Oceanography, 85(1), 92-107.

Stocker, T.F., Johnsen, S.J. 2003. A minimum thermodynamic model for the bipolar seesaw: thermal bipolar seesaw. Paleoceanography, 18, n/a-n/a. doi:10.1029/2003PA000920.

Sylwan, C.A. 2001. Geology of the Golfo San Jorge Basin, Argentina. Geología de la Cuenca del Golfo San Jorge, Argentina. Journal of Iberian Geology, 27, pp.123-158.

Taylor, F.J.R., M. Hoppenrath, and J.F. Saldarriaga. 2008. Dinoflagellate diversity and distribution. Biodiversity and Conservation, 17(2):407–418, https://doi.org/10.1007/s10531-007-9258-3.

Thompson, D.W., Solomon, S. 2002. Interpretation of recent Southern Hemisphere climate change. Science, 296(5569), 895-899.

Thompson, D.W., Wallace, J.M. 2000. Annular modes in the extratropical circulation. Part I: Month-to-month variability. Journal of climate, 13(5), 1000-1016.

Toggweiler, J.R., Russell, J.L., Carson, S.R. 2006. Midlatitude westerlies, atmospheric CO2, and climate change during the ice ages. Paleoceanography, 21(2).

Toggweiler, J.R. 2009. Climate change: Shifting Westerlies. Science, 323, 1434–1435. https://doi.org/10.1126/science.1169823

Tonello, M.S., Mancini, M.V., Seppä, H. 2009. Quantitative reconstruction of Holocene precipitation changes in southern Patagonia. Quaternary Research, 72(3), 410-420.

Van Daele, M., Bertrand, S., Meyer, I., Moernaut, J., Vandoorne, W., Siani, G., De Batist, M. 2016. Late Quaternary evolution of Lago Castor (Chile, 45.6 S): Timing of the deglaciation in northern Patagonia and evolution of the southern westerlies during the last 17 kyr. Quaternary Science Reviews, 133, 130-146.

Versteegh, G.J.M., P. Blokker, K.A. Bogus, I.C. Harding, J. Lewis, S. Oltmanns, A. Rochon, and K.A.F. Zonneveld. 2012. Infra red spectroscopy, flash pyrolysis, thermally assisted hydrolysis and methylation (THM) in the presence of tetramethylammonium hydroxide (TMAH) of cultured and sediment-derived *Lingulodinium polyedrum* (Dinoflagellata) cyst walls. *Organic Geochemistry* 43:92–102, https://doi.org/10.1016/j.orggeochem.2011.10.007.

Villa-Martínez, R., Moreno, P.I. 2007. Pollen evidence for variations in the southern margin of the westerly winds in SW Patagonia over the last 12,600 years. Quaternary Research, 68(3), 400-409.

Violante, R.A. and Parker, G. 2004. The post-last glacial maximum transgression in the de la Plata River and adjacent inner continental shelf, Argentina. Quaternary International, 114(1), pp.167-181.

Wall, D., Dale, B., Lohmann, G.P., Smith, W.K. 1977. The environmental and climatic distribution of dinoflagellate cysts in modern marine sediments from regions in the North and South Atlantic Oceans and adjacent seas. Marine micropaleontology, 2, 121–200.

Waldmann, N., Ariztegui, D., Anselmetti, F.S., Austin Jr, J.A., Moy, C.M., Stern, C., Dunbar, R.B. 2010. Holocene climatic fluctuations and positioning of the Southern Hemisphere westerlies in Tierra del Fuego (54 S), Patagonia. Journal of Quaternary Science, 25(7), 1063-1075.

Wall, D., Dale, B., Lohmann, G., Smith, W. 1977. The environmental and climatic distribution of dinoflagellate cysts in modern marine sediments from regions in the North and South Atlantic Ocean and adjacent seas. Mar. Micropaleontol. 2, 121–200.

Zolitschka, B., Anselmetti, F., Ariztegui, D., Corbella, H., Francus, P., Lücke, A., Wastegård, S. 2013. Environment and climate of the last 51,000 years–new insights from the Potrok Aike maar lake Sediment Archive Drilling project (PASADO). Quaternary Science Reviews, *71*, 1-12.

Zonneveld, K.A.F., Bockelmann, F., Holzwarth, U. 2007. Selective preservation of organic-walled dinoflagellate cysts as a tool to quantify past net primary production and bottom water oxygen concentrations. Marine Geology, 237, 109–126. doi:10.1016/j.margeo.2006.10.023

Zonneveld, K. A., Pospelova, V. 2015. A determination key for modern dinoflagellate cysts. Palynology, 39(3), 387-4